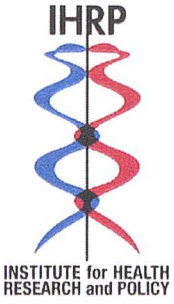

Lanthanide complexes of phthalimide and phthalamate containing ligands: synthesis, photophysical properties and their potential applications

A THESIS

Submitted in partial fulfillment of the requirement of

London Metropolitan University

for the degree of

DOCTOR OF PHILOSOPHY

Presented by

Gaoyun Chen

BSc (Hons), AMRSC

Faculty of Life Sciences

London Metropolitan University

166 – 220 Holloway Road

London N7 8DB

October 2012

Abstract

Molecular sensors and switches have made important contributions to biomedical devices and molecular computational operations. There are numerous molecular designs using a fluorophore linked through a spacer group to a receptor(s), with a wide dynamic range, directional precision, target specificity, and molecular logic capability. Tb(III) and Eu(III) metal ions have natural luminescence lifetimes in the order of milliseconds. As a result they have been used as probes that allow discrimination between probe emission and background fluorescence using time-resolved techniques. Unfortunately the free ions themselves absorb light poorly so cannot provide the sensitivity often required of a probe or a sensor. Their performance however can be improved dramatically by the coordination of the metal ions to organic chelate ligands containing appropriate organic fluorophores.

This project is based on the design and synthesis of Tb(III) and Eu(III) complexes of phthalimide and phthalamate derivatives as responsive lanthanide complexes. Phthalimide and phthalamate compounds are organic chromophores. Four acyclic phthalimide derivatives, L^1, L^3, L^5 and L^7, were prepared through condensation reaction of phthalic anhydride and the corresponding amine derivatives in *glacial* acetic acid. These phthalimide derivatives, L^1, L^3, L^5 and L^7, were then hydrolysed under basic conditions to yield the desired phthalamate compounds, L^2, L^4, L^6 and L^8. The yields of these phthalamate derivatives (L^2, L^4, L^6 and L^8) were 50%-70%. They are fully characterised by ^1H and ^{13}C NMR spectroscopy, elemental analysis, mass spectrometer, IR and melting point analysis.

A series of macrocycles with *N*-substituted phthalimide pendant arm(s) $L^{9\text{-}12}$ were synthesised. The macrocyclic phthalimide derivatives were prepared by incorporating *N*-bromoalkyl phthalimide onto tri-tert-butyl-1,4,7,10-tetraazacyclododecane-1,4,7-triacetate, di-tert-butyl-1,4,7,10-tetraazacyclododecane-1,4-diacetate and mono-tert-butyl-1,4,7,10-tetraazacyclododecane-monoacetate through nucleophilic substitution reactions. Removal of t-butyl functions and retention of phthalimide was achieved in trifluoroacetic acid to yield the final products (6%-14%). 1,4,7,10-Tetraazacyclododecane was alkylated on its 4 nitrogen sites by phthalimide

function with a propyl bridge to yield L^{13} (10%). $L^{9\text{-}13}$ were fully characterized by ^{1}H and ^{13}C NMR spectroscopy, elemental analysis, mass spectrometer, IR and melting point analysis. Apart from L^{1}, L^{3}, L^{4}, L^{5} and L^{10} all the phthalimide and phthalamate derivatives synthesised in this thesis are new.

The optimal metal-to-ligand ratio of 1:2 was established for acyclic phthalamate-based terbium complexes, whereby the best antennae effects on the luminescence properties of these complexes were observed. The highest luminescence level of $[Tb(L^{2})_2]^-$, $[Tb(L^{4})_2]^-$, $[Tb(L^{6})_2]^{3-}$ and $[Tb(L^{8})_2]^-$ was observed at pH *ca.* 6, but it was quenched at pH>7. These four terbium complexes exhibited long emission lifetimes of the order of sub-milliseconds.

Luminescence features of $[TbL^{9}]$, $[TbL^{10}]$, $[TbL^{11}]^+$ and $[TbL^{12}]^{2+}$ showed rather weak luminescence under acidic conditions. The luminescence was enhanced under basic conditions while phthalimide functions were hydrolysed to phthalamates. Their phthalamate-based macrocyclic terbium complexes ($[TbL^{9H}]^-$, $[TbL^{10H}]^-$, $[TbL^{11H}]^-$, $[TbL^{12H}]^-$, and $[TbL^{13H}]^-$) exhibited high quantum yields (Φ) and long lifetimes (τ) of the order of milliseconds at pH *ca.* 6. The values of Φ and τ were 46% and 2.4 ms respectively for $[TbL^{9H}]^-$, which was one of the top three terbium complexes benefiting from the macrocyclic architecture. Eu^{3+} complexes gave luminescence, but a rather weak antennae effect was observed. The results showing different number of chromophores appended on the macrocycle and the size of linkers have a significant effect on Φ.

The high efficiency of energy transfer could be quenched in the presence of particular metal ions (such as Cu^{2+}, Fe^{2+}, Co^{2+}, Ni^{2+} and Fe^{3+}) for these terbium complexes, $[Tb(L^{2})_2]^-$, $[TbL^{9H}]^-$ and $[TbL^{13H}]^-$. $[Tb(L^{2})_2]^-$ and $[TbL^{13H}]^-$ were responsive to Cu^{2+} and Fe^{3+}, while $[TbL^{9H}]^-$ was responsive to Cu^{2+} and Co^{2+}. Quenching rate constants (*kq*) of these complexes in the presence of quenchers showed that Cu^{2+} has the most significant quenching effect on the luminescence of $[Tb(L^{2})_2]^-$.

An NOR mode molecular logic gate system is devised on the basis of using these three terbium complexes, $[Tb(L^{2})_2]^-$, $[TbL^{9H}]^-$ and $[TbL^{13H}]^-$, in the presence of responsive metal ions. In $[Tb(L^{2})_2]^-$ and $[TbL^{13H}]^-$, their luminescence was switched

on in the absence of both Cu^{2+} and Fe^{3+}. This luminescence could be switched off when either Cu^{2+} or Fe^{3+} or both of them were present. The same logic could be applied in $[TbL^{9H}]^{-}$ where two inputs were Cu^{2+} and Co^{2+}.

Abbreviations

A	absorption
aq	aqueous
Ar	aromatic
approx	approximately
^{t}Bu	t-butyl
calc'd	calculated
conc	concentrated
cyclen	1,4,7,10-tetraazacyclododecane
DEPT	distortionless enhancement by polarization transfer
DMA	dimethylacetamide
DMF	dimethylformamide
DPA	dipicolinic acid
ESI	electrospray ionization
ET	energy transfer
Eu	Europium
F	fluorescence
HEPES	4-(2-hydroxyethyl)-1-piperazineethanesulfonic acid
HMBC	heteronuclear multiple bond correlation
HOMO	highest occupied molecular orbitals

HSQC	heteronuclear correlation through single quantum coherence
IMS	industrial methylated spirit
ISC	intersystem crossing
IUPAC	International Union of Pure and Applied Chemistry
J	coupling constant
k_q	quenching rate constant
L	ligand/luminescence
La	lanthanum
Ln	lanthanide
LUMO	lowest unoccupied molecular orbitals
MHz	megahertz
m.p.	melting point
NMR	nuclear magnetic resonance
P	phosphorescence
PET	photoinduced electron transfer
Phth	phthalimide
ppm	parts per million
q	number of bound water molecule
RT	room temperature
S/N	signal-to-noise ratio

S_0	ground state
S_1	singlet excited state
sat'd	saturated
T_1	triplet excited state
TLC	thin layer chromatography
TMS	tetramethylsilane
Tris	tris(hydroxymethyl)aminomethane
Ts	tosyl
TSP - d_4	deuterated 3-(trimethylsilyl)propionate-2,2,3,3- acid sodium salt
UV	ultraviolet
v	volume
w	weight
λ	wavelength
δ	chemical shift
Φ	quantum yield
τ	lifetime
$\bar{\upsilon}$	frequency

Acknowledgements

I am indebted to my supervisor, Professor Annie Bligh, for her guidance, encouragement and supervision to this project. My thanks also go to Dr Nick Chatterton for his support and comment throughout the duration of this work, and Dr Nick Wardle for his advice on the organic synthesis in this project.

I would not have been able to perform any of the experiments described without help and instruction from staff in the Institute for Health Research and Policy and the Science Centre at London Metropolitan University, especially Mr John Crowder for his suggestions on NMR studies, Mr Alan Bashall for the mass spectrometer and Mr Stephen Boyer for the elemental analyses. My appreciation is also extended to the technical staff, in particular Miss Pramila Haria, Mr Brian Whiting, Mr John Morgan, Mr Eric Coleman and Mr Phil Vidler.

This work was also made possible with help from Dr Ed Welbeck, Dr Olumuyiwa, Xinyu Li, Yifan Zhang, Miao Jin, Ali Saleh for their ideas, assistance and practical tips on using laboratory equipments in general. I am grateful to the School of Human Sciences, London Metropolitan University for the financial support.

Last but not least, I would like to say a big thank-you to my wife, Dr Xiaobei Pan and all the family members for their never ending support, which I could not have done without.

Declaration

The work presented in this thesis is the original work of the author, unless referenced to other sources. This thesis has been composed by the author and has not been submitted in whole or part for any other degree.

Gaoyun Chen

Date: 1st October 2012

Table of Contents

List of Figures

List of Tables

Ligand nomenclatures

Ligand	Structure	IUPAC name
L^1	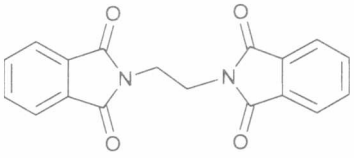	2,2'-(ethane-1,2-diyl)diisoindoline -1,3-dione
L^2	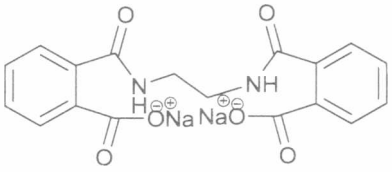	sodium 2,2'-(ethane-1,2-diylbis (azanediyl)) bis(oxomethylene)dibenzoate
L^3	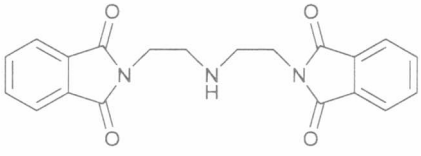	2,2'-(2,2'-azanediylbis(ethane-2,1 -diyl))diisoindoline-1,3-dione
L^4	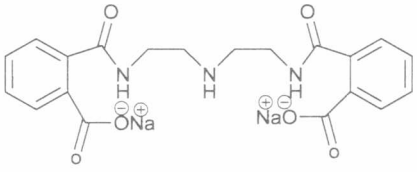	sodium 2,2'-(2,2'-azanediylbis(ethane -2,1-diyl)bis(azanediyl)) bis(oxomethylene)dibenzoate
L^5	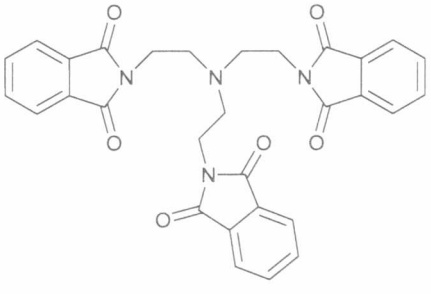	2,2',2''-(3,3',3''-nitrilotris (propane-3,1-diyl)) triisoindoline-1,3-dione

L^6 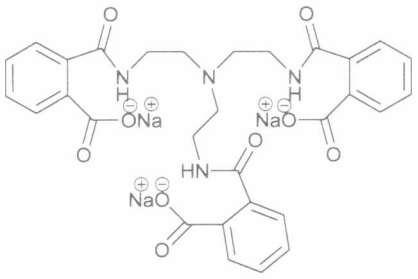

sodium 2,2',2''-(3,3',3''-nitrilotris (propane-3,1-diyl)tris(azanediyl)) tris(oxomethylene)tribenzoate

L^7 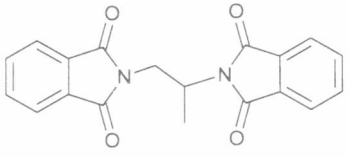

2,2'-(propane-1,2-diyl) diisoindoline-1,3-dione

L^8 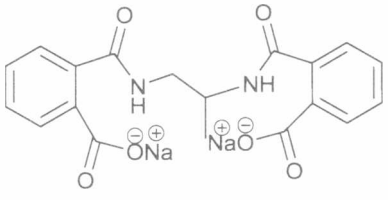

sodium 2,2'-(prorane-1,2-diyl bis(azanediyl)) bis(oxomethylene)dibenzoate

L^9 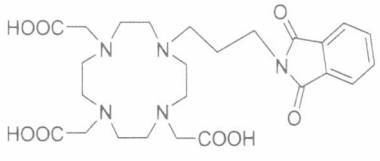

2,2',2''-(10-(3-(1,3-dioxoisoindolin-2-yl) propyl)-1,4,7,10-tetraazacyclododecane -1,4,7-triyl)triacetic acid

L^{9H} 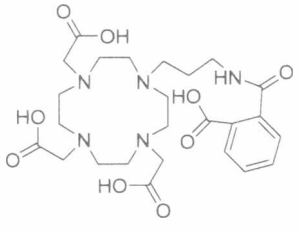

2,2',2''-(10-(3-(2-carboxybenzamido)propyl)-1,4,7,10-tetraazacyclododecane-1,4,7-triyl)triacetic acid

L^{10} 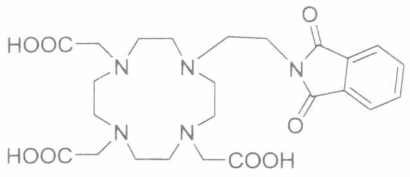

2,2',2''-(10-(2-(1,3-dioxoisoindolin-2-yl) ethyl)-1,4,7,10-tetraazacyclododecane -1,4,7-triyl)triacetic acid

L^{10H} 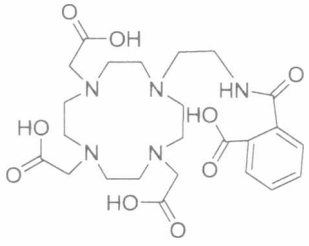

2,2',2'''-(10-(2-(2-carboxybenzamido) ethyl)-1,4,7,10-tetraazacyclododecane -1,4,7-triyl)triacetic acid

L^{11} 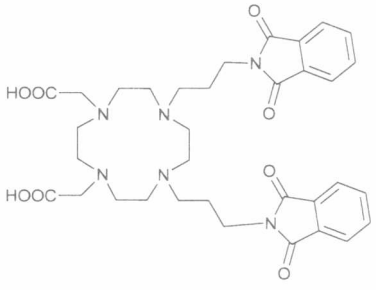

2,2'-(7,10-bis(3-(1,3-dioxoisoindol in-2-yl)propyl)-1,4,7,10- tetraazacyclododecane-1,4-diyl) diacetic acid

L^{11H} 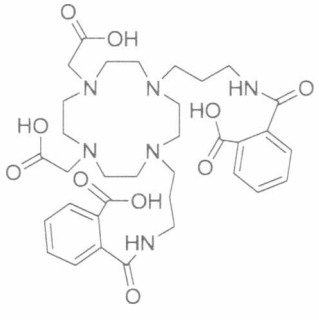

2,2'-(3,3'-(7,10-bis(carboxymethyl)-1 ,4,7,10-tetraazacyclododecane-1,4-diyl) bis(propane-3,1-diyl))bis(azanediyl) bis(oxomethylene)dibenzoic acid

L^{12} 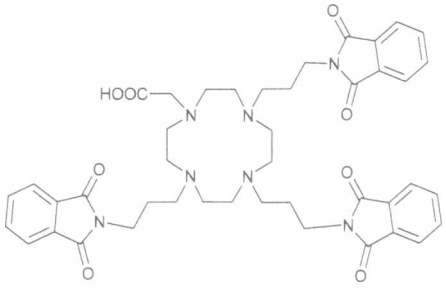

2-(4,7,10-tris(3-(1,3-dioxoisoindol in-2-yl)propyl)-1,4,7,10- tetraazacyclododecan-1-yl) acetic acid

L^{12H}

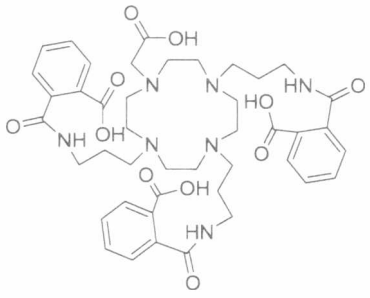

2,2',2''-(3,3',3''-(10-(carboxymethyl)-1,4,7,10-tetraazacyclododecane-1,4,7-triyl) tris(propane-3,1-diyl))tris(azanediyl) tris(oxomethylene)tribenzoic acid

L^{13}

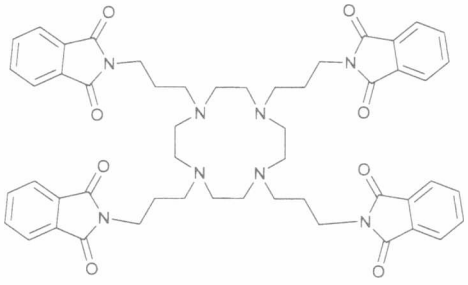

2,2',2'',2'''-(3,3',3'',3'''-(1,4,7,10-tetraazacyclododecane-1,4,7,10-tetrayl)tetrakis(propane-3,1-diyl)) tetraisoindoline-1,3-dione

L^{13H}

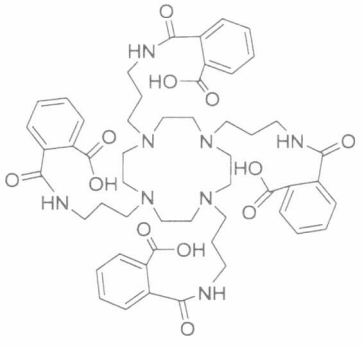

2,2',2'',2'''-(3,3',3'',3'''-(1,4,7,10-tetraazacyclododecane-1,4,7,10 -tetrayl)tetrakis(propane-3,1-diyl)) tetrakis(azanediyl)tetrakis(oxomethylene) tetrabenzoic acid

DO3A-t-butyl ester

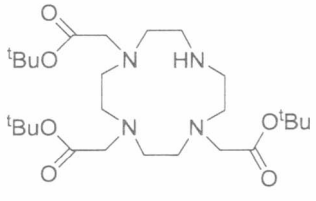

tert-butyl 2,2',2''-(1,4,7,10-tetraazacyclododecane-1,4,7-triyl) triacetate

DO2A-t-butyl ester

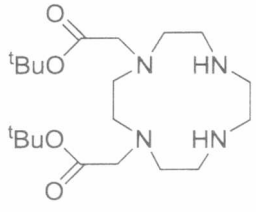

tert-butyl 2,2'-(1,4,7,10-tetraazacyclododecane-1,4-diyl) diacetate

DO1A-t-butyl ester

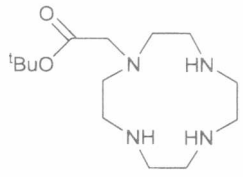

tert-butyl 2-(1,4,7,10-tetraazacyclododecan-1-yl) acetate

Chapter One Introduction

1.1 Molecular switches

In recent years, electronic devices have been developed from relatively large size and energy consumption to compact in size and less energy consumption.[1] A molecular switch is a molecular level device, and has electronic switching features.[2] The first concept of a molecular switch was introduced by *Wringhton et al* and it was one of the most investigated topics in the last 20 years.[3]

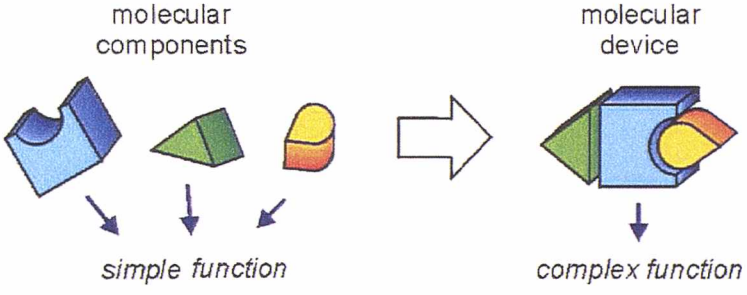

Figure 1.1 A molecular device with its molecular components[8]

The concept has been widely accepted since supramolecular chemistry was born in the late 1970s.[4-7] Molecular switches are composed of a number of small molecular components. Each component performs a simple function while an entire molecule performs a more complex function (Figure 1.1). It responds to one or more specific chemical species, in which the relative component is activated and resulting in an external output.[8, 9] In one word, molecular switches perform via electronic or energy rearrangement to give relative signals.[10, 11]

1.1.1 Principle of molecular switches

Molecular switches have been studied due to their extensive potential applications, such as chemical sensors, biological detectors and medical diagnostics.[12, 13] In general, the invention of molecular switches has the same principles on binary logics in computers. All the information is presented as numbers, '1' for presence and '0' for absence. When the functional molecule accepts the correct information from an input, it is switched on, as '1'. If the input information does not match the condition, then the molecule will not be activated and it shows '0', as off.[14]

The performance of a molecular switch can be divided into three parts: input, receptor and output.[15] Input is an external subject which is expected to activate the molecular switch. The receptor is responsive to designed input information. The receptor then converts the input information to a simply detectable output signal.[16]

1.1.2 Molecular switches and their logics

As it is introduced above, a molecular switch has its own logic. There are mainly two different types of molecular switches, single-input molecular switches and double-input molecular switches.[17] Three-input molecular switches are also designed, and they are developed on the combination of single-input and double-input molecular switches. Hence it has the same basic principles.

1.1.2.1 Single-input system

A single-input molecular switch is a system which can be activated only by one specific input, such as temperature, pH or some particular chemical species. All other un-related inputs lead to switch off, '0', This single-input system is illustrated in Table 1.1 by the principle on binary logic:[18]

Table 1.1 Logic table of a single-input molecular switch

Input	Output
0	0
1	1

1.1.2.2 Double-input system

A single-input system tests one thing at a time and this may not be useful enough and its potential application is limited in a more complex environment. So another type of molecular switch: double-input system is developed on the basis of single-input system. Herein two various inputs and one output signal are involved in the molecular switch. These two inputs are combined in one system and can be

detected at a time. The most widely used double-input molecular switch systems: OR, XOR, AND and INHIBIT,[17] are illustrated below:

Table 1.2 Logic table of OR system

Input 1	Input 2	Output
0	0	0
0	1	1
1	0	1
1	1	1

OR is a system (Table 1.2) which can be activated when either Input 1 or Input 2 or both of them are present.[19] An example of OR mode molecular switch (Figure 1.2, Compound **1**) here was invented by *Bharadwaj*.[20]

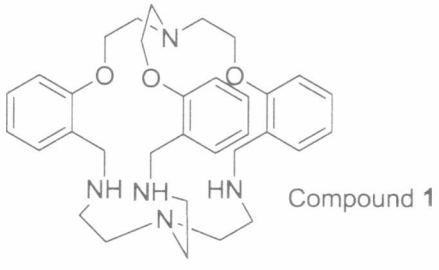

Figure 1.2 Structure of compound **1**

In a dry THF solution of compound **1** ($1x10^{-6}$ M), the quantum yield of this is enhanced from 0.1% to 12% when Zn^{2+} ($1x10^{-4}$ M) or Pb^{2+} ($1x10^{-4}$ M) or both are added.[20]

Table 1.3 Logic table of XOR system

Input 1	Input 2	Output
0	0	0
0	1	1
1	0	1
1	1	0

The first XOR system was reported from the laboratories of *Balzani* and *Stoddart*.[21] XOR is a system (Table 1.3) which can be activated when either Input 1 or Input 2 is present. The only difference between XOR and OR is that the molecule is switched off when both these two inputs occur in the XOR mode.

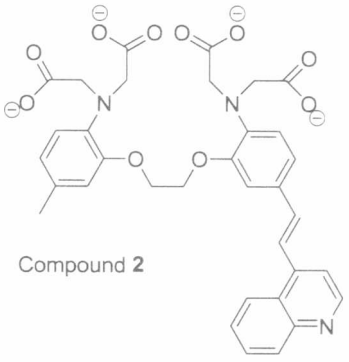

Figure 1.3 Structure of compound **2**

In Figure 1.3, compound **2** is sensitive to either the presence of H^+ or Ca^{2+}. The UV absorbance at $\lambda_{390\ nm}$ of the aqueous solution of compound **2** ($1x10^{-5}$ M) is enhanced by *ca.* 40% while H^+ ($1x10^{-5}$ M) or Ca^{2+} ($1x10^{-3}$ M) is present in the solution.[22, 23]

Table 1.4 Logic table of AND system

Input 1	Input 2	Output
0	0	0
0	1	0
1	0	0
1	1	1

AND is a system (Table 1.4) which can be activated only when both Input 1 and Input 2 are present.[24] *Baron* discovered a molecular switch which utilized glucose dehydrogenase and horseradish peroxidase.[25]

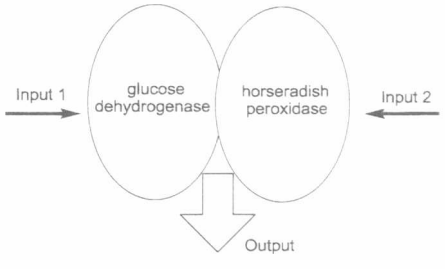

Figure 1.4 A molecular switch based on AND system

As shown in Figure 1.4, when both glucose (Input 1) and peroxide (Input 2) are present, they can be converted into gluconic acid and water. This results in an enhanced absorbance at $\lambda_{240\ nm}$, from 0.25 to 1.0 a.u.[25]

Table 1.5 Logic table of INHIBIT system

Input 1	Input 2	Output
0	0	0
0	1	0
1	0	1
1	1	0

The INHIBIT mode involves a combination of AND and OR, in which the system (Table 1.5) can be activated only with the presence of Input 1 while Input 2 is absent. The difference between INHIBIT and single-input system is that a single-input molecular switch can be activated in any environment which contains the particular input. However an INHIBIT system is switched on only when a specific input appears without the other input in the environment.[26]

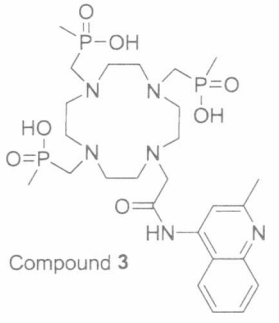

Compound **3**

Figure 1.5 Structure of compound **3**

The first INHIBIT mode molecular switch was reported by *Gunnlaugsson* (Figure 1.5, compound **3**). The luminescence of compound **3**-based lanthanide was observed only in an oxygen free acid solution.[27]

1.1.3 Design of a molecular switch

In order to design a widely acceptable molecular switch, the most attractive part is its output signal. As a molecular switch, its output signals can be light, heat, and motion. Nowadays, light is the most widely used output signal because of its straightforward convenient observation. Here is a widely applied molecular switch, benzylamine. It was invented by *Maroawetz* in 1976, and one of its applications is acting as a pH indicator by its fluorescence.[28-31] Benzylamine is sensitive to different pH, which shows rather weak fluorescence under basic condition whilst a

significant enhanced fluorescent emitting at $\lambda_{283\ nm}$ under acidic condition (Figure 1.6). So its well-detectable output signal is the bright emission in UV region.[32]

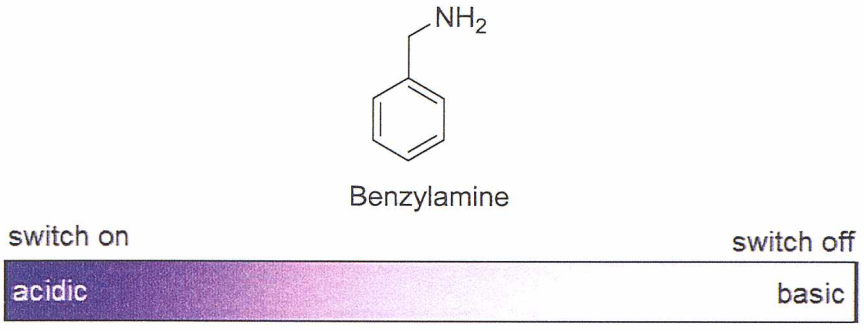

Figure 1.6 A pH dependent molecular switch of benzylamine

According to the principle on molecular logic, benzylamine is a single-input system. The level of the pH in a solution is converted into intense colour, which is based on two different states, "on" for emission and "off" for no emission.

Basically, benzylamine is an assembly of three components, receptor, fluorophore and spacer.[17, 33] According to the structure of benzylamine (Figure 1.7), amine is the receptor for pH, benzene is the fluorophore and methylene is the spacer which links the fluorophore and the receptor.

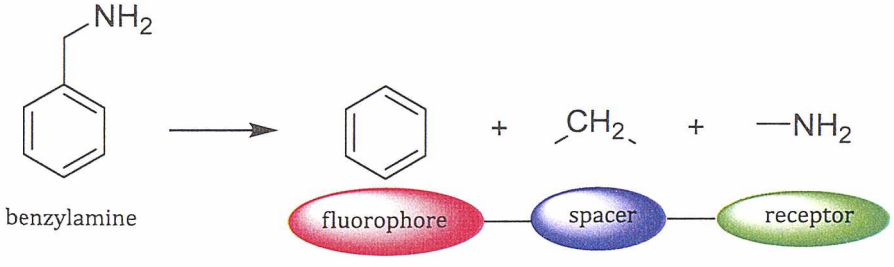

Figure 1.7 Components of benzylamine

In this case, benzene can emit UV fluorescence at $\lambda_{284\ nm}$ when this molecule is activated, in another word, fluorophore is the output signal. The amine function is sensitive to different input information, such as pH in this case. The spacer is methylene which links amine and benzene.[34] The input information is received by amine and then it is transferred to the benzene through methylene group, converting the input information into output signal in fluorescence.

1.1.4 Photoinduced electron transfer (PET)

The receptor is the most important part which governs the switching process and enables recognition of a particular input. So far photoinduced electron transfer (PET) is the most widely accepted theory to explain how a luminescent molecular switch works.[35] But this theory is suitable for a receptor containing amine functions.

Here the explanation of PET mechanism is still focused on benzylamine. Firstly, the molecule is activated under acidic conditions while it emits fluorescence. An incoming photon is absorbed by the benzene group, one electron in its ground state (highest occupied molecular orbital, HOMO) is promoted to the excited state (lowest unoccupied molecular orbital, LUMO), i.e., $\pi \rightarrow \pi^*$ of the benzene.[36] Then this excited electron in benzene group will decay from the LUMO to HOMO by emitting fluorescence. Meanwhile, the protonated amine function (ammonium cation) has lower HOMO level than that of benzene and its electrons always stay at HOMO level (Figure 1.8a) due to the inappropriate excitation wavelengh.[37] This process results in an emission of benzylamine, called switched on.

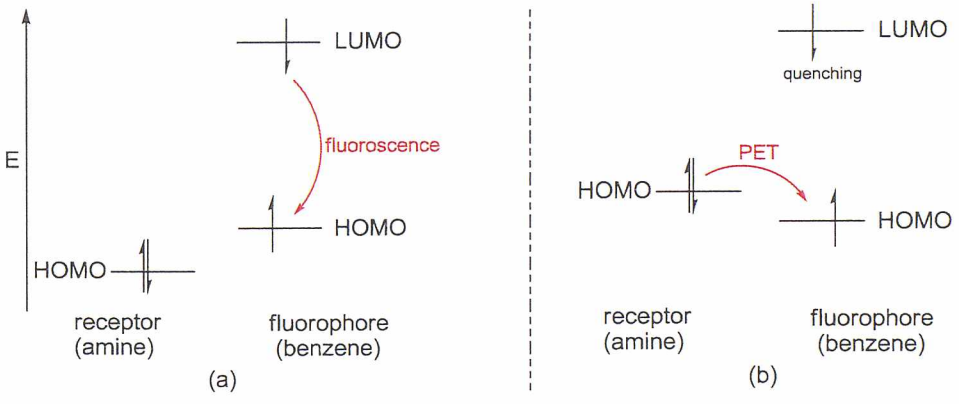

Figure 1.8 Frontier energy level diagram of (a) switched on status and (b) switched off status by PET

The molecular fluorescence is not observed under basic conditions, switched off. The amine function is unprotonated and its HOMO level is higher than that of benzene, causing PET.[38] The electron on HOMO of amine shifts to the HOMO level of benzene. Therefore, the HOMO level of benzene is filled and the energy is released through non-radiative process rather than fluorescence (Figure 1.8b).

Hence, as a responsive receptor, it must have a range of various HOMO levels when it is affected by external inputs, resulting in higher or lower energies than that of the fluorophore's HOMO levels.

1.1.5 Development of output signal

– from organic fluorescence to lanthanide luminescence

Visible molecular switches have recently attracted much attention due to their potential applications in optical research areas.[39] Today most successful systems in the chemical and biological fields contain organic fluorophores.[40] However, the applications are still limited due to the inherent properties of fluorophores, i.e., their short fluorescence lifetimes must compete with natural fluorophores in biological media. Therefore an advanced optical output signal has been developed, which is called lanthanide luminescence.

In the last decades, lanthanide luminescence-based molecular switches have being developed rapidly as part of optical sensing systems due to their long lifetimes and distinctive emission signals.[41] Many lanthanide-based molecular switches have been applied in luminescence assays for biology, chemistry and electroluminescence.[42]

1.2 Lanthanides

1.2.1 Introduction to the lanthanides

The discovery of the lanthanide elements started from the development of yttrium, which was first discovered by *Johann Gadolin* in Scandinavia in 1794. The next 15 rare earth elements were discovered between 1803 (cerium) and 1907 (lutetium) while the last one, artificial promethium was synthesized in 1947.[43]

Lanthanides are also known as f-block elements. The electronic configuration of lanthanide involves the progressive filling of the 4f electron shell. To form the ions, electrons are removed first from the outer 6s and 5d orbitals, so that their ionic

electron configurations from La^{3+} to Lu^{3+} are [Xe] $4f^n$ (n = 0 – 14).[44] The outer 5s and 5p orbitals are not shielded completely by the partially filled inner 4f orbitals.[45] With increasing atomic number, the nuclear charges are increased, giving rise to a more effective attraction between nuclei and the outer shell electrons, resulting in radii contraction.[46] Due to the lanthanide contraction, the atomic radius of lutetium (period 6) is about 5 pm smaller than that of yttrium (period 5).[47]

1.2.2 Coordination chemistry of lanthanide

All of the trivalent lanthanide ions share a number of common coordination properties, and exhibit little variability across the entire series. In general, all the lanthanide ions are classified as a type of hard acid by Pearson's rules.[48] Therefore, it is expected that these metal ions form more stable complexes with highly electronegative hard bases, in the order of O>N>S.[49, 50]

The 4f orbitals are inner orbitals and have little or no effect on participating in bonding. Therefore 4f orbitals do not play an important role in coordinating as the d- orbital elements. As a result of their independency from the influence of the ligands, crystal ligand effects are very small.[51] Because there is no directional interaction between a lanthanide cation and ligands, the coordination numbers and complex formations are determined almost by the ligands characteristics, such as donor groups, conformational properties and sizes.[52]

Coordination numbers between two to twelve are known in lanthanide complexes.[53] However, the most common coordination numbers are ranging from nine (La - Eu) to eight (Dy - Lu).[54, 55]

1.2.3 Luminescence properties of Tb^{3+} and Eu^{3+}

The luminescence properties of lanthanides have been studied by researchers for decades.[56] In general, most lanthanide ions are luminescent, but some are more

emissive than others. Tb^{3+} and Eu^{3+} are the most studied metal ions used in luminescent molecular switches.[43]

1.2.3.1 Spectroscopic features of Tb^{3+} and Eu^{3+}

An observation of luminescence is dominated by the energy gap (ΔE) between the lowest excited states and the ground states. This determines whether or not a lanthanide ion exhibits good luminescence emission. All the luminescence occurs from the excited states of the metal ions. From the energy distribution diagram below (Figure 1.9),[57] it appears that Eu^{3+} and Tb^{3+} are the only two ions in which the energy states are well separated.

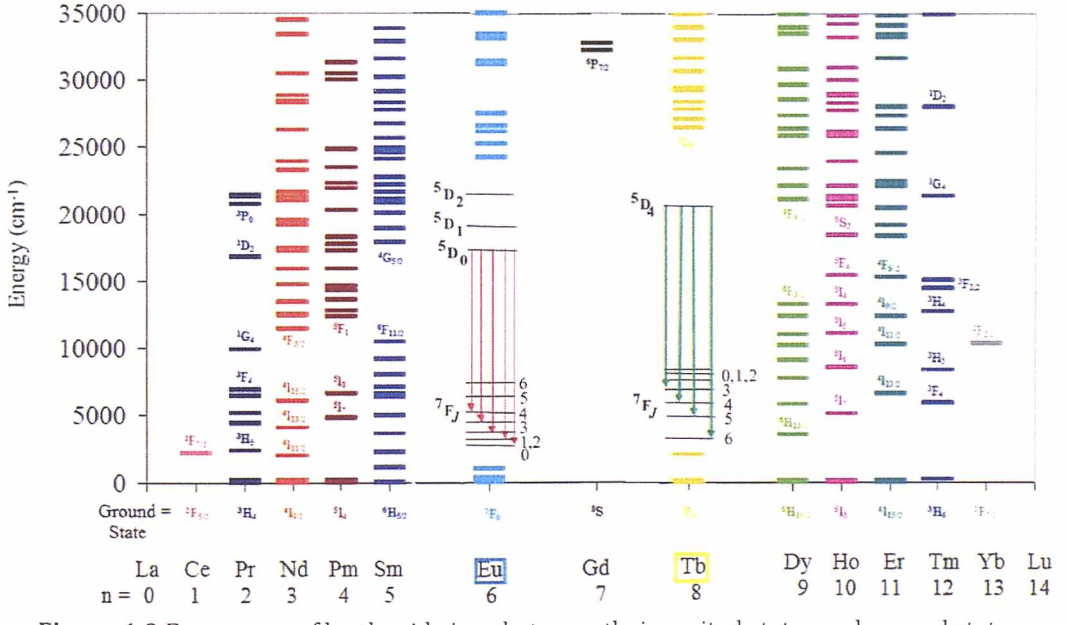

Figure 1.9 Energy gap of lanthanide ions between their excited states and ground states

The luminescence is observed more significantly while the energy decays from the lowest excited states to the ground states for lanthanide ions. The lowest excited states are $^5D_0$ (E = 17200 cm^{-1}) and $^5D_4$ (E = 20500 cm^{-1}) for Eu^{3+} and Tb^{3+} respectively.[58] These deactivations are $^5D_0 \rightarrow {}^7F_J$ (J = 0 – 4) and $^5D_4 \rightarrow {}^7F_J$ (J = 6 – 3) transitions for Eu^{3+} and Tb^{3+} respectively (Figure 1.9), while they exhibit red and green emissions.[59] A significant energy gap between excited states and ground states of Gd^{3+} is observed, but it emits in a broad wavelength regions which interferes with the emission spectra of organic compounds,[60] e.g., both Gd^{3+} and azadipyrromethene dyes emit at *ca.* $\lambda_{600\text{-}800\ nm}$.[61, 62]

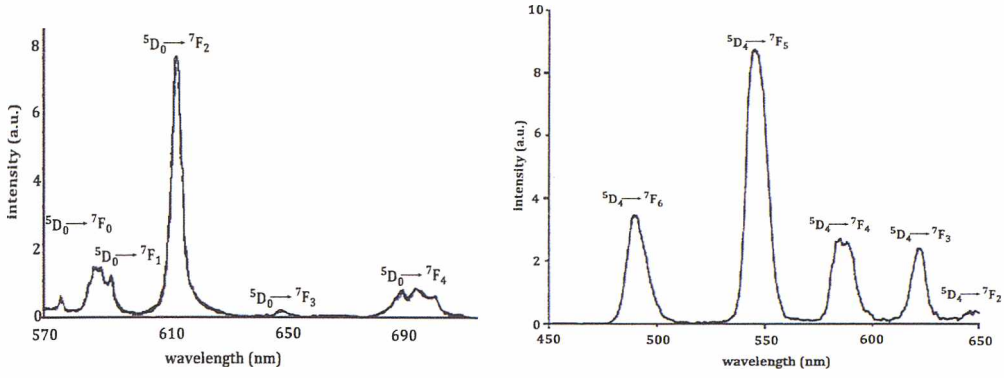

Figure 1.10 Luminescence transition for Eu^{3+} (left), and Tb^{3+} (right)

The most significant luminescent transitions for Eu^{3+} and Tb^{3+} are $^5D_0 \rightarrow {}^7F_2$ and $^5D_4 \rightarrow {}^7F_5$ respectively (Figure 1.10). Experimentally, the highest luminescence intensities of either lanthanide ions are observed at these transitions. In addition, both $^5D_0 \rightarrow {}^7F_2$ and $^5D_4 \rightarrow {}^7F_5$ are relatively the most sensitive transitions and potentially good probes for external environment changes.[63]

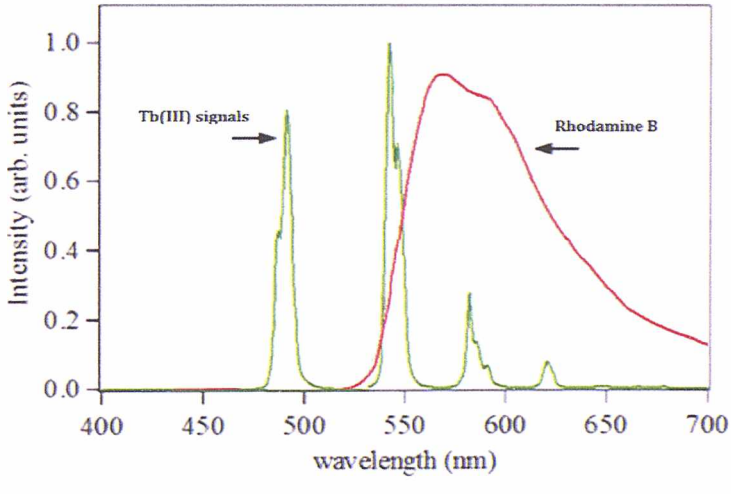

Figure 1.11 Luminescence emission spectra of Tb^{3+} and rhodamine B

Moreover, both Tb^{3+} and Eu^{3+} exhibit distinctive emission bands. Because the 4f electron shells of both Tb^{3+} and Eu^{3+} are well-shielded from their outer 5s and 5p shells, the trivalent ions are almost un-affected by the surrounding environment. This leads to narrow emission bands as defined signatures for Tb^{3+} or Eu^{3+}.[64] This advantage can be observed in the comparison of the luminescence emission spectrum of Tb^{3+} with that of an organic fluorophore (Figure 1.11). The luminescence emission of Tb^{3+} shows a much more distinctive signal than that of rhodamine B.

1.2.3.2 Lifetime

The luminescence lifetime (τ) of the excited state of a lanthanide ion is an important term to measure the deactivation process by radiative process. It is not a time defining how long the lanthanide ion exhibits in its excited state, but is rather the deactivation time needed for excited state population to reduce to 1/e of its initial population.[65]

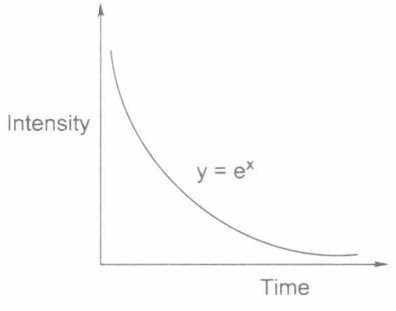

Figure 1.12 The relationship between luminescence intensity and delay time

In an experiment, the plot of luminescence intensity against delay time is an exponential function (Figure 1.12). However, the calculation of the lifetime depends on the decay rate of the luminescence. In other word, the lifetime can be calculated from the luminescence decay rate constant k_f. It is well defined as follows:[66]

$$\tau = 1/k_f \qquad \textbf{Equation 1}$$

where k_f is the decay rate of luminescence intensities *vs* delay time.

The luminescence lifetime of lanthanide ions can be as long as milliseconds, in contrast to that of organic fluorescence in nanoseconds.[67] The lifetime of Tb^{3+} can be observed as milliseconds, whilst the lifetime of rhodamine B is just *ca.* 1.72 nanoseconds. The lifetime of Tb^{3+} is about 100000 times longer than that of rhodamine B. The long lifetime of lanthanide ions is because it is transition forbidden.[68] According to *Laporte's Selection Rule*, $s \rightarrow p$ transition is allowed whilst $f \rightarrow f$ transition is forbidden. However despite being forbidden, this is in fact observed experimentally. Therefore both Tb^{3+} and Eu^{3+} have extraordinarily long luminescence lifetimes of milliseconds due to f-f transitions.[69]

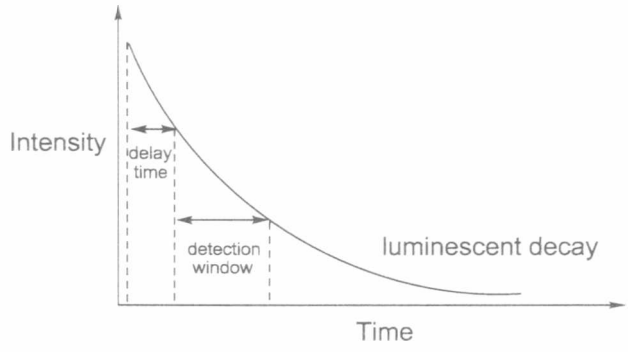

Figure 1.13 Time-resolved luminescence measurement

Because of the extremely long lifetimes of lanthanide ions luminescence in contrast to organic fluorophores, lanthanides have a high signal-to-noise ratio (S/N). The influence of short-lived background fluorescence and scattered light can be reduced to a negligible level by a method termed time-resolved luminescence measurement (Figure 1.13).[70] Experimentally, this is achieved using a light source to excite the sample with a delay time of the order of 10 – 100 nanoseconds. After a period of this time, all the background and scattered light will decay to zero whilst the lanthanide intensity remains at a high level.

1.2.3.3 Number of water molecules

The number of lanthanide ion bound water molecules was first measured by *Horrocks et al.*[71] The number was obtained by measuring the luminescence lifetimes of Tb^{3+} and Eu^{3+} in H_2O and D_2O respectively. The number of bound water molecules is also called the hydration state (q), mainly depending on the ligand design. This method was later reviewed by *Parker et al*, and the resultant equation is shown below (Equation 2):[72]

$$q = A_{Ln}(1/\tau H_2O - 1/\tau D_2O - \alpha_{Ln}) \quad \textbf{Equation 2}$$

where A_{Tb} is 5, A_{Eu} is 1.2; α_{Tb} is 0.06, α_{Eu} is 0.25.

1.2.3.4 Quantum yield

Quantum yield (Φ) is introduced here to give the probability of excited states decaying by luminescence rather than by non-radiative processes. Quantum yield

is basically a ratio of absorbed photons to emitted photons.[73] The most widely used method for calculating quantum yield was developed by *Williams et al.*, which involves the use of well characterised standard samples with known Φ value (Equation 3).[74]

$$\Phi_T = \Phi s \left(\frac{Grad_T}{Grad_S}\right)\left(\frac{\eta^2_T}{\eta^2_S}\right) \qquad \textbf{Equation 3}$$

where T and S are referred to the test and standard sample respectively. *Grad* is the gradient from the plot of integrated luminescence intensity *vs* absorbance, and η is the refractive index of solvents used.[75]

1.2.3.5 Vibrational quenching of lanthanide ions excited states in solutions

Excited states of lanthanide ions can decay through luminescence, or they can decay through non-radiative process, resulting from vibrational quenching by other molecules. Quenching of the excited states of lanthanide ions has been investigated for a long time.[76] It has been demonstrated that the vibrational quenching of lanthanide excited states is associated with the interaction of O-H oscillators as well as N-H, C-H and C-O oscillators.[77] The vibrational quenching occurs while the excited states of lanthanide ions are close to the different vibrational energy of solvent molecules.

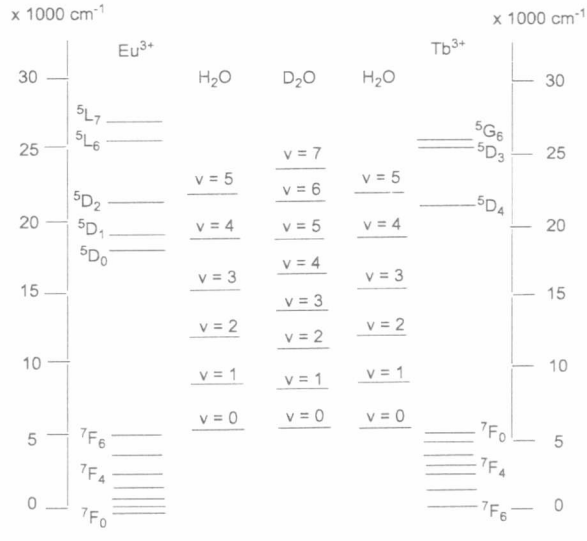

Figure 1.14 Energy levels of Tb^{3+}, Eu^{3+} and OH oscillators

The energy gap between the luminescence excited state and the ground state is approximately 12000 cm^{-1} for Eu^{3+} and 15000 cm^{-1} for Tb^{3+}.[77] The smaller the energy gap, the more easily its luminescence process can be quenched through non-radiative processes by high energy vibrations, such as O-H oscillators in solvent molecules.[78] The vibrational frequency of O-H is ~ 3300 – 3500 cm^{-1}.[79] Thus it might be expected that higher lying vibrational levels of O-H oscillators may be close in energy to the excited states of Eu^{3+} and Tb^{3+}. It is known that relatively efficient quenching of Eu^{3+} excited states occurs with the third vibrational level of proximate O-H oscillators (ν_{OH}), and with the fourth to Tb^{3+} excited states (Figure 1.14). The quenching is found to be inversely proportional to the energy gap between the two states of the metal ions. Therefore Tb^{3+} is less effectively quenched by O-H oscillators due to less Franck-Condon overlap.[80]

However, O-D oscillators have lower vibrational frequency, ~ 2200 – 2400 cm^{-1}, and any energy matching is only possible with even higher vibrational states. Consistent to the less quenching ability of Tb^{3+}, it has less Franck-Condon overlap. O-D oscillator is at least 200 times less effective at vibrational quenching than the corresponding O-H oscillators.[72]

1.2.3.6 Absorption features of Tb^{3+} and Eu^{3+}

Due to *Laporte's selection rules*, the forbidden f-f transition leads to very low absorption abilities of lanthanide ions. Their molar extinction coefficients are less than 4 M^{-1} cm^{-1}.[81] All free lanthanide ions absorb energy poorly unless excited by a very powerful light source, such as laser.[69]

Hence, in order to overcome this disadvantage, a lanthanide ion must be coordinated by an organic chromophore. Then a lanthanide ion can be excited indirectly through energy transfer. A coordinated organic chromophore transfers the energy to a lanthanide ion.[69] Hence lanthanides always occur as complexes.

1.2.4 Design of a luminescent lanthanide complex

To design a luminescent lanthanide complex, an organic chromophore must be coordinated with a lanthanide ion so the lanthanide ion can be sensitized by the organic chromophore. This organic chromophore functions as an 'antennae', absorbing incident light and then transferring this excitation to the lanthanide ion (Figure 1.15). This is also defined as the 'antennae effect'.

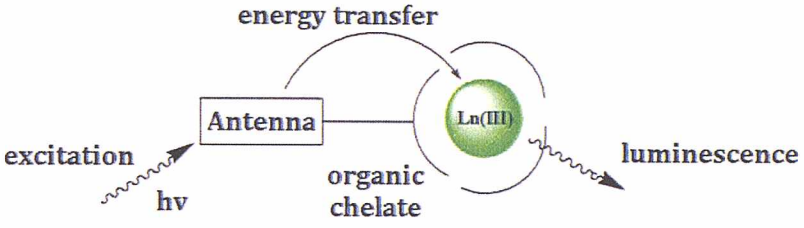

Figure 1.15 'Antennae effect' of a lanthanide complex

The commonly accepted energy transfer process from the antennae to the excited states of central Ln^{3+} (Figure. 1.16) is described by *Crosby* and *Whan*.[82] The electron in an antennae is promoted to its excited singlet state (S_1), and then it can either return to the ground state (S_0) by emitting fluorescence or via a non-radiative intersystem crossing (ISC) from the excited singlet state to the excited triplet state (T_1). At this time it may either return to the ground state (S_0) through phosphorescence or alternatively undergo energy transfer from its excited triplet state to an excited state of a Tb^{3+} or Eu^{3+}. After this energy transfer, the energy undergoes a luminescence emission to the ground state. However lanthanide luminescence could be quenched at this stage through a non-radiative vibrational energy transfer, especially the O-H oscillators in solvent molecules.[79, 83]

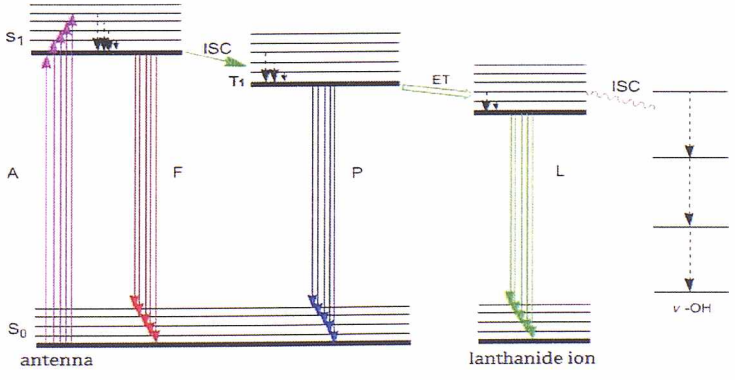

Figure 1.16 Energy transfer process from absorption to emission described by *Crosby* and *Whan*. (A: absorption; F: fluorescence; P: phosphoresce; L: luminescence; S_0: ground state; S_1: excited singlet state; T_1: excited triplet state; ISC: inter-system crossing; ET: energy transfer)

1.2.4.1 'Antennae effect'-based luminescent lanthanide complex

In order to obtain a luminescent lanthanide complex, the organic chromophore-containing ligand is designed for coordinating a lanthanide ion. Here is an example of a phthalamide derived ligand, which is designed to sensitise four different lanthanide ions, Tb^{3+}, Eu^{3+}, Dy^{3+} and Sm^{3+}.[84] All these complexes show bright luminescence with various colours in methanol (Figure 1.17).

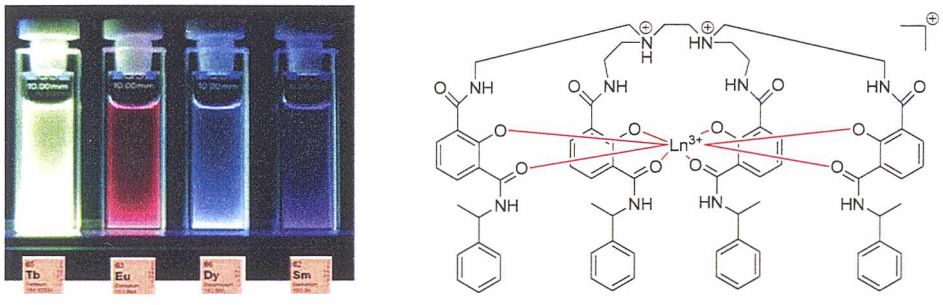

Figure 1.17 Luminescence of four different lanthanide complexes based on phthalamide[84]

The phthalamide functions are designed as 'antennae' in the complexes, they can absorb energy and transfer it onto the excited states of lanthanide ions through eight coordinate bonds.

Luminescence is observed on these four lanthanide complexes, but the Tb^{3+}-based complex shows the highest quantum yield of 64% and the longest lifetime of 1.3 ms. The quantum yields of other three complexes are less than 3%, and lifetimes of those are shorter than 0.9 ms.

1.2.4.2 Intersystem crossing (ISC)

An organic chromophore undergoes an energy transfer from its singlet excited states to its triplet excited states by ISC. To obtain an efficient energy transfer from the antennae to a lanthanide ion, this organic chromphore should be able to efficiently transfer its energy to triplet excited state first.

The probability of ISC is more favourable when the vibrational levels of the triplet excited state and the singlet state are very close. Nevertheless, it is known that a heavy atom (with an atomic number greater than that of the carbon atom e.g.,

those containing iodine or bromine[85]) can facilitate ISC when it is coordinated with an organic chromophore. [86]

1.2.4.3 Förster-Dexter theory

Förster-Dexter theory is used to describe a single non-radiative energy transfer that occurs between a donor (antennae) and an acceptor (lanthanide ion). Förster-Dexter theory is based on two different models: Förster and Dexter (Figure 1.18). The Förster model was first developed on the basis of electric dipole-dipole interactions, and was later extended by Dexter to include electron exchanges.[87, 88]

The Förster process is a non-radiative dipole-dipole interaction (Coulombic interaction), which is based on a resonance theory of energy transfer. In this process, a deactivation of the donor species generates an electric field, which stimulates the excitation of the receptor.[89]

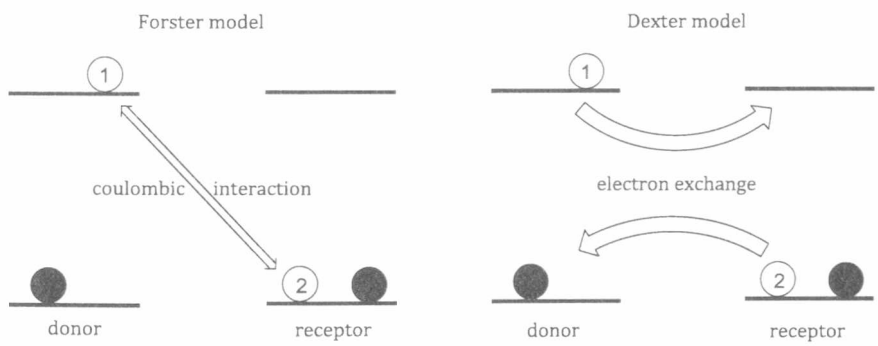

Figure 1.18 Förster-Dexter theory, Coulombic interaction by the Foster model and electron exchange by the Dexter model

In the Dexter process, a double electron transfer occurs between the donor and the acceptor. This is a very short range process since it requires the overlap of the orbitals of the two species.[89]

The main difference between these two processes is the distance over which these interactions can occur. The Förster process occurs efficiently over very long distances (~80 Å) whereas in the Dexter process the transfer happens over much shorter distances (<10 Å). In the Förster process, an overlap between the emission spectrum of the donor and the absorption spectrum of the acceptor is required. In

contrast, the Dexter process requires spatial overlap between the donor and acceptor orbitals.

Therefore, the Dexter process is less likely to occur for energy transfer in a lanthanide complex, as it would require availability of the 4f orbitals for bonding, which is not the case as they are inner orbitals.[90-92] Therefore the energy transfer between the triplet excited state of an antenna and the excited state of a lanthanide ion is more generally accepted to be a Förster dipole-dipole interaction process.

1.3 Responsive molecular switches-based on lanthanides

From the above descriptions, it becomes apparent that several requirements are necessary to design a highly responsive luminescent lanthanide complex:[69] (1) a coordinated antennae function should have a high molar extinction coefficient so as to harvest light efficiently; (2) a ligand should have high denticity to coordinate with the lanthanide ion tightly and shield bound water molecules; and (3) a receptor function should be responsive to one or more particular external inputs.

1.3.1 Description of a responsive lanthanide complex model

As a responsive lanthanide complex, the lanthanide ion must be coordinated with one or more ligands. Because of the low extinction coefficient of lanthanide ions and the responsive requirements of the complex,[93] a ligand must contain three parts to achieve a desired responsive molecular switch: chelating function, antennae and receptor (Figure 1.19).[94] The antennae is usually an organic chromophore which can absorb energy in the UV or visible region, and then transfers the energy to the excited state of the coordinated lanthanide ion. The receptor is a functional part which can react with particular external inputs so that it can affect the luminescence features of the complex. The chelating function is very much clearly to coordinate the central lanthanide ion. This model can be illustrated for a range of responsive lanthanide complexes.

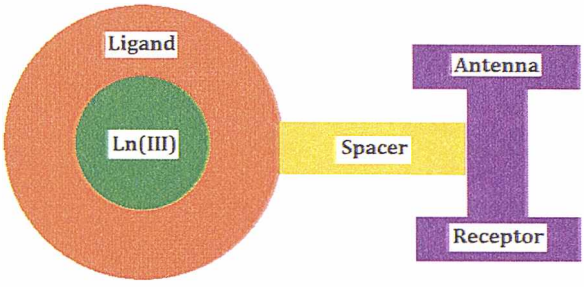

Figure 1.19 A responsive lanthanide complex model

Upon the recognition of one or more particular external inputs, the sensitisation properties of the antennae could be modulated, such as the excited state's energy, or a structural change, hence affecting the energy transfer process. Consequently, the effect on antennae will be reflected in the luminescence properties of its coordinated lanthanide ion, such as luminescence intensity, lifetime and quantum yield. On the other hand, recognition could also occur directly on the lanthanide ion, leading to an increase/decrease of luminescence with bound solvent molecules, such as water.

Nowadays, the most widely designed molecular switches are used for chemical sensors. Below are given some examples of lanthanide complexes which have potential applications as pH sensors and cation/anion detectors.

1.3.2 Examples of lanthanide complexes as pH sensors

A terbium complex of compound **4** (Figure 1.20) is a pH dependent molecular switch, in which the luminescence of $[Tb(\mathbf{4})]^{+}$ is modulated by PET from (X) to (terpyridyl).[95] Amine derived functional groups (X) are the receptor of the ligand and its benzene functions are the antenna. In its unprotonated form, the amines quench the excited states of benzene functions via a PET mechanism. Because of this quenching, the luminescence of the lanthanide ion is reduced significantly. Under acidic conditions, PET is removed and the complex emits a bright colour. The quantum yields of this Tb^{3+} complex at different pH are shown in Figure 1.21.[96]

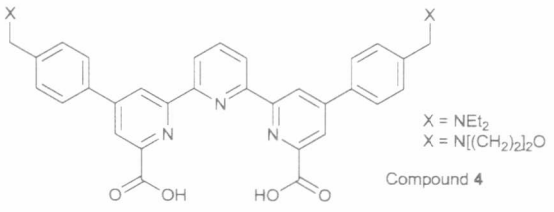

Figure 1.20 Structure of compound **4**

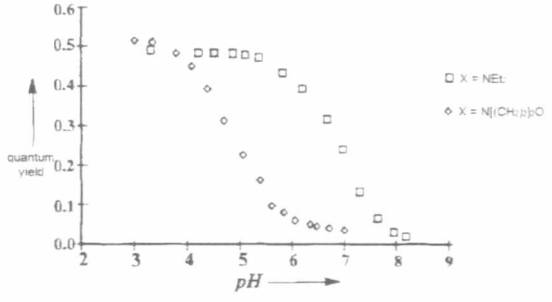

Figure 1.21 Quantum yield against pH of $[Tb(\mathbf{4})]^{+}$[96]

The wavelength of the maximal absorption of $[Tb(\mathbf{4})]^{+}$ is at $\lambda_{285\ nm}$, and gives emission bands mainly at $\lambda_{544\ nm}$. It is obvious that $[Tb(\mathbf{4})]^{+}$ gives distinguishable quantum yields at pH 3 and 8, 49% and 3% when X = NEt_2 and 51% and 5% when X = $N[(CH_2)_2]_2O$, respectively.[96]

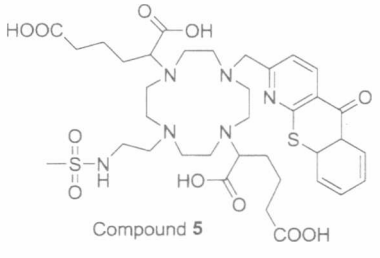

Figure 1.22 Structure of compound **5**[97]

A macrocyclic ligand (compound **5**, Figure 1.22)-based Eu^{3+} complex has been reported and two emission bands appeared at $\lambda_{627\ nm}$ and $\lambda_{680\ nm}$ as the pH is raised from 5 to 8.[97] The plot of the emission intensity ratio of $\lambda_{680\ nm}/\lambda_{587\ nm}$ versus pH is shown in Figure 1.23. A Number of water molecules of zero is obtained over the entire pH range, with a higher emission intensity ratio at pH 8 (1.2) than at pH 4.5 (0.1).[98]

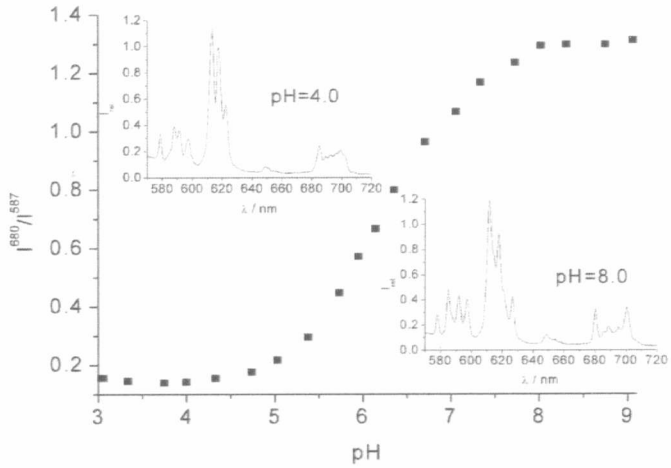

Figure 1.23 pH titration of Eu^{3+} complex-based on compound **5**[98]

The emission spectrum of [Eu(**5**)]$^-$ is sensitive to the coordination provided by the ligand.[58] Under acidic conditions, the protonated sulphonamide nitrogen atom is not coordinating the Eu^{3+} ion. Under basic conditions, the Eu^{3+} ion is coordinated with sulphonamide. This is most apparent in changes in the form of luminescence intensity of $\lambda_{680\ nm}/\lambda_{587\ nm}$ (Figure 1.23).[99, 100]

1.3.3 Examples of lanthanide complex as cation or anion detectors

A Tb^{3+} complex based on compound **6** (Figure 1.24) is derived from polyhydroxy dicarboxylic acid, and it has been demonstrated to be an anion detector in aqueous solution.[64] The complex is responsive to F^-, Cl^-, Br^-, I^-, CN^-, NO_3^-, NO_2^-, SO_4^{2-}, CO_3^{2-} and PO_4^{3-}. These anions interact with Tb^{3+} and enhance the luminescence intensity of the $^5D_4 \rightarrow {}^7F_5$ transition, especially for the carbonate anion.

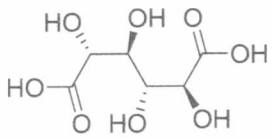

Compound **6**

Figure 1.24 Structure of compound **6**

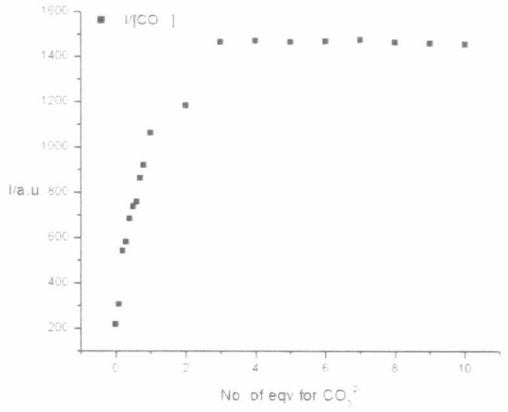

Figure 1.25 Luminescence intensity of $[Tb(\mathbf{6})_2]^-$ against mol equivalent of carbonate anions

With an increase of ~3 mol equivalents of carbonate anions in a $[Tb(\mathbf{6})_2]^-$ solution, the luminescence intensity at $\lambda_{544\,nm}$ is enhanced significantly and maintained at this high luminescence level with addition of further carbonate anions (Figure 1.25). The enhancement at luminescence is believed to be due to the effect of the numerous OH groups in the acid, which interact strongly with the anions through hydrogen bonding.[101]

An Eu^{3+} complex has been demonstrated the use for application in sensing of metal cations using displacement assays.[102] The formation of a ternary complex between a cyclen-based (compound **7**, Figure 1.26) Eu^{3+} complex and the water soluble antennae 4,7-diphenyl-1,10-phenanthroline-disulfonate (BPS), gives rise to the formation of Eu-BPS, a red emitting complex. BPS is being a known ligand for the selective sensing of Fe^{2+},[103] therefore the Eu^{3+} emission of Eu-BPS can be modulated through the displacement of the BPS antennae in the presence of Fe^{2+} (Figure 1.27).[102]

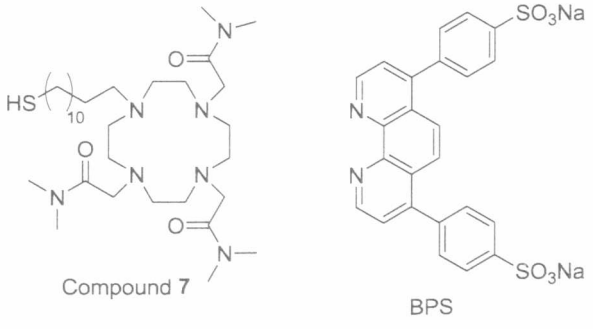

Figure 1.26 Structures of compound **7** and BPS

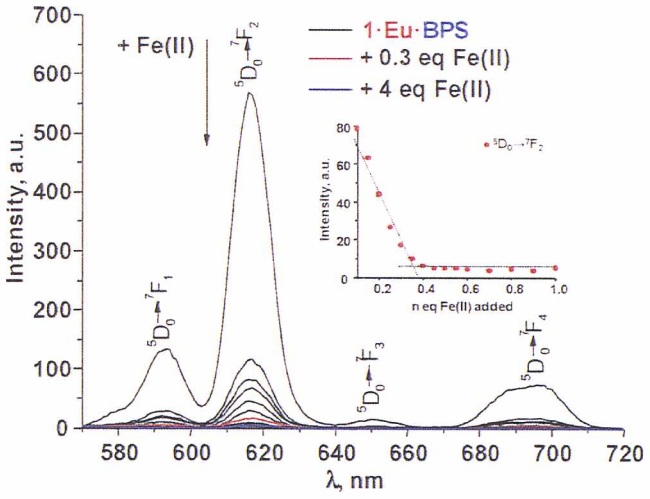

Figure 1.27 luminescence intensity changes of $[Eu(7)]^{3+}$ with addition of Fe^{2+}

The changes in the Eu^{3+} emission in HEPES buffer solution at pH 7.4 in the presence of Fe^{2+} (~4 equiv.) are shown above (Figure 1.27). The emission intensity decreased significantly at 0.33 equivalent of Fe^{2+}. The quenching is observed not only in Eu^{3+} emission, but also in the fluorescence of BPS when Fe^{2+} is added. This confirmed that the displacement of the antennae from the ternary complex and thus the formation of $Fe(BPS)_3$ in solution, quenching the luminescence of Eu^{3+}.[104]

1.3.4 Phthalimide derivatives in luminescent molecular switches

Kanaoka and co-workers have demonstrated that phthalimides undergo a number of interesting photochemical reactions.[105] Like their aromatic ketone functions, the excited state of phthalimide participates in photocyclization. The *N*-alkyl phthalimide leads to preferential γ-hydrogen atom abstraction as part of *N*-heterocyclic ring-forming reactions (Scheme 1) with long time exposure to a powerful light source.[106]

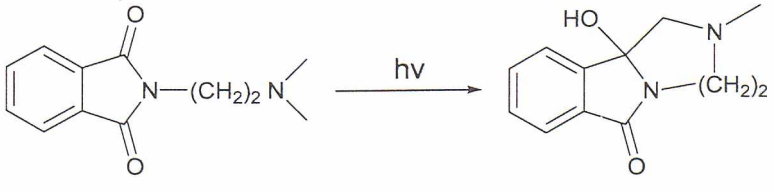

Scheme 1 N-heterocyclic ring-forming reactions

1.3.4.1 Photophysical properties of phthalimide and its derivatives

Besides the sensitive photochemical reactions of phthalimide, one of the most attractive aspects of these compounds is their roles as organic chromophores. The most likely accepted levels to sensitize Eu^{3+} and Tb^{3+} through energy transfer are 17,200 cm^{-1} ($\lambda_{580\ nm}$) and 20,400 cm^{-1} ($\lambda_{290\ nm}$) respectively, so the triplet excited state level of the antennae should be above 22,000 cm^{-1} ($\lambda_{460\ nm}$) in theory.[63] The lowest triplet excited state of phthalimide is at *ca.* 22,222 cm^{-1} ($\lambda_{450\ nm}$).[107] Hence the phthalimide function presumably is a suitable antennae for both Eu^{3+} and Tb^{3+}in terms of the energy transfer process.

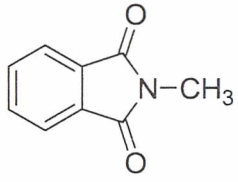

Figure 1.28 Structure of *N*-methyl phthalimide

A phthalimide-based organic chromophore, *N*-methyl phthalimide (Figure 1.28), exhibits fluorescence with remarkably low quantum yields of 0.01 or even less in solution at rt. For *N*-methyl phthalimide in acetonitrile (with excitation wavelength at $\lambda_{390\ nm}$), its fluorescence quantum yield is 0.08% and lifetime is only 0.19 ns.[108] However the triplet state lifetime in the same solvent is in the range of 2–10 μs at RT in the absence of oxygen.[109] Because the ISC quantum yield of phthalimide can reach 80%, it can be concluded that the phosphorescence dominates the decay pathway,[109] and that the phosphorescence decay process is more favourable for energy transfer from the antennae to lanthanide ions (*cf.* Section 1.2.4.2).

1.3.4.2 Conformation changes of phthalimide to phthalamate

Phthalimide has been proved to be a good pH dependent receptor, its imide function can be hydrolysed at pH 9 – 10 to generate phthalamate.[110] The UV spectrum of the hydrolysis process is shown in Figure 1.29. The maximal absorption wavelength of phthalamate ($\lambda_{272\ nm}$) differs from that of phthalimide ($\lambda_{300\ nm}$). Therefore it is believed that as an antenna, the conformational change of phthalimide may have the potential effects on the coordination between

lanthanide ion and ligand, resulting in different energy transfer efficiency. Hence the conformation change may lead to a potential establishment of a phthalimide-based lanthanide complex for pH sensors.[110, 111]

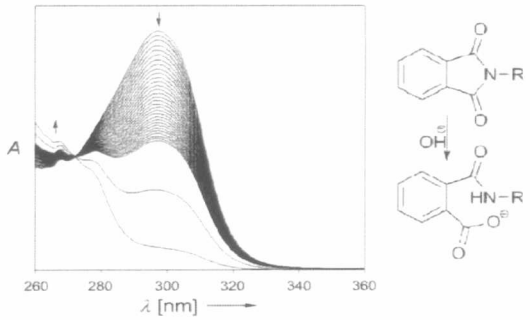

Figure 1.29 UV spectrum of phthalimide converts to phthalamate by NaOH[112], the absorbance at *ca.* $\lambda_{300\ nm}$ is replaced by the absorbance at *ca.* $\lambda_{270\ nm}$

1.3.4.3 Analogues of phthalimide in luminescent molecular switches

According to the largest reported literatures of luminescent molecular switches, none of highly luminescent lanthanide complexes were designed on the basis of phthalimide as an antenna.[43, 69, 78, 113] However, some were designed on the basis of phthalimide analogues, such as phthalamide.[114] A series of phthalamide-based (Compound **8**, **9** and **10**) Eu^{3+} complexes were reported, of which the luminescence intensities were significantly responsive to pH (Figure 1.30).

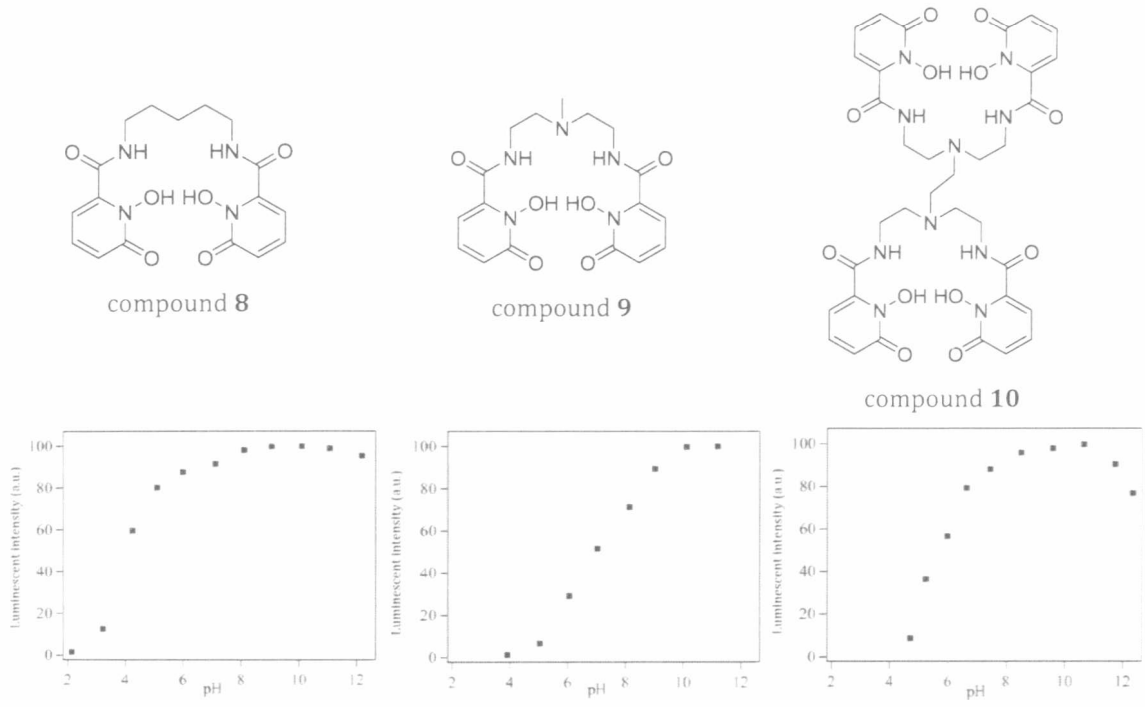

Figure 1.30 A series of hydroxypyridine-based (compound **8**, **9** and **10**) Eu^{3+} complexes and their modulation of luminescence intensities against pH

Under acidic conditions, these ligands were all protonated, resulting in no energy transfer and luminescence quenching. Under basic conditions, complexations occurred and the luminescence intensities were enhanced significantly. The lifetimes of all three Eu^{3+} complexes in 0.1M Tris buffer aqueous solution (pH *ca.* 7.5) were in the range of 0.5 – 0.7 ms and quantum yields were between 4% – 20%.[115, 116]

1.4 Aims and objectives

One of the primary objectives of this work was the investigation of luminescence properties of phthalimide/phthalamate-based lanthanide complexes and their potential applications as molecular switches. These required the development of both methodology studies for preparing phthalimide/phthalamate-based ligands and luminescence properties investigations of their lanthanide complexes under different conditions, such as pH.

With this goal in mind, the preparation methods of phthalimide/phthalamate-based ligands were first studied. A series of cyclic phthalimide/phthalamate-based

ligands and macrocyclic phthalimide-based ligands were prepared. Extensive work involving photophysical properties and coordination characteristics were carried out to understand the subsequent complexation reactions. Once this was established, the work was extended to luminescence studies of lanthanide complexes based on these ligands. The metal-to-ligand ratio was first established, followed by the luminescence measurements at various pH. Lifetimes and quantum yields were measured and the potential applications in metal ion detectors of these terbium and europium complexes were investigated.

Chapter Two Synthesis and characterization of acyclic phthalimide and phthalamate derivatives

2.1 Introduction

Phthalimides belong to a class of attractive compounds in photochemistry, but they are not good chelating agents for binding metal ions due to their planar geometric structures. The coordination chemistry of $TiCl_4$ and phthalimide shows that nitrogen is not participating in coordination.[117] Since the two carbonyl groups of a phthalimide have a fixed planar orientation, coordinating to the same metal ion is precluded. So there are two possible coordination modes available to phthalimide: first, as a bidentate ligand where the two C=O groups coordinate to two metal ions, and second, as a monodentate ligand, resulting in the formation of a 1:2 metal-to-ligand adduct.[118]

With the amide function acting as bidentate in phthalimide, the Ti^{4+} centre has a coordination number of six, and a metal-halide-metal bridging structure is observed (Figure 2.1a). When the amide function acts as a monodentate ligand, however, a 1:2 metal-to-ligand adduct results, where only one C=O group per phthalimide coordinates to the central metal ion giving it an octahedral configuration (Figure 2.1b).

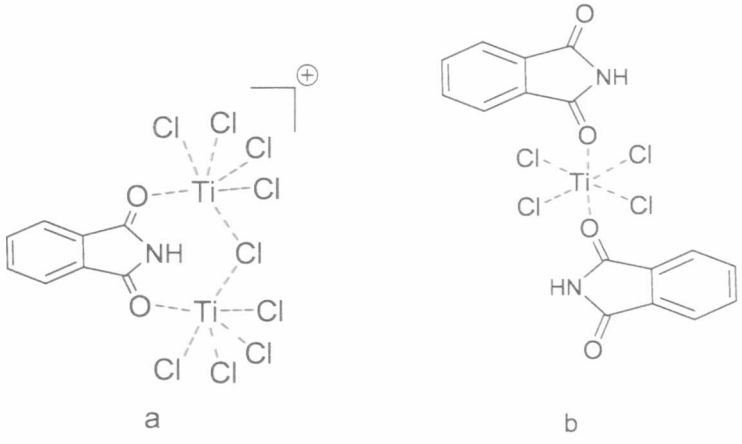

Figure 2.1 Coordination structure of (a) phthalimide as a bidentate ligand or (b) a monodentate ligand in a titanium complex

Therefore in order to increase the chelating effect of a ligand, more than one phthalimide function is required.

However, a class of hydrolysed phthalimide compound (phthalamate) is more widely applicable. It exhibits a structure similar to dipicolinic acid (DPA) (Figure 2.2). As an excellent antennae and chelating agent, DPA exhibits efficient energy transfer to lanthanide ions and luminescence in its complexes.[119] So it is believed that phthalamates may have potential coordination and antennae abilities for lanthanide ions.

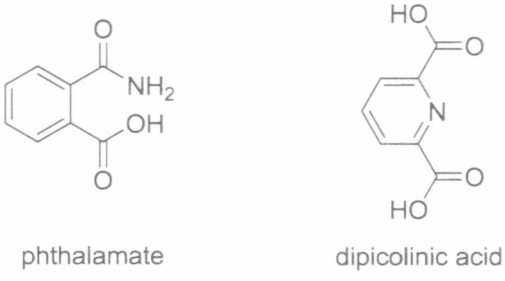

Figure 2.2 Phthalamate and dipicolinic acid

Synthetic routes to phthalimides and phthalamates are derived from phthalic anhydride (Scheme 2).[120]

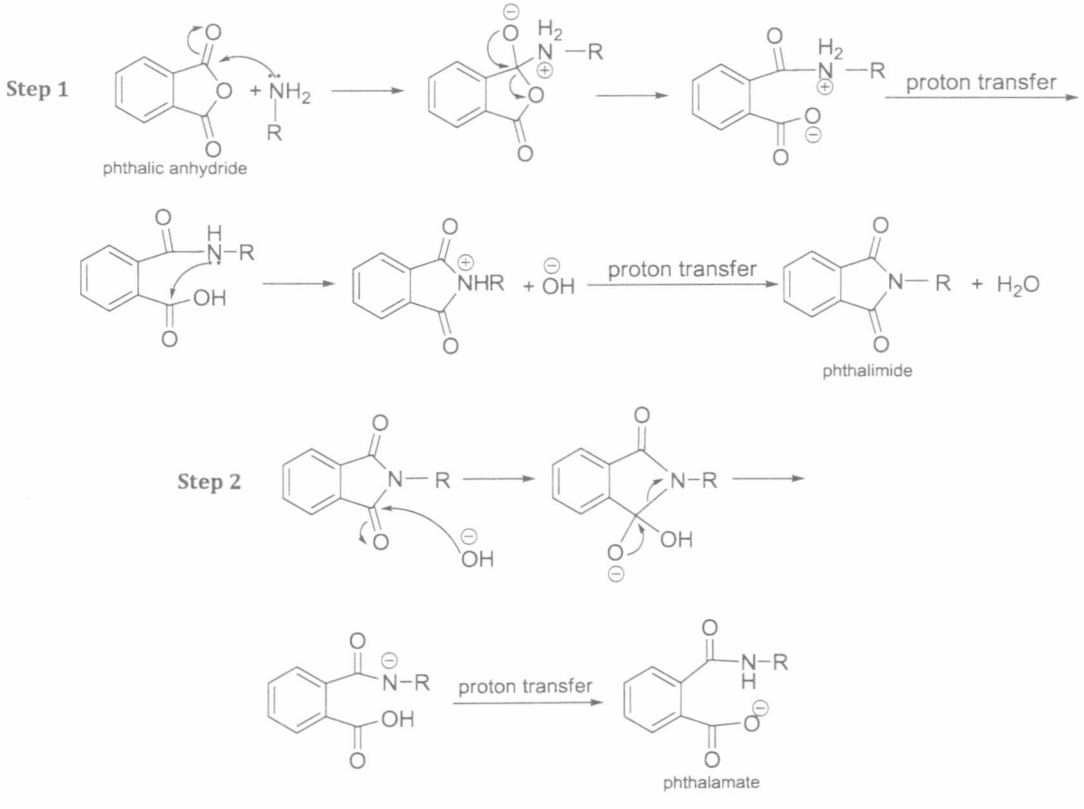

Scheme 2 Synthetic routes to phthalimide (step 1) and phthalamate (step 2)

Phthalamate itself is a multidentate ligand. It contributes one carboxylate function as a hard Lewis base and one amide function for coordinating a lanthanide ion.

Therefore the work in this Chapter was aimed at investigating the possibility of synthesising phthalamate-based polydentate acyclic ligands. It was proposed that one lanthanide ion might coordinate to two or three phthalamate functions of a suitable ligand. It was expected that an increase in energy absorption could be transferred onto the lanthanide ion according to the number of phthalamate functions coordinated. So the design of molecules containing two or three phthalamate functions was studied.

2.2 Experimental

2.2.1 General materials

All reagents and starting materials were used as purchased from commercial sources and used without further purification, unless otherwise noted. Phthalic anhydride, 1,2- diaminoethane, bis(2-aminoethyl)amine, tris(2-aminoethyl)amine and 1,2- diaminopropane were purchased from the Sigma-Aldrich Company Ltd, UK. Absolute ethanols and *glacial* acetic acid were purchased from Fisher Scientific Ltd, UK.

2.2.2 General instruments

NMR spectra were recorded on a Bruker Avance - 500MHz (^{1}H, 500.1 MHz; ^{13}C, 125.8 MHz, Bruker Corporation, UK) NMR spectrometer. Both ^{1}H and ^{13}C NMR spectra were recorded in $CDCl_3$ with tetramethylsilane as the internal reference, or in D_2O with 3-(trimethylsiyl)propionic-2,2,3,3-d_4 acid sodium salt as internal reference. Resonances (δ) are expressed in ppm and J values are given in Hz.

Mass Spectra (HR-ES-MS) were measured by a Waters Q-Tof microTM mass spectrometer (Waters Corporation, UK)

IR spectra (KBr disc) were recorded on a Nicolet 100 FT-IR spectrophotometer (Thermo Scientific, UK).

Melting points were obtained on an Electrothermal digital melting point apparatus, and were uncorrected.

A Flash 2000 Elemental Analyser was used for C, H and N microanalysis (Thermo Scientific, UK).

2.2.3 Synthesis and characterization of L^1 and L^2

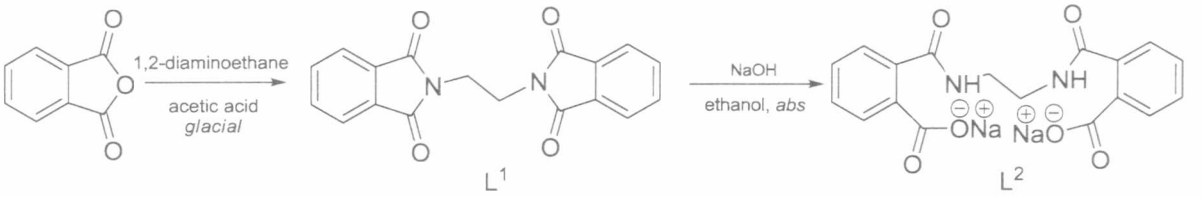

Scheme 3 Synthetic route to L^1 and L^2

A round-bottomed flask was charged with a *glacial* acetic acid solution (150 cm^3) of phthalic anhydride (2.96 g, 19.99 mmol), which was vigorously stirred at RT. Then 1,2-diaminoethane (0.61 g, 10.15 mmol) was added dropwise into the mixture and heated under reflux for 4 h. Thereafter, the solution was cooled and an equal volume of deionised water (150 cm^3) was added. The mixture was left standing overnight at RT to yield a white precipitate. This was isolated on a Büchner apparatus and washed with cold 99IMS (10 cm^3) to give a creamy white solid (L^1, 2.38 g, 74%). m.p. 148-152°C; ES: 321.05 ([M+H]$^+$); Found: C, 64.57; H, 3.66; N, 8.44. Calc'd for $C_{18}H_{12}N_2O_4.0.67H_2O$: C, 65. 06; H, 3.61; N, 8.42; $\delta_H(CDCl_3)$: 4.01 [4H, s, 2xCH_2 (linker)], 7.70 [4H, dd, Ar*H* (Phth)], 7.79 [4H, dd, Ar*H* (Phth)]; $\delta_C(CDCl_3)$: 36.83 [CH_2(linker)], 123.37, 131.90, 134.02 [Ar*C* (Phth)], 168.24 [*C*=O].

A round-bottomed flask was charged with an absolute ethanol suspension (100 cm^3) of L^1 (321.5 mg, ~0.97 mmol). The suspension was heated until the reactant was dissolved completely. An aqueous solution (10 cm^3) of sodium hydroxide (82.1 mg, 2.05 mmol) was added to the flask, maintaining the solution at pH ~9 – 10. The reaction mixture was then heated under reflux for 1 h. Thereafter, the solution was cooled and left standing in the fridge to form a crystallized product. After 24 h, needle-like crystals were obtained. These were isolated by Büchner filtration and washed with cold 99 IMS (5 cm^3). The filtrate was collected and the solvent was reduced to ~20% to obtain more precipitated products, which were

isolated by filtration, washed, and amalgamated with the first crop (L^2, 0.24 g, 60%). m.p. 226-228°C (decomposed); ES: 376.71 ([M-Na]$^-$); Found: C, 48.81; H, 4.03; N, 6.85. Calc'd for $C_{18}H_{14}N_2O_6Na_2.2H_2O$: C, 49.53; H, 4.16; N, 6.42; $\delta_H(D_2O)$: 3.60 [4H, s, 2xCH_2 (linker)], 7.45-7.49 [4H, m, Ar*H* (Phth)], 7.52 [2H, ddd, Ar*H* (Phth)], 7.61 [2H, d, Ar*H* (Phth)]; $\delta_C(D_2O)$: 41.98 [*C*H$_2$ (linker)], 129.91, 130.82, 132.26, 133.12, 137.27, 140.36 [Ar*C* (Phth)], 176.01, 178.79 [*C*=O].

2.2.4 Synthesis and characterization of L^3 and L^4

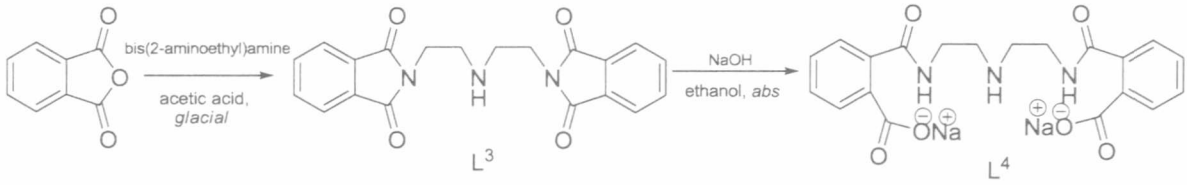

Scheme 4 synthetic route to L^3 and L^4

A round-bottomed flask was charged with a *glacial* acetic acid solution (150 cm^3) of phthalic anhydride (5.01 g, 33.83 mmol), which was vigorously stirred at RT. Then bis(2-aminoethyl)amine (1.73 g, 16.77 mmol) was added dropwise into the mixture and heated under reflux for 5 h. Thereafter, the solution was cooled and evaporated *in vacuo* to give a yellow oil. The crude product was precipitated from a solution of this oil in 99IMS (5 cm^3). This was isolated on a Büchner apparatus and washed with cold 99IMS (3×10 cm^3) and dried in the air for 30 min to give a creamy white solid product (L^3, 5.14 g, 84%). m.p. 160-163°C; ES: 364.11 ([M+H]$^+$); Found: C, 66.28; H, 4.85; N, 11.54. Calc'd for $C_{20}H_{17}N_3O_4$: C, 66.11; H, 4.72; N, 11.56; $\delta_H(CDCl_3)$: 2.95 [4H, t, 2xCH_2 (linker), J = 5.0 Hz], 3.77 [4H, t, 2xCH_2 (linker), J = 5.0 Hz], 7.67-6.69 [4H, dd, Ar*H* (Phth)], 7.71- 7.74 [4H, dd, Ar*H* (Phth)]; $\delta_C(CDCl_3)$: 37.50 [*C*H$_2$(linker)], 47.17 [*C*H$_2$(linker)], 123.13, 132.12, 133.75 [Ar*C* (Phth)], 168.46 [*C*=O].

A round-bottomed flask was charged with an absolute ethanol suspension (100 cm^3) of L^3 (1.82 g, 5.01 mmol). The suspension was heated until the reactant was completely dissolved. An aqueous solution (10 cm^3) of sodium hydroxide (0.41 g, 10.25 mmol) was added to the flask, maintaining the solution at pH ~9 – 10. The reaction mixture was then heated under reflux for 2 h. Thereafter, the solution was

cooled and evaporated *in vacuo* to give a white solid. This was isolated by Büchner apparatus and washed with 99IMS (3×10 cm^3) to give a white solid (L^4, 1.08 g, 49%). m.p. 243-247°C (decomposed); ES: 420.18 ($[M-Na]^-$); Found: C, 54.17; H, 4.29; N, 9.48. Calc'd for $C_{20}H_{19}N_3O_6Na_2$: C, 54.11; H, 4.21; N, 9.60; $\delta_H(D_2O)$: 3.43 [4H, t, 2xCH_2 (linker), J = 5.0 Hz], 3.77 [4H, t, 2xCH_2 (linker), J = 5.0 Hz], 7.39-7.43 [2H, m, Ar*H* (Phth)], 7.47-7.49 [2H, m, Ar*H* (Phth)], 7.50 [2H, m, Ar*H* (Phth)], 7.63[2H, m, Ar*H* (Phth)]; $\delta_c(D_2O)$: 35.91 [CH_2 (linker)], 46.87 [CH_2 (linker)], 126.65, 127.04, 129.87, 130.28, 134.54, 136.29 [Ar*C* (Phth)], 174.19, 175.18 [*C*=O].

2.2.5 Synthesis and characterization of L^5 and L^6

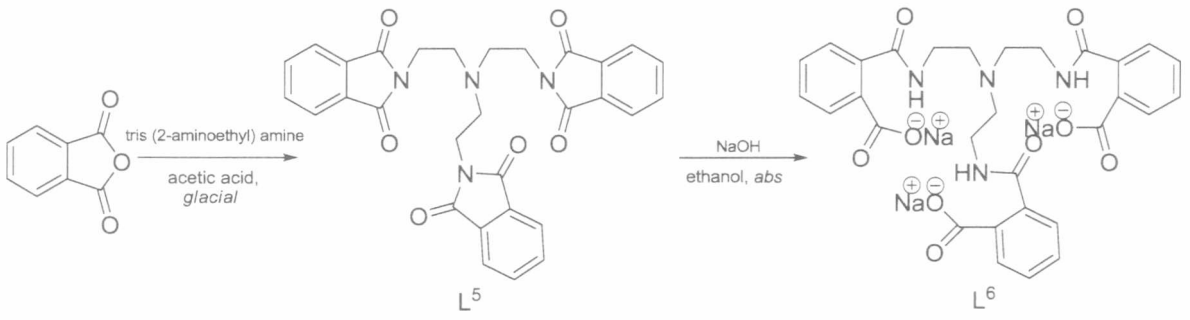

Scheme 5 Synthetic route to L^5 and L^6

A round-bottomed flask was charged with a *glacial* acetic acid solution (150 cm^3) of phthalic anhydride (2.96 g, 19.99 mmol), which was vigorously stirred at RT. Then tris(2-aminoethyl)amine (2.94 g, 20.11 mmol) was added dropwise and the mixture was heated under reflux for 4 h. Thereafter, the solution was cooled and the volume of solvent was reduced to ~50% by evaporation *in vacuo*. Deionised water (150 cm^3) was added and the reaction mixture was left stirring overnight at RT to yield a white precipitate. This was isolated by Büchner apparatus and was washed with cold 99IMS (3×25 cm^3) to give a straw yellow solid (L^5, 10.04 g, 93%). m.p. 172-174°C; ES: 537.48 ($[M+H]^+$); Found: C, 67.00; H, 4.29; N, 10.39. Calc'd for $C_{30}H_{24}N_4O_6$: C, 67.16; H, 4.48; N, 10.45; $\delta_H(CDCl_3)$: 2.91 [6H, t, 3xCH_2 (linker), J = 7.5 Hz], 3.74 [6H, t, 3xCH_2 (linker), J = 7.5 Hz], 7.67 [12H, s, Ar*H* (Phth)]; $\delta_C(CDCl_3)$: 35.35 [CH_2(linker)], 51.54 [CH_2(linker)], 123.04, 132.20, 133.63 [Ar*C* (Phth)], 168.17 [*C*=O].

A round-bottomed flask was charged with an absolute ethanol suspension (100 cm^3) of L^5 (1.07 g, 1.99 mmol). The suspension was heated until the reactant was completely dissolved. An aqueous solution (10 cm^3) of sodium hydroxide (0.24 g, ~6.00 mmol) was added to the flask, maintaining the solution at pH~9 – 10. This reaction mixture was then heated under reflux for 2 h. Thereafter, the solution was cooled and evaporated *in vacuo* while the solvents were reduced to ~20%. Ethanol (10 cm^3) was added to the residue to give a white suspension, and this was left stirring overnight at rt. After 24 h, this was isolated by Büchner apparatus and washed with 99IMS (3×10 cm^3) to give a yellow powder (L^6, 0.81 g, 62%). m.p. 270-273°C (decomposed); ES: 633.35 ([M-Na]$^-$); Found: C, 54.74; H, 4.03; N, 8.39. Calc'd for $C_{30}H_{27}N_4O_9Na_3$: C, 54.85; H, 4.12; N, 8.54. $\delta_H(D_2O)$: 2.69 [6H, t, 3xCH_2 (linker), J = 5.0 Hz], 3.51 [6H, t, 3xCH_2 (linker), J = 5.0 Hz], 7.29-7.36 [6H, m, Ar*H* (Phth)], 7.45-7.55 [6H, m, Ar*H* (Phth)]; $\delta_c(D_2O)$: 40.28 [CH_2 (linker)], 54.68 [CH_2 (linker)], 129.90, 130.92, 132.27, 133.12, 137.23, 140.34 [Ar*C* (Phth)], 175.84, 178.70 [*C*=O].

2.2.6 Synthesis and characterization of L^7 and L^8

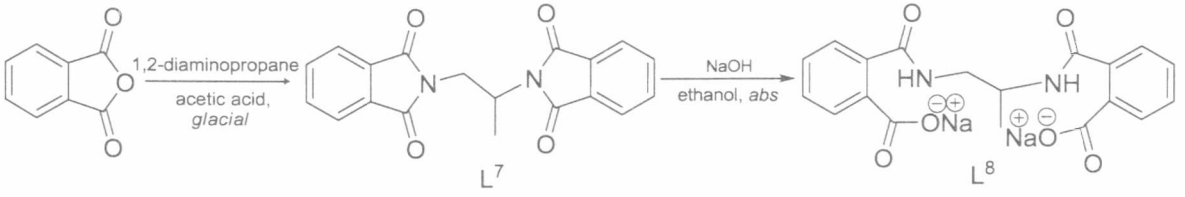

Scheme 6 Synthetic route to L^7 and L^8

A round-bottomed flask was charged with a *glacial* acetic acid solution (100 cm^3) of phthalic anhydride (0.74 g, ~5.00 mmol), which was vigorously stirring at RT. And then 1,2-diaminopropane (0.19 g, 2.57 mmol) was added dropwise into the mixture and heated under reflux for 4 h. Thereafter, the solution was cooled and an equal volume of deionised water (100 cm^3) was added to the flask. It was left standing overnight at RT to yield a white precipitate. This was isolated by Büchner apparatus and washed with cold 99IMS (3×10 cm^3) to give a creamy white solid (L^7, 0.70 g, 86%). m.p. 158-162°C; ES: 335.27 ([M+H]$^+$); Found: C, 68.54; H, 4.35; N, 8.27. Calc'd for $C_{19}H_{14}N_2O_4$: C, 68.26; H, 4.19; N, 8.38; $\delta_H(CDCl_3)$: 1.65 [3H, d, CH_3 (methyl), J = 5.0 Hz], 3.91, 4.39[2H, dd, CH_2 (linker)], 4.67 [1H, m, C*H* (linker)],

7.66-7.70 [4H, m, Ar*H* (Phth)], 7.75-7.79 [4H, m, Ar*H* (Phth)]; δ_C($CDCl_3$): 16.22 [*C*H_3 (methyl)] 40.65 [*C*H (linker)], 46.59 [*C*H_2 (linker)], 123.21, 123.29, 131.5, 131.82, 133.92, 134.01 [Ar*C* (Phth)], 168.10, 168.36 [*C*=O].

A round-bottomed flask was charged with an absolute ethanol suspension (100 cm^3) of L^8 (1.67 g, ~5.00 mmol). The suspension was heated until the reactant was completely dissolved. An aqueous solution (10 cm^3) of sodium hydroxide (0.41 g, 10.25 mmol) was added to the flask, maintaining the solution at pH ~9 - 10. The reaction mixture was then heated under reflux for 1 h. Thereafter, the solution was cooled and evaporated *in vacuo* completely. This was isolated by Büchner apparatus and washed with cold 99IMS (3×5 cm^3) to give an off-white solid (L^8, 1.53 g, 74%). m.p. 235-237°C (decomposed); ES: 391.16 ([M-Na]$^-$); Found: C, 51.46; H, 3.92; N, 6.37. Calc'd for $C_{19}H_{16}N_2O_6Na_2$.0.7 NaOH: C, 51.58; H, 3.78; N, 6.33; δ_H(D_2O): 1.32 [3H, d, C*H*$_3$ (methyl), *J* = 10.0 Hz], 3.46, 3.65[2H, dd, C*H*$_2$ (linker)], 4.32 [1H, m, C*H* (linker)], 7.42-7.61 [8H, m, Ar*H* (Phth)]; δ_c(D_2O): 19.79 [*C*H_3 (methyl)] 47.20 [*C*H (linker)], 48.93 [*C*H_2 (linker)], 129.47, 129.93, 130.72, 130.82, 132.27, 132.29, 133.08, 133.19, 137.50, 137.63, 140.43, 140.55 [Ar*C* (Phth)], 175.41, 176.00, 178.83, 178.95 [*C*=O].

2.3 Results and discussion

2.3.1 Synthesis of phthalimide derivatives, L^1, L^3, L^5 and L^7

All phthalimide derivatives (L^1, L^3, L^5 and L^7) were prepared by the method described in Scheme 2, Step 1. These were basically condensation reactions first introduced by *G. Wanag* in 1939,[121] whereby primary amines attack carbonyl carbons and replace the oxygen while releasing one water molecule. Because liquid amine derivatives fume when exposed to air,[122] a slight molar excess of liquid amine (~5%) was used for these procedures. This was to ensure complete reaction of the phthalic anhydride. The overall synthetic route to these four phthalimide derivatives is shown in Figure 2.3.

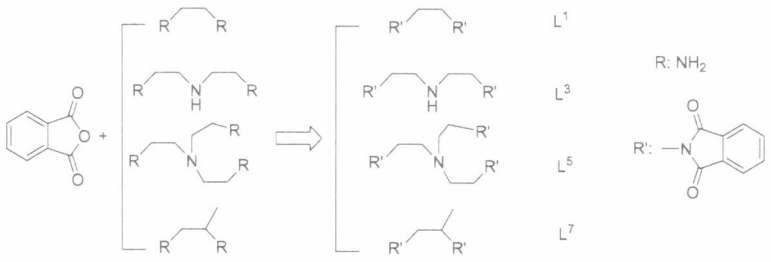

Figure 2.3 Synthetic routes to L^1, L^3, L^5 and L^7

First, the reaction must be achieved under acidic conditions. One of the carbonyl carbons of phthalic anhydride is attacked by a nucleophilic amine function, followed by forming a tetrahedral structure.[123] And then the C-O bond is cleaved. Second, the carbonyl carbon is made more electrophilic due to the fact that the carboxylate oxygen is fully protonated, generating a good leaving group (Scheme 7). This amide intermediate is very unstable and the following intramolecular cyclization step is very fast. Reaction in acetic acid facilitates this step as the protonated hydroxyl function becomes a good leaving group.[11, 124]

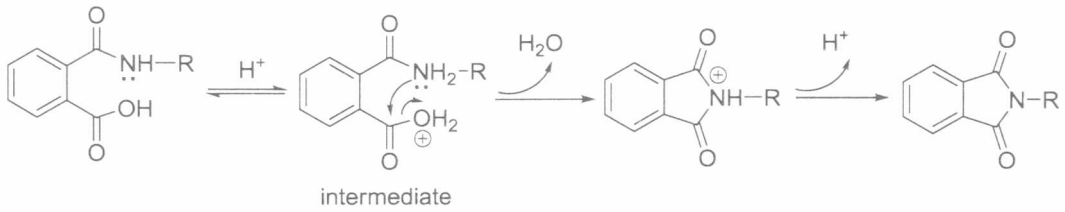

Scheme 7 A good leaving group of protonated hydroxyl function as an intermediate

L^1, L^3, L^5 and L^7 are all creamy white powders. The isolation methods for these four compounds are different, depending on their solubilities in acetic acid and deionised water. L^1 and L^7 were obtained as precipitates in acetic acid when the reaction was finished. In these cases, the crude products were washed with cold 99IMS. For L^5, solvent removal and addition of deionised water was necessary to obtain crude precipitates, which were then triturated with 99IMS to give final products.

However, only a poor yield of L^3 was precipitated from the solution when it was cooled or diluted with deionised water. It seems that the solubility of L^3 in the acetic acid and water mixture is significantly higher than that of the other ligands. Examination of the structures of L^1, L^3, L^5 and L^7 reveals that the only feature

distinguishing from the others is that L^3 exhibits a secondary amine function (Figure 2.4).

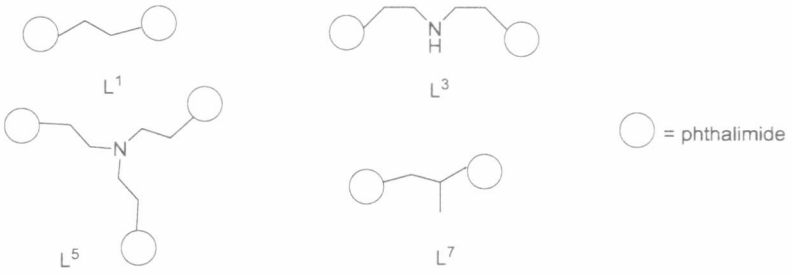

Figure 2.4 Simplified molecular structure of phthalimide derivatives

From the starting primary reactants to final tertiary and secondary amine-based products, the secondary amine function in L^3 more readily interacts with solvent molecules, especially polar solvents, such as acetic acid (Figure 2.5).[125]

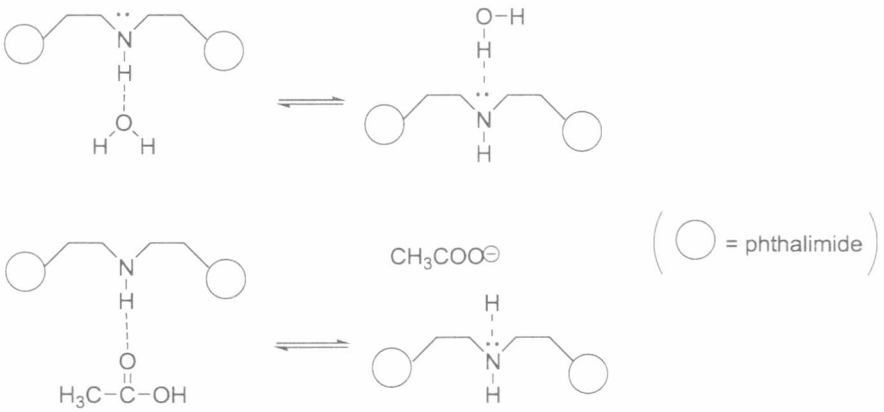

Figure 2.5 Hydrogen bonding between L^3 and acetic acid

The crude oil product (L^3) can be treated with small amount of ethanol, facilitating precipitation after a few hours. It was previously reported that diphthalimido-diethyl ammonium-hydrogen phthalate (DPDAH-HP, Figure 2.6) can be formed by this prodecure,[120] but this compound was not observed in this work according to NMR and elemental analysis results.

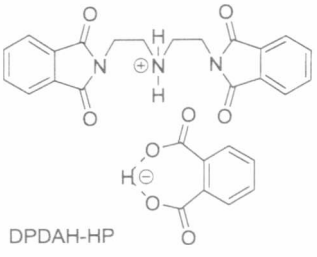

Figure 2.6 Structure of DPDAH-HP

Synthesis of this product in the reported work required addition of a very significant excess of phthalic anhydride into the solution, whereby the excess phthalic anhydride suffered an acid hydrolysis,[110] resulting in the generation of phthalic acid. This interacted with L^3 to form a salt compound.

2.3.2 Synthesis of phthalamate derivatives, L^2, L^4, L^6 and L^8

As mentioned in Section 2.2, L^1, L^3, L^5 and L^7 were all dissolved in absolute ethanol first during the hydrolysis procedures. However due to poor solubilities of phthalimide derivatives in absolute ethanol, employing a diluted solution (~50 mM) was preferred in this work. It was found that the organic solution must be refluxed first before addition of sodium hydroxide.

A slight molar excess of sodium hydroxide (~5%) with respect to phthalimide functions is necessary to complete the reaction, and this excess does not result in any significant decomposition effects, such as further hydrolysis of the phthalamate amide function. This is consistent with the observation in other researchers' work that higher pH does not generate phthalic acid in solution.[110] A very concentrated sodium hydroxide solution was prepared in deionised water in order to minimize the volume of aqueous solution used in the experiment, thereby facilitating precipitation of the products.

Moreover, it is suggested that the pH of phthalimide hydrolysis reactions be maintained between 9 and 10.[126] Actually, the pH of the reaction can reach 11 at the beginning while NaOH is added into the solution, but this drops from pH 11 to pH *ca.* 9 without any additional adjustment after 10 minutes.

As outlined in Scheme 2 (step 2), the hydrolysis reaction consists of two steps. Firstly, an intermediate is formed by nucleophilic attack of hydroxide anion on the carbonyl carbon. The second step involves a proton transfer from oxygen to nitrogen to form the amide function as the imide C-N bond is cleaved.[127, 128] This mechanism can be seen as roughly analogous to that of the hydrolysis of amide function (Scheme 8).

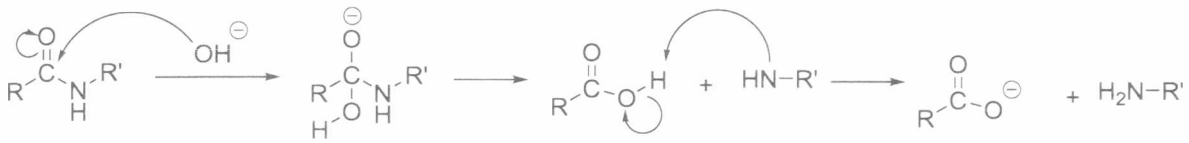

Scheme 8 Basic hydrolysis mechanism of an amide

The preparation of phthalamate derivatives from phthalimides has been well documented by *Tirouflet* and *Trouit*.[129] In their work, base-catalysed hydrolysis of phthalimide was achieved in ethanol-water solution that further hydrolysis of forming phthalic acid anion was precluded. However, *Bruylants et al*[130] have studied the hydrolysis of phthalimide in alkaline media where phthalamate was first formed and further hydrolysed to ammonia (Scheme 9).

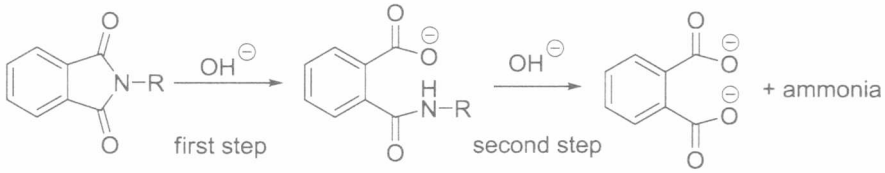

Scheme 9 Completely hydrolysis of phthalimide studied by *Bruylants et al*

The imide bond is hydrolysed far more easily than the amide bond, and the rate of hydrolysis of phthalamate is sensitive to the persisting concentration of hydroxide ions in the solution. Kinetics studies by *Khan et al*[129] established rate constants associated with each step, highlighting the relative difficulty of the second step. Hence, according to the conditions applied in this work, it was concluded that phthalamate derivatives were hardly hydrolysed further due to the limited concentration of hydroxide ion persisting after the first step.

2.3.3 Other methods for synthesizing phthalimides

While the preparatory method for phthalimide employed in this work was successful, the *Gabriel synthesis* is the method most frequently used.[131] In the *Gabriel synthesis*, *N*-substituted phthalimide derivatives are generated through the nucleophilic substitution reactions of potassium phthalimide. However, the ultimate aim of this reaction is to generate an amine, treating the phthalimide derivative as an intermediate.[132] The mechanism of this reaction[133, 134] is illustrated in Scheme 10.

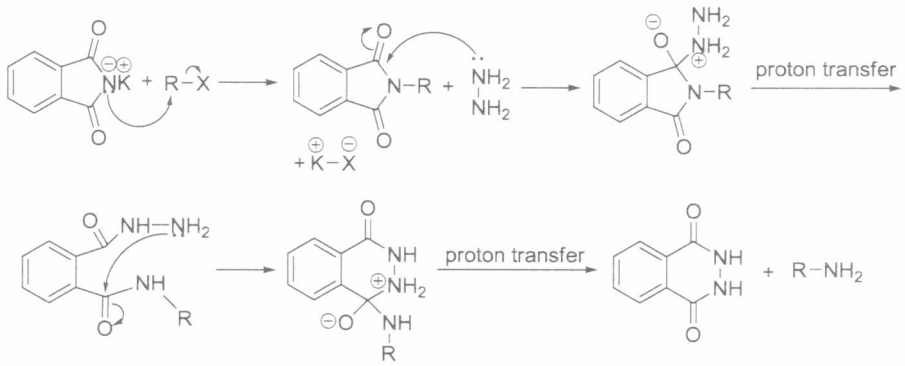

Scheme 10 Mechanism of *Gabriel synthesis*

The hydrolysis of an amide function can be catalysed by either acid or base. In both cases, the mechanism involves addition–elimination via a tetrahedral intermediate. A general scheme of amide hydrolysis is presented in Scheme 11.

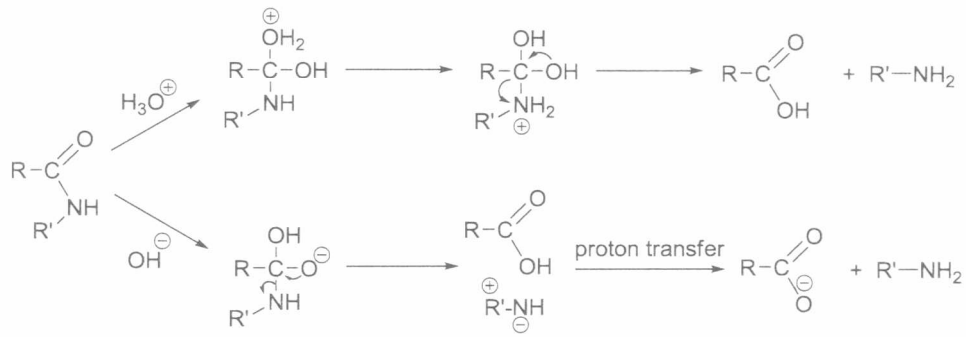

Scheme 11 Acid- and base-catalysed hydrolysis of amide

In acid-catalysed hydrolysis, protonation of the carbonyl oxygen leads to polarization of the carbonyl group, facilitating addition of the water nucleophile. On the other hand, base-catalysed hydrolysis forms a tetrahedral intermediate by the addition of the OH^- nucleophile. Both pathways are irreversible, the first due to protonation of the amine eliminating its nucleophilicity, the second due to suppressed electrophilicity in the deprotonated carboxylate function.

2.3.4 NMR Spectroscopic characterizations of L^{1-8}

2.3.4.1 NMR characterizations of L^1, L^3, L^5 and L^7

Phthalimide derivatives (L^1, L^3, L^5 and L^7) are structurally distinguishable only through the linkages exhibited between phthalimide functions. Interestingly, in ^1H NMR spectra, the splitting patterns associated with the aromatic protons do not follow the first order rule that $n + 1$ for $I = ½$ nuclei rigorously.[135]

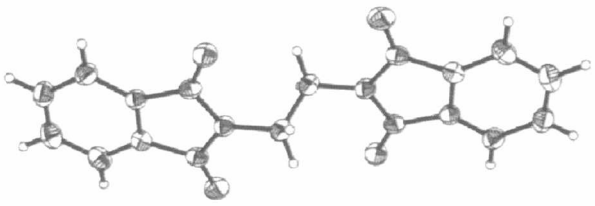

Figure 2.7 Crystal structure of L^1

L^1, L^3, L^5 and L^7 exhibit very similar splitting patterns associated with their aromatic protons, so L^1 is treated as representative of all derivatives in this section during discussion of the spectral features. In fact, the crystal structure of L^1 has been previously reported: a centre of inversion was located at the mid-point of the central C-C bond (Figure 2.7).[136] The two phthalimide functions are therefore parallel, and each half-molecule is essentially planar.

However the aromatic protons do not show two doublet signals as expected. It has been previously reported that *ortho*–disubstituted benzene give rise to complicated second order spectra with many lines.[137] The spectra of phthalimide are usually distinctive in this resonance region, whereby the splitting pattern observed is symmetrical with higher inner peaks.

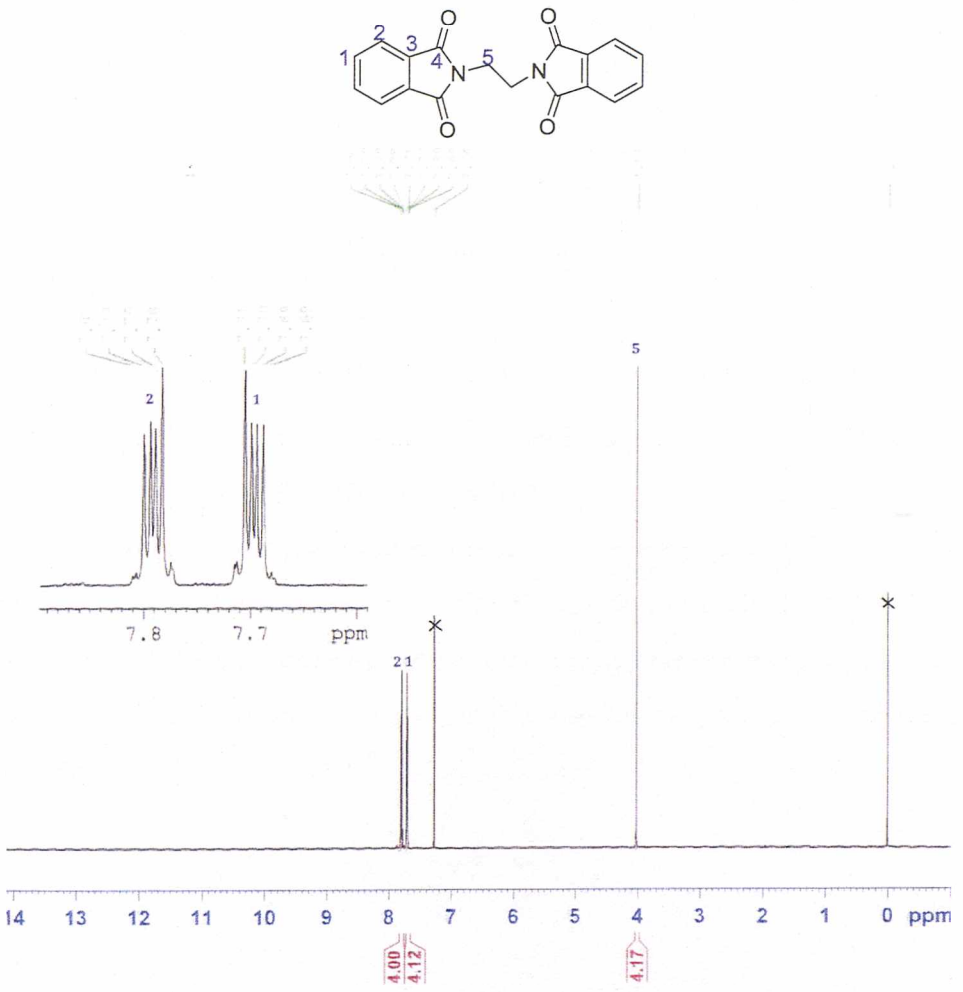

Figure 2.8 ^{1}H NMR spectrum of L^{1}

From the ^{1}H NMR spectrum of L^{1} (Figure 2.8), there are two symmetric doublet of doublet (dd) signals in the aromatic region, which correspond to H^{1} and H^{2} respectively. The dd multiplet signal centred at δ 7.79 ppm is assigned to H^{2}. This is consistent with previous reported studies, in which H^{2} has the downfield resonance of the two.[138, 139] The resonance at δ 4.01 ppm is assigned to the protons of the ethyl linker (H^{5}), all of which are chemically equivalent.

The two dd multiplets associated with the aromatic protons are very distinctive in spectra of phthalimide derivatives. The splitting pattern is widely acknowledged as being a product of second order effects, whereby the ratio of resonance difference to coupling constant ($\Delta\upsilon/J$) is less than 10 in the NMR spectrum.[140] For the aromatic protons in L^{1}, $\Delta\upsilon/J$ is *ca.* 7 by calculation. Hence higher order effects dominate the splitting patterns in this region of the spectrum. Therefore, the

doublet pattern for H^2-H^1 coupling is further split into dd by the coupling of H^2 to $H^{1'}$ (Figure 2.9, left).

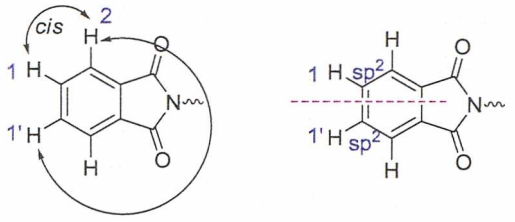

Figure 2.9 Magnetically non-equivalent (left) and chemically equivalent (right)

Clearly, protons H^1 and $H^{1'}$ are interchangeable by 180° rotation about the axis illustrated above (Figure 2.9, right), due to their chemical equivalence. However, these two protons do not have the same spatial relationship with other specified protons (e.g., H^2) and are therefore magnetically non-equivalent.[140] For example, H^1 and $H^{1'}$ have different couplings to H^2, one is a J_{cis} and the other is not, as shown in Figure 2.9. Therefore, the spin coupling system is considered to be AA'BB' for phthalimide.[141-143]

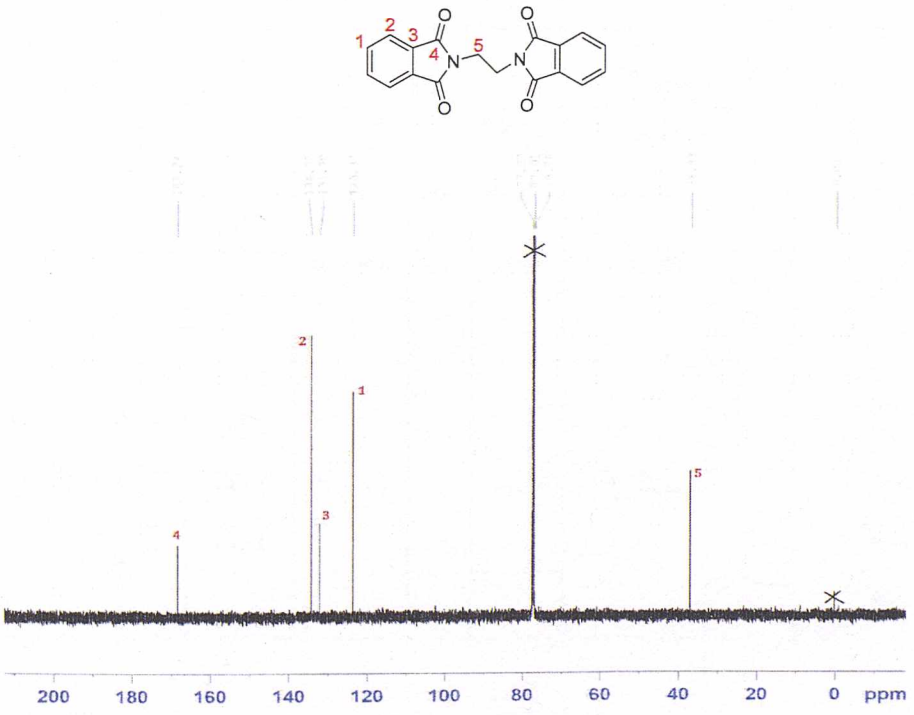

Figure 2.10 ^{13}C NMR spectrum of L^1

The ^{13}C spectra of all phthalimide derivatives studied share many spectral features (Figure 2.10). The resonance at δ 168.24 ppm is assigned to the carbonyl carbon (C^4) in L^1.[144, 145] The resonance at δ 131.90 ppm is assigned to C^3, which has a

similar intensity assigned to C^4, due to the Nuclear Overhauser Effect (NOE), whereby the intensities of carbon resonances in proton-decoupled spectra increase significantly with the number of hydrogen atoms directly attached.[146] As C^3 and C^4 atoms are quaternary, resulting in lower intensities than other hydrogen-attached carbons.[140]

Resonances at δ 123.37 ppm and δ 134.02 ppm belong to C^1 and C^2 respectively, as characterized in other researchers' work.[120] Certainly, the only signal in the aliphatic carbon region, δ 36.03 ppm, corresponds C^5.

NMR spectroscopy is used to identify the structures of all the final products. Both ^1H and ^{13}C NMR spectra of all the phthalimide-based compounds, L^1, L^3, L^5 and L^7 are assigned in Table 2.1-2.4:

Table 2.1 NMR assignments of L^1

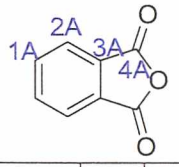						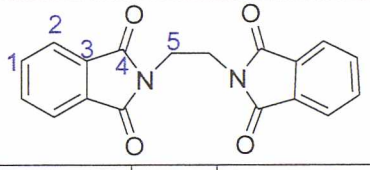		
^1H NMR	H^{1A}	7.99, dd	^1H NMR	H^{5A}	2.65, s	^1H NMR	H^1	7.70, dd
	H^{2A}	8.07, dd					H^2	7.79, dd
							H^5	4.01, s
^{13}C NMR	C^{1A}	125.3	^{13}C NMR	C^{5A}	44.87	^{13}C NMR	C^1	123.37
	C^{2A}	136.1					C^2	134.02
	C^{3A}	131.1					C^3	131.90
	C^{4A}	163.1					C^4	168.24
							C^5	36.83

Table 2.2 NMR assignments of L^3

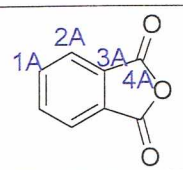			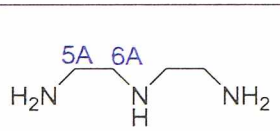			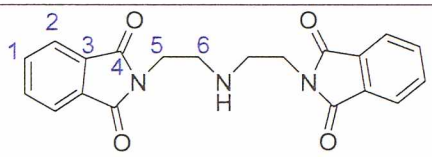		
^{1}H NMR	H^{1A}	7.99, dd	^{1}H NMR	H^{5A}	2.69, t	^{1}H NMR	H^1	7.68, dd
							H^2	7.73, dd
	H^{2A}	8.07, dd		H^{6A}	2.79, t		H^5	3.77, t
							H^6	2.95, t
^{13}C NMR	C^{1A}	125.3	^{13}C NMR	C^{5A}	41.91	^{13}C NMR	C^1	123.13
	C^{2A}	136.1					C^2	132.12
							C^3	133.75
	C^{3A}	131.1		C^{6A}	52.56		C^4	168.46
	C^{4A}	163.1					C^5	47.17
							C^6	37.50

Table 2.3 NMR assignments of L^5

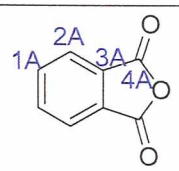			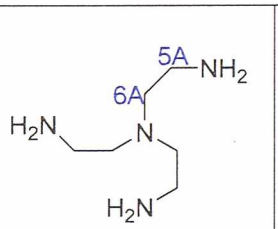			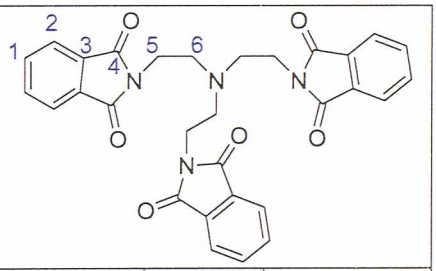		
^{1}H NMR	H^{1A}	7.99, dd	^{1}H NMR	H^{5A}	2.75, t	^{1}H NMR	H^1, H^2	7.76, s
	H^{2A}	8.07, dd		H^{6A}	2.52, t		H^5	3.74, t
							H^6	2.91, t
^{13}C NMR	C^{1A}	125.3	^{13}C NMR	C^{5A}	39.91	^{13}C NMR	C^1	123.04
	C^{2A}	136.1					C^2	133.63
							C^3	132.20
	C^{3A}	131.1		C^{6A}	57.66		C^4	168.17
	C^{4A}	163.1					C^5	51.54
							C^6	35.35

Table 2.4 NMR assignments of L^7

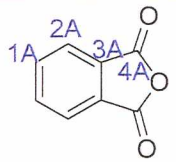			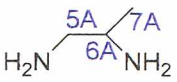			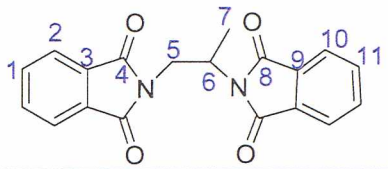		
^{1}H NMR	H^{1A}	7.99, dd	^{1}H NMR	H^{5A}	3.03	^{1}H NMR	H^1, H^{11}	7.68, m
				H^{6A}	2.87		H^2, H^{10}	7.77, m
	H^{2A}	8.07, dd		H^{7A}	1.12		H^5	3.91, dd 4.39, dd
							H^6	4.67, m
							H^7	1.65, d
^{13}C NMR	C^{1A}	125.3	^{13}C NMR	C^{5A}	49.4	^{13}C NMR	C^1, C^{11}	123.21, 123.29
	C^{2A}	136.1		C^{6A}	49.7		C^2, C^{10}	133.92, 134.01
							C^3, C^9	131.50, 131.82
	C^{3A}	131.1		C^{7A}	20.8		C^4, C^8	168.10, 168.36
							C^5	46.59
	C^{4A}	163.1					C^6	40.65
							C^7	16.22

The relatively electron-withdrawing character of the phthalimide function is reflected in the downfield resonance position of H^5 in the products, compared with that of the amine starting material, H^{5A}. This results in the lower electron density surrounding the methylene function in the final products compared with the starting reactants.

2.3.4.2 NMR characterization of L^2, L^4, L^6 and L^8

The hydrolysed ligands, L^2, L^4, L^6 and L^8 show very similar spectral features in their phthalamate functions. The *ortho*–disubstituted benzene with two different functional groups gives rise to more complicated splitting patterns in their ^{1}H NMR spectra. The spin-coupling observed exhibits both first order and higher order effects as discussed in Section 2.3.4.1.

The ^{1}H NMR spectrum of L^2 shows three main signals in the aromatic region and one resonance in the aliphatic region (Figure 2.11). The doublet centred at δ 7.61

ppm exhibiting first order characteristics is assigned to H^3, while the doublet of doublet of doublet (ddd) at δ 7.52 ppm corresponds to H^4. The calculated ratio of the difference of resonance to the coupling constant ($\Delta\upsilon/J$) for H^4 is less than 5,[140] hence second order characteristics are observed in the corresponding multiplet, as well as the splitting patterns of H^5 and H^6.[147] The combined multiplets observed in the range δ 7.44 – δ 7.49 ppm are assigned to H^5 and H^6.

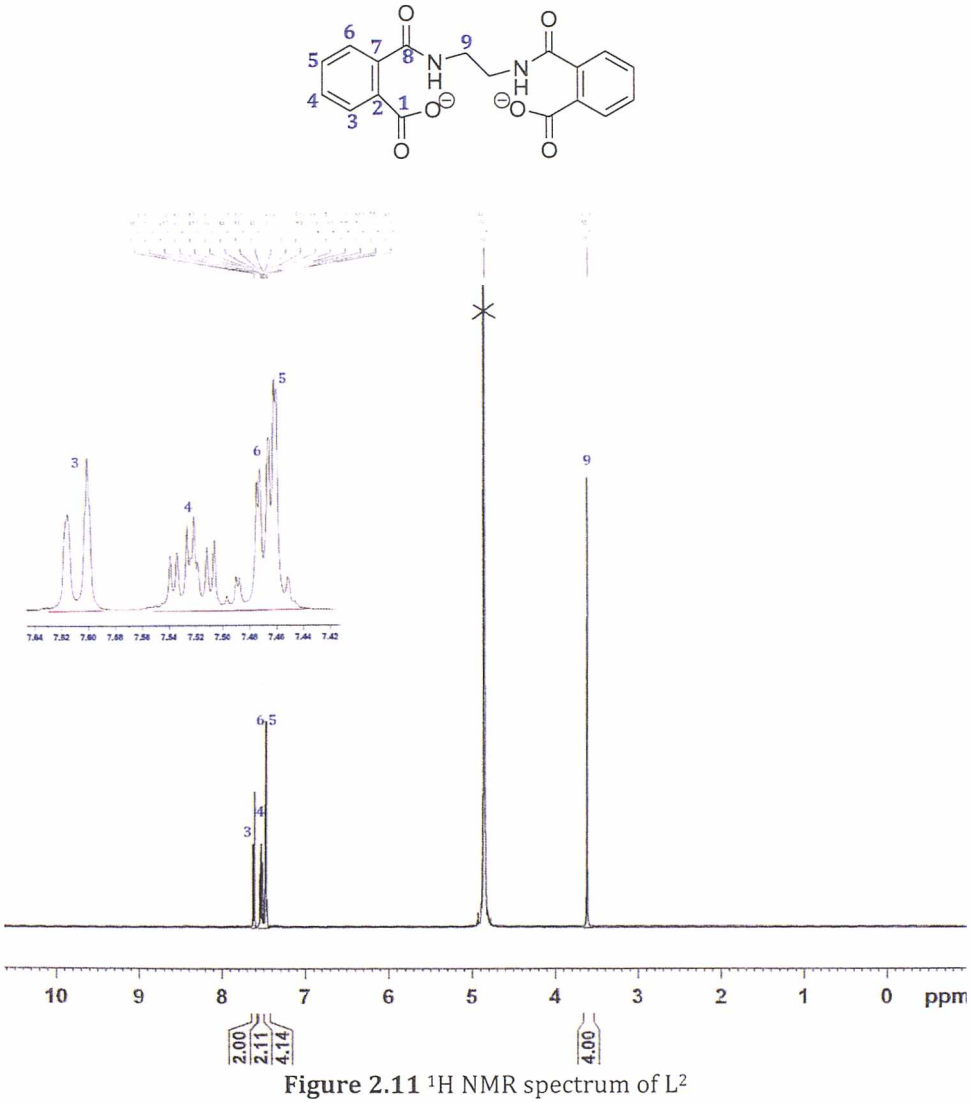

Figure 2.11 ^{1}H NMR spectrum of L^2

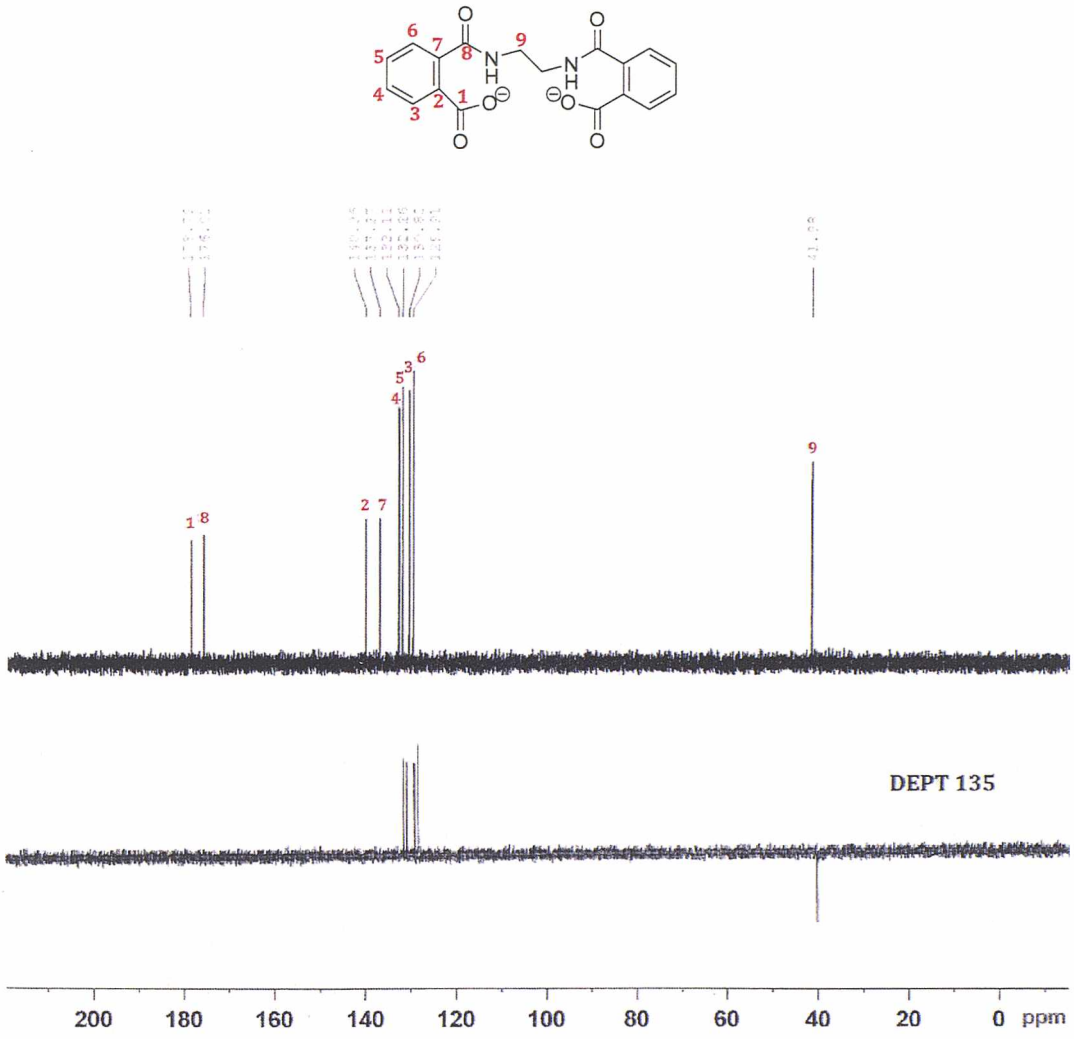

Figure 2.12 ^{13}C NMR spectrum of L^2

The ^{13}C NMR spectrum of L^2 is shown in Figure 2.12. Phthalamate has one carboxylate carbonyl carbon and one amide carbonyl carbon, and resonances at δ 176.01 ppm and δ 178.79 ppm correspond to C^8 and C^1 respectively. Six signals between δ 129.91 ppm and δ 140.36 ppm are assigned to C^{2-7} as indicated above. The resonance at δ 41.98 ppm is assigned to C^9. Spectrum editing with DEPT (pulse angle = 135°) experiment converts the phase of CH_2 carbon resonances to opposite directions with retaining the phase of CH and CH_3 carbon resonances. Quaternary carbon is not shown in DEPT 135° experiments. Hence C^2 and C^7 are distinguished from C^4, C^5, C^3 and C^6 because the resonances of C^2 and C^7 disappearing in DEPT experiments (Figure 2.12), while the assignments of other carbon are assigned by two-dimensional NMR spectra in following sections.

The general distribution of different functional carbons is conveniently distinguished, but the specific assignments of them within same functional group were further determined by *Heteronuclear Multiple Bond Correlation* (HMBC) method, characterising 2, 3 and sometimes 4 bond H-C connectivities.[148]

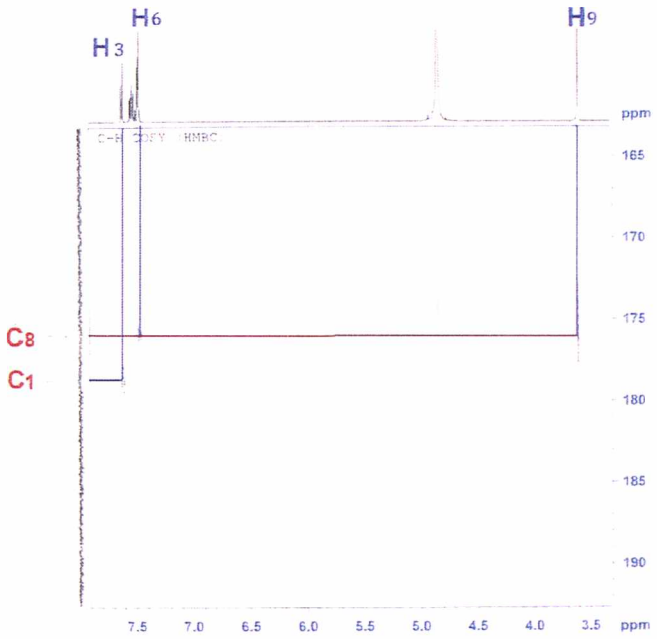

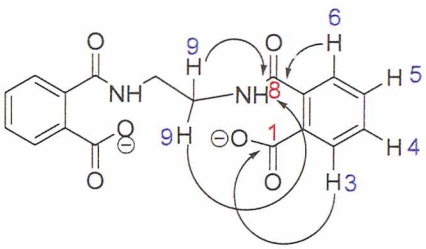

Table 2.5 HMBC couplings of L^2

Hydrogens	Carbons
H^3	C^1
H^6	C^8
H^9	C^8

Figure 2.13 HMBC spectrum of L^2

As the H^9 resonance had been assigned previously, the carbon coupling with H^9 in the HMBC spectrum is identified as the amide carbonyl carbon C^8. So the other carbonyl carbon resonance at δ 178.79 ppm is therefore assigned to C^1. Couplings between $C^{1,8}$ and two aromatic hydrogen atoms are also illustrated in Figure 2.13. According to this HMBC spectrum, the resonances at δ 7.61 ppm and δ 7.47 ppm are assigned to H^3 and H^6 respectively (Table 2.5).

Assignments of the H^3 and H^6 resonances mean that C^2, C^4 and C^5, C^7 can be assigned in the HMBC spectrum. Three-bond couplings between H^3 and carbon atoms are observed in this experiment, so that one aromatic carbon (CH), one aromatic quaternary carbon (C) and one carbonyl carbon (C=O) is revealed. The same coupling features are used for assigning H^6 and its related carbon atoms. From the correlation features in Figure 2.14, the two resonances at δ 132.26 ppm and δ 137.27 ppm are assigned to C^5 and C^7 respectively, and the two resonances at δ 140.36 ppm and δ 133.12 ppm are assigned to C^2 and C^4 respectively (Table 2.6).

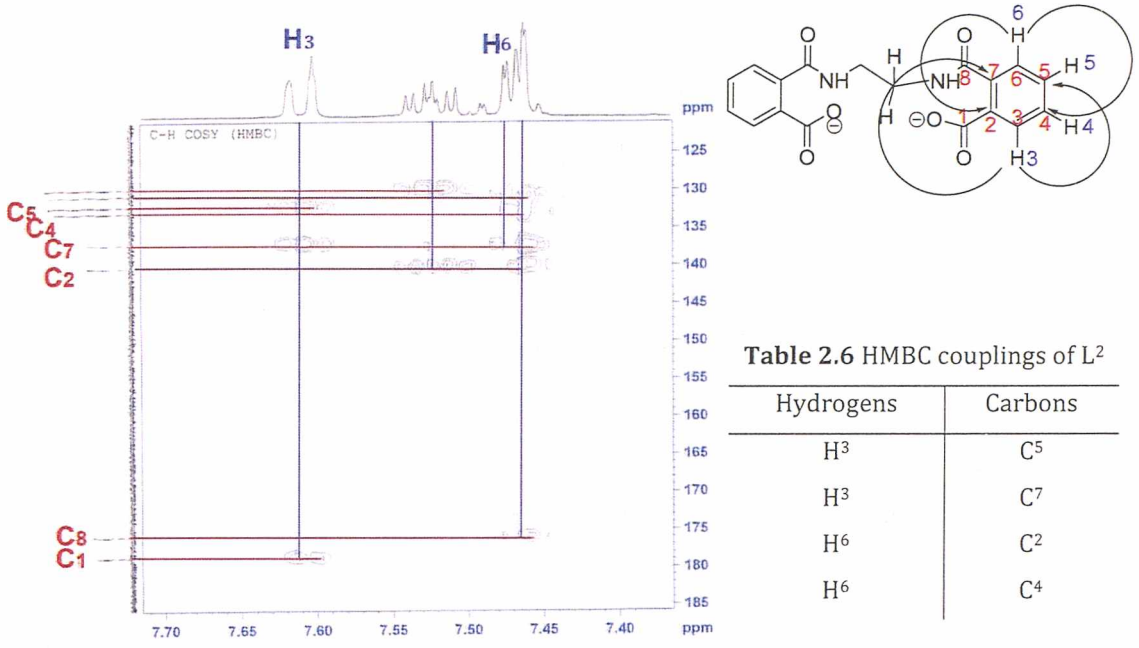

Table 2.6 HMBC couplings of L^2

Hydrogens	Carbons
H^3	C^5
H^3	C^7
H^6	C^2
H^6	C^4

Figure 2.14 HMBC spectrum of L^2

The other hydrogen (H^4, H^5) and carbon (C^3, C^6) are determined by a *Heteronuclear Correlation through Single Quantum Coherence* (HSQC) experiment. In this experiment, one-bond coupling between carbon and their directly attached hydrogen is observed in the spectrum.

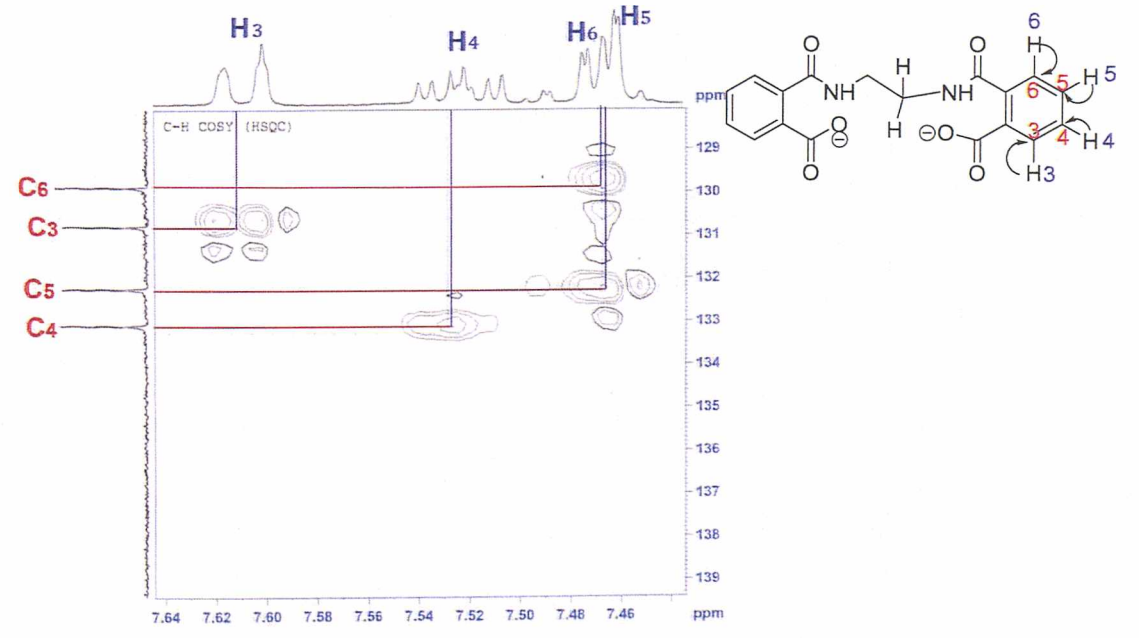

Figure 2.15 HSQC spectrum of L^2

As H^3, H^6 and C^4, C^5 resonances are assigned already, correlated C^3, C^6 and H^4, H^5 resonances can be assigned from the correlations in Figure 2.15. The resonances at δ 7.52 ppm and δ 7.46 ppm are assigned to H^4 and H^5 respectively, and the resonances at δ 130.82 ppm and δ 129.91 ppm are assigned to C^3 and C^6 respectively.

NMR experiments could be applied to determine the occurrence of phthalic anhydride, phthalimide derivatives and phthalamate derivatives efficiently: (1) The splitting pattern of *ortho*-disubstituted benzene in phthalamate is asymmetric rather than the symmetric doublet of doublet signals observed in the ^1H spectrum of in phthalimide. (2) Two resonances are observed in the carbonyl region with low intensities in phthalamate. (3) The aromatic carbon resonances are relocated, with six signals obtained instead of three. The characteristic resonances of starting material (phthalic anhydride), phthalimide derivatives and phthalamate derivatives are shown in Table 2.7.

Table 2.7 ^{13}C NMR resonance of carbonyl carbons of phthalic anhydride and L^1 – L^8

starting material (ppm)	phthalimide derivatives (ppm)	phthalamate derivatives (ppm)
phthalic anhydride 163.10	**L^1** 168.24	**L^2** 176.01 178.70
	L^3 168.46	**L^4** 174.19 175.18
	L^5 168.17	**L^6** 175.85 178.70
	L^7 168.10 168.36	**L^8** 175.41 176.00 178.83 178.95

The full assignments of each compound (L^2, L^4, L^6 and L^8) are shown below:

Table 2.8 NMR assignments of L^2

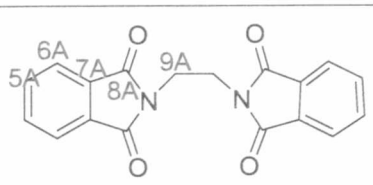			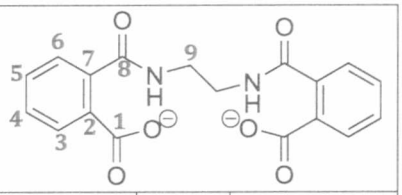		
^{1}H NMR	H^{5A}	7.79, dd	^{1}H NMR	H^3	7.61, d
	H^{6A}	7.70, dd		H^4	7.52, ddd
	H^{9A}	4.01, s		$H^{5,6}$	7.46, m
				H^6	7.47, m
				H^9	3.61, s
^{13}C NMR	C^{5A}	123.37	^{13}C NMR	C^1	178.70
	C^{6A}	134.02		C^2	137.24
	C^{7A}	131.90		C^3	130.82
				C^4	133.12
	C^{8A}	168.24		C^5	132.26
				C^6	129.91
				C^7	140.36
	C^{9A}	36.83		C^8	176.01
				C^9	41.98

Table 2.9 NMR assignments of L^4

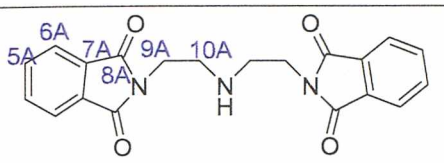

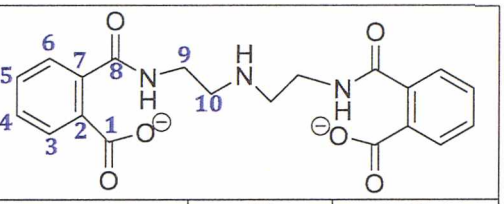

^{1}H NMR	H^{5A}	7.73, dd	^{1}H NMR	H^3	7.63, d
	H^{6A}	7.68, dd		H^4	7.52, ddd
	H^{9A}	3.77, t		H^5	7.41, m
	H^{10A}	2.95, t		H^6	7.47, m
				H^9	3.77, t
				H^{10}	3.47, t
^{13}C NMR	C^{5A}	123.13	^{13}C NMR	C^1	175.18
	C^{6A}	132.12		C^2	134.54
	C^{7A}	133.75		C^3	127.04
				C^4	130.28
	C^{8A}	168.46		C^5	129.87
				C^6	126.65
	C^{9A}	47.17		C^7	136.29
				C^8	174.19
	C^{10A}	37.50		C^9	46.87
				C^{10}	35.91

Table 2.10 NMR assignments of L^6

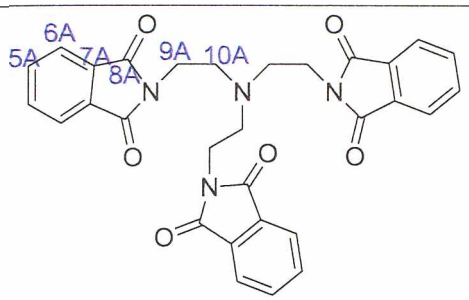			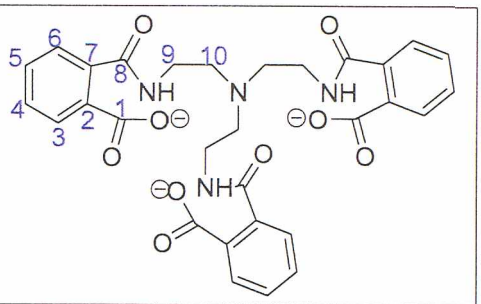		
^{1}H NMR	H^{5A}, H^{6A}	7.76, s	^{1}H NMR	H^3, H^4	7.45 - 7.55, m
				H^5, H^6	7.29 - 7.36, m
	H^{9A}	3.74, t		H^9	3.51, t
	H^{10A}	2.91, t		H^{10}	2,69, t
^{13}C NMR	C^{5A}	123.04	^{13}C NMR	C^1	178.70
				C^2	137.34
	C^{6A}	133.63		C^3	130.92
				C^4	133.12
	C^{7A}	132.20		C^5	132.27
				C^6	129.90
	C^{8A}	168.17		C^7	140.34
				C^8	175.84
	C^{9A}	51.54		C^9	54.68
	C^{10A}	35.35		C^{10}	40.28

Table 2.11 NMR assignments of L^8

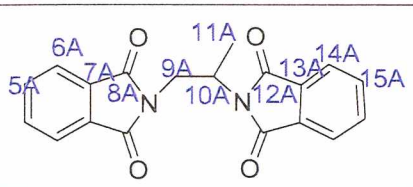			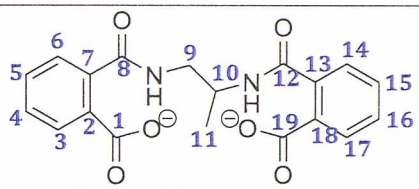		
^{1}H NMR	H^{5A}, H^{15A}	7.77, m	^{1}H NMR	H^3, H^4, H^5, H^6 and H^{14}, H^{15}, H^{16}, H^{17}	7.42 – 7.61, m
	H^{6A}, H^{14A}	7.68, m			
	H^{9A}	3.91, dd 4.39, dd		H^9	3.46, dd 3.65, dd
	H^{10A}	4.67, m		H^{10}	4.32, m
	H^{11A}	1.65, d		H^{11}	1.32, d
^{13}C NMR	C^{5A}, C^{15A}	123.21, 123.29	^{13}C NMR	C^1, C^{19}	178.83, 178.95
	C^{6A}, C^{14A}	133.92, 134.01		C^2, C^{18}	137.50, 137.63
				C^3, C^{17}	130.72, 130.82
	C^{7A}, C^{13A}	131.50, 131.82		C^4, C^{16}	133.08, 133.19
				C^5, C^{15}	132.27, 132.29
	C^{8A}, C^{12A}	168.10, 168.36		C^6, C^{14}	129.47, 129.93
				C^7, C^{13}	140.43, 140.55
	C^{9A}	46.59		C^8, C^{12}	175.41, 176.00
				C^9	48.93
	C^{10A}	40.65		C^{10}	47.20
	C^{11A}	16.22		C^{11}	19.79

2.3.5 Mass spectrometer features of L^{1-8}

The utility of mass spectrometer is to identify the functional groups of a compound.[149] Electrospray (ES) positive or negative mass spectrometer was used for characterizing the ligands in this work. Ions were observed by positive ES with addition of a proton to provide a $[M+H]^+$ cation which is obtained in the mass spectrometer.[150, 151] Therefore M+H signals were obtained for all four phthalimide

derived ligands, L^1, L^3, L^5 and L^7 (Table 2.12). The effect of isotopic ^{13}C is neglected here because of its low natural abundance (1.1%).[152]

Table 2.12 Relative molecular mass of L^1 – L^8 by positive ES and negative ES mass spectrometer

	L^1	L^2	L^3	L^4	L^5	L^6	L^7	L^8
M_r	320.30	400.30	363.37	443.37	536.54	656.54	334.33	414.33
ESI+	321.05		364.11		537.48		335.27	
ESI-		376.71		420.18		633.35		391.16

However the mass spectrometer results of L^2, L^4, L^6 and L^8 were analysed by negative ES experiment. Ligand L^2, L^4, L^6 and L^8 are formed as sodium salts, generating ions in solution. Therefore, the negatively charged electrospray method was used in these cases. M-Na signals were obtained for these ligands.

For the above compounds, the energy required to disrupt intramolecular bonds and intermolecular bonds are comparable.[153] Therefore low energy is used in these experiments, which results in a few big fragments observed in the spectra.

The fragments of L^1 and L^2 assigned in mass spectra are shown below in Figure 2.16. The base peak in the mass spectrum of L^1 corresponds to the proton-ionised molecule. However there is another relative peak of 343.0325 belonging to the sodium-ionised molecule (Figure 2.16). A fragment correlated to the phthalimide function of an m/z value of 147.015 was also observed in the spectrum of L^1.[154] All the other three phthalimide derivatives (L^3, L^5 and L^7) exhibit similar characteristics in their mass spectra.

In the negative EI mode, the complete relative molecule mass of L^2 is not observed due to the ionization process which results in the loss of a sodium atom. The phthalamate group fragment is not observed in the spectrum of L^2 because carboxylate and amine functions are easily fragmented from the original molecule. However, the fragments derived from stepwise loss of sodium atoms and OH species from L^2 and diaminoethane fragment are observed (Figure 2.16). Phthalamate derivatives, L^4, L^6 and L^8 also exhibit similar characteristics in their mass spectra.

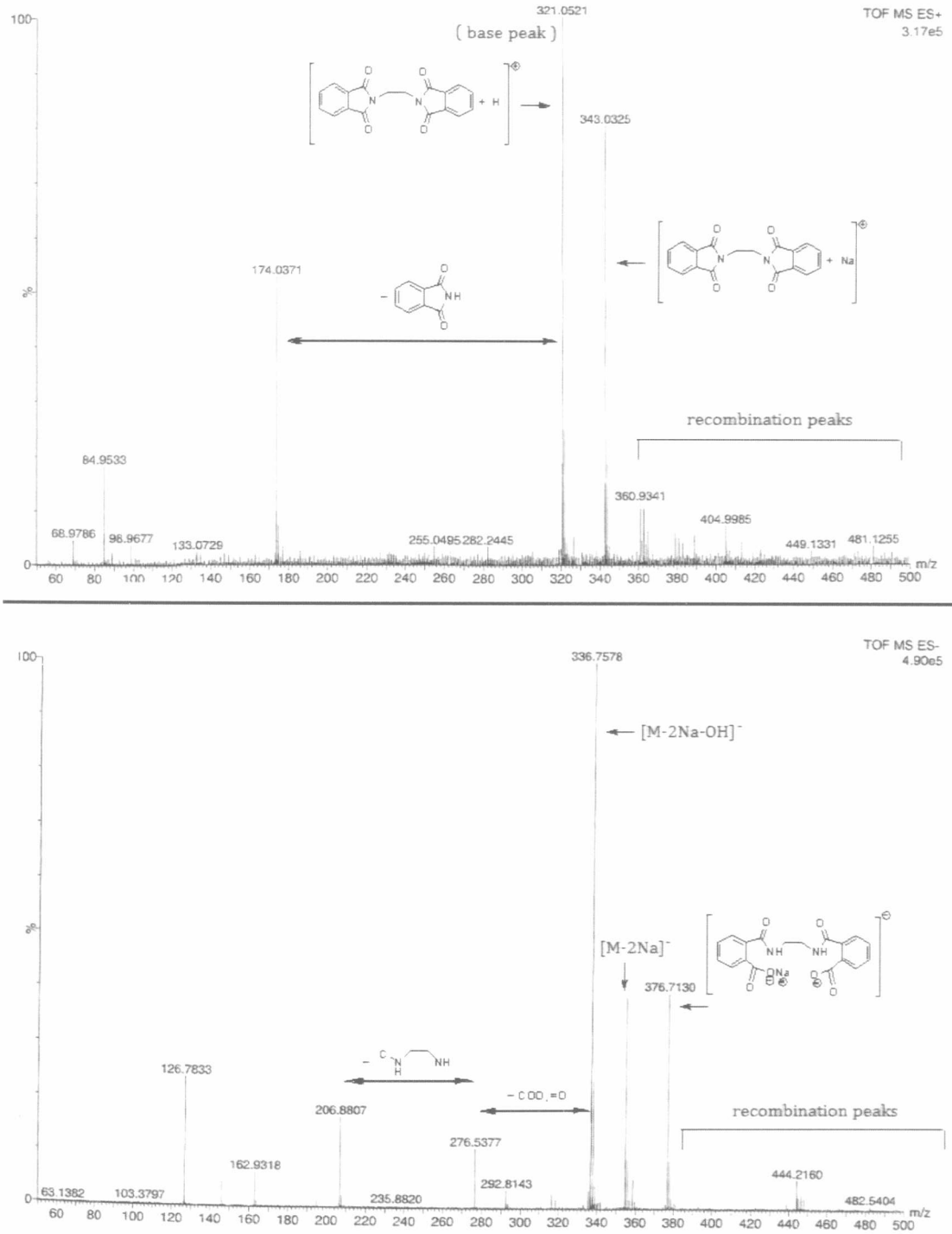

Figure 2.16 Mass spectrometer spectra of L^1 (above) and L^2 (below)

2.3.6 Melting point features of L^1 to L^8

Melting points are indicative of the attractive force between atoms, molecules or ions.[155] From the lowest melting point to the highest of the four phthalimide

derivatives, the order is L^1, L^7, L^3 and L^5 (Table 2.13). Generally, the melting point increases with molar mass, which is consistent with *Brown's* investigation.[156]

Table 2.13 Melting points of L^1 – L^8

	L1	L2	L3	L4	L5	L6	L7	L8
m.p. (^{0}C)	148-152	226-228	160-163	243-247	172-174	270-273	158-162	235-237

The melting point of phthalamates in all these cases is higher than those of phthalimides. These phthalamate derivatives usually start decomposing from 220°C. Ionic bonds are stronger than covalent bonds, resulting in a higher energy requirement for melting the molecule.[157, 158] This is the reason why L^6 has the highest melting point.

2.3.7 Infrared spectroscopy of L^{1-8}

All the experiments for infrared spectroscopy (IR) were studied on potassium bromide discs. For all phthalimide- or phthalamate-based ligands, the characteristic functional groups are the same. Therefore, the five-ring imide function is a characteristic of L^1, L^3, L^5 and L^7. On the other hand, amide and carboxylate functions are well characterised for L^2, L^4, L^6 and L^8. The IR spectra of L^1 and L^2 are shown below (Figure 2.17).

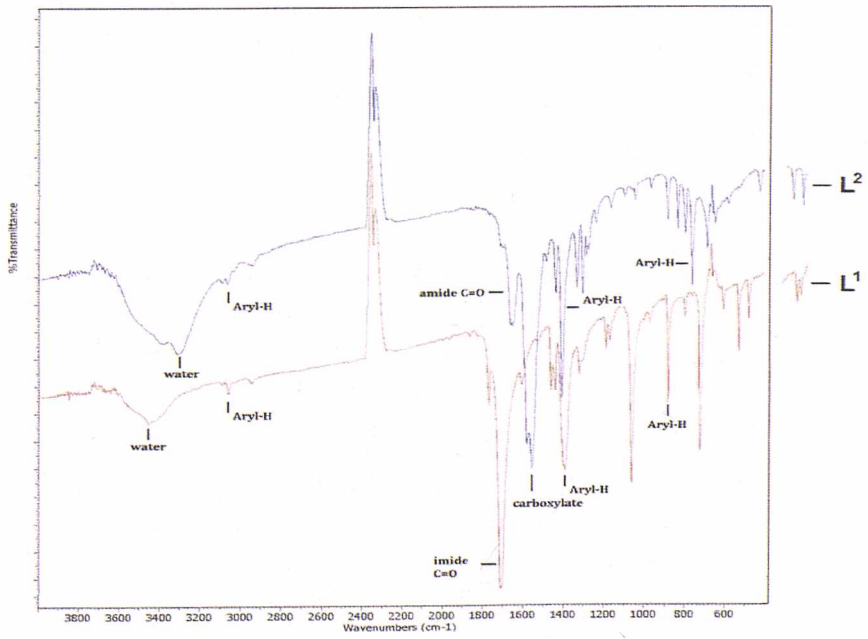

Figure 2.17 IR spectra of L^1 (red) and L^2 (blue)

The detailed assignments of IR features of L^{1-8} are listed below (Table 2.14 and 2.15).[159, 160]

Table 2.14 IR assignments of L^1, L^3, L^5 and L^7

Functional group	Band (cm^{-1})				Intensity	Remarks
	L^1	L^3	L^5	L^7		
water	3459	3455	3461	3460	weak	Residual water in KBr discs gives a broad but weak O – H stretching band
Aryl –H	3064 2952	2943 2866	2976 2940	2975 2953	weak	Usually two stretching bands for unfunctionalised C – H groups and very weak aryl – H in the same region
Aryl –H	797 722	774 757	796 715	798 721	medium to weak	Out of plane C – H bending vibrations, *-ortho*-disubstituted pattern
Aryl C-H	1061	1046	1095	1060	medium to weak	The bands due to C – H in-plane ring bending vibrations, interacting with C – C stretching vibrations,[161] obscure in L^2
Five-ring imide C=O	1713	1710	1710	1708	strong	Strong carbonyl stretching bands[162]
Aryl C=C	1519	1487	1468	1466	medium to weak	C = C alkenes of aromatics, usually very weak and more than one bands

Table 2.15 IR assignments of L^2, L^4, L^6 and L^8

Functional group	Band (cm^{-1})				Intensity	Remarks
	L^2	L^4	L^6	L^8		
water	3304	3297	3283	3273	weak	Residual water in KBr discs gives a broad but weak O – H stretching band
Aryl –H	3071 2943	3064 2917	3062 2968	3062 2972	weak	Usually two stretching bands for unfunctionalised C – H groups and very weak aryl – H in the same region
Aryl –H	766 691	765 690	748 711	750 691	medium to weak	Out of plane C – H bending vibrations, *-ortho*-disubstituted pattern
Secondary 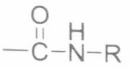	1653	1621	1635	1643	strong	Amide stretching bands of carbonyl
	3380-3420	3350-3400	3350-3400	3300-3400	medium	Secondary amines absorb weakly N – H stretching band with overlaps with water molecules
Carboxylate 	1556 1413	1571 1443	1565 1443	1585 1443	medium	Asymmetric and symmetric stretching bands of carbonyl respectively

2.4 Conclusion

Four phthalimide-based derivatives (L^1, L^3, L^5 and L^7) were successfully prepared by condensation reaction in *glacial* acetic acid. These compounds were further hydrolysed by sodium hydroxide in absolute ethanol-water under reflux temperatures to generate phthalamate-based ligands (L^2, L^4, L^6 and L^8). The yields for generating these eight compounds were 50% - 90%. All these eight compounds were completely characterised by NMR spectroscopy, mass spectrometer, elemental analysis, IR spectroscopy and melting point studies. L^6, L^7 and L^8 are novel derivatives previously unreported.

Chapter Three Synthesis and characterization of macrocyclic ligands

3.1 Introduction

A novel series of macrocyclic compounds has been investigated by *D. Park and A.P. de Silva, et al* for the complexation of lanthanide ions.[113] The 'cage' in a 12-membered ring-based ligand was shown to bind a number of lanthanide ions perfectly.[163] Macrocyclic compounds based on phthalimide has not been investigated much in recent years.[113] However, an analogue of phthalimide, porphocyanine, has been developed for coordinating different metal ions, including lanthanide ions.[219] Porphocyanine incorporates the combined structure of porphyrin (Figure 3.1a) and offers two extra nitrogens in addition to the four pyrrolic nitrogens.[164, 165] A Gd^{3+} complex based on porphocyanine has demonstrated applications in magnetic resonance imaging.[166]

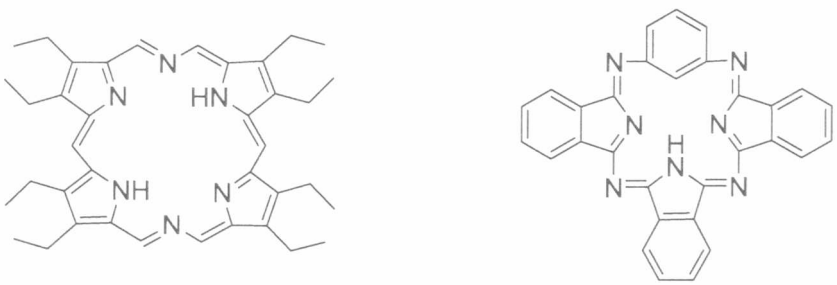

Figure 3.1 Early Ln^{3+} chelating macrocycles: (a) Porphocyanine and (b) Tri*iso*indole macrocycle

However, macrocyclic compounds consisting of conjugated linkages are usually rarely offer the eight/nine donor sites necessary to strongly chelate lanthanide ions.[167, 168] This disadvantage has been demonstrated in tri*iso*indole–benzene (Figure 3.1b). It only has two tertiary nitrogens available for coordinating with a metal ion. The other unsaturated nitrogen atoms suffered electron delocalization, resulting in low basicity and no coordinate bonds. Therefore the luminescence features of La^{3+} complexes based on tri*iso*indole–benzene are not well observed due to quenching by bound solvent molecules.[169]

Hence another type of ligand based on the 12-membered tetraaza macrocycle, 1,4,7,10-tetraazacyclododecane (cyclen), was investigated in this work,

incorporating four pendant arms onto the nitrogen atoms, with the potential to increase the denticity of the ligand.[170]

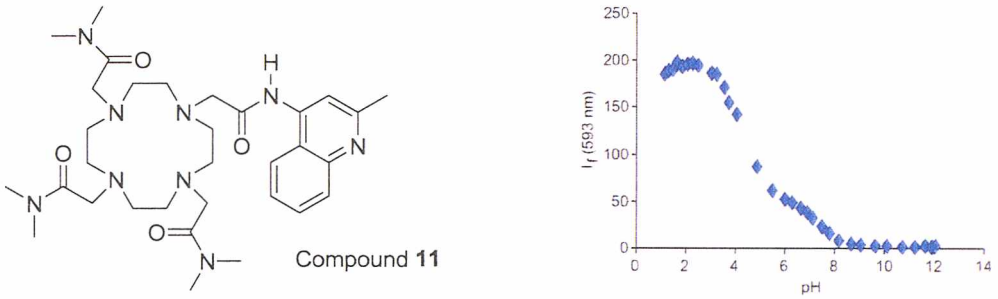

Figure 3.2 Structure of compound **11** and the luminescence of its Eu^{3+} complex at various pH

An example of a macrocycle-based (1,4,7-tris(dimethyl{carbamoylmethyl})-10-(2-methyl-4-quinolylethanamide)-1,4,7,10-tetraazacyclododecane, compound **11**, Figure 3.2) is a cyclen-based compound. The Eu^{3+} complex of which was synthesized in previous research.[171] This ligand proved an ideal design in terms of coordination number and energy transfer, and this Eu^{3+} complex has been applied as a pH dependent sensor in deionised water. $[Eu(\mathbf{11})]^{3+}$ is excited at $\lambda_{330\,nm}$ and emits at $\lambda_{593\,nm}$, the luminescence of this complex is switched on under acidic condition, and switched off under basic condition (Figure 3.2).[172]

In this Chapter, all macrocylic compounds described were based on the cyclen structure. The synthetic route to cyclen follows the method reported by *Atkins* and *Richman* (Scheme 12).[173]

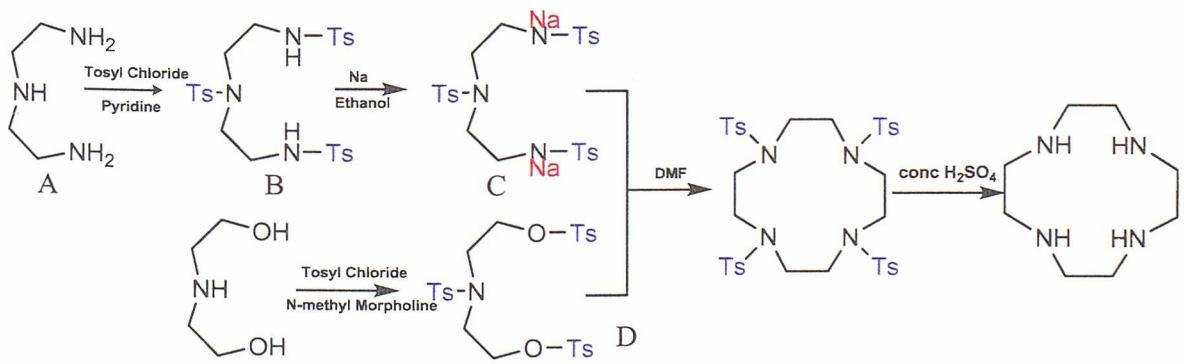

Scheme 12 Synthetic route to cyclen

This pathway involves a 1+1 cyclization, exploiting the acidity of secondary tosylamide functions in B caused by the electron withdrawing character of the tosyl function (*p*-toluenesuofonyl). Hence, the deprotonated nucleophile

tris(tosyl)-diethylenetriamine species (C) reacts with bistosylate derivatives (D) in a nucleophilic substitution at high dilution in DMF, to generate the protected macrocycle (Figure 3.3).[174, 175, 176]

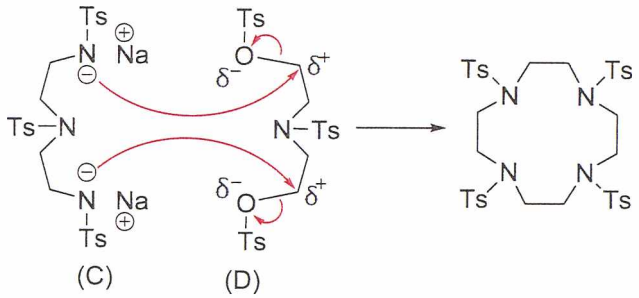

Figure 3.3 Cyclization to generate 1,4,7,10-tetrakis(*p*-toluenesulfonyl)-1,4,7,10-tetraazacyclododecane

The nucleophilic substitution reaction is facilitated as the O-Ts function of D[177], which is a very good leaving group, removed by the attack of tosylamido nucleophilic functions during C-N bond formulation.[173] Thereafter, the tosyl protecting groups are removed in concentrated sulfuric acid at 105°C, generating the cyclen sulfuric acid salt. This is neutralized by saturated KOH solution followed by continuous extraction in chloroform.

It is known that carboxymethyl function is a good Lewis base for coordinating lanthanide ions.[40, 178] Therefore the aim of this part of the study was to design a series of cyclen-based ligands consisting of carboxymethyl and phthalimide functions.

3.2 Experimental

3.2.1 General materials

All reagents and starting materials were used as purchased from commercial sources and used without further purification, unless otherwise stated. Bromopropyl phthalimide, bromoethyl phthalimide and triethylamine were purchased from the Sigma Aldrich Company Ltd, UK. Dimethylformamide, acetonitrile, chloroform and methanol dichloromethane were purchased from Fisher Scientific Ltd, UK. Dimethylformamide and methanol were dried over

molecular sieves, diethyl ether was dried over sodium metal and all were stored at RT.

1,4,7,10-Tetraazacyclododecane (cyclen) was prepared according to the method reported by *Atkins* and *Richman*.[173] The HBr salt of 1,4,7-Tris(carboxymethyl-t-butyl-ester)-1,4,7,10-tetraazacyclododecane (DO3A-t-butyl ester) was prepared from cyclen according to the method reported by *Schultze* and *Bulls*.[179] The 1,4,-Bis(carboxymethyl-*t*-butyl-ester)-1,4,7,10-tetraazacyclododecane (DO2A-t-butyl ester) was prepared according to the method published by *Li* and *Wong*.[180] The relative molar mass of these reactants were calculated according the results from elemental analyses.

3.2.2 General instruments

NMR spectra were recorded on a Bruker Avance - 500MHz (^{1}H, 500.1 MHz; ^{13}C, 125.8 MHz, Bruker Corporation, UK) NMR spectrometer. Both ^{1}H and ^{13}C NMR spectra were recorded in $CDCl_3$ with tetramethylsilane as the internal reference, or in D_2O with 3-(trimethylsiyl)propionic-2,2,3,3-d_4 acid sodium salt as internal reference. Resonances (δ) are expressed in ppm and J values are given in Hz.

Mass Spectra (HR-ES-MS) were measured by a Waters Q-Tof microTM mass spectrometer (Waters Corporation, UK)

IR spectra (KBr disc) were recorded on a Nicolet 100 FT-IR spectrophotometer (Thermo Scientific, UK).

Melting points were obtained on an Electrothermal digital melting point apparatus, and were uncorrected.

A Flash 2000 Elemental Analyser was used for C, H and N microanalysis (Thermo Scientific, UK).

TLC was performed on pre-coated silica plates (Whatman Al Sil G/UV, 250 mm layer) in different solvent systems. Column chromatography was performed over

Sorbsil C60 silica gel (60 mesh particle size) or Aldrich silica gel (Merck grade 10180, 63-200 mesh particle size).

3.2.3 Synthesis and characterization of L^9

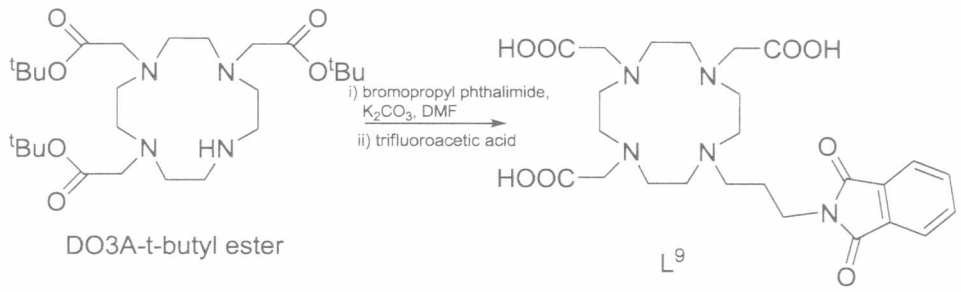

Scheme 13 Synthetic route to L^9

A round-bottomed flask was charged with an anhydrous DMF suspension (7 cm^3) of DO3A-t-butyl ester HBr salt (2.69 g, 4.01 mmol), *N*-(3-bromopropyl)phthalimide (1.29 g, 4.81 mmol) and anhydrous K_2CO_3 (1.328 g, 9.61 mmol). The mixture was vigorously stirred in anhydrous conditions at RT for 6 days. The mixture was then decanted into dichloromethane (150 cm^3), washed with deionised water (6×100 cm^3) and saturated brine (2×100 cm^3), and dried over $MgSO_4$. The solvent was evaporated *in vacuo* to yield a yellow oil which was subjected to column chromatography (stationary phase - silica gel, eluent - CH_2Cl_2/MeOH 7:1 v /v; desired fractions, R_f 0.65). Thereafter, the collected fractions were combined and the solvents were evaporated *in vacuo.* The residue was dissolved in a stirred chloroform solution (15 cm^3) which was charged with trifluoroacetic acid (20 cm^3) and the reaction mixture was stirred under anhydrous conditions at RT for 4 h. The solvent was evaporated *in vacuo* and the residue was azeotroped twice with chloroform. An acetone (3 cm^3) solution of the residue was added dropwide to diethyl ether (100 cm^3) and this was isolated by Büchner apparatus to give a crude solid. This precipitation procedure was repeated, followed by trituration of the separated solid in diethyl ether, yielded a creamy white solid (L^9, 643.7mg, 19% from DO3A-t-butyl ester). m.p. 127-130°C. ES: 534.4 ([M+H]$^+$); Found: C, 41.97; H, 4.55; N, 8.12. Calc'd. for $C_{25}H_{35}N_5O_8.2.75CF_3COOH.H_2O$: C, 42.33; H, 4.59; N, 8.10%. $\delta_H(D_2O)$: 2.17 [2H, t, CCH_2C (linker), J = 10 Hz]; 3.00-3.17, 3.39-3.49, 3.60-3.64 [22H, m]; 3.76 [2H, t, J = 5 Hz]; 3.89 [2H, s]; 7.80-7.86 [4H, m, (Ar*H*, Phth)]; $\delta_C(D_2O)$: 25.40

[C*C*H$_2$C (linker)]; 37.65 [N*C*H$_2$'s (linker)]; 51.34, 52.74, 54.17, 54.80, 56.07, 58.90 [N*C*H$_2$'s (DO3A segment)]; 126.35, 134.11, 137.71 [Ar*C*, (Phth)]; 172.88, 173.37, 176.99 [*C*=O];

3.2.4 Synthesis and characterization of L^{10}

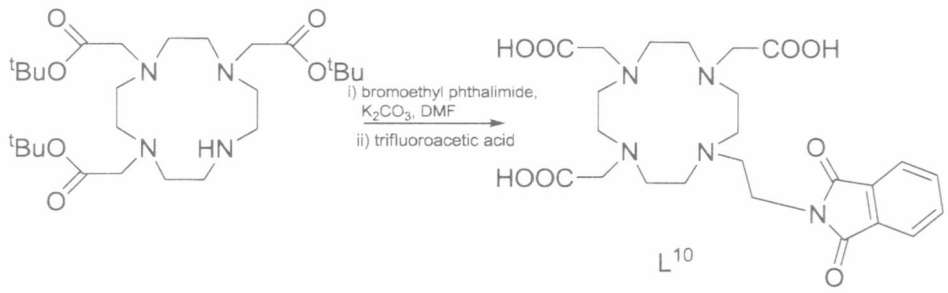

Scheme 14 Synthetic route to L^{10}

A round-bottomed flask was charged with a methanolic solution (10 cm^3) of DO3A-t-butyl ester HBr salt (638.8 mg, 1.01 mmol) and KOH (86.7 mg, 1.55 mmol). The solvent was evaporated *in vacuo*. The residue was redissolved in dichloromethane (20 cm^3) and filtered before evaporating again to leave a colourless syrup. Anhydrous K_2CO_3 (182.3 mg, 1.31 mmol) and *N*-2(bromoethyl)phthalimide (325.5 mg, 1.28 mmol) were added to this, followed by anhydrous DMF (10 cm^3). This mixture solution was vigorously stirred at RT in anhydrous conditions for 5 days. The solution was then evaporated *in vacuo* and the residue was redissolved in dichloromethane (70 cm^3). This was washed with deionised water (4×50 cm^3) and saturated NaCl (50 cm^3), and dried over Na_2SO_4. Evaporation *in vacuo* yielded a straw oil which was introduced to column chromatography (stationary phase - silica gel, eluent - CH_2Cl_2/MeOH 7:1 v/v; desired fractions, R_f 0.64). Thereafter, the collected fractions were combined and the solvents were rotary evaporated *in vacuo*. The residue was dissolved in a stirred chloroform solution (10 cm^3) which was charged with trifluoroacetic acid (10 cm^3) and the reaction mixture was stirred under anhydrous conditions at RT overnight. The solution was then evaporated *in vacuo* and the residue was redissolved in methanol (1 cm^3). A methanol (1 cm^3) solution of the residue was added dropwide to diethyl ether (50 cm^3) and this was isolated by Büchner apparatus to give a crude solid. This precipitation procedure was repeated, followed by trituration of the separated

solid in diethyl ether, yielded a hygroscopic solid (L^{10}, 135.5 mg, 14.11% from DO3A-t-butyl ester). m.p. 90°C (hygroscopic); ES: 520.15 ([M+H]$^+$); Found: C, 42.97; H, 4.96; N, 8.91. Calc'd. for $C_{24}H_{33}N_5O_8.2CF_3COOH.2H_2O$: C, 42.90; H, 5.02; N, 8.94%. $\delta_H(CD_3OD)$: 3.16[2H, s] 3.45, 3.53, 3.65, 3.68, 3.73, 3.74, 3.76, [22H, m]; 4.17. [2H, s]; 3.94 [2H, t, J = 15 Hz)]; 7.79-7.88 [4H, s, (Ar*H*, Phth)], $\delta_C(CD_3OD)$: 33.54, 37.75 [N*C*H$_2$'s (linker)]; 52.90, 54.04, 54.15, 55.89 [N*C*H$_2$'s (DO3A segment)]; 124.42, 133.28, 135.73 [Ar*C*, (Phth)]; 162.36, 162.64, 169.62, 169.78 [*C*=O].

3.2.5 Synthesis and characterization of L^{11}

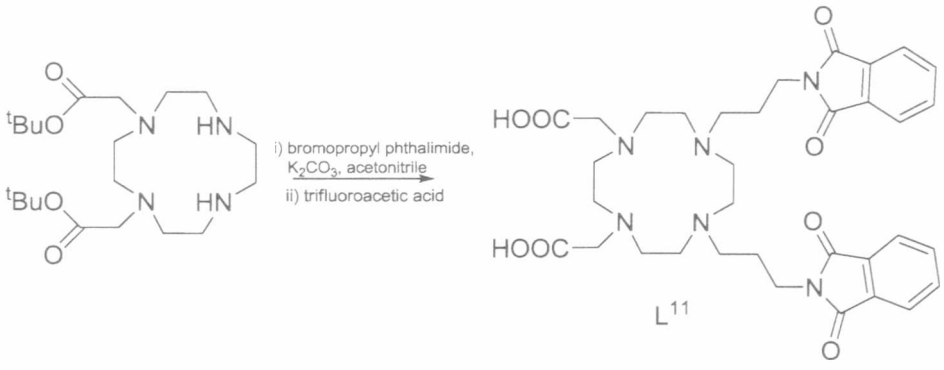

Scheme 15 Synthetic route to L^{11}

A round-bottomed flask was charged with an acetonitrile (50 cm^3) solution of DO2A-t-butyl ester (~1.00 g, 2.16 mmol), *N*-(3-bromopropyl)phthalimide (1.66 g, 6.19 mmol), triethylamine (3.30 g, 32.58 mmol) and anhydrous K_2CO_3 (0.20 g, 1.45 mmol) were stirred under anhydrous condition at 60°C for 5 days. The mixture was then decanted into dichloromethane (100 cm^3), washed with deionised water (3x80 cm^3), and dried over $MgSO_4$. The solvent was evaporated *in vacuo* to give a brown oil which was subjected to column chromatography (stationary phase - silica gel, eluent - CH_2Cl_2/MeOH 10:1 v/v; desired fractions, R_f 0.60). Thereafter, the collected fractions were combined and the solvents were evaporated *in vacuo.* The residue was dissolved in a stirred chloroform solution (25 cm^3) which was charged with trifluoroacetic acid (25 cm^3) and the reaction mixture was stirred in anhydrous conditions at RT for 4 h. The mixture was evaporated *in vacuo* and the residue was redissolved in chloroform (25 cm^3) and trifluoroacetic acid (25 cm^3) solution, stirred for further 4 h. The solution was evaporated *in vacuo*. An acetone

(1.5 cm^3) solution of the residue was added dropwise to diethyl ether (100 cm^3) and this was isolated by Büchner apparatus to give a crude solid. This precipitation procedure was repeated, followed by trituration of the separated solid in diethyl ether, yielded an off–white solid (L^{11}, 362.7 mg, 11% from DO2A-t-butyl ester). m.p. 122-125°C; ES: 663.39 ([M+H]$^+$); Found: C, 47.68; H, 4.31; N, 7.68. Calc'd. for $C_{34}H_{42}N_6O_8.3.5CF_3COOH.0.5CH_3OH$: C, 46.82; H, 4.58; N, 7.62%. $\delta_H(CD_3OD)$: 2.14, 2.18 [4H, broad, s, CC*H*$_2$C (linker)]; 3.06, 3.16, 3.44, 3.48, 3.51, 3.61 [20H, m]; 3.31-3.44 [4H, broad]; 3.75 [4H, t, J = 15 Hz]; 7.79-7.82 [8H, m, (Ar*H*, Phth)]; $\delta_C(CD_3OD)$: 25.21 [C*C*H$_2$C (linker)]; 36.62 [N*C*H$_2$'s (linker)]; 51.15, 51.53, 52.92 [N*C*H$_2$'s (DO2A segment)]; 124.27, 133.38, 135.49 [Ar*C*, (Phth)]; 169.94[*C*=O].

3.2.6 Synthesis and characterization of L^{12}

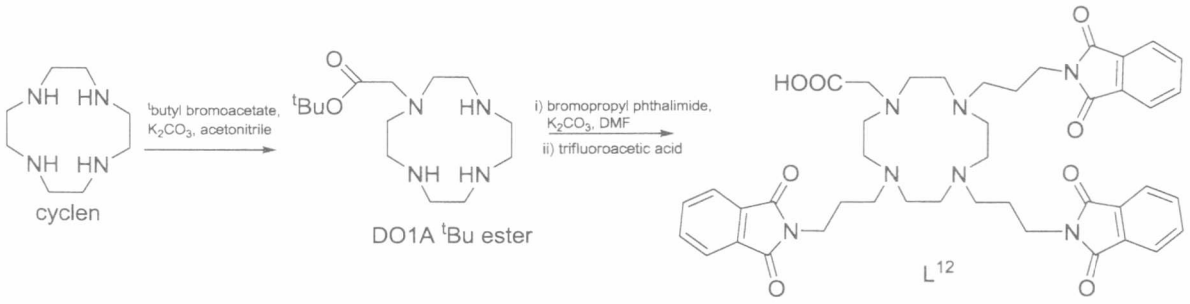

Scheme 16 Synthetic route to L^{12}

A round-bottomed flask was charged with a suspension of anhydrous acetonitrile suspension (30 cm^3) of 1,4,7,10-tetraazacyclododecane (0.82 g, 4.8 mmol) and finely ground anhydrous K_2CO_3 (0.66 g, 4.8 mmol). This was heated to 50-60°C under N_2. A solution of t-butyl bromoacetate (0.31 g, 1.6 mmol) in dry acetonitrile (10 cm^3) was then added dropwise. Thereafter, the suspension was heated at 60°C for 5 h under N_2 at which time a second portion of t-butyl bromoacetate (0.31 g, 1.6 mmol) in dry acetonitrile (10 cm^3) was added dropwise and the reaction mixture heated at 55-60°C for a further 15 h. The solution was filtered and the solvent was evaporated *in vacuo* to yield a colourless oil which was subjected to column chromatography (stationary phase - silica gel, eluent - CH_2Cl_2/MeOH/NH_3(0.88w/v)10:5:1 v/v/v; R_f 0.45-0.60), leaving a colourless oil as *N*-(carbo[1,1-dimethylethoxy]methyl)-cyclen (DO1A-t-butyl ester, 378.2 mg, 27% from cyclen). m.p. 147-149°C ES: 287.3 ([M+H]$^+$); Found: C, 58.68; H, 10.32; N,

19.42. Calc'd. for $C_{14}H_{30}N_4O_2$: C, 58.74; H, 10.49; N, 19.58%. $\delta_H(CDCl_3)$: 0.80-1.30 [1H, broad, s, N*H*]; 1.45, 1.47 [9H, s, CH_3's, t-butyl]; 2.30-3.30 [18H, broad]; $\delta_C(CDCl_3)$: 28.17, 28.20 [*C*H_3's, ^{t}Bu]; 45.24, 45.94, 46.05, 46.95, 51.75, 57.01 [N*C*H_2's]; 80.98 [*C*Me_3, ^{t}Bu]; 170.94 [*C*=O].

A round-bottomed flask was charged with an anhydrous DMF suspension (5 cm^3) of DO1A-t-butyl ester (0.36 g, 1.2 mmol), *N*-(3-bromopropyl)phthalimide (1.05 g, 3.92 mmol) and anhydrous K_2CO_3 (0.57 g, 4.1 mmol) was vigorously stirred under anhydrous conditions at RT for 12 days. The mixture was then decanted into dichloromethane (150 cm^3), washed with deionised water (6×100 cm^3) and saturated brine (1×100 cm^3), and dried over $MgSO_4$. The solvent was evaporated *in vacuo* yielded a yellow oil which was subjected to column chromatography (eluent - CH_2Cl_2/MeOH 8:1 v/v; desired fractions, R_f 0.60). The intermediate fractions were amalgamated as a hygroscopic oil. This was dissolved in dichloromethane solution (5 cm^3), and treated with trifluoroacetic acid (10 cm^3). The reaction mixture was stirred under N_2 at RT for 4.5 h, evaporated *in vacuo*. An acetone (2.5 cm^3) solution of the residue was added dropwide to diethyl ether (20 cm^3) and this was isolated by Büchner apparatus to give a crude solid. This precipitation procedure was repeated, followed by trituration of the separated solid in diethyl ether, yielded a creamy white solid (L^{12}, 85.2 mg, 6% from *N*-(carbo[1,1-dimethylethoxy]methyl)-1,4,7,10-tetraazacyclododencane). m.p. 94-97°C; ES: 793.5 ($[M+H]^+$); Found: C, 51.72; H, 4.45; N, 8.56. Calc'd. for $C_{43}H_{49}N_7O_8.3CF_3COOH$: C, 51.85; H, 4.59; N, 8.64%. $\delta_H(CD_3OD)$: 1.80, 1.94, 2.14 [6H, broad, m's, CC*H*$_2$C (linker)]; 2.35-4.20 [28H, broad]; 7.70-7.95 [12H, broad, (Ar*H*, phth)]; $\delta_C(CD_3OD)$: 23.99, 26.39, 28.81 [C*C*H_2C (linker)]; 35.59, 35.76, 35.92, 36.11, 36.73, 36.93 [N*C*H_2's (linker)]; 46.69, 50.74, 50.97, 51.51, 52.85, 53.12, 54.08, 54.77, 55.40 [N*C*H_2's (cyclen ring)]; 124.13, 124.16, 124.21, 124.24, 124.30, 124.40, 135.32, 135.43, 135.44, 135.46, 135.51 [Ar*C*, phth]; 133.33, 133.37 [Ar*C*, phth]; 169.84, 169.88, 169.92, 169.97, 175.49 [*C*=O].

3.2.7 Synthesis and characterization of L^{13}

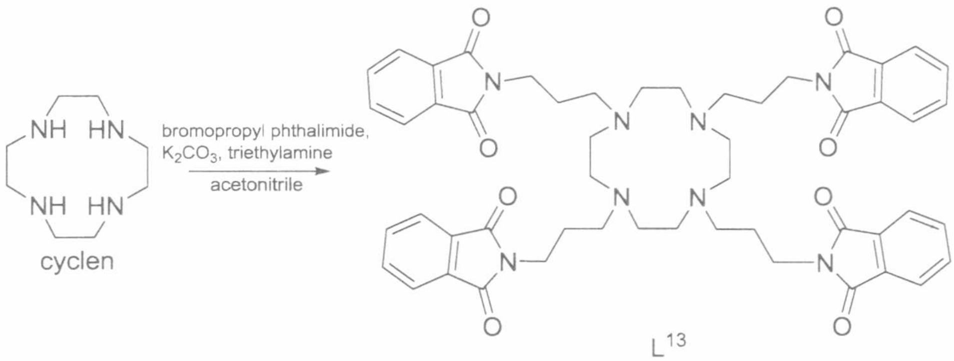

Scheme 17 Synthetic route to L^{13}

A round-bottomed flask was charged with an acetonitrile (50 cm^3) suspension of cyclen (515.6 mg, 3 mmol), triethylamine (6.072 g, 60.12 mmol) and anhydrous K_2CO_3 (301.1 mg, 2.18 mmol). An acetonitrile solution (20 cm^3) of *N*-(3-bromopropyl)-phthalimide (4.821 g, 17.99 mmol) was stirred under anhydrous conditions at 60°C. The mixture was stirred between 60~65°C for 7 days. Thereafter, the suspension was filtered using a Büchner apparatus. The filtrate was then evaporated *in vacuo*, and the residue was redissolved in dichloromethane (100 cm^3), washed with deionised water (3×100 cm^3), and dried over anhydrous $MgSO_4$. The residue was dissolved in methanol (3 cm^3) and diluted by deionised water (7 cm^3). The separated brown oil was isolated and dissolved in a minimal volume of chloroform (1 cm^3). This was diluted by diethyl ether (50 cm^3) and was left standing overnight. The final brown suspension was filtered using a Büchner apparatus to yield a straw coloured powder (L^{13}, 288.3 mg, 10% from cyclen). m.p. 108-111°C; ES: 921.56 ($[M+H]^+$); Found: C, 63.54; H, 6.30; N, 11.40. Calc'd. for $C_{52}H_{56}N_8O_8.3H_2O$: C, 63.87; H, 6.35; N, 11.46%. $\delta_H(CDCl_3)$: 1.77, 1.79 [8H, broad, s, CCH_2C (linker)]; 2,62, 2.64, 2.65, 2.80, 2,82, 2.83, 2.95, 3.09[24H, m]; 3.65, 3.68, 3.70, 3.71, 3.73, 3.74, 3.76 [8H, m]; 7.62-7.80 [16H, broad, m, (Ar*H*, phth)]; $\delta_C(CDCl_3)$: 26.94 [CCH_2C (linker)]; 36.15 [NCH_2's (linker)]; 49.31, 50.52, 52.39 [NCH_2's of cyclen)]; 123.05, 123.26, 123.40, 131.88, 131.92, 133.84, 133.95, 134.17 [Ar*C*, Phth]; 168.16, 168.26, 168.29 [*C*=O].

3.3 Results and discussion

3.3.1 Synthesis of intermediates: DO1A-t-butyl ester, DO2A-t-butyl ester, and DO3A-t-butyl ester

The synthetic procedures employed for cyclen, DO2A-t-butyl ester and DO3A-t-butyl ester have been described in the previous work.[173, 180] However, the method for DO1A-t-butyl ester does not follow previously reported procedures. Hence DO1A-, DO2A- and DO3A-t-butyl ester are discussed here.

3.3.1.1 Isolation of DO1A-t-butyl ester

DO1A-t-butyl ester was prepared using an excess (1.5 equivalents) of cyclen to give the 1:1 adduct with a ~27% yield. Product isolation was achieved by column chromatography, and the product was characterised by ^{1}H NMR spectroscopy, the spectrum revealing the anticipated integral ratio of 9:16 for resonances associated with t-butyl methyl protons and cyclen methylene protons respectively.

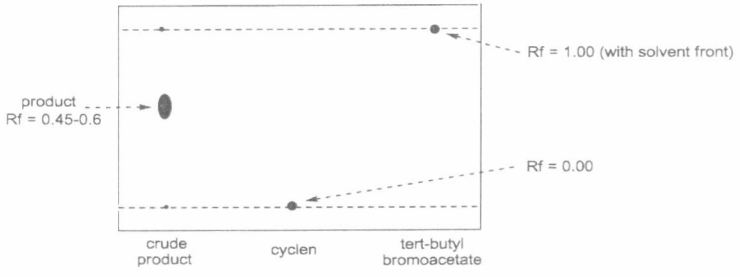

Figure 3.4 TLC results for isolating DO1A t-butyl ester

A typical TLC separation for a crude product mixture containing DO1A-t-butyl ester, cyclen and t-butyl bromoacetate, employing dichloromethane/methanol/0.88 ammonia (10:5:1, v/v/v) as eluent system, is shown in Figure 3.4. The structure of silica gel consists of a lattice of silicon and oxygen, exhibiting residual hydroxyl groups on the surface, accounting for much of its adsorptive properties.[181]

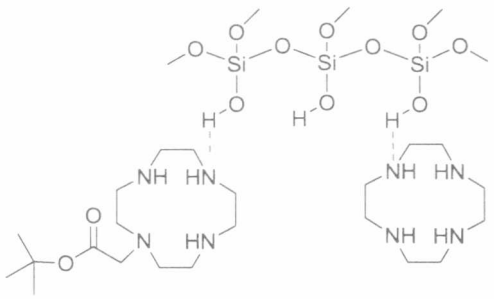

Figure 3.5 Interaction between sorbents and solutes

The desired product contains one primary and three secondary amine functions and therefore interacts strongly with silica-based stationary phases in chromatography columns and TLC plates (Figure 3.5).[182, 183] Therefore, ammonia (0.88 w/v) is added into the mobile phase system to move the compound off the baseline.

3.3.1.2 Synthesis of DO2A-t-butyl ester and DO3A-t-butyl ester

Both DO2A-t-butyl ester and DO3A-t-butyl ester were prepared as HBr salts in this work following the *Li* and *Wong's* method[184], and the *Schultze* and *Bull's* method respectively.[184] Therefore their synthesis and characterizations are discussed only briefly here.

For preparing DO2A-t-butyl ester, it was found that two mol equivalents of electrophiles were sufficient to generate the product. Interestingly, isomers such as the 1,7- disubstituted product were not generated by the method used in this work. This has been reported to be due to the selectivity and distribution of $CHCl_3$/triethylamine in the reaction mixture.[180] The final product was crystallized from acetone/water (9:1) and washed with a minimum amount of acetone.

An excess of the electrophile reagent was needed in order to generate the DO3A-t-butyl ester. In this work, 3.5 mol equivalents of t-butyl bromoacetate reagent were used. The product precipitated from a very concentrated DMA solution in 24 h.

These two intermediates show very similar NMR spectra to those associated with DO1A-t-butyl ester, in terms of the resonance of multiplets and associated splitting patterns. Differences in the spectra relate to the integral ratios between methyl

protons of the t-butyl group and methylene protons of the tetraazacyclododecane system. Detailed characterization of the HBr content in sample was deduced through microanalysis.

3.3.2 Synthesis of L^9

Ligands L^9 – L^{12} consist of a tetraazacyclodecane macrocyclic system derivatised at *N*-sites, with methyl carboxylate and *N*-alkylated phthalimide functions, giving rise to many shared spectroscopic feature. Therefore, the synthetic method and characterization of L^9 are discussed as a typical example.

As discussed in Section 3.3.1.2, the DO3A-t-butyl ester is prepared as an HBr salt. The decrease of *N*-site nucleophilicity in the cyclen is well-documented.[185] Hence removal of HBr is necessary for successful reaction. For this purpose a molar excess of K_2CO_3 (4.8 mol equivalents) is employed in anhydrous DMF. Because the condition of the alkaline mixture solution is achieved by K_2CO_3, the solvent must be anhydrous. Any water present in the DMF can dissolve K_2CO_3 and hydrolyse phthalimide under mild basic conditions.

The nucleophilic substitution reaction of the *N*-alkylated phthalimide function is considered to follow an S_N2 pathway. The electrophilic centre of the *N*-(3-bromopropyl)phthalimide reagent is a primary carbon centre, and not sterically hindered (Scheme 18).[186]

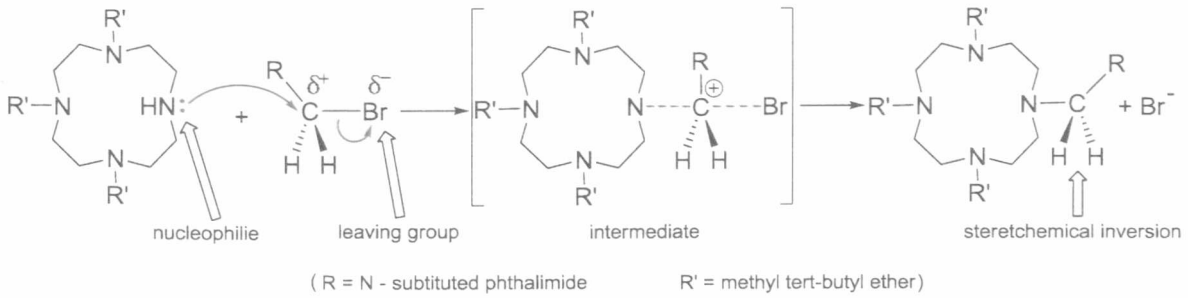

Scheme 18 S_N2 reaction pathway of synthesizing N-alkylated cyclen

S_N2 reaction profiles are facilitated in polar aprotic solvent media (e.g., DMF, DMSO).[187, 188] Such media stabilise activated complexes in which some degree of charge separation is observed, while attracting hydrogen from the amine function,

increasing the nucleophilicity of the nucleophile (Figure 3.6a).[189] Polar protic solvents (e.g., methanol) can solvate a nucleophile through H-bonding interactions, thereby stabilising the initial nucleophile state. (Figure 3.6b).[190]

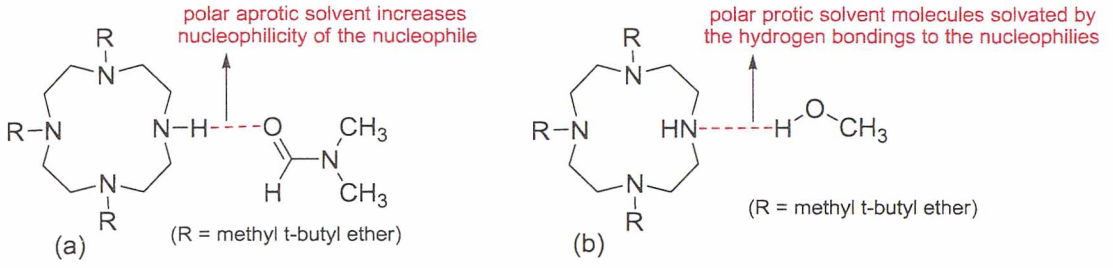

Figure 3.6 Stabilisation of activated complex by polar aprotic solvent and solvation of nucleophile by polar protic solvent

Crude products were successfully purified by column chromatography using dichloromethane/methanol (7:1, v/v) eluent systems. However, the amphipathic nature of these molecules results in surfactant behaviour and significant adsorption onto the stationary phase. This in turn influences yields to varying degrees according to factors including the surface area of the stationary phase. Hence the choice of stationary phase was a practical consideration in this work, and normal grade silica gel (e.g., 63 – 200 mesh particle sizes) was found to be optimal for this purpose. Desired fractions were identified by NMR and amalgamated for further use. Thereafter, t-butyl ester functions were subjected to removal with trifluoroacetic acid (Scheme 19).[191, 192]

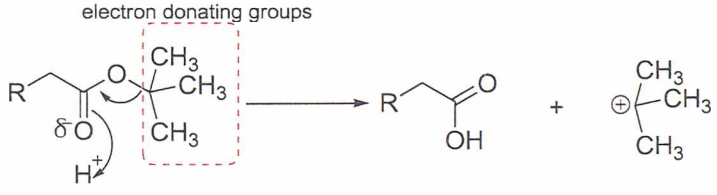

Scheme 19 Removal of t-butyl function by trifluoroacetic acid

According to the NMR spectroscopy and microanalysis results, the final product is a trifluoroacetate salt. The structure of such an adduct of 1,4,7-tris(carboxymethyl)-1,4,7,10-tetraazacyclododecane (H_3DO3A) has been investigated before (Figure 3.7).[193] The two protonated amine functions interact with the remaining two nitrogen atoms and the carboxylate carbonyl oxygen atoms.[185]

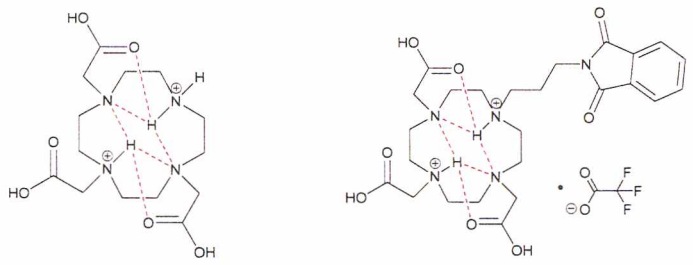

Figure 3.7 L^9 incorporating with trifluoroacetic acid

The final product (L^9) was obtained from trifluoroacetic acid, and no further neutralization procedure was carried out in this work. It is believed that an intramolecular H-bonding network coordinates $2H^+$ in the macrocyclic ring, generating the $[H_2L^9]^{2+}\cdot CF_3COO^-$ salt species (Figure 3.7).[185]

3.3.3 Synthesis of $L^{10\text{-}13}$

In all cases, *N*-substituents to the cyclen systems are appended by nucleophilic substitution reactions. $L^{10\text{-}12}$ were prepared in two steps, and derivatisation of the remaining free cyclen *N*-sites (in DO3A-, DO2A- and DO1A-t-butyl esters) with *N*-alkyl phthalimide is the first step. The crude products of this step were purified by column chromatography using dichloromethane/methanol eluent systems. Meanwhile, the second step involved removal of t-butyl functions and retention of phthalimide. L^{13} was prepared by one-step nucleophilic substitution reaction on the four N-sites of cyclen in acetonitrile/triethylamine at reflux temperature. Four phthalimide functions were appended onto the cyclen at the same time. The overall yields of these four compounds were 6-11%.

3.3.3.1 Synthesis of L^{10}

L^{10} differs from L^9 in relation to the ethyl linker used to append the cyclen and phthalimide functions. Hence, *N*-(2-bromoethyl)phthalimide reagent was used in the preparation scheme, which was identical to that of L^9 in all other aspects. The characterization of L^{10} is very similar to L^9. Hence, the mechanism of making this compound is analogous to Section 3.3.2.

3.3.3.2 Synthesis of L^{11}

Acetonitrile solutions of triethylamine were employed for this reaction. Acetonitrile is a polar aprotic solvent and a system with triethylamine as the base of choice was reported previously for generating 1,4 di-substituted cyclen.[180] Product retention on the column in chromatography separations proved problematic, and use of a high polarity eluent system (dichloromethane: methanol = 7:2, v/v) had no significant effect on retention.

3.3.3.3 Synthesis of L^{12}

L^{12} has the lowest yield (6%) out of all five macrocyclic ligands. In this case, when the crude product is isolated through column chromatography, the desired product is adsorbed to the stationary phase strongly. The chromatographic purification for this product takes longer than for $L^{9\text{-}11}$ and yields the lowest amount of product. According to the molecular structure, the only difference for these ligands is that the number of phthalimide functions appended onto the cyclen. It seems that the strength of interaction between compound and stationary phase for these ligands corresponds to the number of phthalimide functions present. This is consistent with the amphipathic nature of the phthalimide function, which results in its surfactant properties.

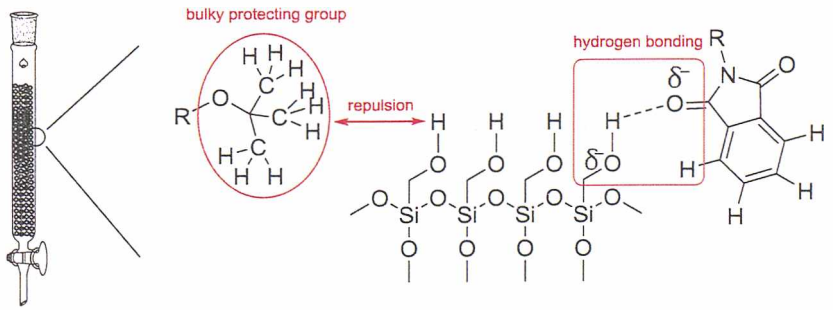

Figure 3.8 Interactions between functional groups and stationary phase

The purification process of column chromatography mainly depends on the polarity of the eluent and the adsorbents.[194] The surface of the silica gel is comprised of hydroxyl functions.[194] The electron donating carbonyl functions of phthalimide form hydrogen bonding with the hydroxyl function on the silica gel

surface (Figure 3.8).[195, 196] L^{12} has three phthalimide groups and exhibits the highest absorption with the stationary phase, resulting in lowest eluting yields. Meanwhile, t-butyl group is a bulky protecting group, which has relatively repulsion effect and lowest interaction with hydroxides (Figure 3.8).[197, 198] The high polarity methanol can somewhat dissolve silica gel,[199] therefore the highest proportion of methanol tried in this experiment is 30% (v/v).

3.3.3.4 Synthesis of L^{13}

L^{13} consists of 4 *N*-(bromopropyl)-phthalimide functions appended to the cyclen ring system. It has been previously noted in substitution reactions involving cyclen that the auxiliary base has an important role in achieving four *N*-alkylated reaction.[200] The four *N*-sites of cyclen can be alkylated by the same substituents in acetonitrile and triethylamine system in the presence of potassium carbonate.[180, 201] After 7 days, all the cyclen is fully alkylated with propylphthalimido functions. The purification procedure depends on the solubilities of L^{13} in different solvents. L^{13} is insoluble in deionised water and diethyl ether, while triethylamine and potassium bromide are soluble in water and unreacted excess *N*-(3-bromopropyl)phthalimide is soluble in diethyl ether (Scheme 20).[202]

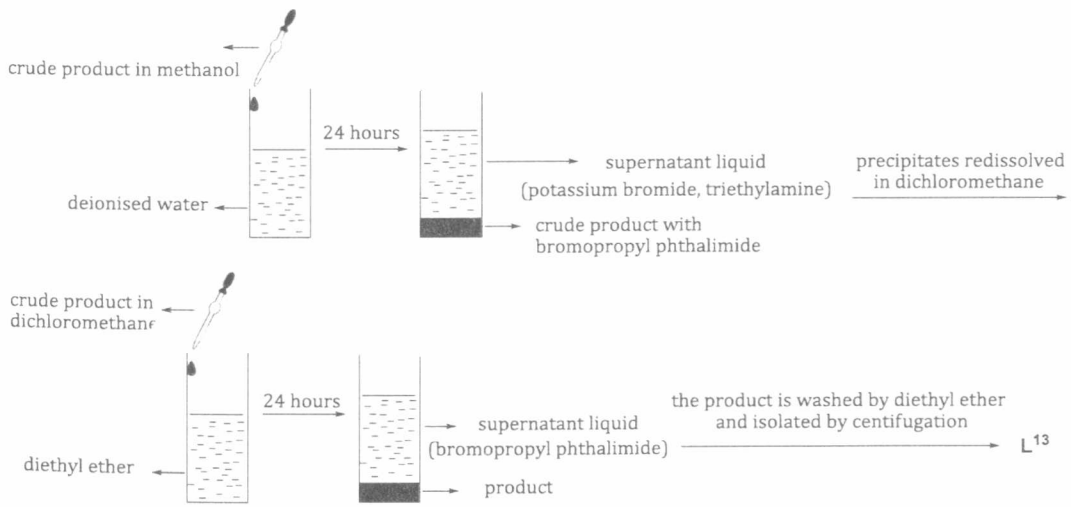

Scheme 20 Purification process of L^{13}

3.3.4 NMR characterizations

3.3.4.1 NMR characterization of DO1A-t-butyl ester

Prominent features in the ^{1}H NMR spectrum of DO1A-t-butyl ester are associated with the methylene groups of the alicyclic system and a t-butyl group. The resonances of the methylene protons do not give sharp splitting patterns (Figure 3.9). Poor resolution of multiplets in this region (δ 2.3 – δ 3.0 ppm) is due to bulky structure and non-rigid conformation associated with the alicyclic system.[203]

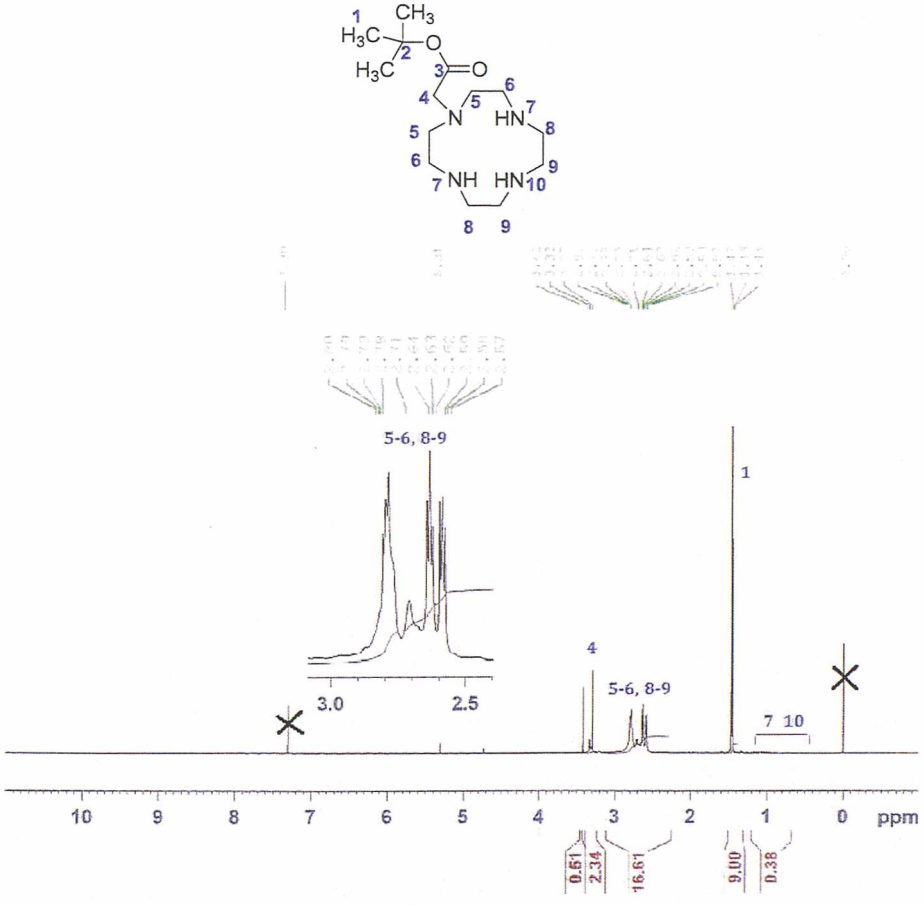

Figure 3.9 ^{1}H NMR spectrum of DO1A-t-butyl ester

The ^{1}H NMR spectrum of DO1A-t-butyl ester is shown in Figure 3.9. The sharp signals at δ 1.45 ppm and δ 1.47 ppm correspond to methyl protons of the t-butyl groups, exhibiting the anticipated 9H integral. A very broad peak at *ca.* δ 0.80 – δ 1.30 ppm with low intensity is assigned to NH protons.[204] Another distinctive resonance in the spectrum is located at δ 3.29 ppm, exhibiting a 2H integral, which is assigned to methylene protons, H^4.[184] The multiplet resonances between δ 2.57 –

δ 2.80 ppm, correspond to the methylene protons of the cyclen system, H^5, H^6, H^8 and H^9.

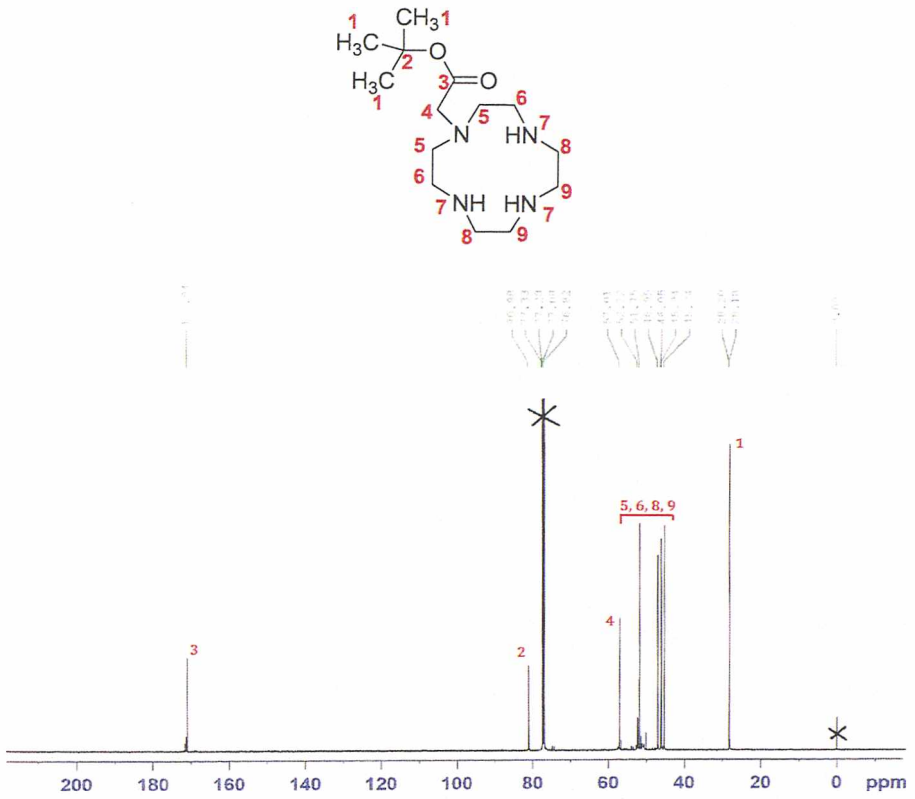

Figure 3.10 ^{13}C NMR spectrum of DO1A-t-butyl ester

The ^{13}C NMR spectrum of DO1A-t-butyl ester is shown in Figure 3.10. The NMR spectrum assignment for this product is referenced to the well-known DO3A-t-butyl ester.[179] The sharp signals at δ 28.17 ppm and δ 28.20 ppm are assigned to t-butyl carbon (C^1). The downfield resonance at δ 170.94 ppm of spectrum is assigned to the carbonyl carbon of C^3, which shows low intensity in the carbonyl carbon region of ^{13}C NMR spectrum. Another low intensity resonance at δ 80.98 ppm is assigned to quaternary carbon of the t-butyl group (C^2). The resonance at δ 57.01 ppm is assigned to the methylene bridge carbon (C^4). The peaks with resonances of δ 45.24, δ 45.94, δ 46.95 and δ 51.57 ppm are assigned to the rest methylene carbon of cyclen (C^5, C^6, C^8 and C^9).

The full NMR characterization of DO1A-t-butyl ester is shown below (Table 3.1).

Table 3.1 NMR assignments of DO1A-t-Bu ester

DO1A-t-butyl ester				
^{1}H NMR			^{13}C NMR	
	resonance (ppm)	number of protons		resonance (ppm)
H^1	1.45, 1.47	9	C^1	28.18, 28.20
H^4	3.33	2	C^2	80.98
$H^{7,10}$	0.80 - 1.30	1	C^3	170.94
$H^{5,6,8,9}$	2.57 - 2.80	16	C^4	57.01
			$C^{5,6,8,9}$	45.24, 45.94, 46.95, 51.57

3.3.4.2 NMR characterization of the precursor to L^9

L^9 was prepared from DO3A-t-butyl ester. The t-butyl ester intermediate, 1-(3-phthalimidopropyl)-4,7,10-tris(1-carbo-[1,1-dimethyl[ethoxymethyl)-1,4,7,10-tetraazacyclododecane was isolated by column chromatography and desired fractions were identified by ^{1}H NMR spectroscopy according to the ratio of integral values corresponding to methyl protons and aromatic protons in the spectrum, and then amalgamated for further use.

The ^{1}H NMR spectrum of the t-butyl ester precursor to L^9 in $CDCl_3$ is shown in Figure 3.11. In this case, the resonance at δ 1.45 ppm corresponds to methyl protons of the t-butyl functions, assigned to H^{15} and H^{19}. Another two multiplets located between δ 7.7 – δ 7.9 ppm are assigned to the four aromatic protons of the phthalimide function. The broad resonances observed in the region δ 1.8 – δ 3.7 ppm are assigned to methylene protons of cyclen and propyl functions. The integral ratio of ~27:4 for protons of these respective functions indicates that the desired product has been generated.

A triplet corresponding to the central methylene group of the propyl linker is clearly observed at ~δ 1.8 ppm. The broad resonance reflects poor resolution of the conformation associated with the cyclen ring system on the NMR time-scale, a feature enhanced by the presence of bulky t-butyl groups on substituent

functions.[205] However, the total integral in this region is in a reasonable agreement. Evidence of residual DMF and dichloromethane solvents were observed at δ 2.8, δ 2.9 and δ 5.3 ppm respectively (Figure 3.11).

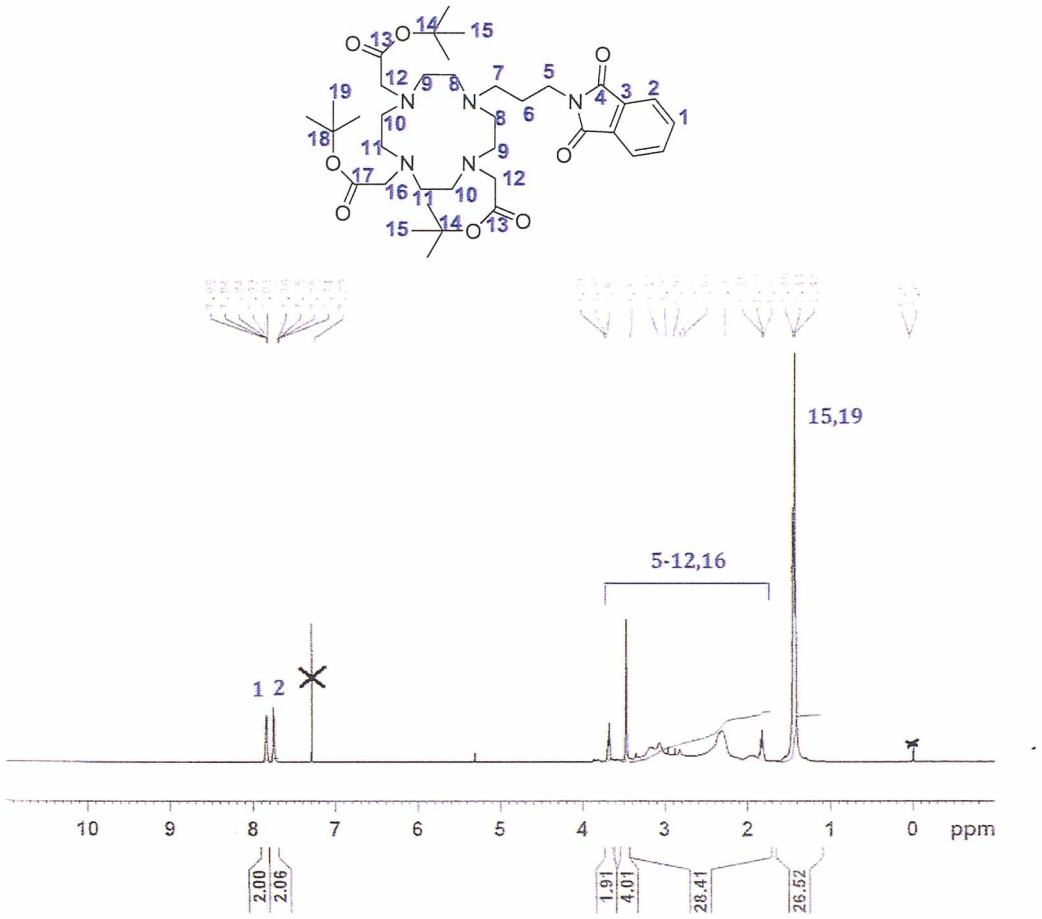

Figure 3.11 ^{1}H NMR spectrum of 1-(3-phthalimidopropyl)-4,7,10-tris(1-carbo-[1,1-dimethyl[ethoxymethyl)-1,4,7,10-tetraazacyclododecane

3.3.4.3 NMR characterization of L^9

As discussed and shown in Figure 3.7, the final product (L^9) is formed as a salt with trifluoroacetic acid.

The ^{1}H NMR spectrum of L^9 is shown in Figure 3.12. The resonances at δ 7.80 - δ 7.86 ppm are assigned to H^1 and H^2. This splitting feature of phthalimide aromatic protons has been discussed in Chapter 2. The relatively broad resonance at δ 2.17 ppm is assigned to protons of the central methylene function on the propyl linker (H^6).[206] The downfield resonance at δ 3.89 ppm is assigned to methylene protons

of the propyl linker (H^7). The triplet signal at δ 3.76 ppm is assigned to methylene protons of the propyl linker (H^5).[207] Resonances at δ 3.05 – δ 3.17 ppm and δ 3.39 – δ 3.49 ppm are assigned to the H^{8-12} and H^{14}.[208]

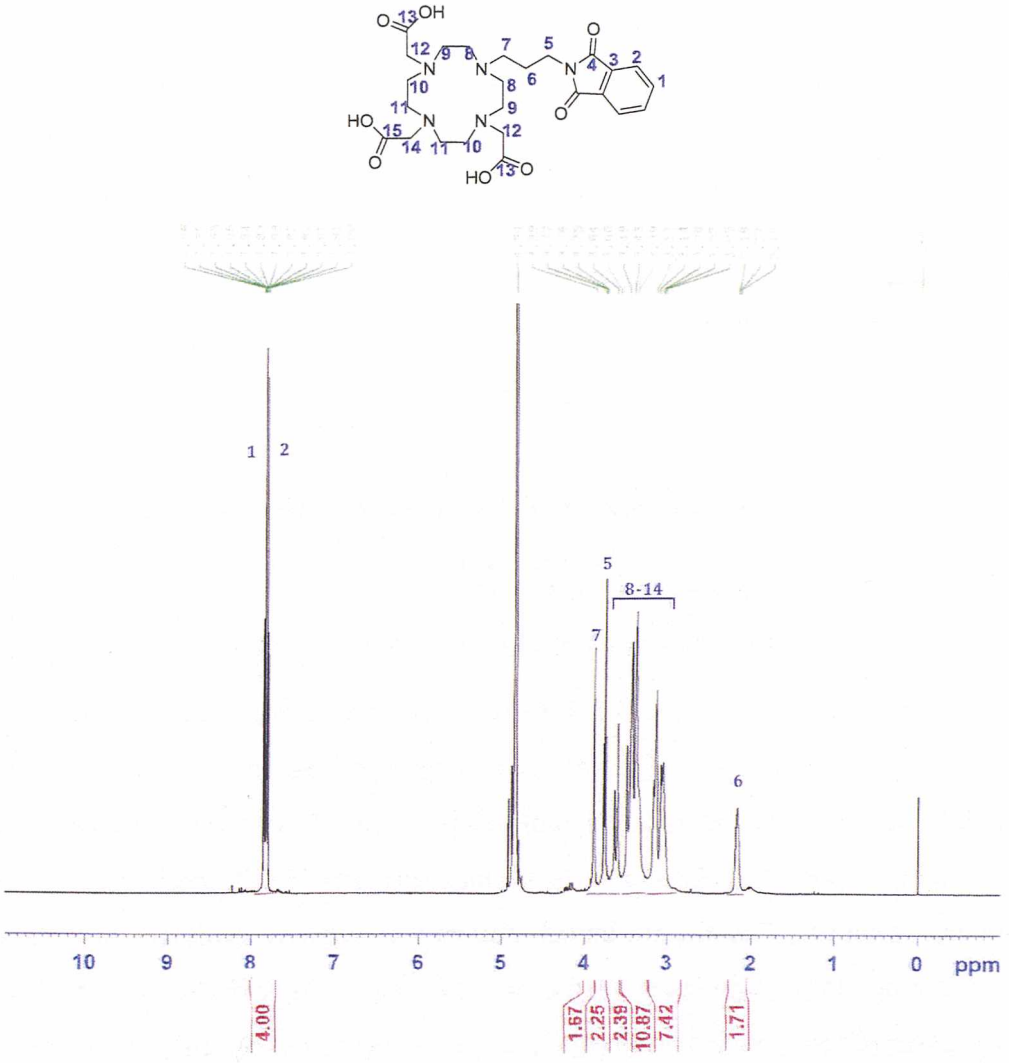

Figure 3.12 ^{1}H NMR spectrum of L^9

The ^{13}C NMR spectrum of L^9 is shown in Figure 3.13. The two quartets at δ 119 and δ 166 ppm are assigned to the alpha-carbon and carbonyl carbons respectively of TFA. While the ^{13}C spectrum illustrated is proton-decoupled, carbon-fluorine coupling is still observed.[209] The quartet at ~δ 119 ppm is a 1-bond coupling of 3 chemically equivalent fluorines with the alpha carbon. Meanwhile the quartet at ~δ 166 ppm is derived from a two-bond coupling involving the 3 equivalent fluorines with the adjacent carbonyl carbon.

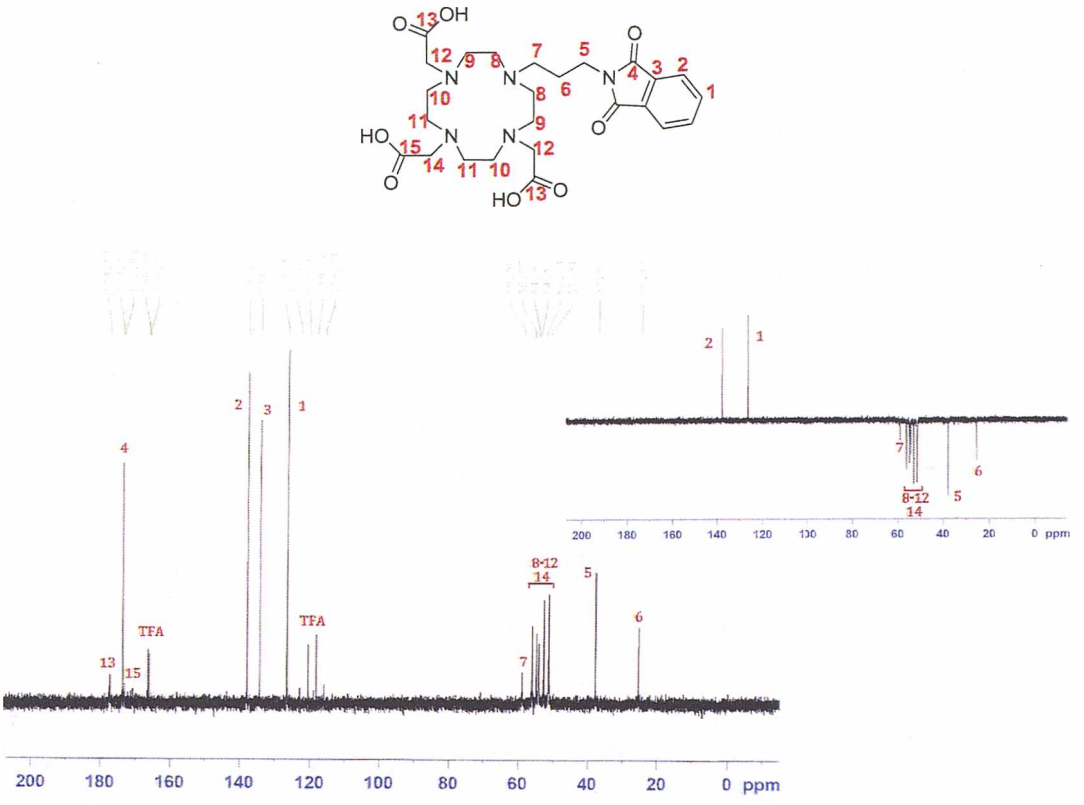

Figure 3.13 ^{13}C NMR spectrum of L^9 (insert with DEPT-135°)

Four typical phthalimide signals located at δ 173.37, δ 137.71, δ 134.11 and δ 126.35 ppm are observed in Figure 3.13. As has been well-characterised in analogous compounds in Chapter 2, these four resonances are assigned to C^4, C^2, C^3 and C^1 respectively.[138, 210] The resonances at δ 176.99 ppm and δ 172.88 ppm indicate that the three methyl carboxylate functions (C^{13}, C^{15}) are not chemically equivalent and are divided into two chemically non-equivalent sets. All other resonances correspond to the methylene carbon of the cyclen and the propyl linker, which have similar chemical environments and can not be identified exactly.

The structure of L^9 was further established by two-dimensional NMR spectroscopy, HMBC and HSQC, in which the coupling relationships between protons and carbons are illustrated.

The methylene protons of the linker between cyclen and phthalimide can be assigned by the HMBC experiment (Figure 3.14). In general, the spectrum exhibits characterising 2, 3 and sometimes 4 bond H-C connectivities (Table 3.2).[211, 212]

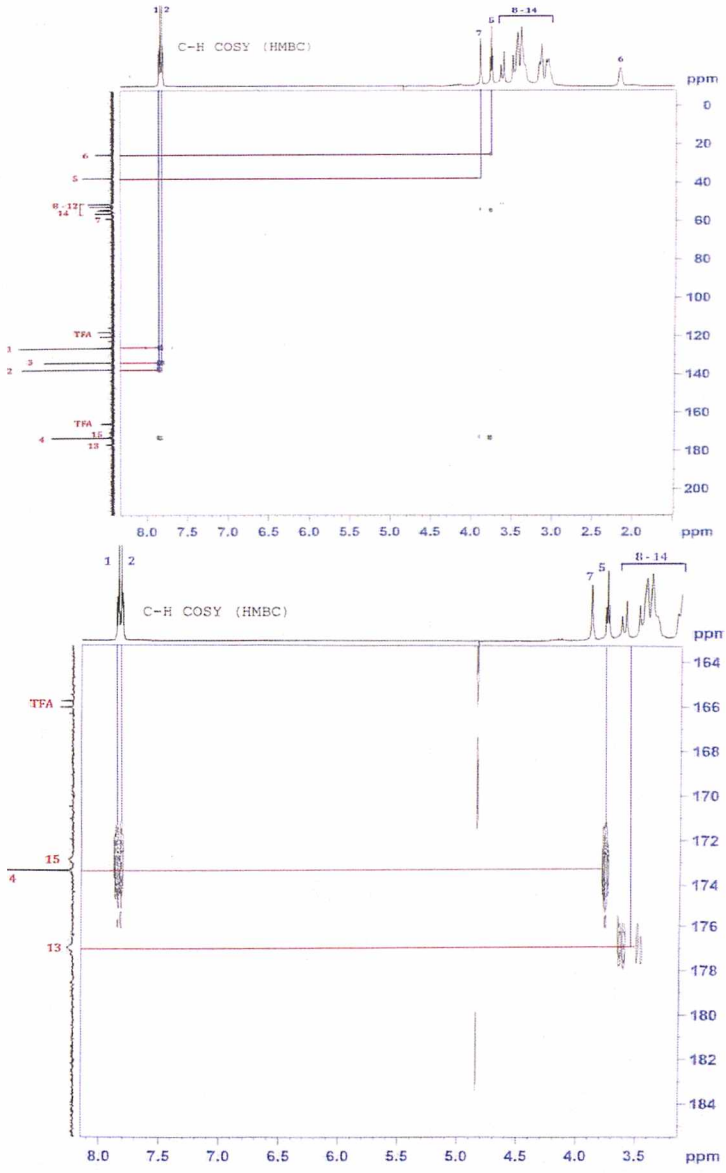

Figure 3.14 HMBC NMR spectra of L^9

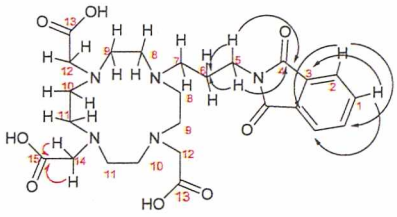

Table 3.2 HMBC coupling of L^9

Hydrogens	Carbons
H^1	$C^{2,3,4}$
H^2	$C^{1,2,4}$
H^5	$C^{4,6}$
H^7	C^5

The HSQC NMR spectrum (Figure 3.15) shows the coupling of carbon atoms with directly attached protons.

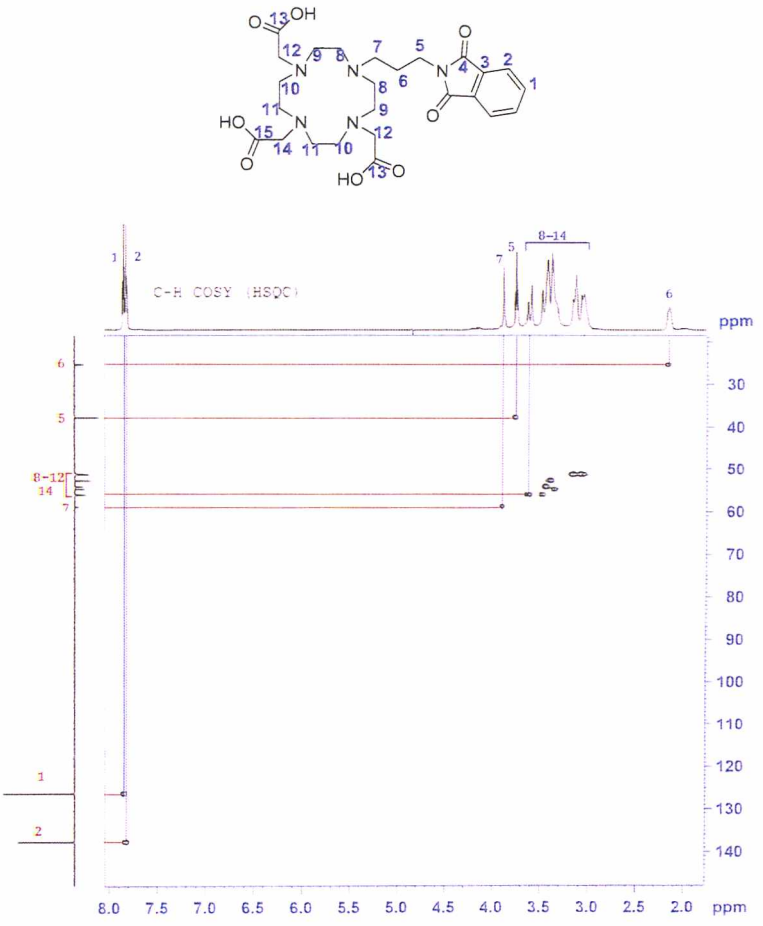

Figure 3.15 HSQC NMR spectrum of L^9

All anticipated one-bond C-H couplings were observed in the HSQC NMR spectrum (Figure 3.15). Examination of the structure of L^9 reveals that the resonances of $C^{8,9}$ are not well-distinguished from $C^{10,11}$. Although 1-bond C-H connectivities can be observed in HSQC, all the methylene protons and carbons have very similar chemical environments and are not defined.

The inter- and intra-molecular hydrogen bonding between phthalimide and carboxylic acid were reported before (Figure 3.16).[213,214, 215,216] This could also explain the poor resolution and complicated C-H couplings observed in HMBC and HSQC spectra.

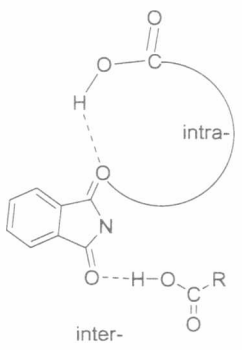

Figure 3.16 Intra and inter-molecular hydrogen bonding between carboxylic acid and phthalimide

3.3.4.4 NMR characterizations of L^{9-13}

Ligand L^{9-13} share many structural and spectral features. However, the splitting patterns observed in the ^1H NMR spectra of L^{10-13} are not as clear as is shown in L^9. This is due to the fact that the more phthalimide functions involved in the compound, the greater the size of the molecule. This influences signal resolution. Therefore only a few distinctive resonances were clearly assigned to the corresponding protons and carbons, including the middle methylene function of the propyl linker, phthalimide protons and carbonyl carbons. Table 3.3-3.7 show the characteristic NMR assignments for L^{9-13}.

Table 3.3 NMR assignments of L^9

L^9	^1H NMR		^{13}C NMR	
	Hydrogen atoms	Resonance (ppm)	Carbon atoms	Resonance (ppm)
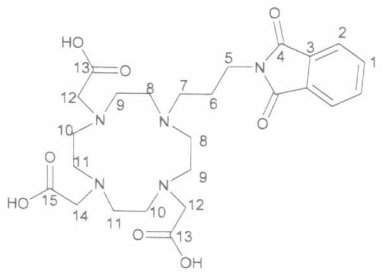	$H^{1,2}$	7.80 - 7.86	C^1	126.35
			C^2	137.71
	H^6	2.17	C^3	134.11
			C^6	25.04
	$H^{5,7-11}$ and $H^{12,14}$	3.00 - 3.89	$C^{5,7-11}$ and $C^{12,14}$	37.65, 51.34, 52.74, 54.17, 54.80, 56.07, 58.90
			$C^{4,13,15}$	172.88, 173.37, 176.99

Table 3.4 NMR assignments of L^{10}

L^{10}	^1H NMR		^{13}C NMR	
	Hydrogen atoms	Resonance (ppm)	Carbon atoms	Resonance (ppm)
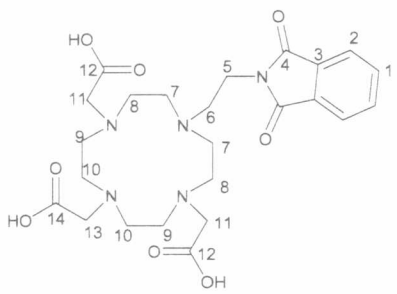	$H^{1,2}$	7.79- 7.88	C^1	124.42
			C^2	135.73
			C^3	133.28
	$H^{5,7\text{-}11}$ and $H^{12,14}$	3.16 - 3.94, 4.17	$C^{5,7\text{-}11}$ and $C^{12,14}$	33.54, 37.75, 52.90, 54.04, 54.15, 55.89
			$C^{4,13,15}$	162.36, 162.64, 169.62, 169.78

Table 3.5 NMR assignments of L^{11}

L^{11}	^1H NMR		^{13}C NMR	
	Hydrogen atoms	Resonance (ppm)	Carbon atoms	Resonance (ppm)
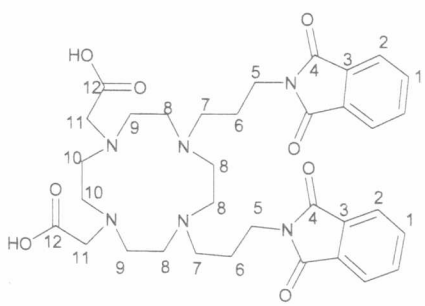	$H^{1,2}$	7.80 - 7.86	C^1	124.27
			C^2	135.19
	H^6	2.17	C^3	133.38
			C^6	25.21
	$H^{5,7\text{-}11}$	3.00 - 3.89	$C^{5,7\text{-}11}$	36.62, 51.15, 51.53, 52.92
			$C^{4,12}$	169.94

Table 3.6 NMR assignments of L^{12}

L^{12}	^1H NMR		^{13}C NMR	
	Hydrogen atoms	Resonance (ppm)	Carbon atoms	Resonance (ppm)
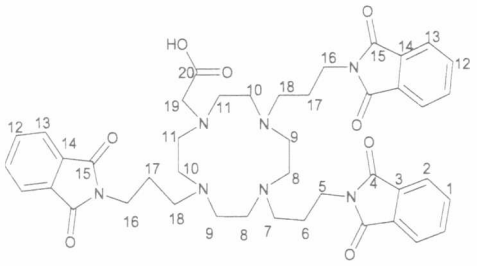	$H^{1, 2, 12, 13}$	7.70 – 7.95	$C^{1, 12}$	124.13, 124.16, 124.21, 124.24, 124.30, 124.40,
			$C^{2, 13}$	133.33, 133.37
	$H^{6, 17}$	1.80, 1.94, 2.14	$C^{3, 14}$	135.32, 135.43, 135.44, 135.46, 135.51
			$C^{6, 17}$	23.99, 26.39, 28.81
	$H^{5, 7-11}$ and $H^{16, 18, 19}$	2.35 – 4.10	$H^{5, 7-11}$ and $H^{16, 18, 19}$	35.59, 35.76, 35.92, 36.11, 36.73, 36.93, 46.69, 50.74, 50.97, 51.51, 52.85, 53.12, 54.08, 54.77, 55.40
			$C^{4, 15, 20}$	169.84, 169.88, 169.92, 169.97, 175.49

Table 3.7 NMR assignments of L^{12}

L^{13}	^1H NMR		^{13}C NMR	
	Hydrogen atoms	Resonance (ppm)	Carbon atoms	Resonance (ppm)
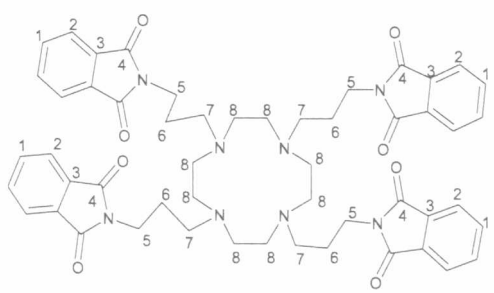	$H^{1, 2}$	7.62 – 7.80	C^1	123.05, 123.26, 123.40,
			C^2	133.84, 133.95, 134.17
	H^6	1.77, 1.79	C^3	131.88, 131.92
			C^6	26.94
	$H^{5, 7, 8}$	2.62 – 3.76	$C^{5, 7, 8}$	36.15, 49.31, 50.52, 52.39
			C^4	172.88, 173.37, 176.99

3.3.5 IR features of the ligands

3.3.5.1 IR features of DO1A-t-butyl ester

DO1A-t-butyl ester was a colourless oil, and it was prepared as a Nujol mull for IR analysis. The IR spectrum is shown in Figure 3.17. Nujol itself has a long chain hydrocarbon. It mainly shows six bands in infrared spectrum,[217] which are at 2955, 2925, 2854, 1463, 1377 and 438 cm^{-1}.

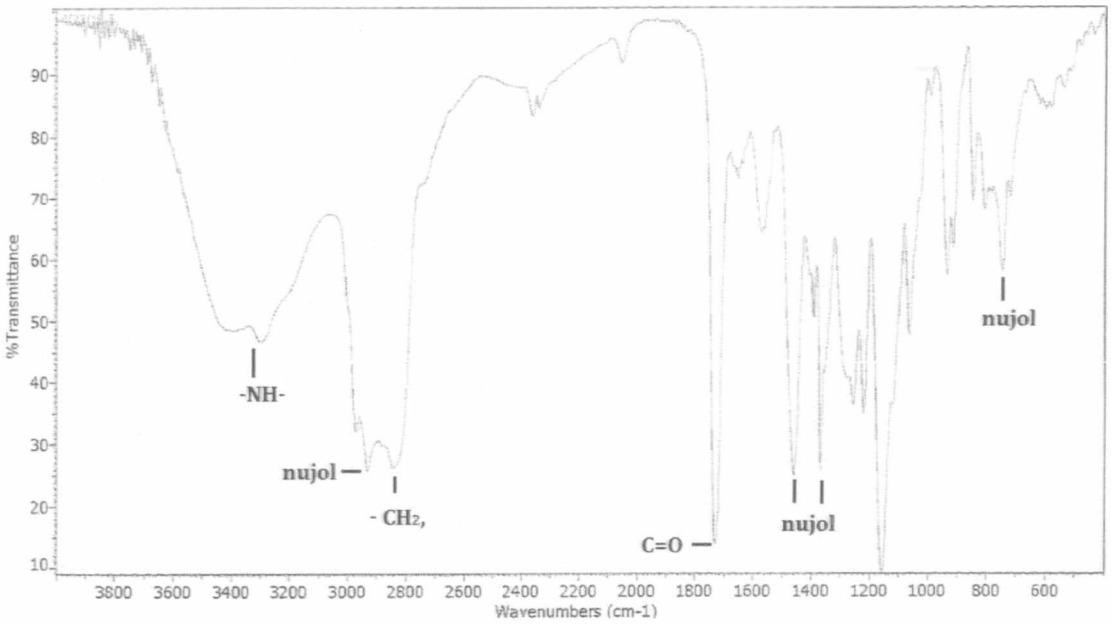

Figure 3.17 IR spectrum of DO1A-t-butyl ester

The detailed IR spectroscopy assignments of DO1A-t-butyl ester are shown in table 3.8.[218]

Table 3.8 IR assignments of DO1A-t-butyl ester[218]

Functional group	Band (cm^{-1})	Intensity	Remarks
$-CH_3$, $>CH_2$	2846	Strong	Usually 2 or 3 peaks overlapped
$-CH_3$, $>CH_2$	1459	Medium	Asymmetrical deformations
$-CH_3$	1392, 1367	Medium	Symmetrical deformations
$>N-H$	3299 - 3400	Weak	Unsymmetrical and the symmetrical stretching, secondary amine absorbs weakly
$>N-H$	1571	Weak	Sharp bending vibrations peak
C=O	1731	Strong	Sharp and strong stretch band dominates this region of the spectrum

3.3.5.2 IR features of L^9

All the major anticipated absorbance bands associated with the carboxylate function and phthalimido 5-membered ring imide structure are observed in the IR spectrum of L^9 (Figure 3.18). Our particular interest is the region near $\bar{\upsilon}$=1710 cm^{-1}, where a main frequency of C=O band is observed ($\bar{\upsilon}$=1710 cm^{-1}) in conjunction with two shoulders. In 1964, *Matsuo* reported three intense bands near 1600 cm^{-1} in the IR spectrum of potassium phthalimide,[219, 220] and these were confirmed and characterised by *Hase*[221] as 1587 cm^{-1} for vibrational carbonyl band; and 1596 and 1610 cm^{-1} for phthalimide ring stretching.[222, 223] However, this absorbance pattern is not as clearly observed in the spectrum of L^9 in which the phthalimido frequency of C=O overlap with those of the carboxylic acid function.[215] In general the frequency of C=O for N-alkylated phthalimide derivatives occur as a strong absorption, between $\bar{\upsilon}$=1730-1645 cm^{-1}.[138, 161] The results obtained in this work is consistent with the work investigated by *Matsuo* and *Hase*.

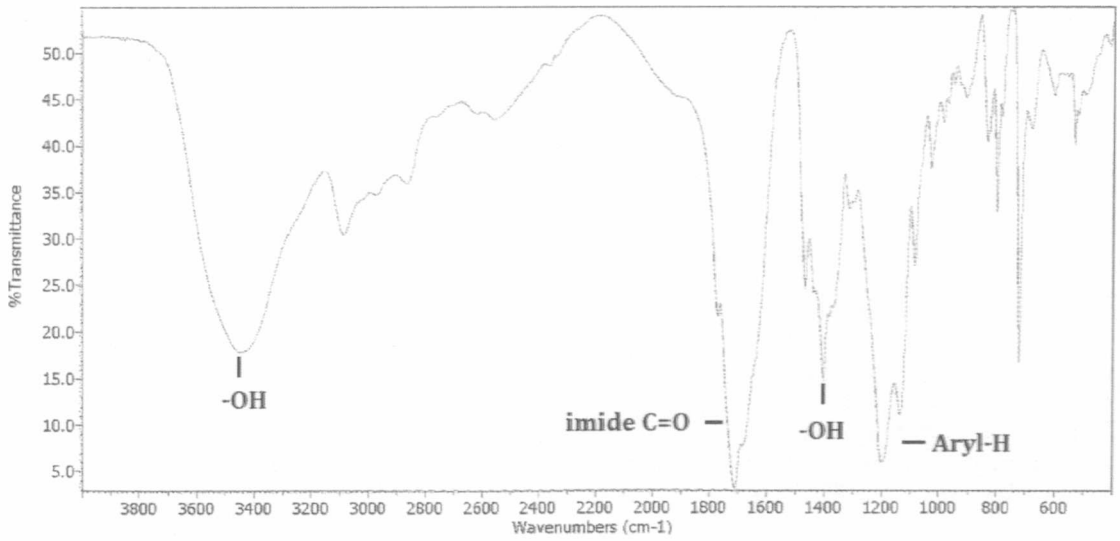

Figure 3.18 IR spectrum of L^9

The detailed assignments for the IR spectrum of L^9 are recorded in Table 3.9.

Table 3.9 IR assignments of L^9

	Band (cm^{-1})	Intensity	Remarks
-OH	3417, 1403	strong	Sharp and usually broad, OH bending vibrations
Aryl -H	800, 1468	weak, medium to weak	Usually two stretching bands for unfunctionalised C - H groups and very weak aryl - H in the same region, C-H bending vibrations
Five-ring imide C=O	1710	strong	Strong carbonyl stretching bands[162]
Aryl C-H	1086	medium to weak	The bands due to C-H in-plane ring bending vibrations, interacting with -C stretching vibrations[161]
Aryl C=C	1468	medium to weak	C = C alkenes of aromatics, usually very weak and more than one band
Carboxylate C=O	1710	strong	Very sharp of this peak dominates this region of the spectrum

3.3.5.3 IR features of L^{9-13}

The IR spectroscopy results of L^{10-12} are very similar; the characteristics of these compounds are corresponding to carboxylic acid and phthalimide groups. The three products, L^{10-12}, show the same characteristic bands as L^9. However, the band around 1710 cm^{-1} corresponding to phthalimide groups is the only distinctive peak which determines the generation of the phthalimide carbonyl of L^{13}. The detailed IR data of L^{9-13} are shown in Table 3.10.

Table 3.10 IR correlation table of L^{9-13}

	Band (cm^{-1})					Intensity
	L^9	L^{10}	L^{11}	L^{12}	L^{13}	
-OH	3417, 1403	3422, 1426	3418, 1402	3417, 1400	-	strong
Aryl -H	800, 1468	807, 1456	800, 1468	721, 1468	720, 1466	weak, medium to weak
Five-ring imide C=O	1710	1716	1709	1710	1708	strong
Aryl C-H	1086	1092	1136	1132	1035	medium to weak
Aromatic C=C	1468	1456	1468	1468	1466	medium to weak
Carboxylate C=O	1710	1716	1709	1710	1708	strong

3.3.6 Mass spectrometer features

3.3.6.1 Mass spectrometer features of L^9

The positive EI mass spectrometer result of L^9 (Figure 3.19) shows a relative molecular mass of 534.37. The obtained relative mass is the $[M+H]^+$ of L^9, which is also the base peak in the spectrum. However, another peak of sodium ionised molecule of L^9 ($[M+Na]^+$) is observed in the spectrum as well. The ionisation process in mass spectrometer can be achieved by ion attachment ionisation, employing H^+ and Na^+ ions.

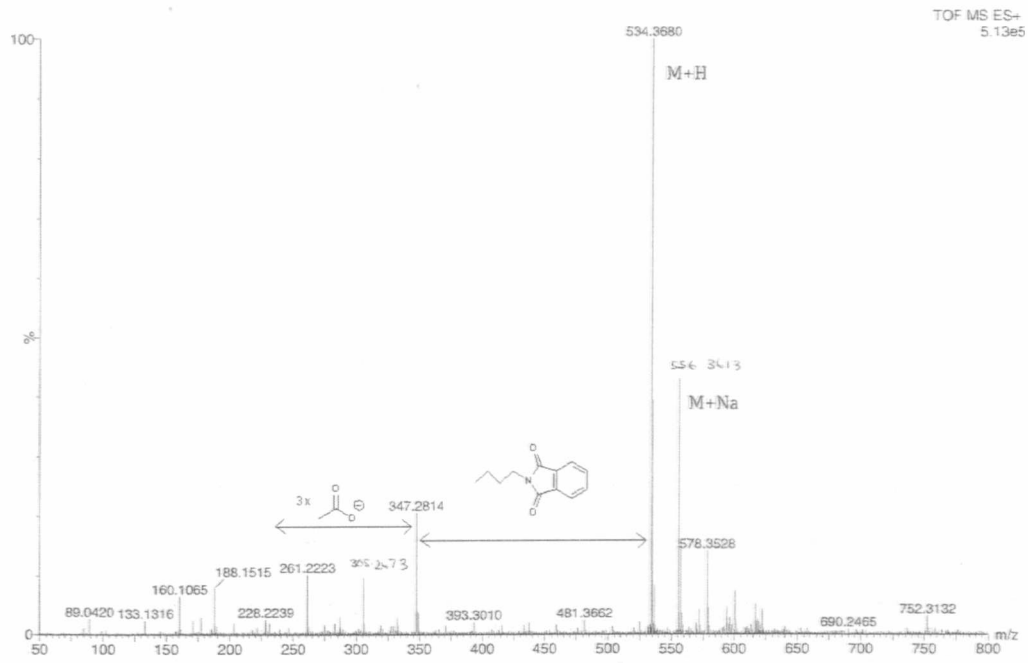

Figure 3.19 Mass spectrum of L^9

Due to the ionization by H^+ and Na^+ ions, both $[M+H]^+$ and $[M+Na]^+$ of L^9 are observed in the spectrum. A fragment of the propyl-phthalimide function is also observed. Three carboxylate functions are fragmented while an m/z value of 228.22 is observed. Hence the functional groups of L^9 are generally confirmed by these fragmentations.

3.3.6.2 Mass spectrometer characterizations of L^{9-13}

The mass spectrometer results of L^{9-13} were obtained by positive ES experiment. The relative molecular mass observed for all these compounds correspond to proton ionised $[M+H]^+$ molecules (Table 3.11).

Table 3.11 Mass spectrometer results of L^{9-13}

	L^9	L^{10}	L^{11}	L^{12}	L^{13}
Expected molecular mass	533.5	519.5	662.7	791.9	921.1
Observed relative molecular mass $(M + H)^+$	534.4	520.2	663.4	793.5	921.6

By analyses of fragment peaks, it is possible to clearly identify the number of phthalimide and carboxylate groups present in each ligand structure.

3.4 Conclusion

Herein five novel macrocyclic compounds, L^{9-13}, were synthesized. All these compounds were prepared through nucleophilic substituent reactions in polar aprotic solvent. L^{9-12} were isolated from column chromatography, by eluting by dichloromethane/methanol mixture mobile phase. Their t-butyl functions were removed in TFA, yielding the compunds as trifluoroacetic acid salts. L^{13} was isolated from the mixture according to its solubility in methanol-water solution and diethyl ether. The average yields of the compounds were between 6% - 14%, and the methodology used in the Chapter was validated by the analyses. All these five novel compounds were characterised by ^1H and ^{13}C NMR spectroscopy, IR spectroscopy, mass spectrometer, microanalysis and melting point analysis.

Chapter Four pH dependent Tb^{3+} and Eu^{3+} complexes

4.1 Introduction

In recent years, the use of the modulation of lanthanide luminescence has led to the development of molecular switches.[224] Ideally, they are developed on the basis of the construction of chromophore-receptor moieties. The operating principle of these molecular logic gates is the transmission between inputs and outputs.[23] Generally, such luminescence-based logic operations have been successfully reported as detectors in chemical, biological and environmental fields.[225] One of the most widely investigated aspects is pH sensors.[226]

In this work, all the studies were focused on the modulation of luminescence at different pH values. Two of the complexes derived from L^3 have been studied before.[110] Both of the ligands were acyclic polydentate systems, utilizing the phthalimide or phthalamate as a chromophore to sensitize lanthanide ions (Figure 4.1). One was a partially hydrolysed compound from L^3, which had one phthalimide function and one phthalamate function (compound **12**). The other ligand was a fully hydrolysed compound from L^3, which had two phthalamate functions (L^4).

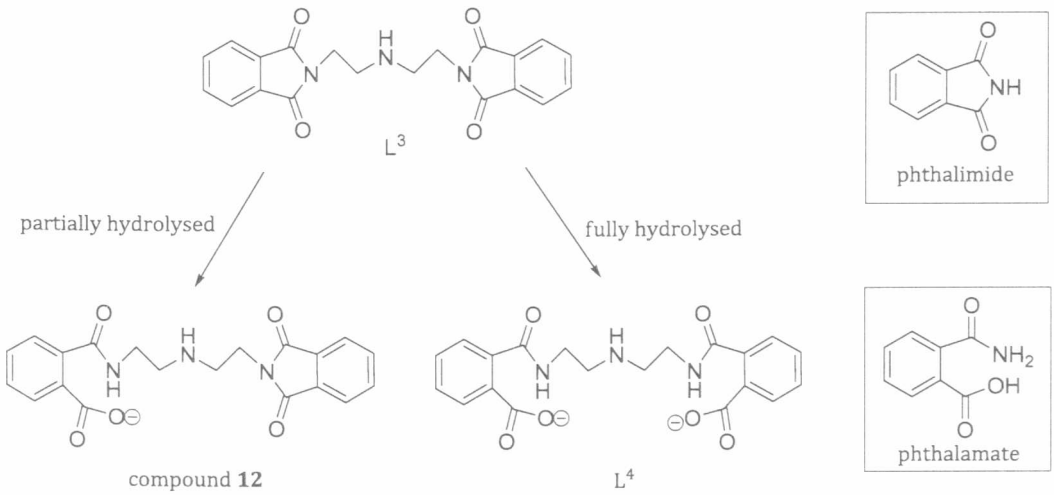

Figure 4.1 Partially hydrolysed compound from L^3 (left), and its fully hydrolysed compound (right)

The work from the previous investigation showed that phthalamate functions transferred energy more efficiently than phthalimide functions. A L^4-based Tb^{3+} complex showed luminescence at RT,[227] but this was partially quenched through

metal-to-ligand energy back transfer. According to the previous investigation of L^4, we firstly hypothesized that the three new phthalamate-based compounds, L^2, L^6 and L^8 would perform as good organic chromophores to sensitize lanthanide ions.

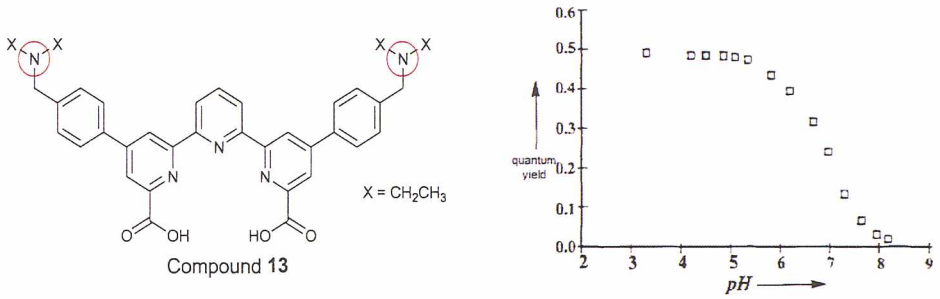

Figure 4.2 Structure of compound **13** and the quantum yield against pH of its Tb^{3+} complex

When lanthanide complexes act as pH sensors, the switching process is predominantly dominated by PET.[69, 228] *de Silva* has reported a pH dependent molecular switch of [Tb(**13**)]$^+$ (Figure 4.2).[95] The complex was excited at $\lambda_{285\,nm}$ and showed strongly pH sensitive emission for the $^5D_4 \rightarrow {}^7F_5$ transition.[96] [Tb(**13**)]$^+$ displayed varying quantum yields as a function of pH (3% and 49% at pH 8 and pH 3 respectively).[95] In their unprotonated forms, the amine functions quench the excited states of the antennae via a PET mechanism. However, upon protonation of the amine functions, the PET quenching was removed, causing enhanced emission. Therefore the second hypothesis in this Chapter is that the pH may cause different efficiency of energy transfer, possibly via a PET mechanism, if amine functions are present in the ligand system.

However it is known that acyclic chelates have low denticity, leading to low thermodynamic stability of the resultant complexes, thus limiting their use in further practical applications.[229] One solution to this is coupling the chromophore to a macrocyclic unit so as to ensure high thermodynamic stability in the complexes and circumvent this problem. DO3A, DO2A, and DO1A systems are known to have high thermodynamic stabilities.[230] Five phthalimide derived macrocyclic compounds were prepared as described in Chapter 3. Four of the ligands, L^{9-12}, are water soluble and their phthalimide functions can be hydrolysed to phthalamates and so their Tb^{3+} complexes may have application as pH sensors: this is the third hypothesis of this Chapter. L^{13} is not soluble in water, hence

luminescence studies of its Tb^{3+} complex were performed on the tetraphthalamate form of L^{13}.

4.2 Experimental

4.2.1 General materials

All reagents and starting materials were used as purchased from commercial sources and used without further purification, unless otherwise noted. Terbium(III) chloride hexahydrate 99.9% and europium(III) nitrate pentahydrate 99.9% were purchased from the Sigma-Aldrich Company Ltd, UK. Ligands were synthesized according to the methods described in Chapter 2 and 3.

4.2.2 General instruments

NMR spectra were recorded on a Bruker Avance - 500MHz (^1H, 500.1 MHz; ^{13}C, 125.8 MHz, Bruker Corporation UK) NMR spectrometer. Both ^1H and ^{13}C NMR spectra were recorded in D_2O with 3-(trimethylsiyl)propionic-2,2,3,3-d_4 acid sodium salt as internal reference if required. Resonances (δ) are expressed in ppm and J values are given in Hz.

UV-Vis spectrophotometry was measured using a UV-1800 Shimadzu spectrophotometer (Shimadzu Scientific Instruments, US).

A semi micro prepared pH electrode was used for pH measurements, connected to a Jenway 3510 pH meter (Fisher Scientific Ltd, UK).

Luminescence measurements were carried out using a LS-50 spectrometer (Perkin Elmer Ltd, UK).

The luminescence measurements were measured by operating the spectrometer in phosphorescence mode with a 0.00 ms delay time, 200 ms cycle time, 10.00 ms gate time and a flash count of 5. All the emission spectra utilized a 350 nm cut-off of the standard photomultiplier type and an automatic photomultiplier voltage as given by the instructions in the operators' manual. All emission spectra of these

metal complex solutions were measured in a fluorescence quartz cuvette (45 mm × 12.5 mm × 12.5 mm) and excited at λ_{272nm} (10 and 4 mm path lengths for excitation and emission, respectively).

4.2.3 Luminescence studies of acyclic phthalamate-based Tb^{3+} complexes $[Tb(L^2)_2]^-$, $[Tb(L^4)_2]^-$, $[Tb(L^6)_2]^-$ and $[Tb(L^8)_2]^-$

4.2.3.1 Solution preparations of L^1 and L^2

A stock solution of L^1 ($5x10^{-4}$ M) was prepared in chloroform. An aqueous stock solution of L^2 was prepared as $1x10^{-3}$ M. UV spectra of these two solutions were recorded.

4.2.3.2 Molar extinction coefficient measurements of L^{1-8}

Stock solutions of phthalimide derivatives (L^1, L^3, L^5 and L^7) were prepared in chloroform as $5x10^{-4}$ M and then their concentrations were diluted to $2.5x10^{-4}$ M, $1.25x10^{-4}$ M, $6.25x10^{-5}$ M and $3.125x10^{-5}$ M. Stock solutions of phthalamate derivatives (L^2, L^4, L^6 and L^8) were prepared in deionised water as $1x10^{-3}$ M and then their concentrations were diluted to $5x10^{-4}$ M, $2.5x10^{-4}$ M, $1.25x10^{-4}$ M and $6.25x10^{-5}$ M. The molar extinction coefficients of these four phthalimide derivatives were measured by calculating the slope of the absorbance against concentration plot.[231]

4.2.3.3 Metal-to-ligand ratio studies of Tb^{3+}-acyclic complexes

The most prevalent metal-to-ligand ratio in solution was obtained using a metal-to-ligand titration and recording the luminescence spectrum. Phthalamate-based acyclic ligands (L^2, L^4, L^6 and L^8, $1x10^{-3}$ M) were prepared in HEPES (2-[4-(2-hydroxyethyl)-1-piperazine]-ethane sulfonic acid) buffer solution ($5x10^{-2}$ M) at pH 6. An aqueous solution of Tb^{3+} ($1x10^{-3}$ M) was prepared in HEPES ($5x10^{-2}$ M) at pH 6. Hereafter, the solution of Tb^{3+} was mixed with that of each ligand in differing volumes: 1:0, 1:0.5, 1:1, 1:2, 1:3, 1:4, 1:5 and 1:6. All these test solutions were then

diluted by HEPES buffer to ensure a fixed concentration of Tb^{3+} ($1x10^{-4}$ M). The luminescence intensities of Tb^{3+} at $\lambda_{544\ nm}$ were collected for each test solution. And the results were recorded from three independent measurements.

4.2.3.4 Luminescence studies of acyclic-based Tb^{3+} complexes $[Tb(L^2)_2]^-$, $[Tb(L^4)_2]^-$, $[Tb(L^6)_2]^{3-}$ and $[Tb(L^8)_2]^-$

Solutions were prepared using a metal-to-ligand ratio of 1:2, as obtained from Section 4.2.3.3. The luminescence spectra of these four complex solutions were recorded.

4.2.3.5 pH dependent studies of $[Tb(L^2)_2]^-$, $[Tb(L^4)_2]^-$, $[Tb(L^6)_2]^{3-}$ and $[Tb(L^8)_2]^-$

The complex solutions were prepared by mixing Tb^{3+} and each ligand in deionised water. The concentration of Tb^{3+} in each test solution was fixed at $1x10^{-4}$ M. The pH of these four complex solutions ($[Tb(L^2)_2]^-$, $[Tb(L^4)_2]^-$, $[Tb(L^6)_2]^{3-}$ and $[Tb(L^8)_2]^-$) was initially adjusted to *ca.* 3.5 by addition of HCl ($1x10^{-2}$ M). Hereafter, the pH was increased using NaOH ($1x10^{-2}$ M). The luminescence spectra of each complex solution at various pH values (*ca.* 3.5, 4, 5, 6, 7, 8, 9, 10 and 11) were recorded. Both excitation and emission slit widths were set at 5 nm. A curve of luminescence intensity against pH was plotted for $[Tb(L^2)_2]^-$, $[Tb(L^4)_2]^-$, $[Tb(L^6)_2]^{3-}$ and $[Tb(L^8)_2]^-$.

4.2.3.6 Lifetime measurements of $[Tb(L^2)_2]^-$, $[Tb(L^4)_2]^-$, $[Tb(L^6)_2]^{3-}$ and $[Tb(L^8)_2]^-$

$Tb(L^2)_2]^-$, $[Tb(L^4)_2]^-$, $[Tb(L^6)_2]^{3-}$ and $[Tb(L^8)_2]^-$ were prepared in HEPES buffer ($5x10^{-2}$ M) solutions at pH *ca.* 6. The concentration of Tb^{3+} in each test solution was fixed at $1x10^{-4}$ M. The luminescence intensity at $\lambda_{544\ nm}$ of Tb^{3+} was measured with various delay time (0.00 – 2.00 ms). A plot of luminescence intensity against delay time was recorded for each complex solution and the lifetime (in ms) was calculated as the reciprocal of rate constant derived from these curves. For each

complex solution, the experiment was repeated under the same conditions using D_2O in place of deionised water. The reported lifetime values resulted from three independent measurements.

4.2.4 Luminescence studies of macrocycle-based Tb^{3+} complexes

The macrocycle complex solutions were prepared by mixing Tb^{3+} and each ligand in a 1:1 ratio. The concentration of each test solution was fixed at 6.25×10^{-5} M. The pH of the solutions was increased using NaOH (1×10^{-3} – 5×10^{-5} M) and decreased using HCl (1×10^{-3} – 5×10^{-5} M). Luminescence spectra were recorded at a series of different pH values.

4.2.4.1 Molar extinction coefficients measurements of phthalimide-based macrocycles (L^{9-12}) and phthalamate-based macrocycles (L^{9H-13H})

Stock solutions of L^{9-12} and L^{9H-13H} were prepared in deionised water as 6.25×10^{-5} M and then diluted to 3.13×10^{-5} M, 1.56×10^{-5} M, 7.812×10^{-6} M and 3.91×10^{-6} M. The molar extinction coefficients were measured by calculating the slope of the plot of absorbance against concentration.[231]

4.2.4.2 Luminescence studies of $[TbL^9]$, $[TbL^{10}]$, $[TbL^{11}]^+$ and $[TbL^{12}]^{2+}$

Complex solutions were prepared by mixing Tb^{3+} (5×10^{-3} M) and each macrocyclic ligand (L^{9-11}, 5×10^{-3} M; L^{12}, 2.5×10^{-3} M) in deionised water. The metal-to-ligand ratio for these four Tb^{3+} complexes was 1:1. The solutions were then diluted by deionised water to achieve the desired test concentrations of 6.25×10^{-5} M. The initial pH of these test solutions was observed to be *ca.* 3 – 4. This was then adjusted with NaOH (1×10^{-3} – 5×10^{-5} M). Luminescence spectra of all the solutions were recorded by excitation at $\lambda_{272\ nm}$. Both excitation and emission slit widths were set at 2.5 nm. L^{13} was not soluble in deionised water. Hence its luminescence spectrum was not measured at this stage.

4.2.4.3 Luminescence studies of $[TbL^{9H}]^-$, $[TbL^{10H}]^-$, $[TbL^{11H}]^-$, $[TbL^{12H}]^-$ and $[TbL^{13H}]^-$

Ligands L^{9H-13H} were obtained by hydrolysing their phthalimide-based ligands (L^{9-13}) with NaOH. The concentrations of these five test solutions were prepared at $6.25x10^{-5}$ M in deionised water. The initial pH of these test solutions was at *ca.* 11 – 12. This was then adjusted with HCl ($1x10^{-3}$ – $5x10^{-5}$ M). Luminescence spectra of all the solutions were recorded by excitation at $\lambda_{272\ nm}$. Both excitation and emission slit widths were set at 2.5 nm.

4.2.4.4 Luminescence studies of $[EuL^9]$, $[EuL^{9H}]^-$, $[EuL^{11}]^+$ and $[EuL^{11H}]^-$

The complex solutions were prepared by mixing Eu^{3+} ($5x10^{-3}$ M) and ligand (L^9 and L^{11}, $5x10^{-3}$ M) in deionised water. The test solutions were then diluted with deionised water to achieve desired concentrations of $6.25x10^{-5}$ M. Luminescence spectra were recorded by excitation at $\lambda_{272\ nm}$, while the pH of the test solutions was adjusted with NaOH ($1x10^{-3}$ – $5x10^{-5}$ M).

$[EuL^{9H}]^-$ and $[EuL^{11H}]^-$ were prepared at $6.25x10^{-5}$ M in deionised water. Luminescence spectra were recorded by excitation at $\lambda_{272\ nm}$, while the pH of the test solutions was adjusted with HCl ($1x10^{-3}$ – $5x10^{-5}$ M). Both excitation and emission slit widths were set at 2.5 nm

4.2.4.5 Lifetime and quantum yield measurements of macrocycle-based complexes

The complex solutions were prepared at $6.25x10^{-5}$ M at desired pH values. The luminescence intensities for Tb^{3+} ($\lambda_{544\ nm}$) and Eu^{3+} ($\lambda_{615\ nm}$) were recorded at differing delay times (0.00 – 5.50 ms). A curve of luminescence intensity against delay time was plotted for each complex solution and the lifetime was calculated from the reciprocal of rate constant. For each complex solution, the experiment was repeated under the same conditions using D_2O in place of deionised water. And the reported lifetime values resulted from three independent measurements.

Quantum yield (Φ) was measured in deionised water at the desired pH values. The value was obtained relative to known standard samples with absolute Φ values.[74] The calculation was carried out according to equation 3:

$$\Phi_T = \Phi S \left(\frac{Grad_T}{Grad_S}\right)\left(\frac{\eta^2_T}{\eta^2_S}\right) \quad \text{Equation 4}$$

Here the tris(dipicolinate) complex, $[Tb(dpa)_3]^{3-}$, (Φ=26.5%, pH *ca.* 6)[232] was used as the reference for the terbium complexes. The consistency of data was checked by measuring the quantum yield of the $[Tb(dpa)_3]^{3-}$ against rhodamine B (Φ=65 % in absolute ethanol).[233] Reported lifetime values resulted from three independent measurements.

4.3 Results and discussion

4.3.1 Luminescence studies of acyclic phthalamate-based Tb^{3+} complexes

4.3.1.1 UV studies of ligands (L^{1-8})

The molar extinction coefficients of all the phthalimide and phthalamate derivatives described here have not been evaluated before and it is important to evaluate the nature of the electronic transition involved in order to establish how efficiently the organic chromophore can harvest light as this is important for the antennae effect.[231, 234] Hence the starting point for this study was to record the UV spectra of phthalimide and phthalamate derivatives.

The UV absorption spectral data of L^1 and L^2 are shown in Figure 4.3. The UV spectrum of L^1 in chloroform exhibits three main absorption bands at $\lambda_{225\,nm}$, $\lambda_{240\,nm}$ and $\lambda_{294\,nm}$. These bands are consistent with previous studies: both acetophenones and phthalimide derivatives show absorption between $\lambda_{200\,nm}$-$\lambda_{400\,nm}$.[235] The absorption bands at $\lambda_{225\,nm}$ and $\lambda_{240\,nm}$ were assigned to π-π* absorption transitions of the aromatics.[236-238] The most broad absorption band centred at $\lambda_{294\,nm}$ is π-π* transition involving the carbonyl group and benzene ring.[239]

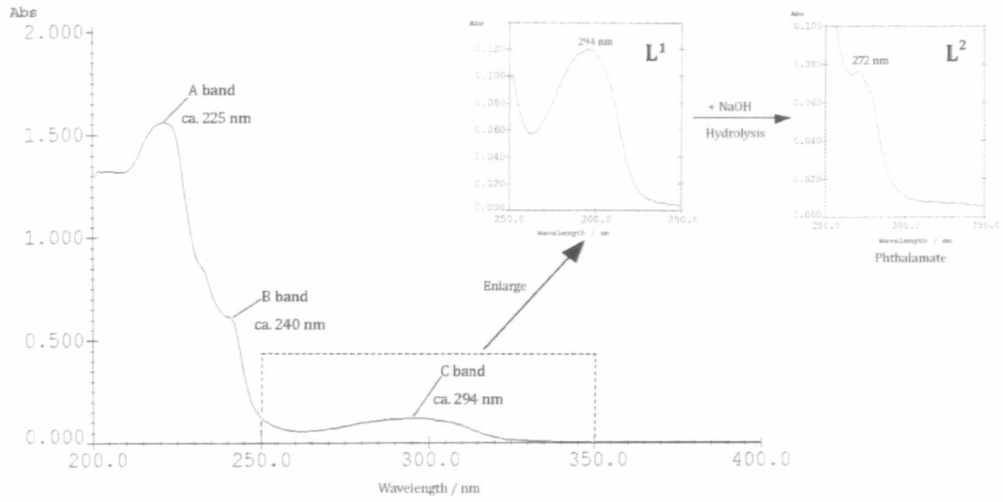

Figure 4.3 UV spectra of L^1 and L^2

On conversion to the phthalamate, the absorption band at $\lambda_{294\ nm}$ is replaced by a new band of L^2 formed at $\lambda_{272\ nm}$ in deionised water. Although different solvent system may affect this wavelength shift, the cleavage of five-membered imide ring system is thought to cause the formation of the new lowest absorption band.[235] The absorption band at $\lambda_{272\ nm}$ is believed to be a π to π* transition of the aromatic function of phthalamate function, as inferred from the absorption transitions of benzoic acid.[240-242]

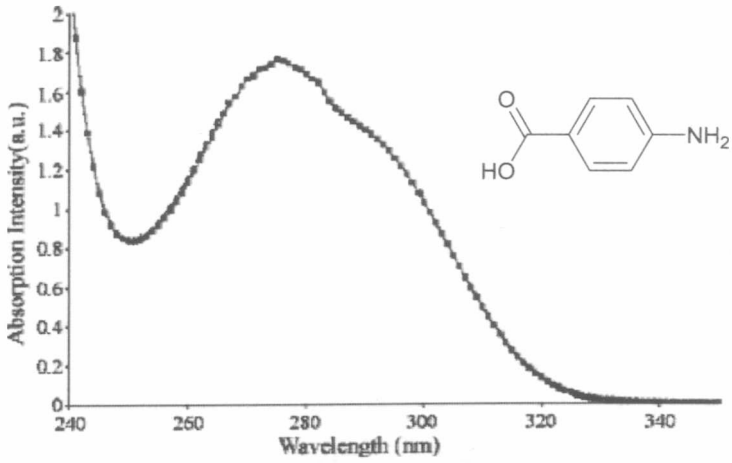

Figure 4.4 UV spectrum of *p*-amino benzoic acid[243]

Figure 4.4 shows the UV spectrum of *p*-amino benzoic acid ($1x10^{-3}$ M) in 0.1 M HCl.[243] The absorption band at the highest wavelength for *p*-amino benzoic acid is *ca.* $\lambda_{275\ nm}$. This is very close to the π and π* transition of the aromatic functions of L^2.

The molar extinction coefficients (M^{-1} cm^{-1}) were measured for L^1, L^3, L^5 and L^7 at $\lambda_{294\ nm}$ in chloroform, and L^2, L^4, L^6 and L^8 at $\lambda_{272\ nm}$ in deionised water. The calculated extinction coefficients of L^{1-8} are shown in Table 4.1, in which L^5 has the highest molar extinction coefficient out of the four phthalimide derivatives. Clearly, at the same concentration, the more phthalimide functions involved in a molecule, the higher the molar extinction coefficient observed and the more efficiently the molecule absorbs energy. For the same reason L^6 has the highest molar extinction coefficient out of the four phthalamate derivatives.

Table 4.1 Molar extinction coefficients of L^{1-8}

UV absorbance against concentration	Ligand	Molar extinction coefficient (M^{-1} cm^{-1})
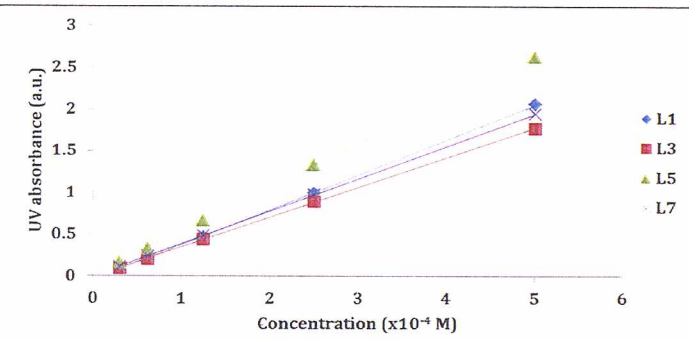	L^1	4200
	L^3	3600
	L^5	5300
	L^7	4000
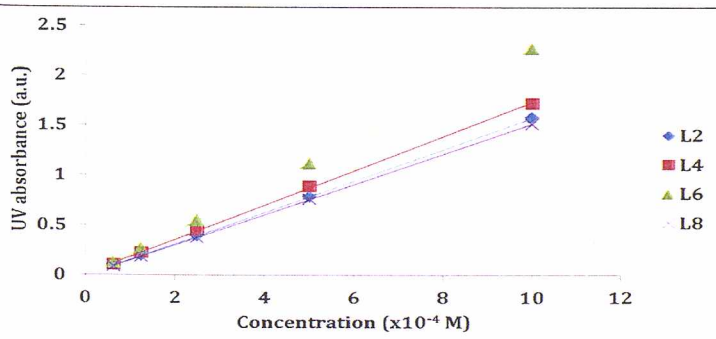	L^2	1600
	L^4	1700
	L^6	2300
	L^8	1600

4.3.1.2 UV studies of acyclic phthalamate ligand-based complexes

When Tb^{3+} was added into the ligand solutions (L^2, L^4, L^6 and L^8), it was found that the UV spectra of the complexes were identical to those observed for free ligands, indicating that the excited state of the free ligand was not significantly affected by the complexation with Tb^{3+}. In other words, the energy gap between π and π* of the aromatic function of the ligand was not changed with addition of Tb^{3+}.

It is known that lanthanide ions have large ionic radii and high affinities for hard donor atoms and ligands with oxygen atoms due to *Pearson's* 'hard and soft acids and bases theory'.[244] Lanthanide ions more likely coordinate to multicarboxylate ligands, which are usually employed in the establishment of stable lanthanide complexes.[245] Hence Tb^{3+} is more likely to bind strongly to the carboxylate functions of the phthalamate functions.

4.3.1.3 Metal-ligand ratio studies on the basis of acyclic ligands (L^2, L^4, L^6 and L^8)

A Tb^{3+} centre can accommodate 9 coordinate bonds with one multidentate ligand or several small monodentate ligands.[246] An individual phthalamate function contains one amide and one carboxylate group. Hence there are two possibilities of metal-to-ligand ratio to establish a Tb^{3+}-phthalamate complex. Firstly, one phthalamate function can chelate one Tb^{3+} and form a relatively stable 7-membered ring. In this case, the metal-to-ligand ratio is dominated by the number of phthalamate function in a ligand. This type of ratio was reported previously for L^4 (Figure 4.5), with five lanthanide ions (Eu^{3+}, Gd^{3+}, Pr^{3+}, La^{3+} and Nd^{3+}) coordinated with L^4 in a 2:1 metal-to-ligand ratio.[110] However, in this case, each Ln^{3+} may have been further coordinated by solvent molecules, such as water, resulting in luminescence quenching.

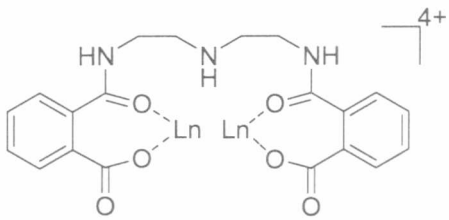

Figure 4.5 Proposed coordination of Tb^{3+} with L^4, under 2:1 metal-to-ligand ratio

Secondly, one Tb^{3+} can coordinate more than one ligand. Below is a proposed coordination between Tb^{3+} and two L^4 (Figure 4.6). Eight coordinate bonds are contributed from the ligand and the final coordination site is filled by a solvent molecule. In this case, the Tb^{3+} is surrounded by two equivalents of ligand molecules minimising the effects from solvent molecules. The desired

luminescence on the basis of 1:2 metal-to-ligand ratio could be higher due to less quenching from solvents.[247]

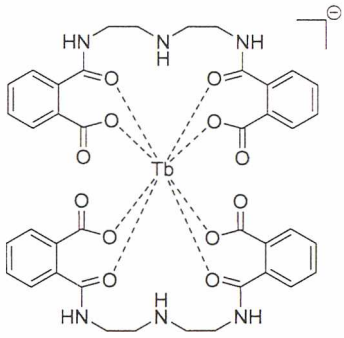

Figure 4.6 Proposed coordination of Tb^{3+} with L^4, under 1:2 metal-to-ligand ratio

This work aimed to design a highly luminescent lanthanide complex on the basis of phthalamate derived ligands (L^2, L^4, L^6 and L^8). Therefore the method used here for investigating the optimal metal-to-ligand ratio is to measure the luminescence intensity. The highest luminescence intensity is taken as the most efficient energy transfer under ambient conditions. The luminescence intensities against metal-to-ligand ratio for each Tb^{3+}-based complexes are shown below (Figure 4.7):

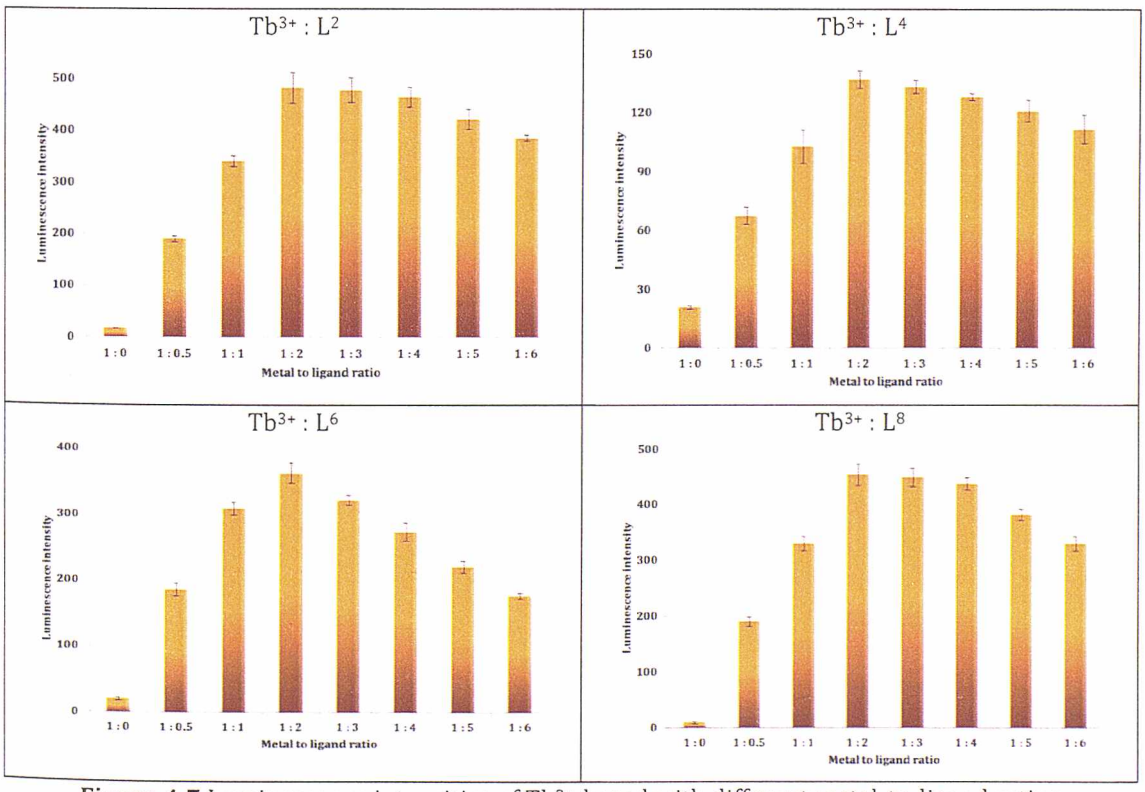

Figure 4.7 Luminescence intensities of Tb^{3+}-based with different metal-to-ligand ratios (mean ± S.D. of triplicate measurements)

According to the results shown in Figure 4.7, Tb^{3+} shows rather weak luminescence without any coordinating ligand present, as expected. Luminescence is enhanced significantly when a ligand is added into the solution, and reaches the highest luminescence level at metal-to-ligand ratio of 1:2 for all these four systems. This suggests that these ligands are tetradentate systems, hence the highest luminescence of 1:2 metal-to-ligand ratios.

However, further addition of ligand beyond the 1:2 ratio reduces the luminescence intensities for all the systems. To explain this feature we assume that only the free ligands and the metal complexes are excited at $\lambda_{272\ nm}$. By adding excess ligand which does not complex to the metal ion centre, a relatively larger percentage of the total energy is absorbed by the free ligand rather than exciting Tb^{3+} complex. The effect of this maybe to reduce the overall antennae effects observed and hence the observed luminescence (Figure 4.8)

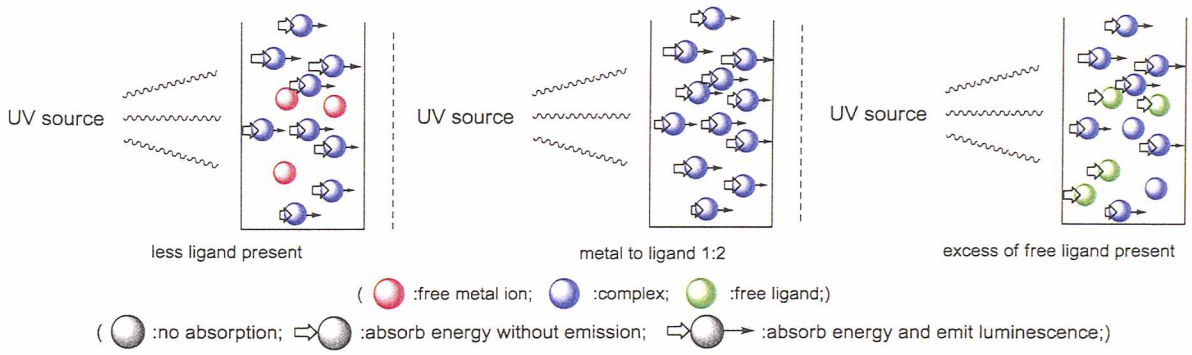

Figure 4.8 Energy absorbed by free ligand or Tb^{3+} complex

The luminescence of L^6-based Tb^{3+} complex decreases significantly when compared to the other three complexes, on addition of excess ligand. This is not surprising in that under the same mole concentration, L^6 has the most phthalamate functions, leading to the strongest ability to absorb energy. So the most significant reduction of the luminescence intensity is observed on the metal-to-ligand ratio studies of L^6.

In conclusion, the best metal-to-ligand ratio on the basis of acyclic phthalamates (L^2, L^4, L^6 and L^8) is 1:2. In this mol ratio, the complexes show the highest luminescence at pH *ca.* 6. The antennae effect is observed in these complexes. At

the same time, $[Tb(L^2)_2]^-$ shows the strongest luminescence, followed by $[Tb(L^8)_2]^-$ and $[Tb(L^6)_2]^{3-}$. $[Tb(L^4)_2]^-$ shows the lowest luminescence intensity (Figure 4.9).

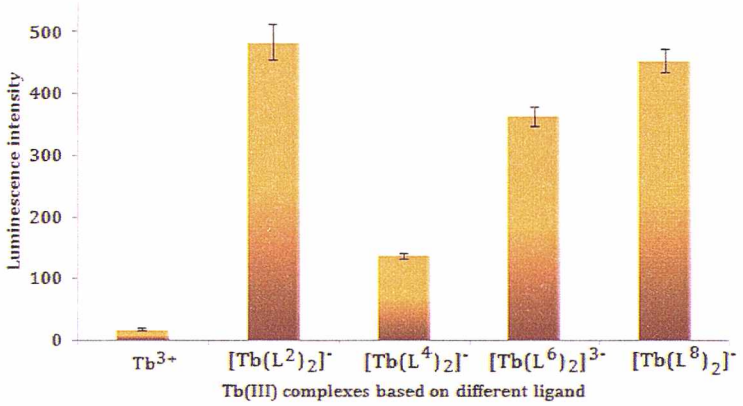

Figure 4.9 Luminescence intensities of free Tb^{3+} ion and Tb^{3+} complexes of 1:2 metal-to-ligand ratio (mean ± S.D. of triplicate measurements)

From the luminescence intensity of each Tb^{3+} complex under the same conditions, it shows that $[Tb(L^2)]^-$ performs the best antennae effect. It is proposed that L^2 has the simplest, least sterically demanding structure thereby providing the tightest conformation to shield any coordination by solvent molecules, resulting in less luminescence quenching.[84]

There is slightly weaker luminescence observed for $[Tb(L^8)_2]^-$ compared to $[Tb(L^2)_2]^-$. The only difference between the ligands here comes from the extra methyl function of L^8. This methyl function is more likely to act as a bulky group preventing efficient coordination of the ligand (Figure 4.10).[248] Steric repulsion will make the complex have a lower formation constant, hence less luminescence as there is likely to be 1:2 complex present in solution.

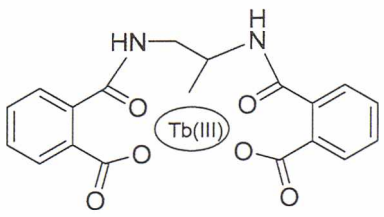

Figure 4.10 Steric repulsion between methyl function and metal ion

Although L^6 has three phthalamate functions, the energy transfer is not as efficient as expected. It was reported that a phthalimide-based analogue of L^6, in other words, L^5, is not rigid in solution. Four different conformations were observed in a

previous report (Figure 4.11).[120] A similar lack of rigidity was observed in this work that, as the splitting pattern of ^{1}H NMR spectrum of L^5 is poorly resolved. One singlet peak is shown for aromatic protons, rather than a doublet of doublet pattern which is observed in other three compounds (L^1, L^3 and L^7).[120]

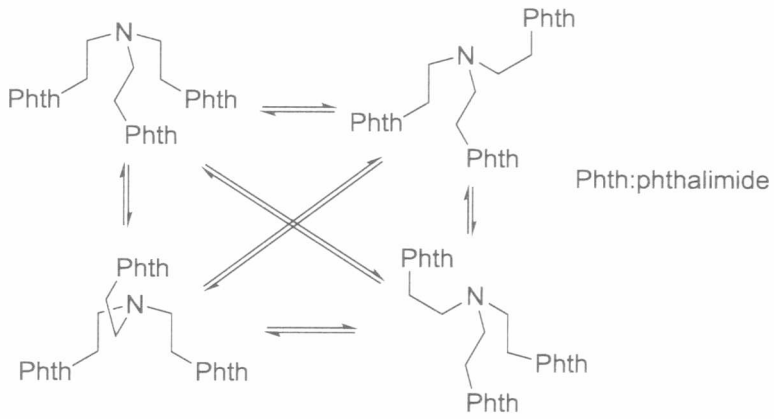

Figure 4.11 Four different conformations of L^5 reported in solution[120]

This non-rigid conformation of L^5 could be extended to L^6. It might be expected that the coordination to the Tb^{3+} could fix the coordinated phthalamate groups. The metal-to-ligand ratio studies of L^6 suggest that one Tb^{3+} is coordinated with two L^6. Therefore the Tb^{3+} is proposed to coordinate only two phthalamate functions from one L^6. This selectivity leads to a free un-coordinated phthalamate function, which absorbs energy but probably acts as weak antennae.

On the other hand, in the metal-to-ligand ratio studies, it is found that the increased luminescence is relatively smaller when a second mol equivalent of L^6 is added to the solution. This indicates that antennae effect is more significant in $[TbL^6]$ rather than $[Tb(L^6)_2]^{3-}$ per mole of coordinated ligand. This maybe suggests that the 1:1 complex involving coordination of all three phthalamates is relatively favourable for this system when compared to the 1:2 system for L^6. The addition of a second L^6 molecule may lead to a smaller proportion of 1:2 complex generated when compared to the other phthalamate systems and hence a smaller increase in luminescence. The proposed coordination between Tb^{3+} ion and L^6 is shown in Figure 4.12.

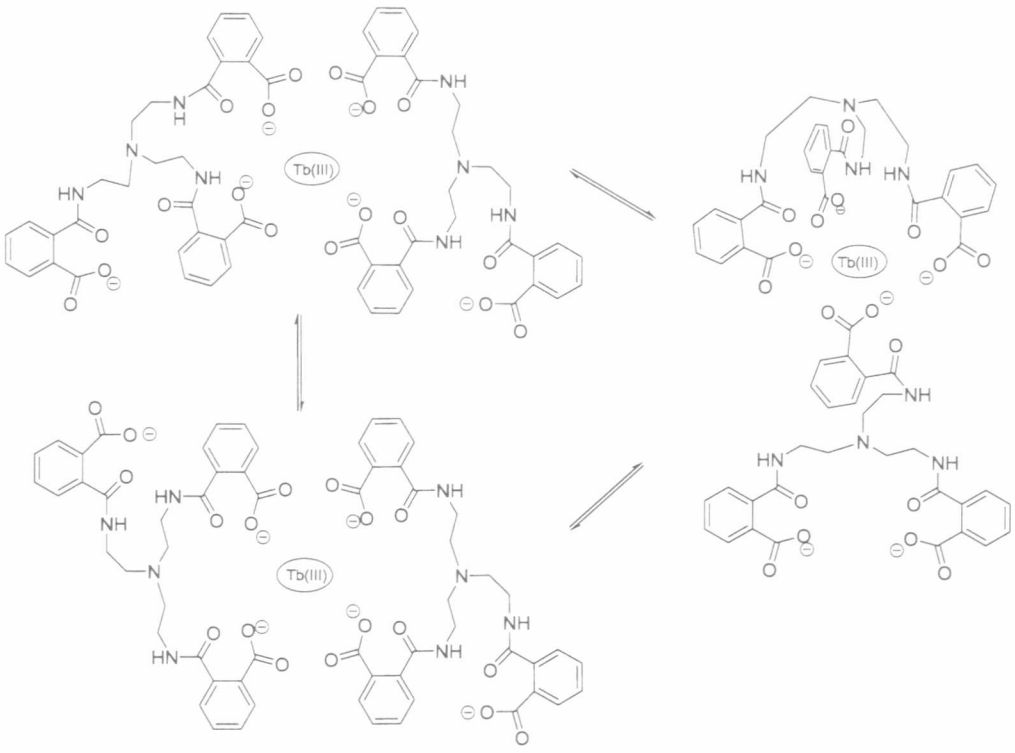

Figure 4.12 Proposed coordination modes between Tb^{3+} and L^6

$[Tb(L^4)_2]^-$ shows the lowest luminescence intensity in these four acyclic terbium complexes. It was reported before that metal-to-ligand back energy transfer occurred on L^4-based Tb^{3+} complex at rt, due to small energy gap between Tb^{3+} and L^4.[110] However, this factor does not dominate the weak luminescence observed, because all four ligands (L^2, L^4, L^6 and L^8) are phthalamate derived as should have the same excited states and therefore they will all have the same energy gap between their excited states and excited state of Tb^{3+}. In other words, if metal-to-ligand back energy occurs on $[Tb(L^4)_2]^-$, then it must occur on the other three complexes. There must be some other factor causing such weak luminescence.

The secondary amine function between two phthalamate functions could coordinate with Tb^{3+} and quench the luminescence by N-H oscillators.[79] It has been reported that the efficiency of luminescence quenching by N-H oscillators is governed by the distance between lanthanide ion centre and the N-H oscillators, a quenching effect was observed over 4.5 Å from the lanthanide ion centre.[170] In addition, the secondary amine function has a reasonably high p*K*a so may well be protonated at pH 6, resulting in hydrogen bonding with water molecules.[249] Although this water molecule might not bound with lanthanide ion directly, it was

reported that the quenching by O-H oscillator could be extended to 3.6 Å.[250] Hence this hydrogen bonding could lead to luminescence quenching by proximal water molecules.

4.3.1.4 Luminescence studies of $[Tb(L^2)_2]^-$, $[Tb(L^4)_2]^-$, $[Tb(L^6)_2]^{3-}$ and $[Tb(L^8)_2]^-$ at various pH values

It was demonstrated in Section 4.3.1.3 that for all the acyclic complexes studied the optimal, in terms of luminescence, metal-to-ligand ratio was 1:2. In order to minimise the changes in complex concentrations, the concentrations of NaOH and HCl used to adjust pH were $1x10^{-2}$ M, leading to small volume changes on addition of acid or base.

The initial pH values for all these four Tb^{3+} complex solutions were adjusted to *ca.* 3.5. The emission spectrum was collected for each complex solution at various pH values. The highest pH value studied was at *ca.* 11.5. The plots of luminescence intensities ($\lambda_{544\ nm}$) against pH for each terbium complex are shown in Figure 4.13.

Terbium complexes of	Luminescence intensities against pH
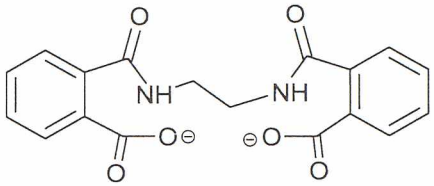 L^2	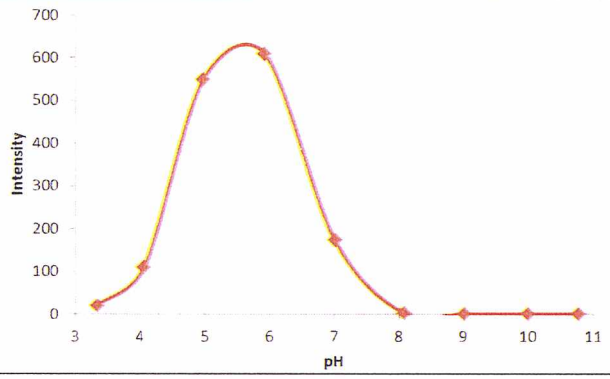
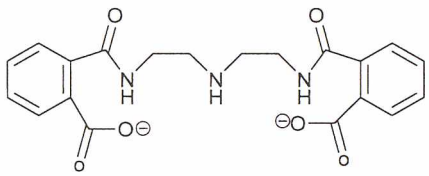 L^4	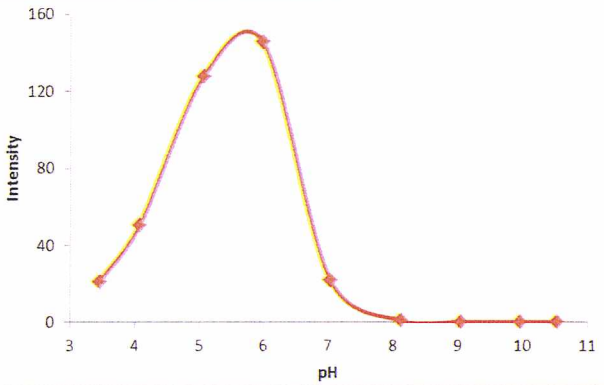
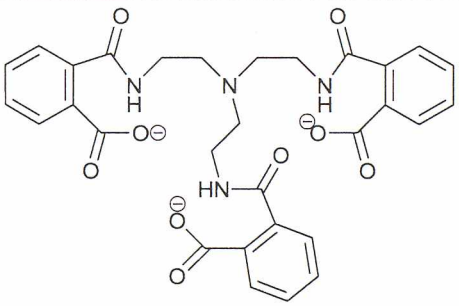 L^6	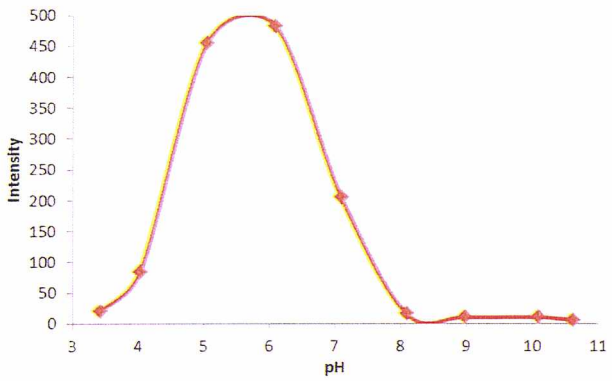
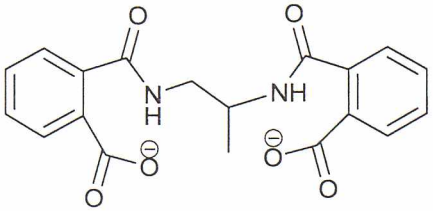 L^8	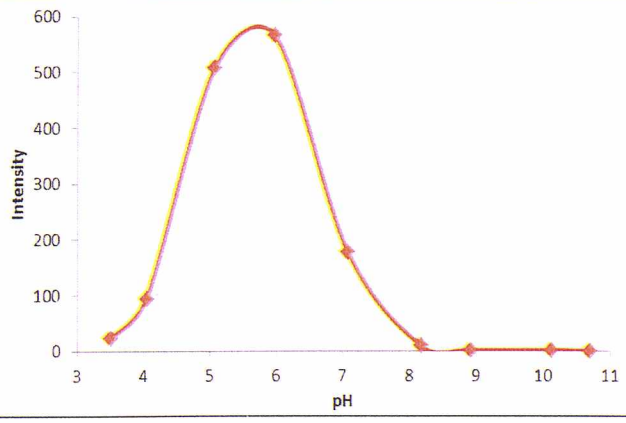

Figure 4.13 Luminescence measurements of each Tb^{3+} complex at various pH values

The luminescence studies for all four complexes show rather weak luminescence under acidic conditions, where the pH is less than 4. As pH is increased, the luminescence is enhanced significantly until pH *ca.* 6. Thereafter, it is reduced significantly between pH 6 – 8, indeed more than 50% luminescence is lost within one pH unit. As a result, we believe that the mechanisms that affect luminescence are the same, regardless of the systems. Herein the luminescence changes of $[Tb(L^2)_2]^-$ are described throughout the pH titration and the mechanism is believed to be as follows:

Firstly, the amide function is usually protonated on the carbonyl oxygen atom under strong acidic conditions (pKa ~ -1).[251] Acetic acid has a p*K*a of *ca.* 4.6, the carboxylate function of L^2 is protonated under acidic conditions, resulting in a carboxylic acid function at pH's less than 4 (Figure 4.14).[252] Under these conditions, the protonated ligand in aqueous solution does not coordinate to Tb^{3+}.

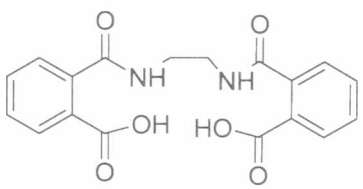

Figure 4.14 Structure of protonated L^2 in aqueous solution when pH is less than 4

Secondly, with increase of pH from 4 to *ca.* 6, the carboxylic acid group is deprotonated, generating carboxylate anions which effectively coordinate to lanthanide cations.[253] The concentration of H^+ is decreased while pH is raised, so the concentration of complex is increased thereby enhancing luminescence as the H^+ ions do not compete so successfully with lanthanide ions for binding to the ligand. On the other hand, as a hard Lewis acid, Tb^{3+} is expected to form complexes with highly electronegative hard Lewis bases, in the order of O>N>S.[49, 50] So a Tb^{3+} is more likely to coordinate with amide carbonyl oxygens rather than the amide nitrogens. The proposed coordination of $[Tb(L^2)_2]^-$ at pH *ca.* 6 is shown in Figure 4.15.

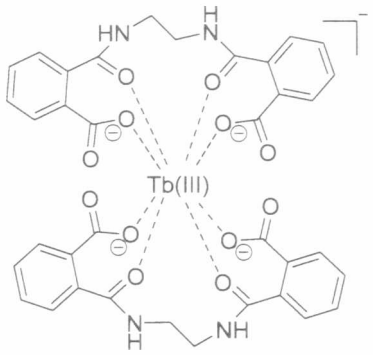

Figure 4.15 Proposed coordination of $[Tb(L^2)_2]^-$ at pH *ca.* 6

Thirdly, the luminescence is observed to be completely disappeared when pH is greater than 8. Although luminescence quenching under a basic condition was reported for non-protonated amines via PET (*cf.* Figure 4.2),[254] there is no amine function in L^2 so this mechanism can be discounted.

The largest reduction of luminescence intensity for $[Tb(L^2)_2]^-$ occurs between pH 6 – 8, where over ~90% of the total luminescence is quenched. It has been reported by others that an amide containing lanthanide complex has a p*K*a of 5.8-7.9 for the metal bound water molecules.[255, 256] Therefore the quenching in luminescence intensity above pH 6 may be related to the deprotonation of the metal bound water molecule. Potentially, this may be due to changes in the coordination in solution that may reduce efficiency of the antennae effect.

Fourthly, it has been reported that the coordinate bond between Ni^{3+} and amide could be switched from Ni–N to Ni–O under a mildly basic condition (Figure 4.16).[257, 258] This potential effect could be proposed in the lanthanide-based complexes described here.

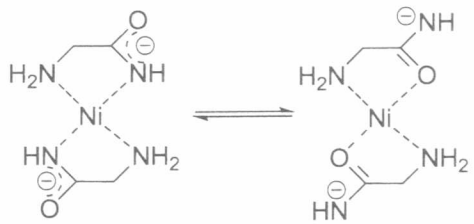

Figure 4.16 Conformation changing of coordinate bond between Ni^{3+} and amide

In order to observe if the coordinate bond is shifted between lanthanide ion and amide, both ^1H NMR experiments of free L^2 and its La^{3+} complex were studied. The

spectrum of L^2 was a background which showed the pH effects on the ligand itself. The experiments were carried out at pH *ca.* 5 and *ca.* 9.

From ^1H NMR spectra of free L^2, it shows that different pH gives rise to different resonance and splitting patterns (Figure 4.17). If the coordinate bond is switched from Ni–N to Ni–O under basic conditions, the most significantly shifted resonances would be the protons of the ethylene linker, because they are adjacent to the amide functions. The resonances at δ 3.692 ppm and δ 3.623 ppm are assigned to the ethylene protons of L^2 at pH 5 and 9 respectively (*cf.* Chapter 3, NMR assignment of L^2).

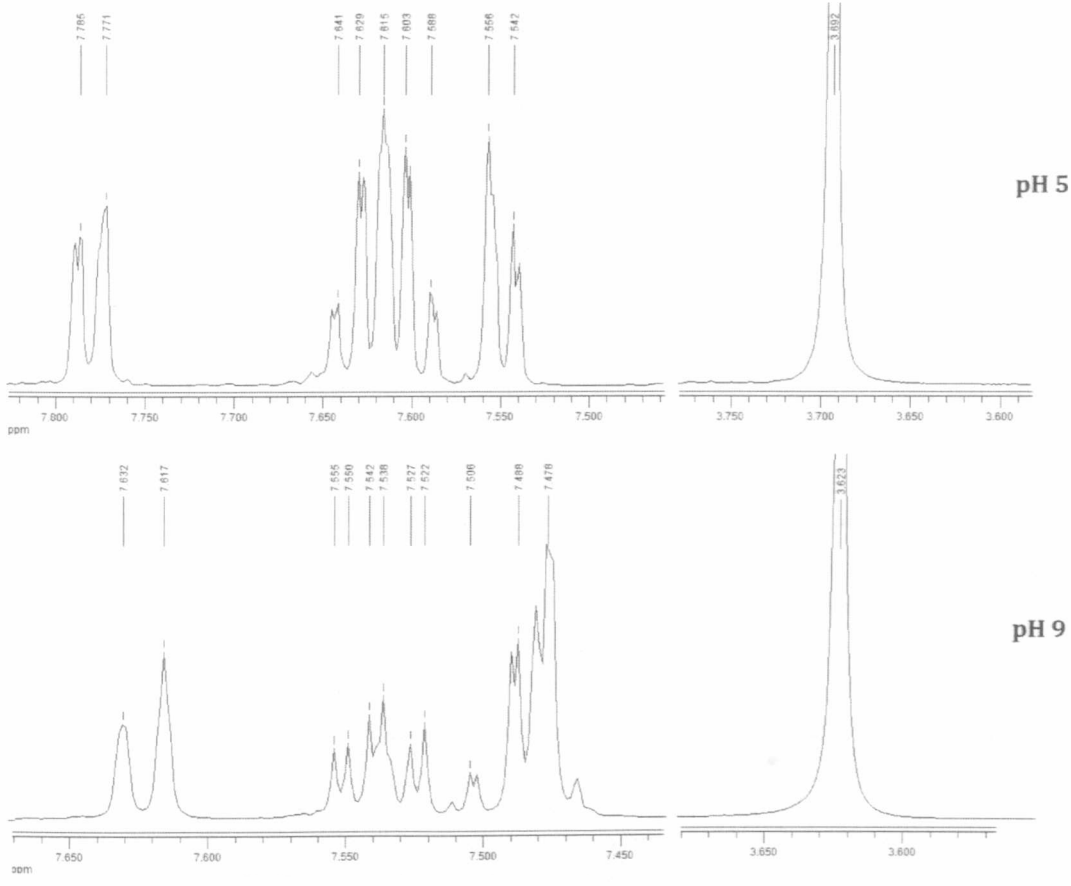

Figure 4.17 ^1H NMR spectra of L^2 at different pH values

^1H NMR spectra of $[La(L^2)_2]^-$ show that the ethylene protons are located at δ 3.692 ppm and δ 3.623 ppm at pH 5 and 9 respectively (Figure 4.18). This indicates that the chemical environment of ethylene protons is not changed significantly. Therefore it is believed that coordinate bond is not switched between La-N and La-

O. Hence the luminescence quenching is more likely due to the bound deprotonated water molecules on the complex.

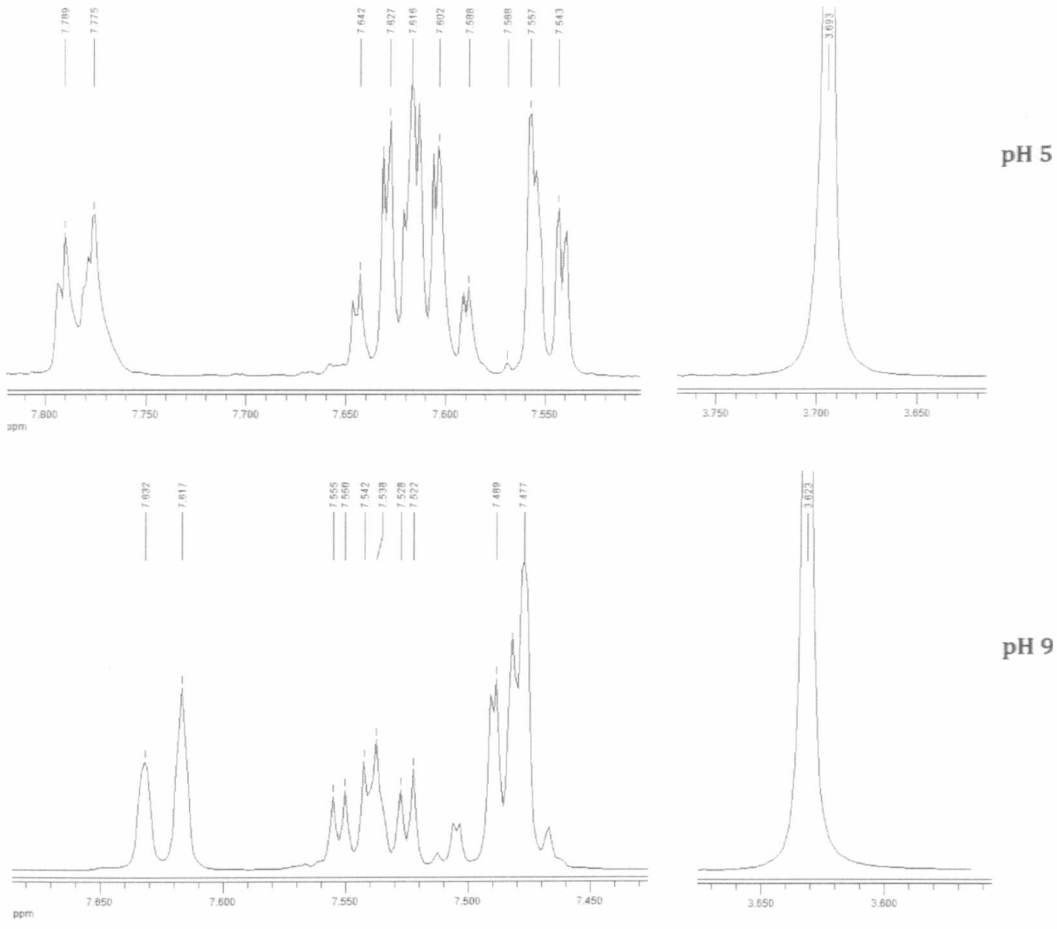

Figure 4.18 ^{1}H NMR spectra of $[La(L^2)_2]^-$ at different pH values

4.3.1.5 Lifetime measurements of $[Tb(L^2)_2]^-$, $[Tb(L^4)_2]^-$, $[Tb(L^6)_2]^{3-}$ and $[Tb(L^8)_2]^-$

The lifetimes of $[Tb(L^2)_2]^-$, $[Tb(L^4)_2]^-$, $[Tb(L^6)_2]^{3-}$ and $[Tb(L^8)_2]^-$ are all at sub-millisecond level (Table 4.2) in HEPES buffer solutions ($5x10^{-2}$ M, pH *ca.* 6). These results indicate that phthalamate functions can transfer energy onto the excited states of Tb^{3+} and generate typical lifetimes of Tb^{3+} luminescence, staying in millisecond to sub-millisecond range. The obtained lifetimes are 100,000 times longer than most organic fluorophores, such as rhodamine B.[69]

Table 4.2 Lifetimes of $[Tb(L^2)_2]^-$, $[Tb(L^4)_2]^-$, $[Tb(L^6)_2]^{3-}$ and $[Tb(L^8)_2]^-$ in HEPES buffer solution at pH *ca.* 6 (mean ± S.D. of triplicate measurements)

Complexes	Lifetime in H_2O (τ/ms)
$[Tb(L^2)_2]^-$	0.38 ± 0.03
$[Tb(L^4)_2]^-$	0.24 ± 0.02
$[Tb(L^6)_2]^{3-}$	0.34 ± 0.04
$[Tb(L^8)_2]^-$	0.34 ± 0.03

The lifetimes of the four terbium complexes were measured in D_2O and the values were between 0.4-0.7 ms. However the calculated number of bound water molecules were bigger than 3. These values show that the coordination number between Tb^{3+} and each ligands is *ca.* 6, which is not the case anticipated. The speciation of the ligands could affect the luminescence of a lanthanide complex, resulting in weak coordination of the complex.[259] Therefore the coordination between Tb^{3+} and each of the ligand needs to be studied further in the future.

4.3.1.6 Potential application of $[Tb(L^2)_2]^-$, $[Tb(L^4)_2]^-$, $[Tb(L^6)_2]^{3-}$ and $[Tb(L^8)_2]^-$ as pH sensors

Since $[Tb(L^2)_2]^-$, $[Tb(L^4)_2]^-$, $[Tb(L^6)_2]^{3-}$ and $[Tb(L^8)_2]^-$ show pH dependent luminescence in their aqueous solutions, they can act as pH sensors. The best application of these complexes would be the dramatic switching off of the luminescence between pH 7 and 8.

An illustration of this is shown in Figure 4.19, where vertical axis is $\log(I/I_0)$, I_0 is the luminescence intensity at pH 8, and I is the luminescence intensity at each particular pH. The measurement of $\log(I/I_0)$ then gives a level of the contrast displayed by each complex with regard to changes in pH values. According this scale, the best contrast for acid/base is $[Tb(L^2)_2]^-$.

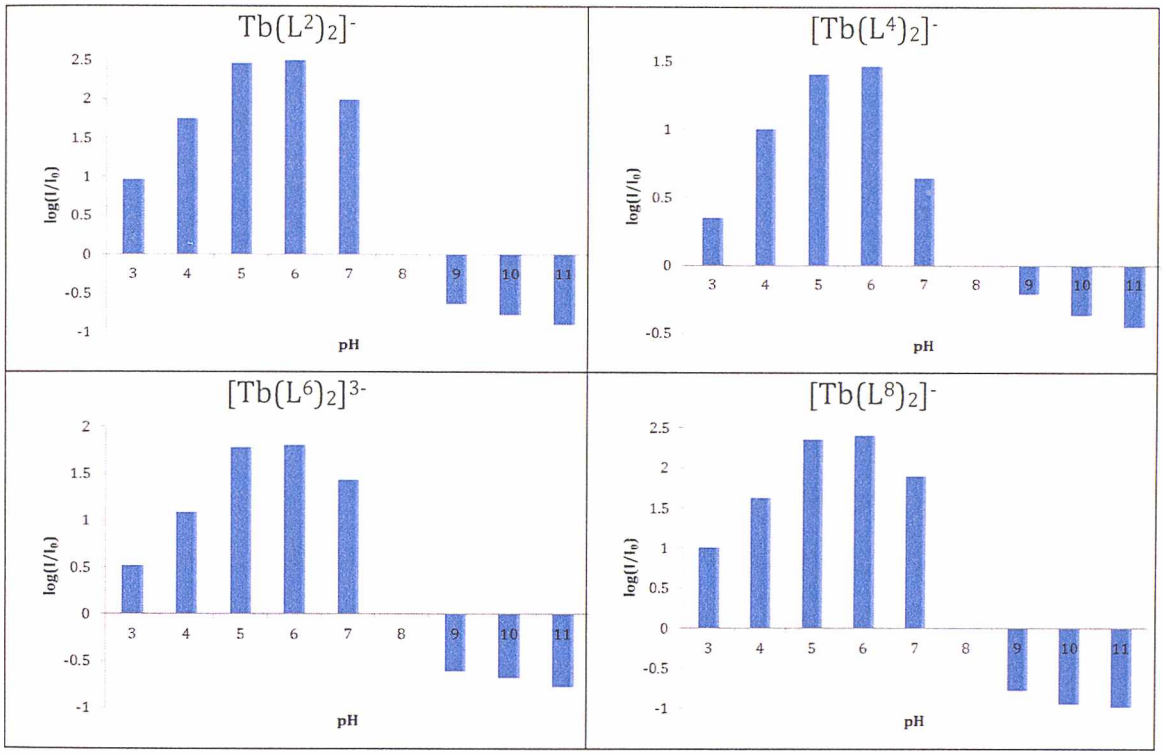

Figure 4.19 Illustration of Tb^{3+} complexes applied as pH sensor

4.3.2 Luminescence of macrocycle-based Tb^{3+} complexes

Before introducing the investigation of the complexes in aqueous solutions, the spectroscopic features of macrocyclic ligands (L^{9-12}) are studied first. Here both UV spectroscopy and ^1H NMR spectroscopy of L^9 are studied at various pH values. The phenomenon observed for L^9 is similar to the other four ligands, as they are all derived on the basis of cyclen and phthalimide functions.

4.3.2.1 UV studies of macrocyclic ligands at different pH

It is well known that phthalimide undergoes hydrolysis under basic conditions, resulting in phthalamate.[110] An absorption band at $\lambda_{300\ nm}$ is observed of L^9 at pH *ca.* 5. With increasing pH, this absorption band is progressively reduced in intensity, whilst another band at $\lambda_{272\ nm}$ is enhanced. A phthalamate-based macrocycle, L^{9H}, is then formed. The absorption band at $\lambda_{300\ nm}$ is completely replaced by the

absorption band at $\lambda_{272\ nm}$ at pH *ca.* 11 (Figure 4.20). This can be explained by the hydrolysis of phthalimide to phthalamate.

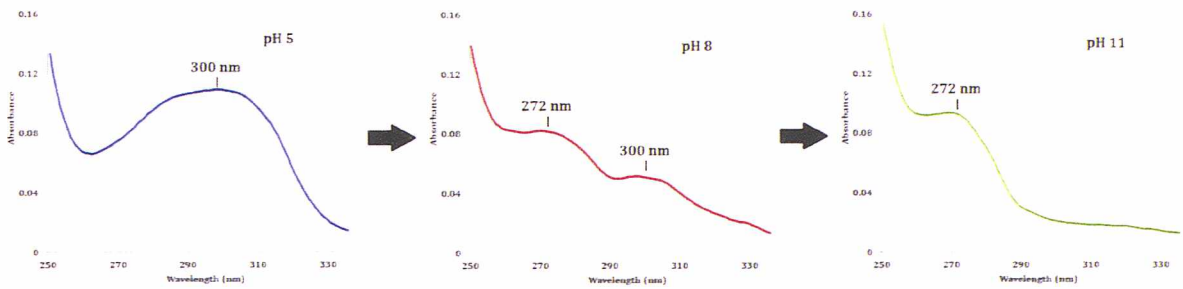

Figure 4.20 UV spectrum of L^9 at various pH values

In addition, further addition of acid into L^{9H} causes a 30% increase of absorbance at $\lambda_{272\ nm}$ when the pH is less than 4 (Figure 4.20). Moreover, the absorption wavelength is not shifted which indicates that the energy gap between ground state and excited state of L^{9H} is not changed. It was reported before that protonation of benzoic acid lead to a partial increase of the UV absorption.[260] This pH is lower than the p*K*a of normal carboxylate functions, hence carboxylic acid is formed in L^{9H}, instead of carboxylate anion.[261] The increase and decrease of the absorbance at $\lambda_{272\ nm}$ and $\lambda_{300\ nm}$ is illustrated in Figure 4.21.

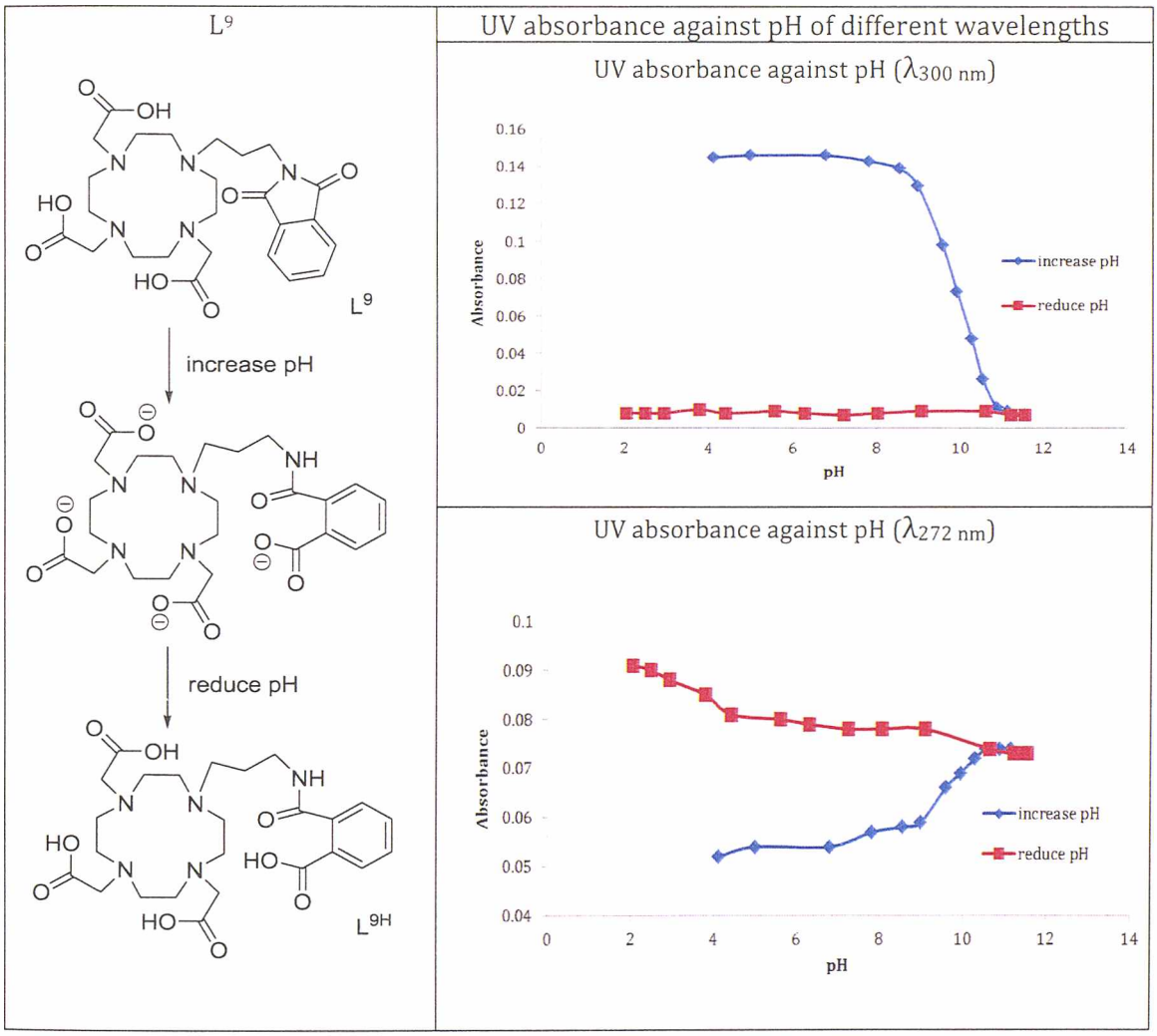

Figure 4.21 UV absorbance against pH at $\lambda_{300\ nm}$ and $\lambda_{272\ nm}$

The extinction coefficients of each ligand in aqueous solutions are shown in Table 4.3. With increased number of phthalimide/phthalamate function in the molecule, the extinction coefficient becomes larger. The more organic chromophore involved in a molecule, the stronger it absorbs energy under the same conditions. However L^{13} is not soluble in deionised water, hence only molar extinction coefficient of its hydrolysed form, L^{13H}, is studied at $\lambda_{272\ nm}$.

The molar extinction coefficients of these macrocyclic ligands in this work are similar to the results reported of benzoic acid. The absorption spectra of benzoic acid in different solvents were investigated by *H.E. Ungnade and R.W. Lamb* in 1952,[262] in which the calculated molar extinction coefficients were between *ca.* 490–1096 M^{-1} cm^{-1}, depending on the solvents, similar to the values I obtained

here. In addition, phthalimide-based ligands have bigger molar extinction coefficients and longer absorption wavelengths than phthalamate-based ligands, possibly because of the more conjugated cyclic system involved in phthalimides.[263, 264]

Table 4.3 Extinction coefficient of each ligand

Ligand		Molar extinction coefficient (M^{-1} cm^{-1})
L^9	Phthalimide-based ($\lambda_{300\ nm}$)	2400
L^{9H}	Phthalamate-based ($\lambda_{272\ nm}$)	1300
L^{10}	Phthalimide-based ($\lambda_{300\ nm}$)	2400
L^{10H}	Phthalamate-based ($\lambda_{272\ nm}$)	1300
L^{11}	Phthalimide-based ($\lambda_{300\ nm}$)	4000
L^{11H}	Phthalamate-based ($\lambda_{272\ nm}$)	2000
L^{12}	Phthalimide-based ($\lambda_{300\ nm}$)	5800
L^{12H}	Phthalamate-based ($\lambda_{272\ nm}$)	2900
L^{13}	Insoluble in water	-
L^{13H}	Phthalamate-based ($\lambda_{272\ nm}$)	3700

4.3.2.2 ^{1}H NMR studies of macrocyclic ligands at various pH

The hydrolysis process from phthalimide to phthalamate is also observed in ^{1}H NMR experiments. In this study, I focus on the protons of aromatic functions. These observations lead to the same conclusions as the results obtained in UV spectra that phthalimide undergoes hydrolysis under basic conditions.

The ^{1}H NMR spectra (Figure 4.22) of L^9 show that the phthalimide function is retained under acidic conditions. The first signal corresponding to the hydrolysed product, L^{9H}, is observed at pH *ca.* 7.7. Both signals from phthalimide and phthalamate are observed in the ^{1}H NMR spectra between pH 8 – 10. This is consistent with that observed in UV spectra that the hydrolysis progress is rather facile at RT and that a mixture of L^9 and L^{9H} exists under mild basic conditions. Phthalimide is completely replaced by phthalamate at pH *ca.* 10.8.

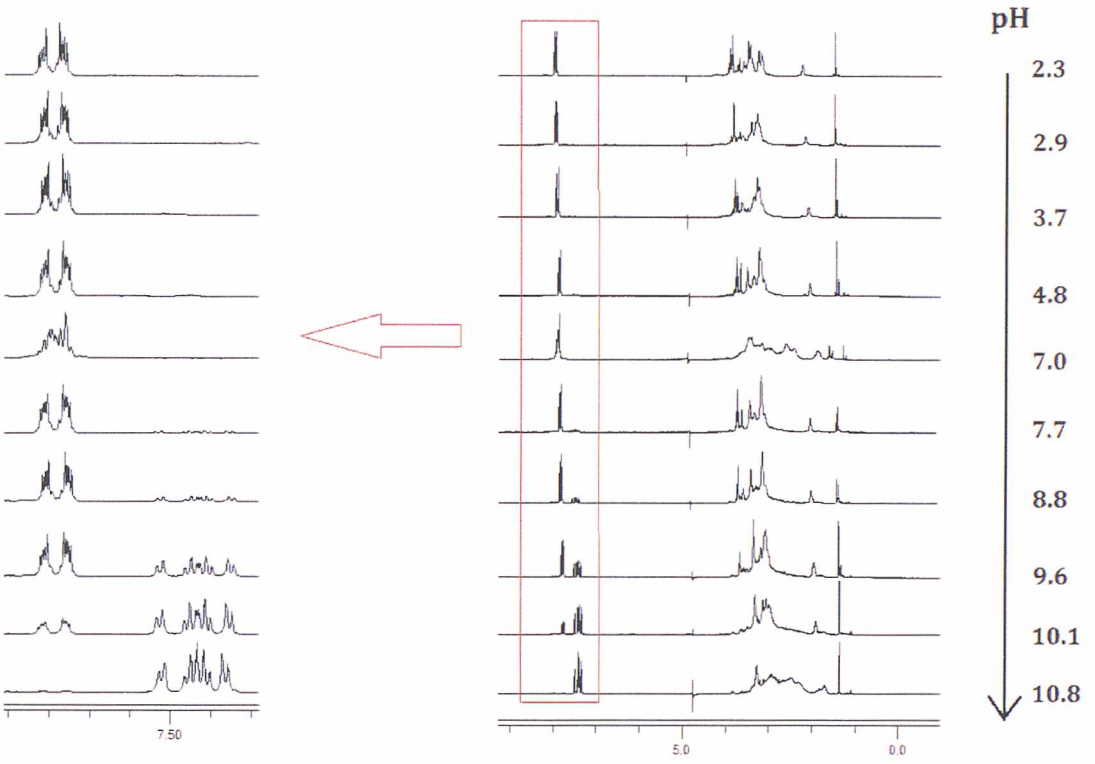

Figure 4.22 ^{1}H NMR spectrum of L^{9} at various pH values

Once the phthalamate function is formed, an additional carboxylate function group is created, which should have greater potential coordination ability with lanthanide ions.

4.3.2.3 Luminescence studies of $[TbL^{9}]$ – $[TbL^{12}]^{2+}$ and $[TbL^{9H}]^{-}$ – $[TbL^{13H}]^{-}$ at various pH

Because L^{9-13} are multidentate macrocyclic ligands, the metal-to-ligand ratio is certainly 1:1. The luminescence studies can be divided into two parts:

Firstly, the initial pH of all the complex solutions, $[TbL^{9}]$ – $[TbL^{12}]^{2+}$, is *ca.* 4. Addition of NaOH into the solutions leads to hydrolysis of the phthalimide function, resulting in the formation of phthalamate-based ligands, $[TbL^{9H}]^{-}$ – $[TbL^{12H}]^{-}$. Enhanced luminescence is observed between pH 8 – 11. L^{13} is not soluble in deionised water, hence it is not investigated at this stage.

Secondly, luminescence studies were carried out on the basis of $[TbL^{9H}]^-$ – $[TbL^{13H}]^-$ at various pH values. The pH is reduced from *ca.* 11 to *ca.* 2 by adding HCl, while luminescence is in general maintained at high level until the pH is less than 4.

The luminescence intensity ($\lambda_{544\ nm}$) against pH for each complex is shown in Figure 4.23:

Phthalimide-based complexes	Luminescence intensity against various pH	Phthalamate-based complexes
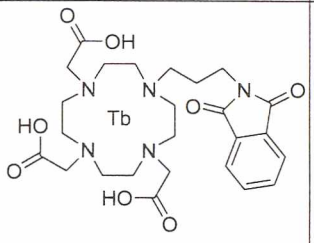 Ligand: L^{9}	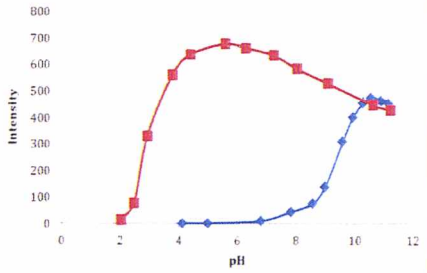	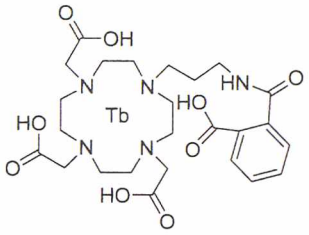 Ligand: L^{9H}
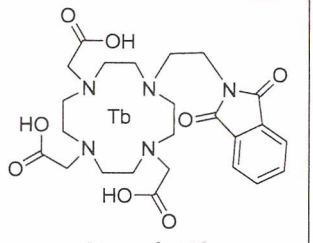 Ligand: L^{10}	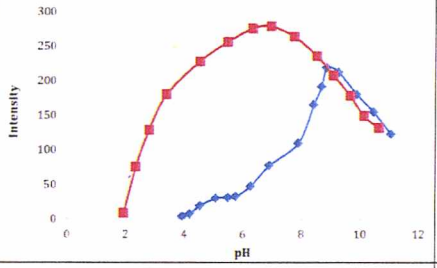	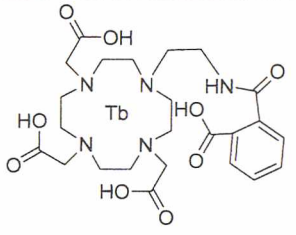 Ligand: L^{10H}
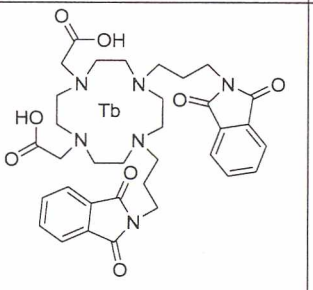 Ligand: L^{11}	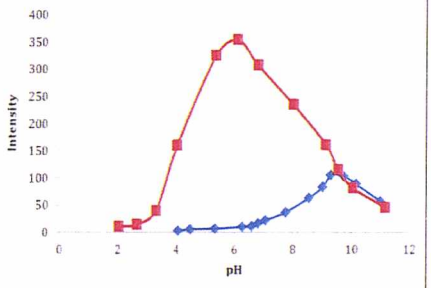	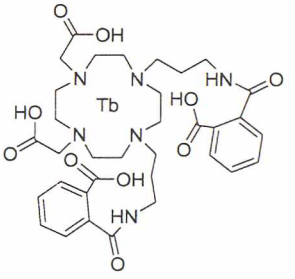 Ligand: L^{11H}
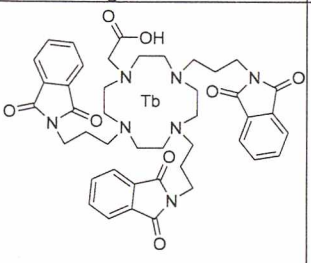 Ligand: L^{12}	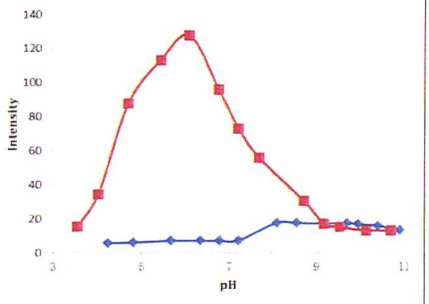	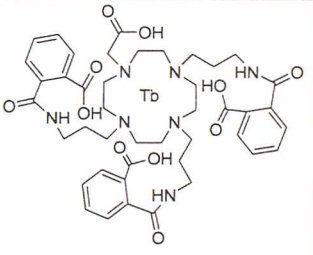 Ligand: L^{12H}
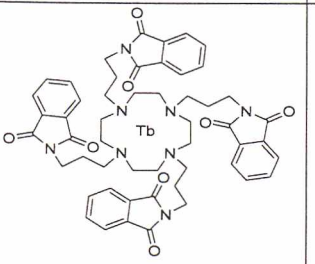 Ligand: L^{13}	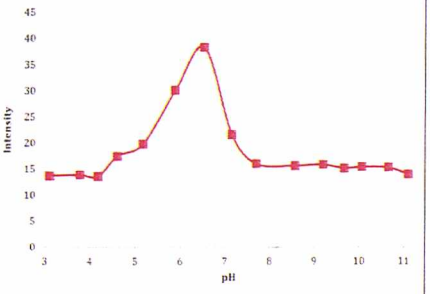	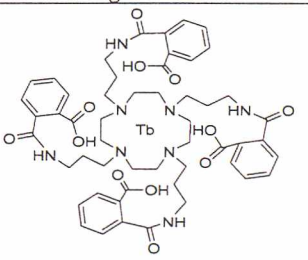 Ligand: L^{13H}

Figure 4.23 Luminescence intensity against pH for each Tb^{3+} complex, λ_{ex}: 272 nm; λ_{em}: 544 nm (blue lines: pH increases from *ca.* 4 to 11; red lines: pH decreases from *ca.* 11 to 2)

From the results shown in Figure 4.23, some significant phenomenon are observed: (1) Luminescence is enhanced with addition of NaOH, as the phthalimide is converted into phthalamate in all the systems studied; (2) Shortening the alkyl bridge between the chromophore and cyclen moiety does not increase the luminescence; (3) The more chromophores present in a ligand, the less enhancement of the luminescence displayed; (4) $[TbL^{9H}]^{-}$ – $[TbL^{13H}]^{-}$ show the highest luminescence level at pH ca. 6. These four observations are discussed in the following sections.

4.3.2.4 Enhanced Tb^{3+} luminescence by increasing the pH

The focus of this study is $[TbL^{9}]$. A rather weak luminescence is observed under the initial acidic conditions. As a comparison, the p*Ka* of acetic acid is 4.78 so it can be presumed that the carboxylate moieties in the DO3A fragment are protonated when pH is less than 5.[265-267] Therefore complex formation is unlikely at low pH because of fully protonated ligand, hence no observed energy transfer on excitation.

Moreover, ^{1}H NMR experiments of L^{9} and $[LaL^{9}]$ at pH *ca.* 4 were performed. The aim of this was to investigate the coordination between L^{9} and La^{3+} at low pH. In this experiment, the ^{1}H NMR spectra show that there is no significant difference in splitting patterns or resonances observed between L^{9} and $[LaL^{9}]$ pH *ca.* 4 (Figure 4.24). In particular, the signals from phthalimide protons do not get affected by the addition of La^{3+} ions and hence this does not affect the chemical environment of phthalimide. This indicates that the complexation between L^{9} and La^{3+} does not occur at pH *ca.* 4, presumably because the ligand is completely protonated.

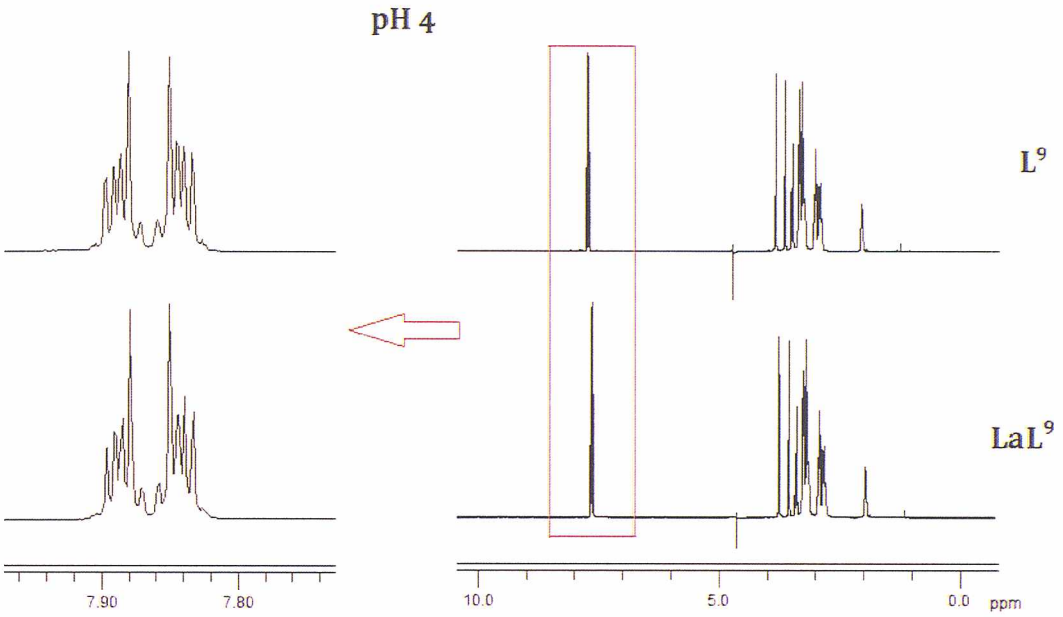

Figure 4.24 ^{1}H NMR spectra of L^9 and [LaL^9] complex at pH 4

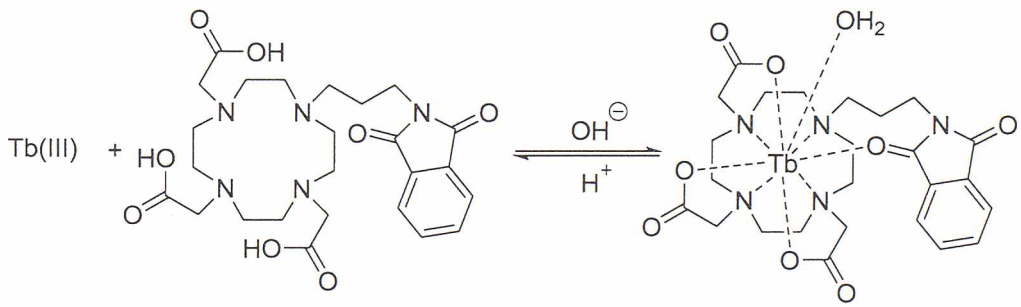

Figure 4.25 Proposed structure of free Tb^{3+} and protonated L^9 under acidic conditions and potential coordination under neutral conditions

When the pH is increased from mildly acidic to neutral, the ligand is progressively deprotonated. It can be visualised that eight coordinate bonds can be formed between L^9 and Tb^{3+} (Figure 4.25), in which four coordinate bonds are contributed from the four cyclen amine functions, three coordinate bonds are contributed from the three carboxylate functions and the last one is contributed from the carbonyl function of phthalimide. Moreover, one water molecule could fill the ninth coordinate bond with Tb^{3+}. Energy transfer is expected in this situation, but the luminescence should be quenched to a degree by the coordinated water molecule.

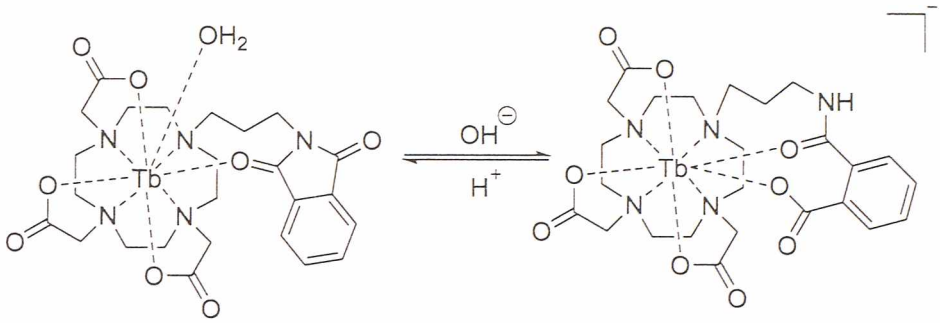

Figure 4.26 Proposed coordination of [TbL^{9}] under mild acidic conditions and [TbL^{9H}]$^{-}$ under basic conditions

Thereafter, [TbL^{9}] is further treated with NaOH. The phthalamate is progressively formed and coordinates to Tb^{3+} by the carboxylate function formed displacing the coordinated water molecule (Figure 4.26). A significant luminescence enhancement is observed under basic conditions. As the new carboxylate function coordinates with the Tb^{3+} ion, creating an antennae effect and, resulting in an efficient energy transfer from the phthalamate chromophore to coordinated Tb^{3+} ion centre (Figure 4.26). The coordination between phthalamate and lanthanide ion can be demonstrated by ^{1}H NMR experiment (Figure 4.27) using the analogous lanthanum complex.

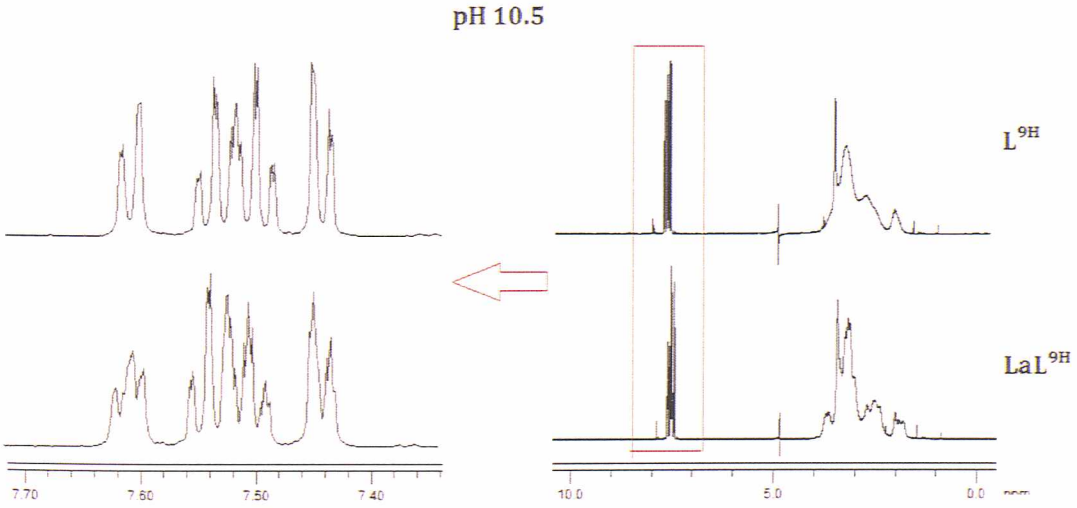

Figure 4.27 ^{1}H NMR spectra of [L^{9H}] and [LaL^{9H}]$^{-}$ at pH *ca.* 10.5

When compared to the ^{1}H NMR spectrum of L^{9} at pH *ca.* 4, the ^{1}H NMR spectrum of L^{9H} at pH *ca.* 10.5 has rather different splitting patterns for the aromatic protons (*cf.* Figure 4.24). This indicates the formation of phthalamate in L^{9H} under basic conditions, replacing phthalimide. On the other hand, the splitting patterns of a

signal at *ca.* δ 7.61 ppm is changed by addition of La^{3+} ion under basic conditions. This coupling signal is assigned to the aromatic proton adjacent to phthalamate carboxylate functions. Therefore this change results from the coordination between carboxylate function of phthalamate in L^{9H} and La^{3+}.

4.3.2.5 Bridge effects between chromophore and lanthanide ion

A luminescence study of $[TbL^{10}]$ shows the same phenomenon as those observed with $[TbL^{9}]$, i.e., that $[TbL^{10H}]^-$ is formed under basic conditions (Figure 4.28). The enhanced luminescence of $[TbL^{10H}]^-$ should have the same mechanism as that described in Section 4.3.2.4. However, it is found that the level of enhanced luminescence intensity of $[TbL^{10H}]^-$ is about 60% weaker than that of $[TbL^{9H}]^-$.

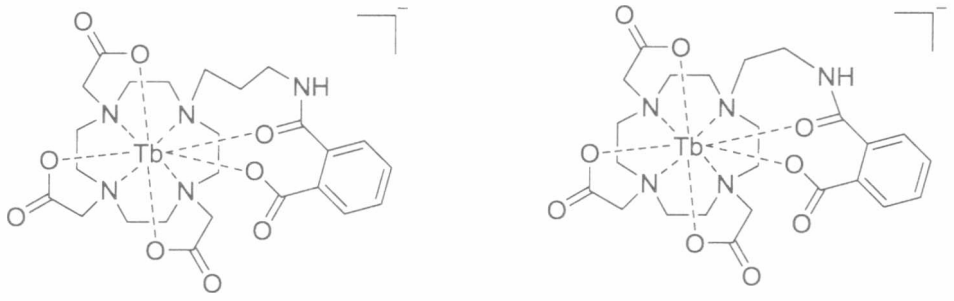

Figure 4.28 Proposed coordination of $[TbL^{9H}]^-$ (left) and $[TbL^{10H}]^-$ (right)

In these phthalamate-based Tb^{3+} complexes, phthalamate is linked by a propyl-bridge with cyclen in $[TbL^{9H}]^-$ whereas an ethyl-bridge links phthalamate and cyclen in $[TbL^{10H}]^-$. The observed luminescence shows that the complex with a propyl-bridge transfers energy more efficiently rather the complex with an ethyl-bridge.

Accordingly, the quantum yields of $[TbL^{9H}]^-$ (36%) and $[TbL^{10H}]^-$ (5.6%) at pH *ca.* 10 demonstrate that the energy transfer and coordination between Tb^{3+} ion centre and ligands are different. The details will be discussed in Section 4.3.2.10.

4.3.2.6 Luminescence studies of the effect of the number of chromophores present in Tb^{3+} DO3A phthalamate complexes

It seems that the luminescence of $[TbL^{11}]^+$ follows the same principles as disscussed in Section 4.3.2.4: there is no coordinate bond between phthalimide and Tb^{3+} at low pH. Energy transfer could occur under mild acidic conditions, but the luminescence may be quenched by bound water molecules. The luminescence is enhanced when $[TbL^{11H}]^-$ is formed under basic conditions, but its enhanced luminescence is weaker than that of $[TbL^{9H}]^-$, although two phthalamate functions are present in $[TbL^{11H}]^-$. The same phenomenon is observed in $[TbL^{12H}]^-$. Generally speaking, increasing the number of chromophores seems to have no effect on the pH dependent behaviour observed with the other phthalamate containing complexes discussed earlier.

The first concern here was that both of the two phthalimide functions in L^{11} may be hydrolysed under basic conditions, so the UV spectra of L^{11} at various pH values were recorded. A plot of UV absorbance at $\lambda_{300\ nm}$ against pH is shown in Figure 4.29. As shown by this figure the absorbance at $\lambda_{300\ nm}$ has completely disappeared at pH *ca.* 11, and this indicates that both the phthalimides in L^{11} were converted into phthalamates under basic conditions, creating L^{11H}.

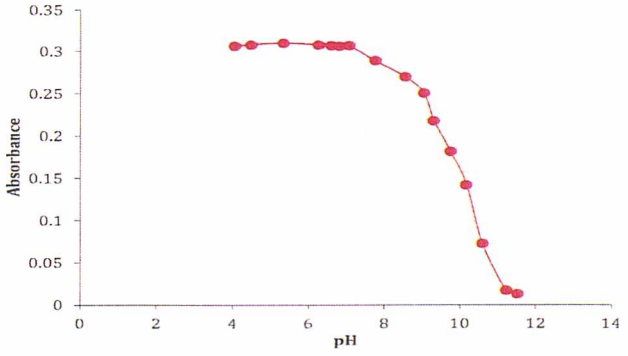

Figure 4.29 UV absorbance at 300 nm against pH of L^{11}

The number of water molecules (q) bound to the Tb^{3+} centre of $[TbL^{9H}]^-$ and $[TbL^{11H}]^-$ were studied measuring the decay rates in H_2O and D_2O, and applying the relationship in Equation 4.[170]

$$q_{Tb} = 5[(\Delta k_{corr})\text{-}0.06] \qquad \textbf{Equation 5}^{170}$$

where Δk_{corr} is the difference between k_{H2O} and k_{D2O}. The measurement shows that the Tb^{3+} centre is coordinated with *ca.* 1.2 water molecule (Table 4.4), thereby eight coordinate bonds between the ligand and the metal ions are proposed for $[TbL^{11H}]^-$.

Table 4.4 Quantum yields (mean ± S.D. of triplicate measurements) and numbers of water molecules (mean ± S.D. of triplicate measurements) of $[TbL^{9H}]^-$ and $[TbL^{11H}]^-$ at pH ca. 10

Tb^{3+} complex	Quantum yield (%)	Number of water molecules
$[TbL^{9H}]^-$	36 ± 4.3	0.11 ± 0.3
$[TbL^{11H}]^-$	8.2 ± 2.5	1.17 ± 0.3

Therefore there are two potential coordinations between L^{11H} and Tb^{3+}: Tb^{3+} can either coordinate with both phthalamates via the carboxylate functions (Figure 4.30a), or coordinate with one phthalamate by its carboxylate and carbonyl functions (Figure 4.30b).

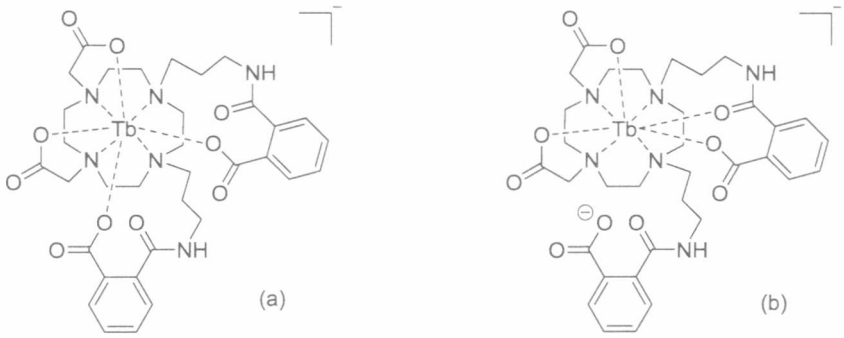

Figure 4.30 Two potentially different coordinations between Tb^{3+} and L^{11H}

The stability constants of Gd^{3+} complexes on the basis of DOTA and compound **14** have been investigated (Figure 4.31), the values of Log(K) were 23.5 and 13.1 respectively.[268] This implies that the Tb^{3+} will be bound to the cyclen amine functions and carboxylate functions appended to cyclen preferentially ahead of the amide carbonyl function on the phthalamate.

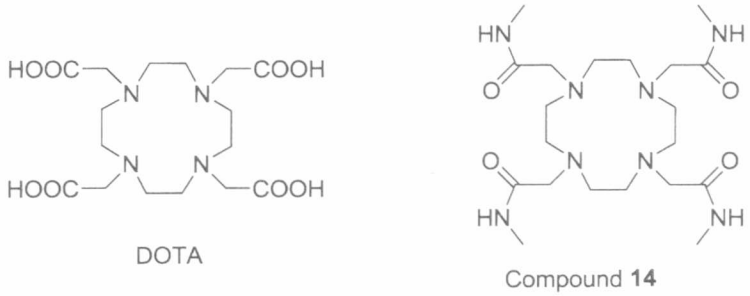

Figure 4.31 DOTA and compound **14**

However, in this work, the pendant arms of L^{11H} have a propyl-bridge and phthalamate functions are more bulky functions than the methyl acetic acid and methyl amide functions shown in Figure 4.31. It has been reported previously that close proximity between antennae and lanthanide ions in particular dipole-dipole interaction were required for efficient energy transfer.[269] Therefore it seems more likely that crowding of the coordination spheres leads to less efficient binding of phthalamates, causing the observed weak antennae effects in $[TbL^{11H}]^-$.

4.3.2.7 Luminescence studies of phthalamate-based Tb^{3+} complexes ($[TbL^{9H}]^-$ – $[TbL^{13H}]^-$) at various pH values

It is found that the maximal luminescence intensity was observed at pH *ca.* 6 for $[TbL^{9H}]^-$ – $[TbL^{13H}]^-$. The luminescence intensities of these five complexes are rapidly reduced between pH 4 – 2; more than 50% luminescence is reduced within one pH unit. This is accounted for the protonation of the ligands which thereby become distal from the central Tb^{3+}.

On the other hand, lower luminescence intensity is observed under basic conditions for $[TbL^{9H}]^-$ – $[TbL^{13H}]^-$ relative to the maximum value at pH *ca.* 6. The reason for this is unclear, however maybe related to presence of unprotonated water molecule species like those suggested in Section 4.3.1.4 for acyclic phthalamates.

4.3.2.8 Lifetime and quantum yield measurements of $[TbL^{9H}]^-$ – $[TbL^{13H}]^-$

The luminescence lifetimes of $[TbL^{9H}]^-$ – $[TbL^{13H}]^-$ at pH *ca.* 10 and 6 were measured in deionised water. Only the quantum yields of $[TbL^{9H}]^-$ and $[TbL^{11H}]^-$ were studied here (Table 4.5). Below is an indicative plot of the decay curve obtained during the luminescence lifetime studies, here is an example for $[TbL^{9H}]^-$ at pH *ca.* 10 (Figure 4.32).

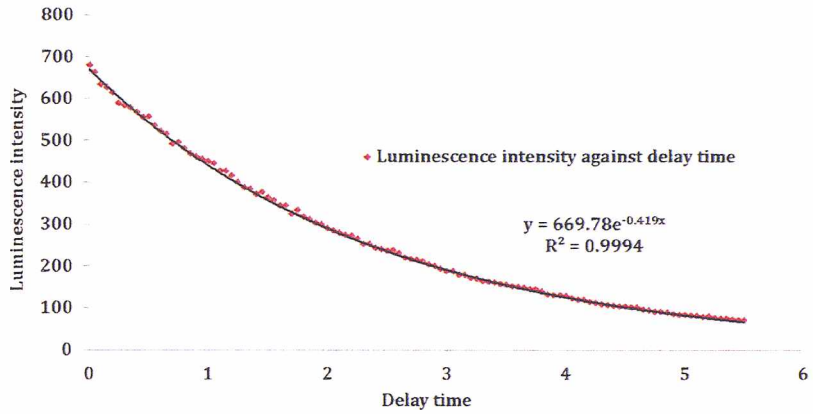

Figure 4.32 Plotted curve of luminescence intensity against delay time of $[TbL^{9H}]^-$ at pH *ca.*10

It is known that the lifetime measures the time at which the luminescence intensity decays to 1/e of its initial level.[43] According to the relationship obtained in Figure 4.32, $y = 669.78e^{-0.419x}$, where y is luminescence intensity and x is delay time, the lifetime is the reciprocal of the decay rate constant, *ca.* 2.4 ms.

Table 4.5 Lifetimes and quantum yields of $[TbL^{9H}]^-$ – $[TbL^{13H}]^-$ at pH *ca.* 10 and 6 respectively (mean ± S.D. of triplicate measurements)

Complexes	pH *ca.* 10		pH *ca.* 6	
	Lifetime (ms)	Quantum yield (%)	Lifetime (ms)	Quantum yield (%)
$[TbL^{9H}]^-$	2.44 ± 0.23	36 ± 4.3	2.39 ± 0.27	46 ± 5.7
$[TbL^{10H}]^-$	2.27 ± 0.21	5.6 ± 1.4	2.13 ± 0.22	
$[TbL^{11H}]^-$	1.84 ± 0.14	8.2 ± 2.5	1.30 ± 0.1	12 ± 2.1
$[TbL^{12H}]^-$	0.36 ± 0.04		0.66 ± 0.06	
$[TbL^{13H}]^-$			0.33 ± 0.03	

The extremely long lifetimes of $[TbL^{9H}]^-$ – $[TbL^{13H}]^-$ are important features that could be applied in time-resolved luminescence measurements. These features are known to have advantages as they allow removal of unexpected background signals, such as biological fluorescence, organic fluorescence and scattered light.[270] It should be noted that $[TbL^{9H}]^-$ is one of the best performing macrocycle-based Tb^{3+} complexes in the literature to date, with both a long lifetime (2.4 ms) and high quantum yield (46%) in deionised water. This is comparable to the previously reported highly luminescent terbium complexes (Table 4.6).[271]

Table 4.6 Reported highly luminescent terbium complexes

Ligand	Lifetime (ms)	Quantum yield (%)	Solvent
Compound **15**[272]	1.66	60	H_2O
Compound **16**[273]	2.60	59	H_2O
Compound **17**[273]	2.45	50	H_2O
Compound **18**[274]	2.22	40	H_2O
Compound **19**[274]	2.52	36	H_2O
Compound **21**[275]	1.34	23	MeOH
Compound **22**[276]	3.28	37	H_2O
Compound **23**[277]	2.40	40	H_2O
Compound **24**[278]	3.00	45	H_2O
Compound **25**[279]	2.75	60	H_2O
Compound **26**[279]	2.82	51	H_2O
Compound **27**[279]	2.65	95	H_2O
Compound **28**[279]	2.28	56	H_2O
Compound **29**[280]	2.03	-	H_2O (HPO_4^{2-})
Compound **30**[280]	2.03	-	H_2O (HPO_4^{2-})
Compound **31**[280]	2.06	-	H_2O (HPO_4^{2-})
Compound **32**[280]	2.16	-	H_2O (HPO_4^{2-})
Compound **33**[275]	1.7	34	H_2O
Compound **34**[281]	4.13	44	H_2O
Compound **35**[281]	3.2	16	H_2O
Compound **36**[275]	1.49	43	H_2O
Compound **37**[282]	1.56	40	H_2O
Compound **38**[282]	2.36	36	H_2O
Compound **39**[283]	1.85	49	H_2O
Compound **40**[72]	3.13	-	H_2O
Compound **41**[72]	3.57	-	H_2O
Compound **42**[72]	3.33	-	H_2O
Compound **43**[72]	3.03	-	H_2O

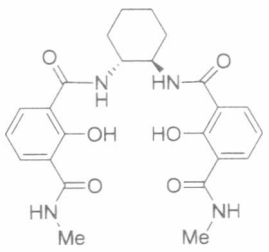

Compound **15**

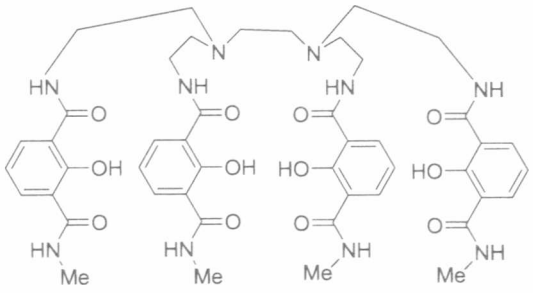

Compound **16**

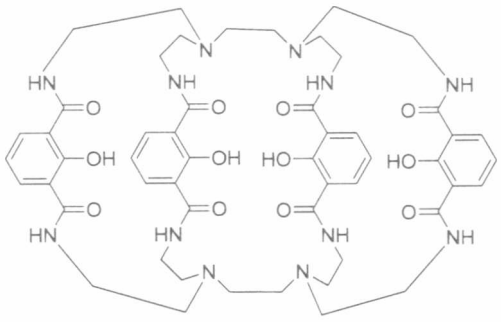

Compound **17**

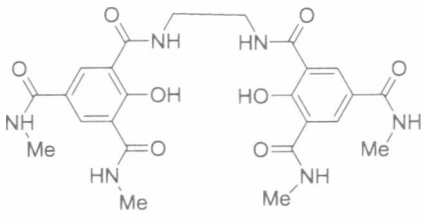

Compound **18**

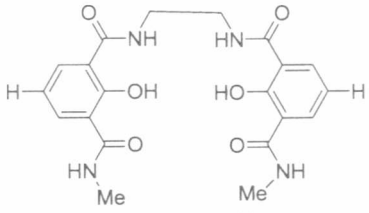

Compound **19**

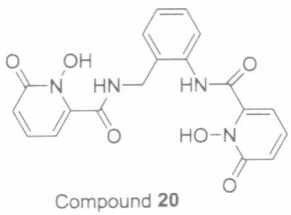

Compound **20**

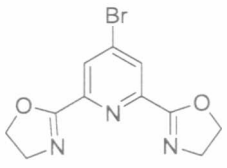

Compound **21**

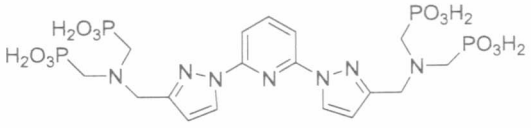

Compound **22**

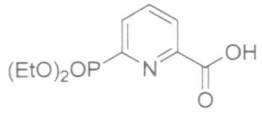

Compound **23**

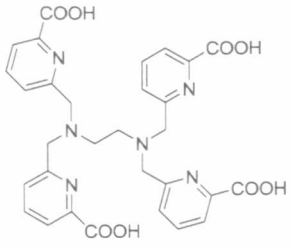

Compound **24**

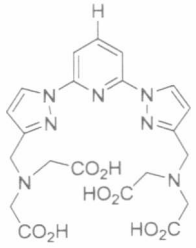

Compound **25**

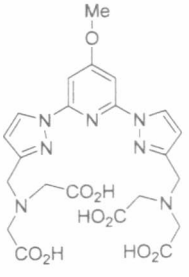

Compound **26**

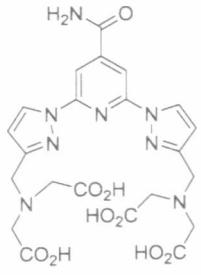

Compound **27**

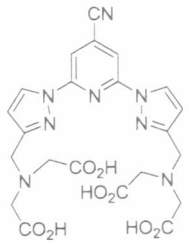

Compound **28**

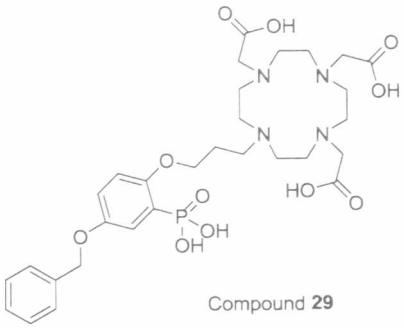

Compound **29**

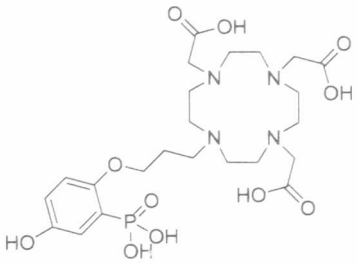

Compound **30**

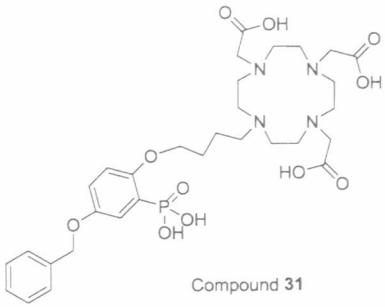

Compound **31**

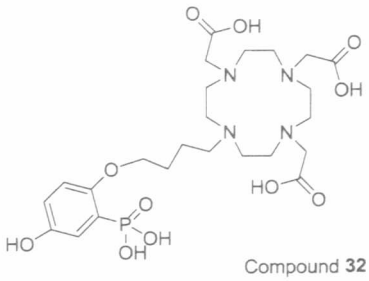

Compound **32**

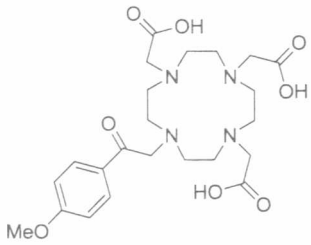

Compound **33**

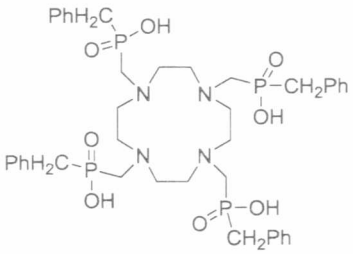

Compound **34**

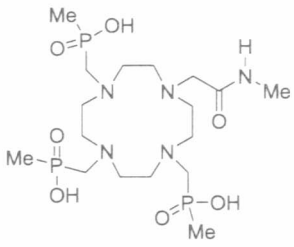

Compound **35**

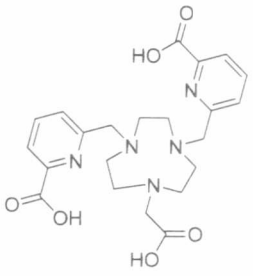

Compound **36**

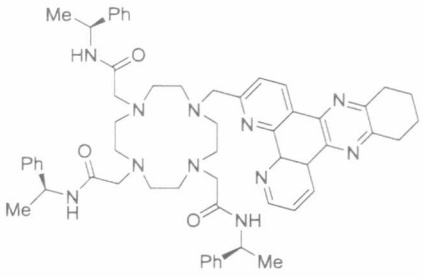

Compound **37**

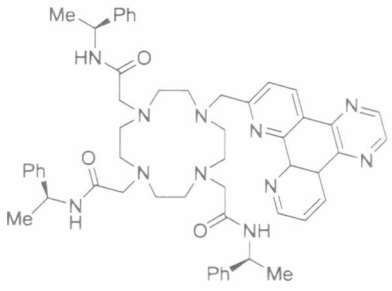

Compound **38**

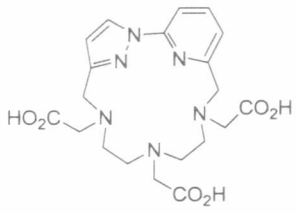

Compound **39**

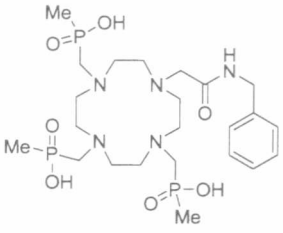

Compound **40**

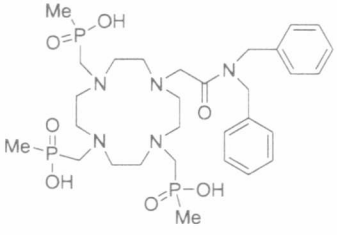

Compound **41**

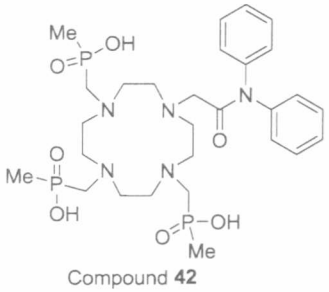

Compound **42**

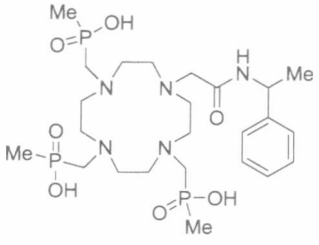

Compound **43**

The structures of Compounds **15 – 43** are shown above. Compounds **15 – 20** are included as they involve the hydroxy*iso*phthalamide moieties, which is possibly the cloest analogue of phthalimide and phthalamate complexes studied here. The highest quantum yield achieved to date using this antennae is 60%, but this utilizes an acyclic ligand, therefore the stability constant for this system will be lower than my macrocyclic systmes. Compounds **22 – 28** involve pyridine derivatives, and the highest quantum yield observed is 95%. However again, these pyridine derivatived ligands suffer the same disadvantage due to their acyclic nature. Compounds **29 – 38** are macrocyclic derivatives. The only comparable complex is [Tb(**34**)]$^{-}$, which has a similar quantum yield (44%) but longer lifetime (4.13 ms). According to the structure of Compound **34**, it could form eight coordinate bonds between ligand and Tb^{3+},[72] therby water molecules could coordinate the Tb^{3+} centre. The other macrocyclic derivatives (**40 – 43**) involve ligands with lower denticity than my

systems hence their luminescence could be quenched by coordinated water molecules.

To sum up, many recently reported highly luminescent Tb^{3+} complexes were designed on the basis of acyclic ligands. According to my literature suvery, the values of quantum yield and lifetime of my complex, $[TbL^{9H}]^-$, is one of the top three systems which benefit from the macrocyclic architecture, and thereby inherent high stability constant, which should be important in any application.

4.3.2.9 Luminescence studies $[EuL^9]/[EuL^{9H}]^-$ and $[EuL^{11}]^+/[EuL^{11H}]^-$

The Eu^{3+} complexes of L^2, L^4, L^6 and L^8 are not investigated in this work, due to the rather weak luminescence observed in the early experiments. However, $[EuL^9]/[EuL^{9H}]^-$ and $[EuL^{11}]^+/[EuL^{11H}]^-$ were studied as their Tb^{3+} analogues had displayed promising characteristics. The luminescence intensity of $[EuL^9]/[EuL^{9H}]^-$ and $[EuL^{11}]^+/[EuL^{11H}]^-$were recorded at various pH values.

Phthalimide-based complexes	Luminescence intensity against various pH	Phthalamate-based complexes
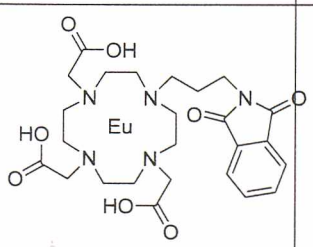 Ligand: L^9	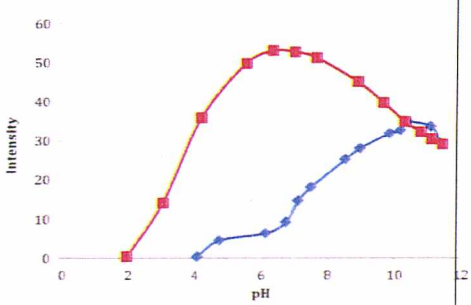	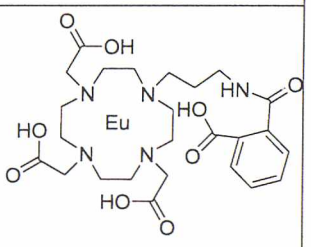 Ligand: L^{9H}
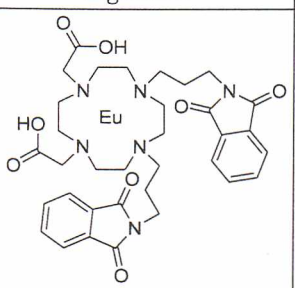 Ligand: L^{11}	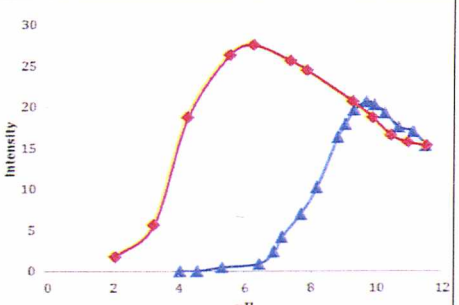	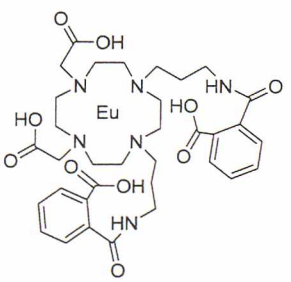 Ligand: L^{11H}

Figure 4.33 Luminescence intensity against pH for $[EuL^9]/[EuL^{9H}]^-$ and $[EuL^{11}]^+/[EuL^{11H}]^-$, ($\lambda_{ex}$: 272 nm; λ_{em}: 615 nm blue plot: increase pH; red plot: decrease pH)

The plots of luminescence intensity against pH of these two Eu^{3+} complexes show the same general characteristics as the analogous Tb^{3+} complexes (Figure 4.33). The luminescence is enhanced significantly by the forming of additional coordinate bond between Eu^{3+} and phthalamate, replacing the coordinated water molecules and creating larger antennae effects.

However, both of the Eu^{3+} complexes show weaker luminescence than Tb^{3+} complexes of the same ligands. The lifetimes and quantum yields of $[EuL^{9H}]^-$ and $[EuL^{11H}]^-$ were measured at pH *ca.*6 (Table 4.7). Since the expected coordination and atomic radius of Eu^{3+} is very similar to those of Tb^{3+}, the reason behind the observed weak luminescence is believed to be the energy transfer efficiency between ligand and Eu^{3+}.

Table 4.7 Lifetimes and quantum yields of $[EuL^{9H}]^-$ and $[EuL^{11H}]^-$ at pH *ca.* 6 (mean ± S.D. of triplicate measurements)

Complexes	Lifetime (ms)	Quantum yield (%)
$[EuL^{9H}]^-$	1.22 ± 0.18	0.5 ± 0.2
$[EuL^{11H}]^-$	1.12 ± 0.11	0.2 ± 0.09

Previous workers have investigated in detail the sensitization of Tb^{3+} and Eu^{3+}, in which the triplet state of its chromophore should be above 20,500 cm^{-1} and 17,500 cm^{-1} for Tb^{3+} and Eu^{3+} respectively.[241] The energy gap between the triplet state of chromophore and the emitting levels of Tb^{3+} and Eu^{3+} should be appropriate, where too big an energy gap results in inefficient energy transfer while too small energy gap results in metal-to-ligand back energy transfer.[284]

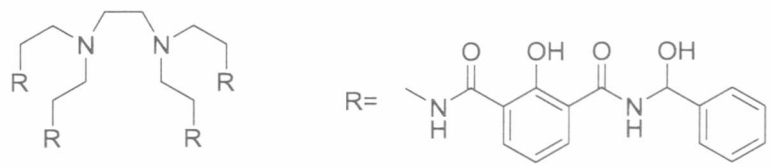

Figure 4.34 Structure of compound **44**

As both complexes contain the same chromophore, the energy gap between Eu^{3+} and the triplet state of phthalamate must be bigger than that for Tb^{3+}. It seems unlikely that any ligand will be successful in sensitizing both lanthanide ions. Hence non-radiative deactivation process is more likely to occur for Eu^{3+}. For example, *Raymond* and his co-workers reported highly luminescent lanthanide

complexes utilizing the hydroxy*iso*phthalimide moiety (Figure 4.34, compound **44**), in which the terbium complex showed a quantum yield of 63% whilst Eu^{3+} had a quantum yield of 2.3%.[84]

4.3.2.10 Quantum yields of these different lanthanide complexes

The energy transfer efficiency from ligand to lanthanide ions can be defined as quantum yield. There are two factors influencing quantum yield significantly:[285] (1) the energy of the triplet state of the ligand and (2) the coordination of the complex.

Since L^{9-12} and L^{9H-13H} contain the same chromophores, either phthalimide or phthalamate, the triplet state of each set of ligands is expected to be the same regardless of the rest of the molecular architecture.

The efficient sensitization displayed by $[TbL^{9H}]^-$ indicates that the triplet state of L^{9H} is slightly higher than the lowest excited state ($^5D_4$) of Tb^{3+}, in order to facilitate energy transfer. The energy level of $^5D_4$ (20500 cm^{-1}) is relatively isolated from its higher excited state (26300 cm^{-1}), while the next excited state above $^5D_0$ for Eu^{3+} is only 1750 cm^{-1} higher in energy.[286] When the triplet state of a ligand is close in energy to the emitting level of Eu^{3+}, energy transfer to the other energy level could occur more efficiently (Figure 4.35).[287]

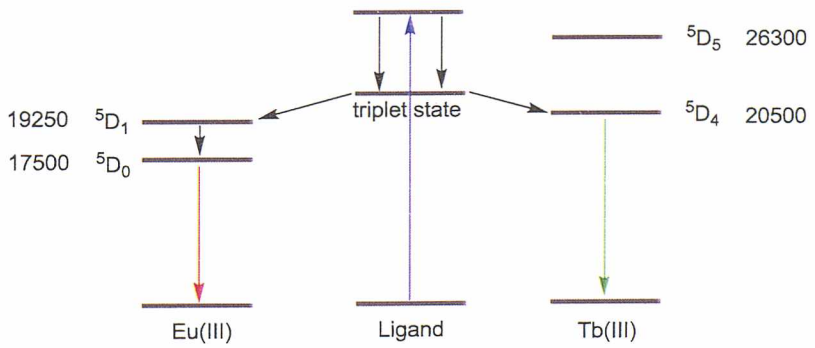

Figure 4.35 Energy transfer between Tb^{3+} or Eu^{3+} and ligand

The relative coordination between lanthanide ions and ligands cause different efficiency of energy transfer. Theoretical methods have been used to design highly luminescent devices with lanthanide complexes. From a theoretical point of view, a

model (Equation 5) describing the energy transfer rates from the triplet state of ligand to the excited state of Eu^{3+} has been proposed by other workers:[288, 289]

$$W_{ET} = \frac{8\pi}{3\hbar}\frac{e^2(1-\sigma_0)^2}{(2J+1)R_L^4}F\langle \alpha' J' \| S \| \alpha J \rangle^2 \times \sum_m \left| \left\langle \phi \left| \sum_k \mu_z(k) s_m(k) \right| \phi' \right\rangle \right|^2$$

Equation 6

where W_{ET} is the energy transfer rate, which is affected by the total spin operator of Eu^{3+} ion (S), the total angular momentum quantum number of Eu^{3+} (J), 4f spectroscopic term (α), the distance from the donor state located at the organic ligand and the Eu^{3+} ion centre (R_L) and the distance dependent screening factor (σ_0). Herein, we focus on the parameter R_L calculated by:[290]

$$R_L = \frac{\sum_i c_i^2 R_{L,i}}{\sum_i c_i^2}$$

Equation 7

where c_i is the molecular orbital coefficient of the atom i contributing to the energy transfer and $R_{L,i}$ is the distance from atom i to the Eu^{3+} ion centre. These two equations can be understood in that the efficiency of energy transfer is affected by the coordination between lanthanide ions and ligands, causing different antennae-to-metal ion distances and angles and hence energy transfer efficiency. Therefore different bridge distance between phthalamate and cyclen may cause different coordination and hence different quantum yields.

4.3.2.11 Potential application of $[TbL^9]$ – $[TbL^{12}]^{2+}$, $[EuL^9]$ and $[EuL^{11}]^+$ as base indicators

The best application of these complexes involves the fact that the luminescence gets turned on between pH 7 and 8. The luminescence of $[TbL^9]$ – $[TbL^{12}]^{2+}$ are rather weak under acidic conditions, whilst their luminescence are significantly enhanced under basic conditions. Similar observations are seen for $[EuL^9]$ and $[EuL^{11}]^+$. The contrast of these complexes in acid/base is illustrated in Figure 4.36. The vertical axis is $\log(I/I_0)$, where I is the luminescence intensity at each particular pH, and I_0 is the luminescence intensity at pH 7. The horizontal axis is pH.

The best contrast is observed on [TbL^9], in which the enhancement of luminescence under basic conditions is most the significant.

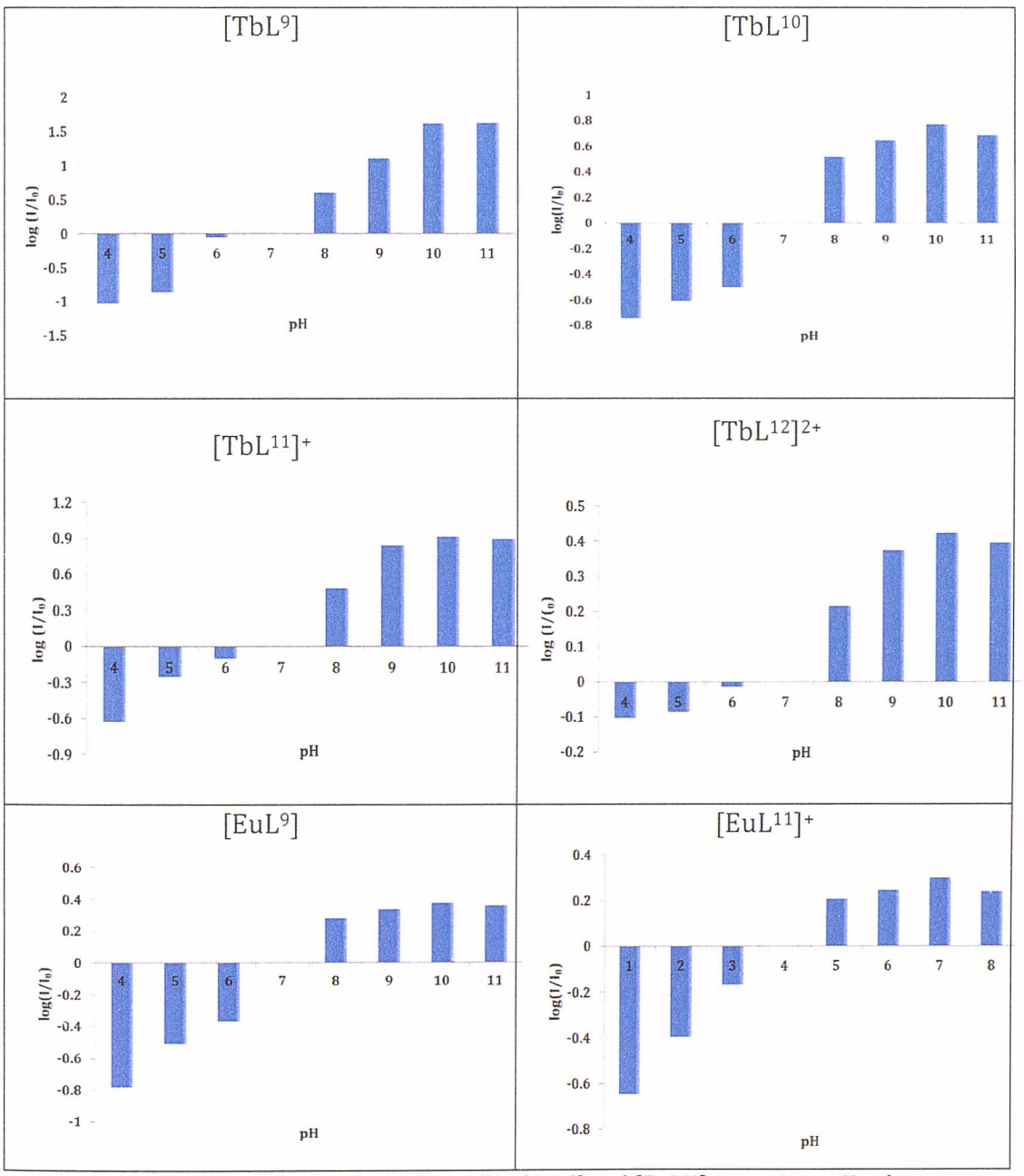

Figure 4.36 Contrast of [TbL^9] – [TbL^{12}]$^{2+}$, [EuL^9] and [EuL^{11}]$^+$ at various pH values

4.4 Conclusion

Four acyclic ligand-based terbium complexes are investigated. The strongest luminescence of [Tb(L^2)$_2$]$^-$ - [Tb(L^8)$_2$]$^-$ are observed at *ca.* pH 6. Their luminescence

is quenched under basic conditions. $[Tb(L^2)_2]^-$ shows the highest luminescence intensity and the longest luminescence lifetime at *ca.* pH 6.

Five novel macrocyclic ligand (L^{9-13})-based complexes are investigated. The luminescence of $[TbL^9]$ – $[TbL^{12}]^{2+}$ are enhanced significantly under basic conditions as $[TbL^{9H}]^-$ – $[TbL^{12H}]^-$ are generated. All these phthalamate-based ligands sensitize more to Tb^{3+} better than Eu^{3+}. The luminescence of $[TbL^{9H}]^-$ – $[TbL^{13H}]^-$ is reduced on addition of acid at low pH because of the protonation of the ligands. The highest luminescence intensities for $[TbL^{9H}]^-$ – $[TbL^{13H}]^-$ are observed at pH *ca.* 6.

$[TbL^{9H}]^-$ shows a long lifetime (2.4 ms) and high quantum yield (46%) in deionised water at pH *ca.* 6. Reviewing comparable terbium complexes, it is worth of note that this complex is one of the top three Tb^{3+} complexes that benefit from macrocyclic architectures, in terms of lifetimes and quantum yields.[43, 64, 67, 84, 278]

Chapter Five Terbium phthalamate complexes as metal ion detectors

5.1 Introduction

Lanthanide complexes have been developed for their potential applications as metal ion detectors by the modulation of their luminescence properties.[111] The design and synthesis of luminescence signalling systems that display large differences between their 'off' (no emission) and 'on' (emissive) states is an attractive area of research within the field of lanthanide complexes.[291]

The spectroscopic features of a lanthanide complex can be affected by the presence of one or more particular metal ions. The UV absorbance of the lanthanide complex can be increased or decreased while luminescence quenching or enhancement has proven useful for the detection of metal ions in solutions. Metal ion detectors detecting essential transition metal ions, such as Cu^{2+}, Zn^{2+}, Hg^{2+}, and Fe^{3+} are currently the most investigated.

Metal ion detectors were first developed by *de Silva and Fabbrizzi et al.*[292] However, only a few of them were using luminescence as output signals. For example, a Tb^{3+} iminodiacetate-cyclen complex, $[Tb(\mathbf{45})]^{3+}$, could selectively detect Cu^{2+} and Hg^{2+} ions (Figure 5.1).[293] In the absence of Cu^{2+} ions, a bright luminescence was observed whereas upon binding to Cu^{2+}, a decrease in emission intensity was detected, being most significant within the addition of ~2 mol equivalents of metal ions.

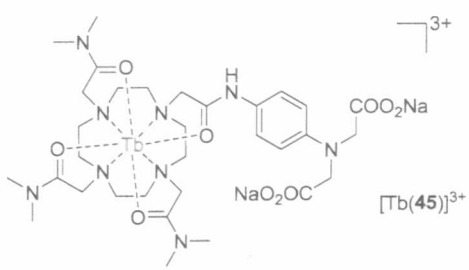

Figure 5.1 Structure of $[Tb(\mathbf{45})]^{3+}$

The luminescence quantum yield of $[Tb(\mathbf{45})]^{3+}$ was reduced as a function of increased Cu^{2+} concentration with *ca.* 65% quenching (Figure 5.2, left). The luminescence lifetime of $[Tb(\mathbf{45})]^{3+}$ was also reduced with addition of Cu^{2+}, from

1.47 ms to 1.18 ms. A similar response was seen with addition of *ca.* 10 mol equivalents of Hg^{2+}, it gave rise to *ca.* 40% luminescence quenching (Figure 5.2, right) and a decreased lifetime of 1.30 ms. These studies were also carried out on Zn^{2+}, Cd^{2+}, Ca^{2+} and Mg^{2+}, which did not lead to any significant changes in the emission of $[Tb(\mathbf{45})]^{3+}$.

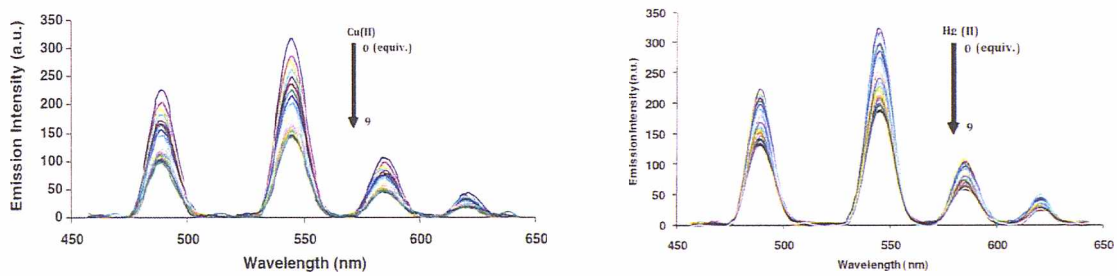

Figure 5.2 Luminescence of $[Tb(\mathbf{45})]^{3+}$ in the presence of Cu^{2+} (left) or Hg^{2+} (right)[293]

The aim of this study is to investigate the potential metal ion detection features of the terbium complex of L^2, L^{9H} and L^{13H} (Figure 5.3). The luminescence features of these complexes were investigated in the presence of different metal ions.

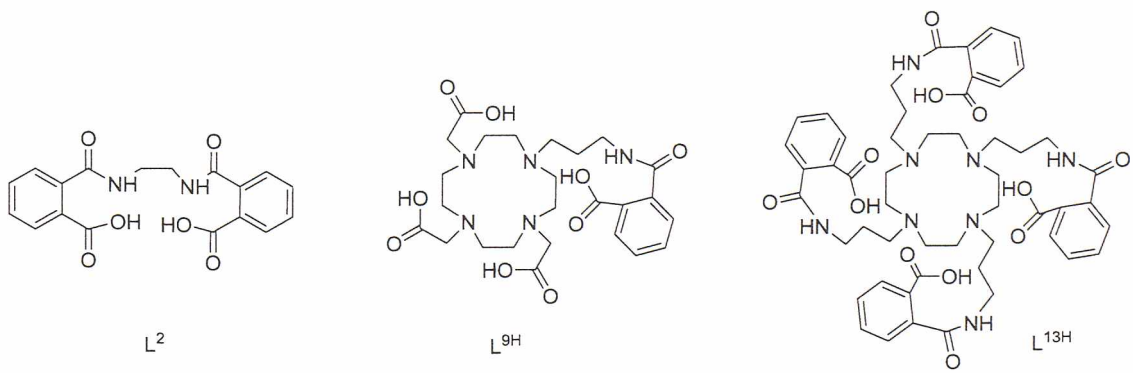

L^2 L^{9H} L^{13H}

Figure 5.3 Structures of L^2, L^{9H} and L^{13H}

5.2 Experimental

5.2.1 General materials

Terbium(III) chloride hexahydrate (99.9%), zinc nitrate hexahydrate (98%), copper(II) nitrate trihydrate (99%), calcium chloride (99.9%), sodium chloride (99.5%), potassium chloride (99%), cobalt(II) chloride hexahydrate (97%), magnesium chloride hyxahydrate (99%), manganese(II) chloride (99%), nickel(II) sulphate heptahydrate (99%), iron(III) sulphate hexahydrate (97%) and iron(II)

sulphate heptahydrate (99%) were purchased from the Sigma–Aldrich Company Ltd, UK and were used without further purification. Buffer solution was prepared by adding 4-(2-hydroxyethyl)-1-piperazineethanesulfonic acid (HEPES) in deionised water and the pH was maintained at *ca.* 6 by HCl or NaOH solutions.

5.2.2 General instruments

NMR spectra were recorded on a Bruker Avance - 500MHz (^{1}H, 500.1 MHz; ^{13}C, 125.8 MHz, Bruker Corporation UK) NMR spectrometer. Both ^{1}H and ^{13}C NMR spectra were recorded in D_2O with 3-(trimethylsiyl)propionic-2,2,3,3-d_4 acid sodium salt as the internal reference. Resonances (δ) are expressed in ppm and J values are given in Hz.

UV-Vis spectrophotometry was measured by a Shimadzu, UV-1800 spectrophotometer (Shimadzu Scientific Instruments, US).

A semi micro prepared pH electrode was used for pH measurements connected to a Jenway 3510 pH meter (Fisher Scientific Ltd, UK).

The luminescence measurements were measured by operating the spectrometer in the phosphorescence mode with a 0.00 ms delay time, 200 ms cycle time, 10.00 ms gate time and a flash count of 5. All the emission spectra utilized a 350 nm cut–off of standard photomultiplier type and an automatic photomultiplier voltage as given by the instructions in the operators' manual. All emission spectra of these metal complex solutions were measured in a fluorescence quartz cuvette (45 mm × 12.5 mm × 12.5 mm) with excitation at $\lambda_{272\ nm}$ (10 and 4 mm path lengths for excitation and emission, respectively).

5.2.3 Luminescence studies of metal ion titrations on $[Tb(L^2)_2]^-$

The stock solutions of Tb^{3+} and L^2 were both prepared in deionised water with concentrations of $5x10^{-3}$ M and $1x10^{-2}$ M respectively. HEPES buffer solution was prepared as $5x10^{-2}$ M and the pH was adjusted by HCl to *ca.* 6. A test solution of $[Tb(L^2)_2]^-$ was prepared by mixing 0.1 cm^3 of the stock solution of Tb^{3+} and 0.1 cm^3

of the stock solution of L^2 in HEPES (4.8 cm^3) solution. Hence the concentration of the final test solution, $[Tb(L^2)_2]^-$, was $1x10^{-4}$ M.

Metal ion solutions, Fe^{3+}, Co^{2+}, Zn^{2+}, Ni^{2+}, Mg^{2+}, Mn^{2+} and Cu^{2+} were all prepared as $1x10^{-2}$ M in HEPES buffer solutions ($5x10^{-2}$ M). Each time 0.1 mol equivalent of metal ions ($5x10^{-3}$ cm^3) was added into the test $[Tb(L^2)_2]^-$ solution. The luminescence intensities ($\lambda_{544\ nm}$) were recorded with excitation at $\lambda_{272\ nm}$. Both excitation and emission slit widths were set at 5 nm. The pH was maintained at *ca.* 6.

5.2.4 ^1H NMR studies of Zn^{2+} and Cu^{2+} titrations on $[La(L^2)_2]^-$

L^2 ($2x10^{-3}$ M) was prepared in Tris buffer (0.01 M) D_2O (0.8 cm^3) and its ^1H NMR spectrum was recorded first. Then the ^1H NMR spectrum of $[La(L^2)_2]^-$ was recorded by adding 0.5 mol equivalent of La^{3+} (0.1 M, $8x10^{-3}$ cm^3) into the L^2 solution. Hereafter, 0.1 mol equivalent of Zn^{2+} ($2x10^{-2}$ M, $4x10^{-3}$ cm^3) was added into $[La(L^2)_2]^-$ sequentially, and the addition was ended at 0.9 mol equivalent of Zn^{2+}.A ^1H NMR spectrum was recorded every time Zn^{2+} was added. This experiment was repeated by addition of Cu^{2+} instead of Zn^{2+}. The solvent signal was used as internal reference.

5.2.5 Luminescence studies of metal ion titrations on $[TbL^{13H}]^-$

Stock solutions of Tb^{3+} ($5x10^{-3}$ M) and L^{13H} ($2.5x10^{-3}$ M) were prepared in deionised water. $[TbL^{13H}]^-$ was prepared by mixing the stock solutions of Tb^{3+} ($5x10^{-2}$ cm^3) and L^{13H} (0.1 cm^3) in HEPES buffer solution ($5x10^{-2}$ M, 3.85 cm^3). The concentration of the final test solution, $[TbL^{13H}]^-$, was $6.25x10^{-5}$ M. All the metal ion solutions, Cu^{2+}, Zn^{2+}, Ca^{2+}, Co^{2+}, Fe^{3+}, Fe^{2+} and Ni^{2+} were prepared as 0.1 M in HEPES buffer solution ($5x10^{-2}$ M).

Each time 0.5 mol equivalent of metal ion solution ($1.25x10^{-3}$ cm^3) was added into $[TbL^{13H}]^-$. The addition was ended at 5 mol equivalents of metal ions in total. The luminescence intensities ($\lambda_{544\ nm}$) were recorded with excitation at $\lambda_{272\ nm}$. Both

excitation and emission slit widths were set at 10 nm. The pH was maintained at *ca.* 6.

5.2.6 Luminescence studies of metal ion titrations on $[TbL^{9H}]^-$

Stock solutions of Tb^{3+} ($5x10^{-3}$ M) and L^{9H} ($5x10^{-3}$ M) were prepared in deionised water. $[TbL^{9H}]^-$ was prepared by mixing the stock solutions of Tb^{3+} ($5x10^{-2}$ cm^3) and L^{9H} ($5x10^{-2}$ cm^3) in HEPES buffer solution ($5x10^{-2}$ M, 3.9 cm^3). The concentration of the final test solution, $[TbL^{9H}]^-$, was $6.25x10^{-5}$ M. All the metal ion solutions, Cu^{2+}, Zn^{2+}, Ca^{2+}, Co^{2+}, Fe^{3+}, Na^+ and K^+ were prepared as $2.5x10^{-2}$ M in HEPES solution ($5x10^{-2}$ M).

Each time 0.2 mol equivalent of metal ion solution ($2x10^{-3}$ cm^3) was added into $[TbL^{9H}]^-$. The addition was ended at 2 mol equivalents of metal ions. The luminescence intensities ($\lambda_{544\ nm}$) were collected with excitation at $\lambda_{272\ nm}$. Both excitation and emission slit widths were set at 2.5 nm. The pH was maintained at *ca.* 6.

5.2.7 Luminescence studies of anion titrations on $[TbL^{9H}]^-$

$[TbL^{9H}]^-$ was prepared under the same conditions described in Section 5.2.6. All the anions HCO_3^-, CO_3^{2-}, Cl^-, I^- and CH_3COO^- were all prepared as $2.5x10^{-2}$ M in HEPES solution ($5x10^{-2}$ M). Each time 0.2 mol equivalent of anion solution ($2x10^{-3}$ cm^3) was added into $[TbL^{9H}]^-$. And 2 mol equivalents of metal ions were added in total. The luminescence intensities ($\lambda_{544\ nm}$) were recorded with excitation wavelength at $\lambda_{272\ nm}$. Both excitation and emission slit widths were set at 2.5 nm. The pH was maintained at *ca.* 6.

5.3 Results and discussion

It has been reported that the modulation of luminescence properties of lanthanide complex was due to the binding affinities of the ligand to the lanthanide in the presence of additional metal ions (such as Cu^{2+}).[292, 294, 295] In Chapter 4, it has been

demonstrated that four acyclic phthalamate-based complexes, $[Tb(L^2)_2]^-$, $[Tb(L^4)_2]^-$, $[Tb(L^6)_2]^{3-}$ and $[Tb(L^8)_2]^-$, showed their highest luminescence at pH *ca.* 6. The same was observed on macrocyclic phthalamate-based complexes, $[TbL^{9H}]^-$, $[TbL^{10H}]^-$, $[TbL^{11H}]^-$, $[TbL^{12H}]^-$ and $[TbL^{13H}]^-$. All these Tb^{3+} complexes have the same receptor functions, phthalamate. Hence the study of the effect on the luminescence of the Tb^{3+} complexes by the addition of transition and alkali metal ions was first focused on $[Tb(L^2)_2]^-$. L^{13H} is a cyclen derived ligand appended with four phthalamate functions, it is an analogue of L^2, so $[TbL^{13H}]^-$ was also selected for this study. The third Tb^{3+} complex, $[TbL^{9H}]^-$, was chosen for its metal ion detector potential because of its high luminescence level under the same conditions (*cf.* Chapter 4).

5.3.1 Spectroscopic studies of metal ion titrations on $[Tb(L^2)_2]^-$

5.3.1.1 UV studies of metal ion titrations on $[Tb(L^2)_2]^-$

It has been reported previously that UV absorption wavelength of lanthanide complex solutions could be increased or decreased with addition of metal ions. So UV measurements of $[Tb(L^2)_2]^-$ were carried out by titrating Mn^{2+}, Fe^{3+}, Co^{2+}, Ni^{2+}, Cu^{2+}, Zn^{2+} and Mg^{2+} ions to the $[Tb(L^2)_2]^-$ solutions.

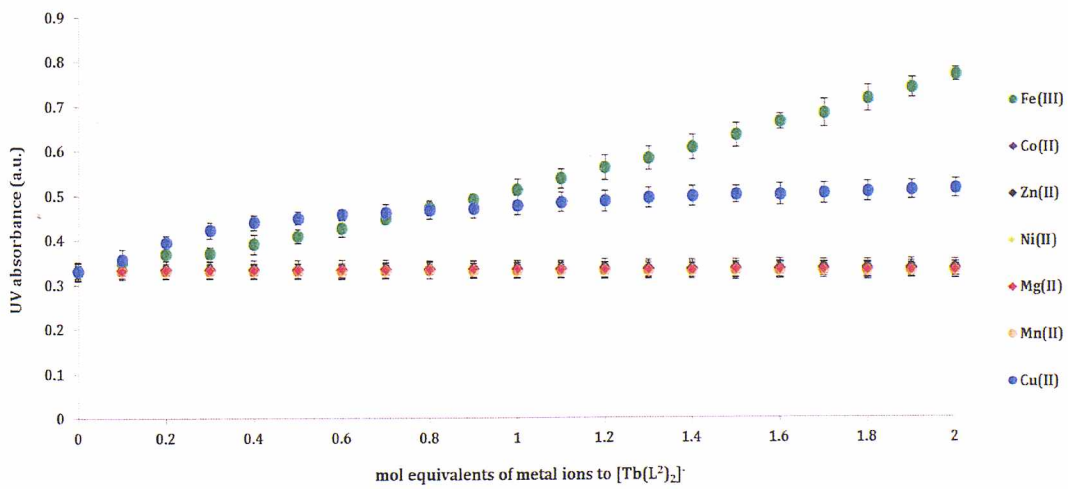

Figure 5.4 UV absorbance ($\lambda_{272\,nm}$) against mol equivalent of metal ions (mean ± S.D. of triplicate measurements)

It shows that the UV absorption at $\lambda_{272\,nm}$ is only affected by Fe^{3+} and Cu^{2+}, whereas no significant changes were observed in the UV absorbance in the presence of other metal ions (Figure 5.4, the data points of Co^{2+}, Zn^{2+}, Ni^{2+}, Mg^{2+} and Mn^{2+} are

overlapped). Because both the concentrations of $[Tb(L^2)_2]^-$ and Fe^{3+} are known, so the relationship between UV absorbance and the concentration of Fe^{3+} could be measured. A plot of the UV absorbance of $[Tb(L^2)_2]^-$ against the concentration of Fe^{3+} in the solution is shown (Figure 5.5), where a straight line is obtained between 0.3 – 2 equivalents.

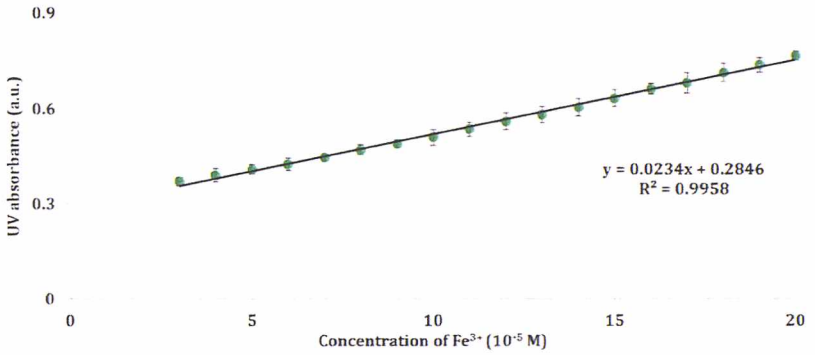

Figure 5.5 UV absorbance against concentration of Fe^{3+} (mean ± S.D. of triplicate measurements)

An increased UV absorbance of $[Tb(L^2)_2]^-$ at $\lambda_{272\ nm}$ is observed with gradual addition of Cu^{2+}. The most significantly increase is observed with addition between 0.1 – 0.5 mol equivalent of Cu^{2+}. There is *ca.* 33% UV absorbance enhanced in the presence of 0.5 equivalent of Cu^{2+}, while further addition of Cu^{2+} (~2 mol equivalents) only shows a 20% increase in the UV absorbance.

Both the UV absorbance at $\lambda_{272\ nm}$ of L^2 and $[Tb(L^2)_2]^-$ were measured in the presence of Cu^{2+} under the same condition so as to investigate the complexation behaviour of the ligand and the Tb^{3+} complex with Cu^{2+} (Figure 5.6).

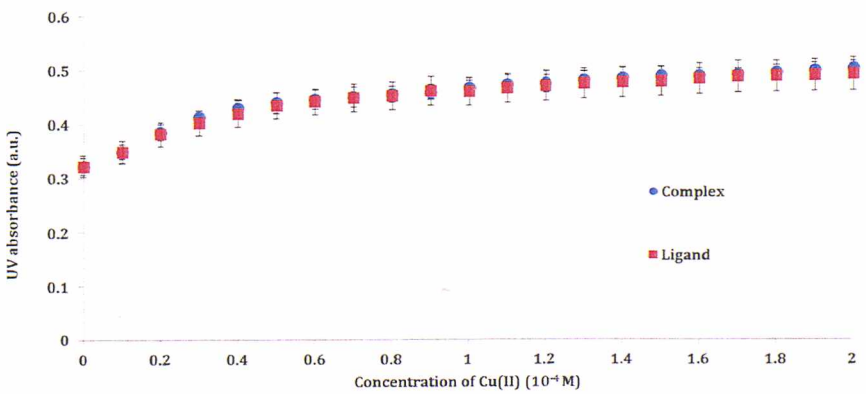

Figure 5.6 UV absorbance (272 nm) against concentration of Cu^{2+}, with or without Tb^{3+} (mean ± S.D. of triplicate measurements)

The results shown in Figure 5.6 indicate that the changes in the UV absorbance is similar when Cu^{2+} is added to L^2 or $[Tb(L^2)_2]^-$. This is consistent with previous reports that changes in the absorption was a result from the interaction between Cu^{2+} and the receptor site of the ligand.[296, 297]

5.3.1.2 Luminescence measurements of $[Tb(L^2)_2]^-$ by addition of different metal ions

The luminescence level of $[Tb(L^2)_2]^-$ was most affected in the presence of Cu^{2+} and Fe^{3+} (Figure 5.7). With the addition of Cu^{2+}, the most significant luminescent reduction occurs between 0.1 – 0.5 equivalent, *ca.* 28% luminescence is reduced. A relatively smaller reduction in luminescence (*ca.* 8%) is observed when Cu^{2+} (0.5 – 2 equivalents) is added. With the addition of Fe^{3+}, the luminescence is reduced by *ca.* 2% with addition of every 0.1 mol equivalent of Fe^{3+}. Analogous titration experiments were carried out on other metal ions (Co^{2+}, Zn^{2+}, Ni^{2+}, Mg^{2+} and Mn^{2+}), however, no significant changes of luminescence were observed.

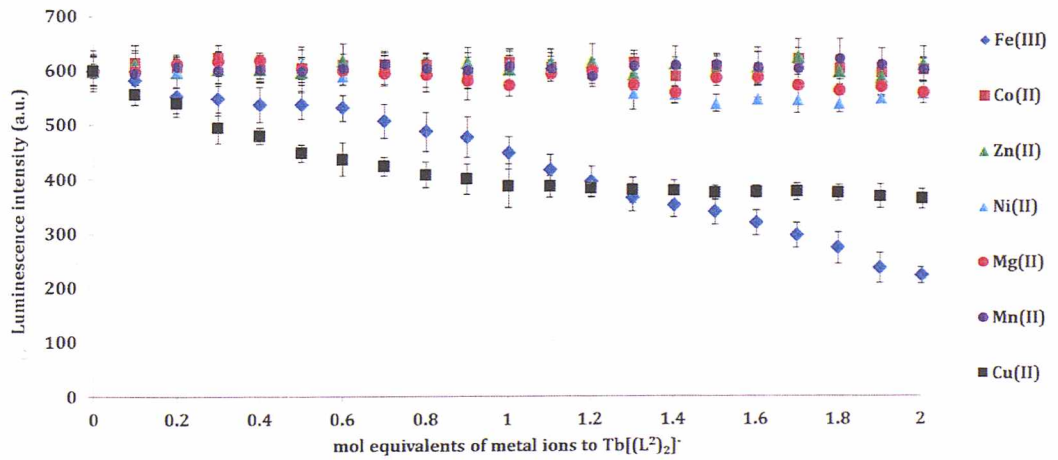

Figure 5.7 Luminescence intensities against different mol equivalent of metal ions to $[Tb(L^2)_2]^-$ (mean ± S.D. of triplicate measurements)

It is worth noting that with the addition of Cu^{2+} in $[Tb(L^2)_2]^-$, the reduced luminescence level is similar to the increased UV absorbance level (Figure 5.8a). The same phenomenon is seen on the experiment of Fe^{3+} titrations (Figure 5.8b). This indicates that the changes of the UV absorbance have a direct effect on the changes of luminescence of $[Tb(L^2)_2]^-$.

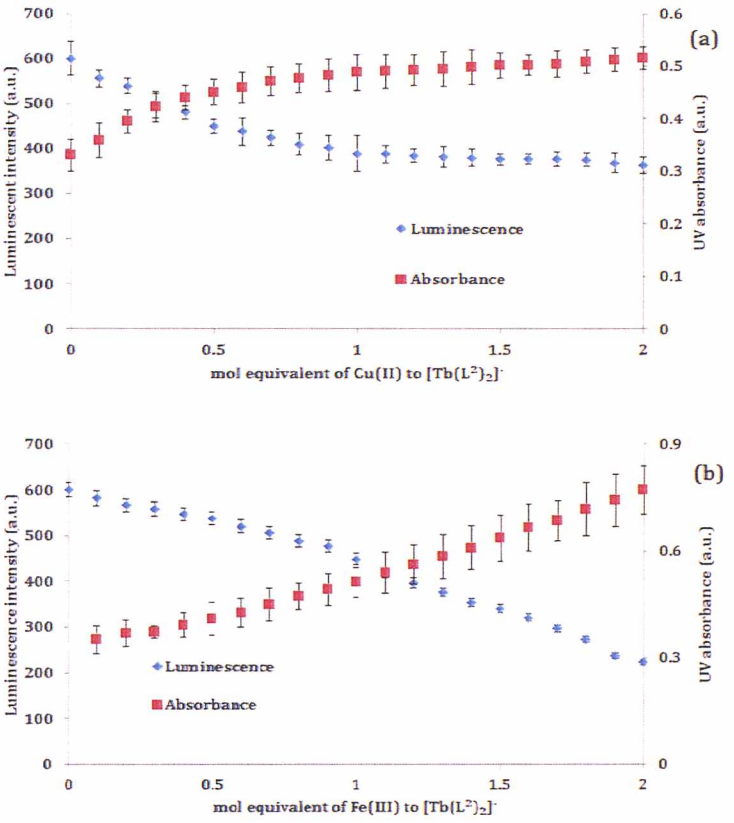

Figure 5.8 Luminescence intensity/absorbance against mol equivalent of (a) Cu^{2+} and (b) Fe^{3+}

It has previously been reported that the coordination of a lanthanide complex could be affected by the presence of metal ions, such as Cu^{2+}.[298] For example, the coordination between Gd^{3+} and the pyridine nitrogen in [Gd(**46**)] could be changed by Cu^{2+} (Figure 5.9).[299] The changes of the coordination are dominated by the binding affinities between metal ions and the receptor sites of the ligands.[300]

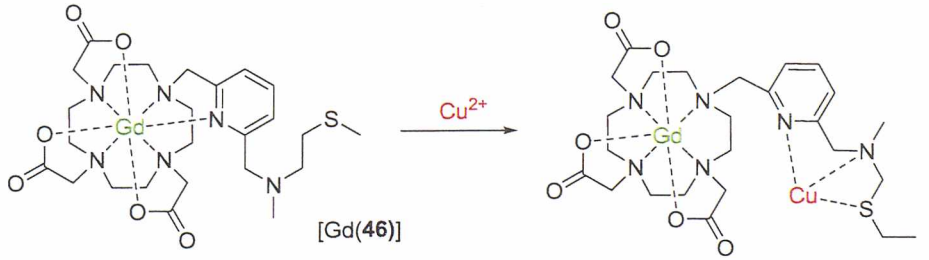

Figure 5.9 Coordination replacement in [Gd(**46**)] by Cu^{2+}

As it was described in Chapter 4, the luminescence quenching of a lanthanide complex was due to the energy transfer from the antennae.[293, 301] The efficiency of energy transfer from the antennae was dominated by the coordination and distance between antennae and lanthanide ions. In this case, the coordination

between phthalamate functions and Tb^{3+} could be affected in the presence of Cu^{2+} in the $[Tb(L^2)_2]^-$ solution, resulting in a weak antennae effect (Figure 5.10). On the other hand, the changes of coordination could increase the chances of vibrational quenching from water molecules. The changes of the coordination occur more significantly in the presence of Fe^{3+}, whereby more luminescence is reduced.

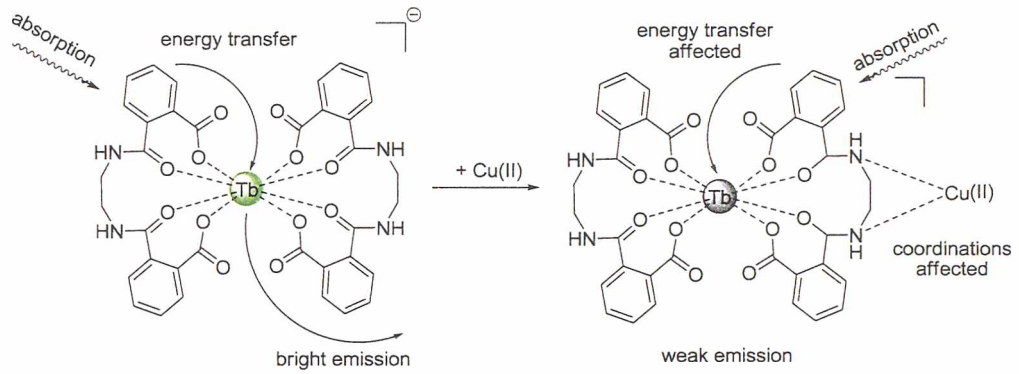

Figure 5.10 Luminescence quenching in the presence of Cu^{2+}

The luminescence was not affected in the presence of other metal ions (Co^{2+}, Zn^{2+}, Ni^{2+}, Mg^{2+} and Mn^{2+}). Selective luminescence quenching can be accounted for the various coordination affinities involving the phthalamate functions.[292] Thus, the quenching is not related to the size and the shape of the metal ions, but is associated with the capability of affecting more or less the coordination between Tb^{3+} and L^2. [302] On the other hand, the pH of the solution also dominates the formation of the coordinate bond between phthalamate functions and the metal ions. In fact, according to *L. Fabbrizzi's* work, the Cu^{2+} complex could be observed with coordinating to amide, whereas a complexation of Ni^{2+} has yet to begin between pH 6 – 7.[292]

5.3.1.3 ^{1}H NMR studies of $[La(L^2)_2]^-$ by addition of Zn^{2+} and Cu^{2+}

In order to investigate any possibilities of decomposition or coordination replacement with addition of Cu^{2+},a ^{1}H NMR spectroscopy experiment was carried out. Because the electron configuration of Zn^{2+} is $[Ar]3d^{10}$, hence it is not paramagnetic, the spectra recorded were used for comparison to those of Cu^{2+}.

The ^{1}H NMR spectra of $[La(L^2)_2]^-$ with the addition of Zn^{2+} at various mol equivalents were recorded (Figure 5.11). A resonance at *ca.* δ 7.60 ppm (H^3 and $H^{3'}$ protons) was shifted to δ 7.64 ppm when La^{3+} was coordinated with L^2. The splitting patterns and chemical shift of the signals were not changed after additions of Zn^{2+}. This indicates that the interaction between Zn^{2+} has no or very little effect on the coordination of the $[La(L^2)_2]^-$ complex.

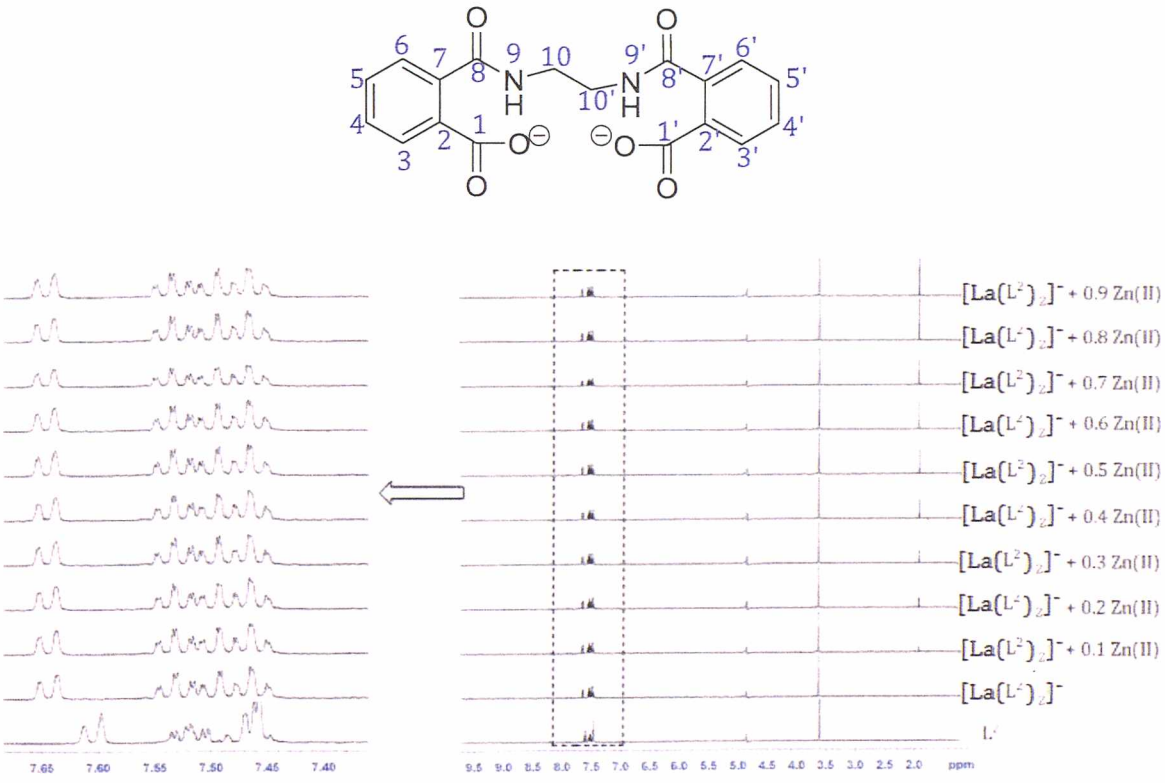

Figure 5.11 ^{1}H NMR spectra of $[La(L^2)_2]^-$ with addition of Zn^{2+}

The ^{1}H NMR spectra of $[La(L^2)_2]^-$ with gradual addition of Cu^{2+} were recorded (Figure 5.12). The resonance at *ca.* δ 7.60 ppm (H^3 and $H^{3'}$) in L^2 was shifted to δ 7.65 ppm, due to the complexation to form $[La(L^2)_2]^-$. An unpaired electron in Cu^{2+} causes a fast paramagnetic relaxation, resulting in very broad NMR signals and unresolved *J* – couplings.[303,304] After the addition of Cu^{2+} at 0.1 mol equivalent (Figure 5.12), the signals of H^3 and $H^{3'}$ protons were broadened, and the rest of the aromatic protons were broadened and shifted at the same time. The signal of ethylene protons (H^{10} and $H^{10'}$) is shifted from δ 3.6 ppm to δ 3.8 ppm. The solvent peak remained at δ 4.85 ppm. The broadening and shifting effects of the ligand after addition as little as 0.1 mol equivalent of Cu^{2+} as observed in the NMR study

confirms the complexation of the Cu^{2+} to the ligand L^2. This may explain the reduction of luminescence intensity in $[Tb(L^2)_2]^-$ as 0.1 mol equivalent addition of Cu^{2+} as observed in Section 5.3.1.2.

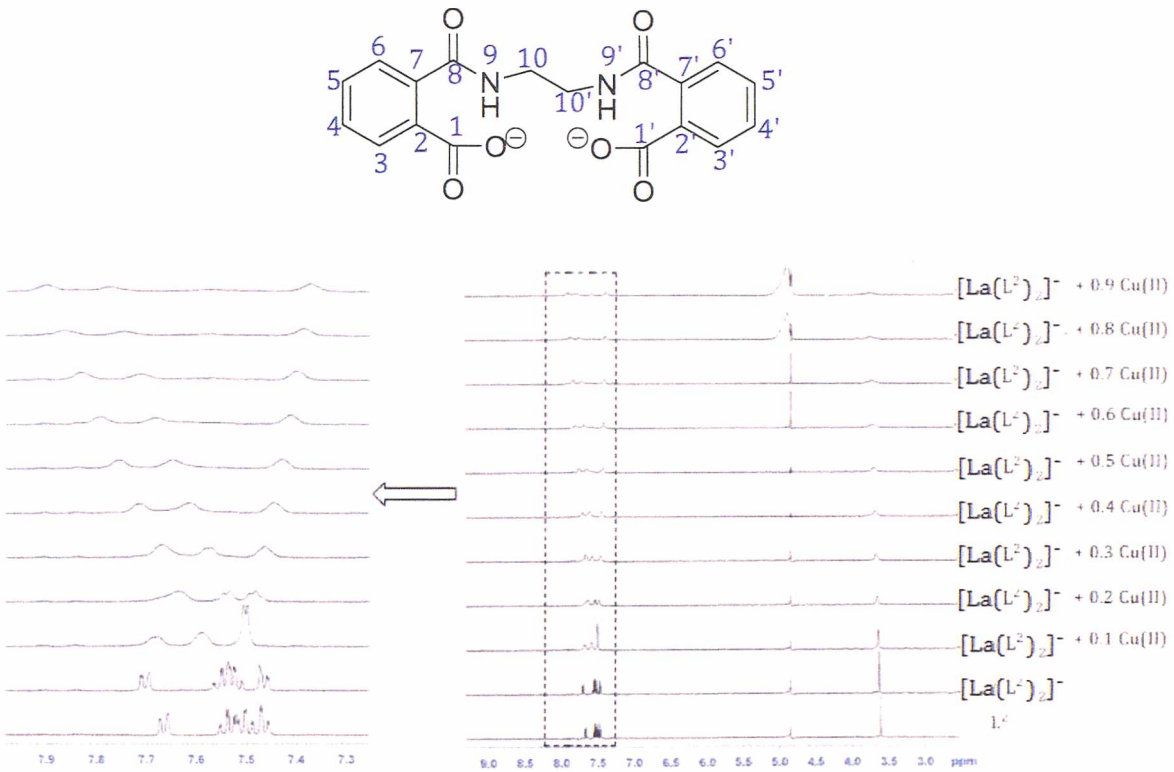

Figure 5.12 ^1H NMR spectra of $[La(L^2)_2]^-$ complex with addition of Cu^{2+}

5.3.1.4 Potential applications of $[Tb(L^2)_2]^-$

$[Tb(L^2)_2]^-$ is clearly responsive to two particular metal ions, Cu^{2+} and Fe^{3+}. So this complex can potentially act as a metal ion detector, in which the luminescence of the solution can be quenched in the presence of Cu^{2+} and Fe^{3+}.

A NOR mode molecular logic for $[Tb(L^2)_2]^-$ can be devised (Table 5.1), in which the luminescence is observed only of a solution without the presence of both Cu^{2+} and Fe^{3+}.

Table 5.1 Conditional logic (NOR) for $[Tb(L^2)_2]^-$

	Input		Output
	Input 1 Cu^{2+}	Input 2 Fe^{3+}	
$[Tb(L^2)_2]^-$	0	0	1
	0	1	0
	1	0	0
	1	1	0

5.3.2 Luminescence studies of metal ion titrations on $[TbL^{13H}]^-$

5.3.2.1 Luminescence studies of $[TbL^{13H}]^-$ with addition of different metal ions

L^{13H} is a macrocyclic ligand based on a cyclen unit with four appended phthalamate functions. It is similar to L^2. An aqueous solution of $[TbL^{13H}]^-$ was treated with different metal ions solutions, Cu^{2+}, Zn^{2+}, Ca^{2+}, Co^{2+}, Fe^{3+}, Fe^{2+} and Ni^{2+}. The luminescence spectra showed that $[TbL^{13H}]^-$ was selectively responsive to Cu^{2+} and Fe^{3+}, which is similar to $[Tb(L^2)_2]^-$ in Section 5.3.1. The most significant luminescence quenching was observed with the addition of 0.1 – 0.5 mol equivalent of Cu^{2+}, where about 70% luminescence was reduced (Figure 5.13) in comparison to 28% for $[Tb(L^2)_2]^-$. Fe^{3+} could reduce the luminescence gradually up until *ca.* 3 mol equivalents at 75%.

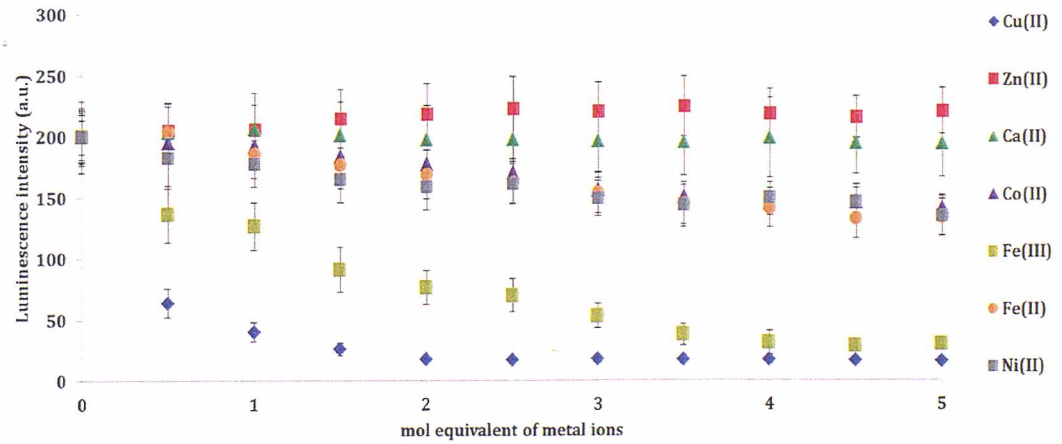

Figure 5.13 Luminescence intensities of $[TbL^{13H}]^-$ against mol equivalent of different metal ions (mean ± S.D. of triplicate measurements)

A rather weak luminescence quenching is observed when Fe^{2+}, Ni^{2+} or Co^{2+} was added. Luminescence quenching for Ni^{2+} and Fe^{2+} by $[Eu(\mathbf{47})]^{3+}$ has been reported previously (Figure 5.14).[305, 306] Therefore the quenching of luminescence in $[TbL^{13H}]^-$ solutions is due to the binding between Fe^{2+}, Ni^{2+} or Co^{2+} to the antennae of $[TbL^{13H}]^-$, but its influence is rather weak.

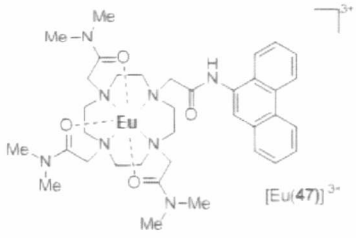

Figure 5.14 Structure of $[Eu(\mathbf{47})]^{3+}$

5.3.2.2 Potential applications of $[TbL^{13H}]^-$

It has been shown that $[TbL^{13H}]^-$ is responsive to two particular transition metal ions, Cu^{2+} and Fe^{3+}. So it can potentially act as a metal ion detector, in which the luminescence of the solution can be quenched by Cu^{2+} and Fe^{3+}. A NOR mode molecular logic gate for $[TbL^{13H}]^-$ can be established similar to that of $[Tb(L^2)_2]^-$ (*cf.* Table 5.1).

5.3.3 Luminescence studies of metal ion titrations on $[TbL^{9H}]^-$

5.3.3.1 Luminescence studies of $[TbL^{9H}]^-$ with addition of different metal ions

$[TbL^{9H}]^-$ has been demonstrated to be the best complex, in terms of lifetime and quantum yield. $[TbL^{9H}]^-$ has additional methyl carboxylate functions appended on the cyclen in the ligand, which is not the case in $[Tb(L^2)_2]^-$ and $[TbL^{13H}]^-$.

An aqueous solution of $[TbL^{9H}]^-$ was treated with different metal ions solutions, Cu^{2+}, Zn^{2+}, Ca^{2+}, Co^{2+}, Fe^{3+}, Ca^{2+} and K^+. The luminescence measurements showed that $[TbL^{9H}]^-$ was selectively responsive to Cu^{2+} and Co^{2+} (Figure 5.15). The most significant luminescence reduction observed during the addition of Cu^{2+} was between 0.2 – 1.0 mol equivalent, where about 65% luminescence intensity was

reduced (Figure 5.15). Co^{2+} reduced the luminescence intensity of $[TbL^{9H}]^-$ more gradually. The additional methyl carboxylate functions presumably have stronger coordination to Co^{2+}.

However, luminescence was not affected by the addition of other metal ions. The luminescence of $[TbL^{9H}]^-$ was not selectively quenched by Ca^{2+}, indicating Ca^{2+} (similar ionic radius to Tb^{3+}) did not replace Tb^{3+} from the macrocyclic ligand and it had very little effect on the antennae binding to the Tb^{3+}.

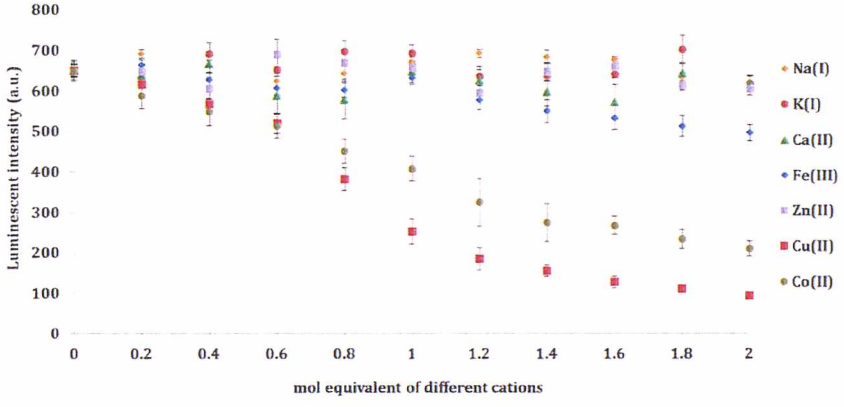

Figure 5.15 Luminescence intensity of $[TbL^{9H}]^-$ with addition of different metal ions (mean ± S.D. of triplicate measurements)

It is widely accepted that the quenching of lanthanide luminescence is a result from the binding between ligand and the added metal ions, but it has also been reported previously that the luminescence of Tb^{3+} can be quenched by Co^{2+} by an energy transfer between these two metal ions. The absorption spectrum of Co^{2+} is between 400 – 600 nm in deionised water, which is similar to the emission spectrum of Tb^{3+}.[307] In addition, this quenching is dominated by the distance between Tb^{3+} and Co^{2+}. For example, a distance of 13.7 Å between Tb^{3+} and Co^{2+} results in an efficient energy transfer, with quantum yield of about 50%.[308, 309] A longer distance decreases the energy transfer efficiency. This can possibly explain the luminescence quenching by Co^{2+} in this study. Both $[Tb(L^2)_2]^-$ and $[TbL^{13H}]^-$ have four phthalamate functions and these bulky molecules creat a steric environment which potentially can shield the interaction between Tb^{3+} and Co^{2+}. In this situation, it seems that the energy on the excited state of phthalamate of $[TbL^{9H}]^-$ could be transferred to the excited state of Tb^{3+}, followed by quenching through further energy transfer to Co^{2+} (Figure 5.16).

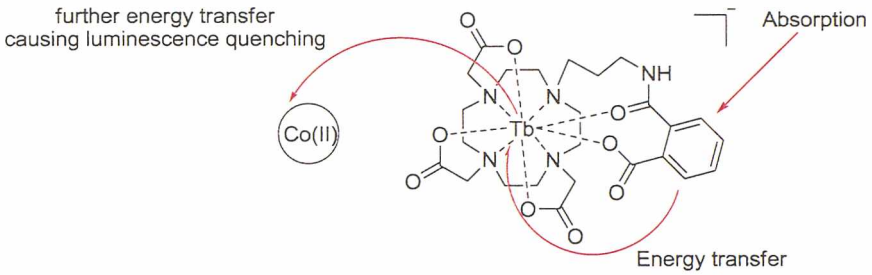

Figure 5.16 Luminescence quenching of $[TbL^{9H}]^-$ by Co^{2+}

Apart from the quenching by metal ions, the presence of some common biological anions, such as chloride, acetate and hydrogen carbonate would lead to descrease/increase in the overall emission intensity of lanthanide complexes.[310] So the luminescence intensity of $[TbL^{9H}]^-$ was also studied with the addition of five anions, Cl^-, I^-, HCO_3^-, CO_3^{2-} or CH_3COO^-.

The luminescence intensity of $[TbL^{9H}]^-$ remains at a similar level upon addition of anions (Figure 5.17). Neither an increase nor decrease of luminescence was observed upon increasing the concentrations of these anions.

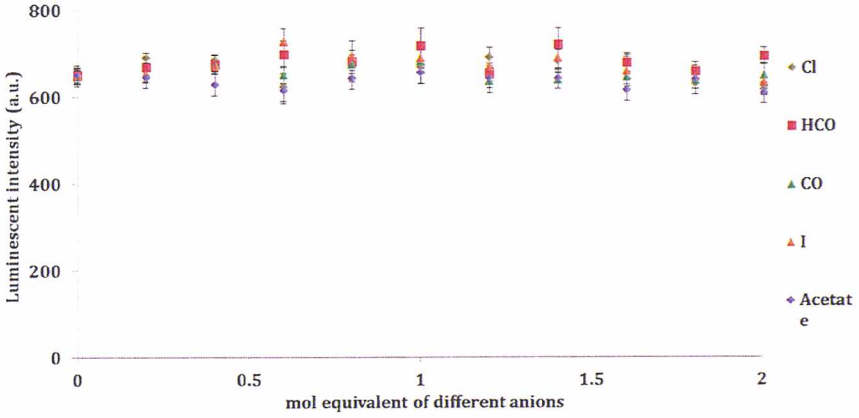

Figure 5.17 Luminescence intensity of $[TbL^{9H}]^-$ with addition of different anions (mean ± S.D. of triplicate measurements)

5.3.3.2 Potential applications of $[TbL^{9H}]^-$

$[TbL^{9H}]^-$ is responsive to two particular transition metal ions, Cu^{2+} and Co^{2+}. So it can potentially act as a metal ion detector, in which the luminescence of the solution can be quenched by Cu^{2+} and Co^{2+}. A NOR mode molecular logic for $[TbL^{9H}]^-$ can be established similar to that of $[Tb(L^2)_2]^-$ (*cf* Table 5.1).

5.3.4 Quenching rate constant measurements

The results in Section 5.3.1 – 5.3.3 have shown that the luminescence of three complexes, $[Tb(L^2)_2]^-$, $[TbL^{13H}]^-$ and $[TbL^{9H}]^-$, can be quenched by particular metal ions. The luminescence quenching rate constant by different metal ions can be estimated by the Stern-Volmer equation which describes the relationship between luminescence intensity and concentration of the quenchers (Equation 7):[311-314]

$$\frac{I_0}{I} = 1 + \frac{k_q}{k_l + k_{nr}}[Q] \quad \textbf{Equation 8}$$

where k_q is a quenching rate constant (M^{-1} s^{-1}), k_l is a luminescence decay rate constant, k_{nr} is a non-radiative decay rate constant, I_0 is the luminescence intensity in the absence of a quencher, I is the luminescence intensity in the presence of a quencher, [Q] is the concentration of the quencher and a plot of I_0/I versus concentration of quencher should yield a straight line with a slope of $k_q/(k_l + k_{nr})$. In this case, $1/(k_l + k_{nr})$ is equal to luminescence lifetime (τ in s) of the complex in the absence of a quencher. The quenching rate constant (k_q) is equal to the slope divided by the lifetime (τ).

The plots of I_0/I versus concentration of each quencher are shown below (Figure 5.18 – Figure 5.20):

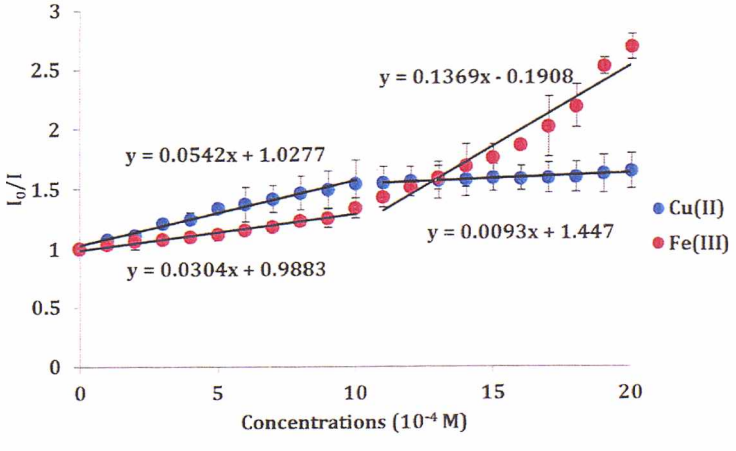

Figure 5.18 I_0/I of $[Tb(L^2)_2]^-$ against the concentrations of Cu^{2+} and Fe^{3+}

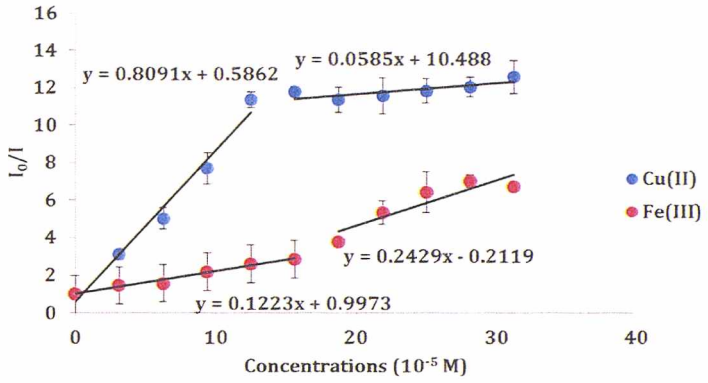

Figure 5.19 I_0/I of $[TbL^{13H}]^-$ against the concentrations of Cu^{2+} and Fe^{3+}(mean ± S.D. of triplicate measurement)

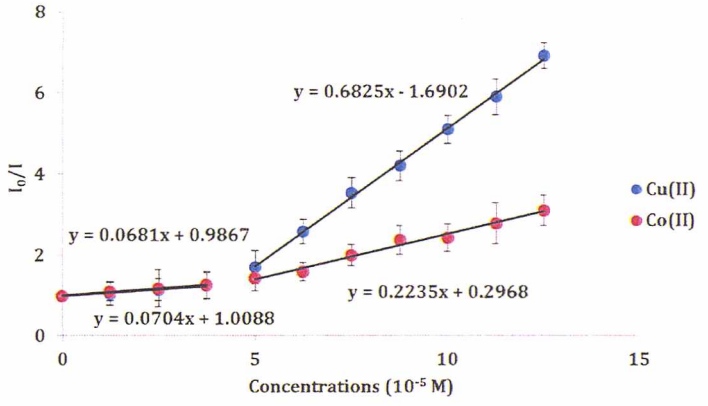

Figure 5.20 I_0/I of $[TbL^{9H}]^-$ against the concentrations of Cu^{2+} and Co^{3+} (mean ± S.D. of triplicate measurement)

With addition of different quenchers (metal ions), a single linear relationship is not observed between the I_0/I and the entire concentrations of quenchers measured. However attempts were made to fit parts of the range of the concentration of quencher. The quenching rate constants were calculated at different ranges of concentrations and presented in Table 5.2 – 5.4.

Table 5.2 Quenching rate constants with addition of Cu^{2+} and Fe^{3+} to $[Tb(L^2)_2]^-$

	Cu^{2+}						Fe^{3+}					
	Concentration ($x10^{-3}$ M)						Concentration ($x10^{-3}$ M)					
	0 – 1.0			1.1 – 2.0			0 – 1.0			1.1 – 2.0		
$[Tb(L^2)_2]^-$	Slope (M^{-1})	τ (ms)	k_q (M^{-1} s^{-1})	Slope (M^{-1})	τ (ms)	k_q (M^{-1} s^{-1})	Slope (M^{-1})	τ (ms)	k_q (M^{-1} s^{-1})	Slope (M^{-1})	τ (ms)	k_q (M^{-1} s^{-1})
	$5.4x10^{-3}$	0.38	14	$9.3x10^{-7}$	0.38	$2.4x10^{-3}$	$3.0x10^{-6}$	0.38	$7.9x10^{-3}$	$1.4x10^{-5}$	0.38	$3.7x10^{-2}$

Table 5.3 Quenching rate constants with addition of Cu^{2+} and Fe^{3+} to $[TbL^{13H}]^-$

	Cu^{2+}						Fe^{3+}					
	Concentration ($x10^{-4}$ M)						Concentration ($x10^{-4}$ M)					
	0 – 1.25			1.56 – 3.13			0 – 1.56			1.88 – 3.13		
$[TbL^{13H}]^-$	Slope (M^{-1})	τ (ms)	k_q ($M^{-1}\,s^{-1}$)	Slope (M^{-1})	τ (ms)	k_q ($M^{-1}\,s^{-1}$)	Slope (M^{-1})	τ (ms)	k_q ($M^{-1}\,s^{-1}$)	Slope (M^{-1})	τ (ms)	k_q ($M^{-1}\,s^{-1}$)
	$8.1x10^{-6}$	2.4	$3.4x10^{3}$	$5.9x10^{-7}$	2.4	$2.5x10^{4}$	$1.2x10^{-6}$	2.4	$5.0x10^{4}$	$2.6x10^{-6}$	2.4	$1.1x10^{3}$

Table 5.4 Quenching rate constants with addition of Cu^{2+} and Co^{2+} to $[TbL^{9H}]^-$

	Cu^{2+}						Co^{2+}					
	Concentration ($x10^{-5}$ M)						Concentration ($x10^{-5}$ M)					
	0 – 3.75			5.0 – 12.5			0 – 3.75			5.0 – 12.5		
$[TbL^{9H}]^-$	Slope (M^{-1})	τ (ms)	k_q ($M^{-1}\,s^{-1}$)	Slope (M^{-1})	τ (ms)	k_q ($M^{-1}\,s^{-1}$)	Slope (M^{-1})	τ (ms)	k_q ($M^{-1}\,s^{-1}$)	Slope (M^{-1})	τ (ms)	k_q ($M^{-1}\,s^{-1}$)
	$6.8x10^{-7}$	0.33	$2.1x10^{3}$	$6.8x10^{-6}$	0.33	$2.1x10^{2}$	$7.0x10^{-7}$	0.33	$2.1x10^{3}$	$2.2x10^{-6}$	0.33	$6.7x10^{3}$

Each k_q depends on the conditions used in the experiment, especially concentration. The numbers can only be compared for the same terbium complex under the same conditions.[315-318] In another word, k_q is only compared within the same table in this work.

- For $[Tb(L^2)_2]^-$, it is shown that the luminescence is quenched most significantly in the presence of Cu^{2+} ($1x10^{-3}$ M) (Table 5.2). In addition, the quenching rate constant was increased when the concentration of Fe^{3+} increased (Table 5.2).

- For $[TbL^{13H}]^-$, the quenching rate constant for Tb^{3+} was not changed significantly in the beginning upon increasing the concentration of Fe^{3+} (Table 5.3) while Cu^{2+} quenched the luminescence of $[TbL^{13H}]^-$ more significantly in the concentration range 0-$1.25x10^{-4}$ M.

- For $[TbL^{9H}]^-$, relatively smaller quenching rate constants were observed when either Cu^{2+} ($3.75x10^{-5}$ M) or Co^{2+} ($3.75x10^{-5}$ M) was present (Table 5.4). With further addition of the quenchers, the quenching rate constant of Cu^{2+} was increased.

5.4 Conclusion

$[Tb(L^2)_2]^-$, $[TbL^{13H}]^-$ and $[TbL^{9H}]^-$ are selectively responsive to different metal ions. The luminescence of all terbium complexes is quenched upon increasing the concentration of Cu^{2+}. Furthermore, Fe^{3+} can quench the luminescence of $[Tb(L^2)_2]^-$ and $[TbL^{13H}]^-$, while $[TbL^{9H}]^-$ is also responsive to Co^{2+}. The selectivity is dominated by the receptors of the ligands, as well as the distance between the metal ions and Tb^{3+}. Various coordination changes between the ligand and Tb^{3+} affect the energy transfer and cause luminescence quenching. The biggest quenching rate constant is observed when Cu^{2+} is added in $[Tb(L^2)_2]^-$.

Chapter Six Conclusion and further work

6.1 Conclusion

Four acyclic phthalimide-based compounds (L^1, L^3, L^5 and L^7) were synthesized in two stages (Scheme 21). They were then hydrolysed under basic conditions, yielding phthalamates (L^2, L^4, L^6 and L^8) of *ca.* 50 – 75%. Phthalimide was appended on cyclen-based macrocyclic systems yielding macrocyclic ligands (L^{9-13}, *ca.* 6 – 14%, Scheme 22). The structures of all the products (L^{1-13}) have been characterized by ^1H and ^{13}C NMR spectroscopy, mass spectrometer, IR spectroscopy and elemental analysis.

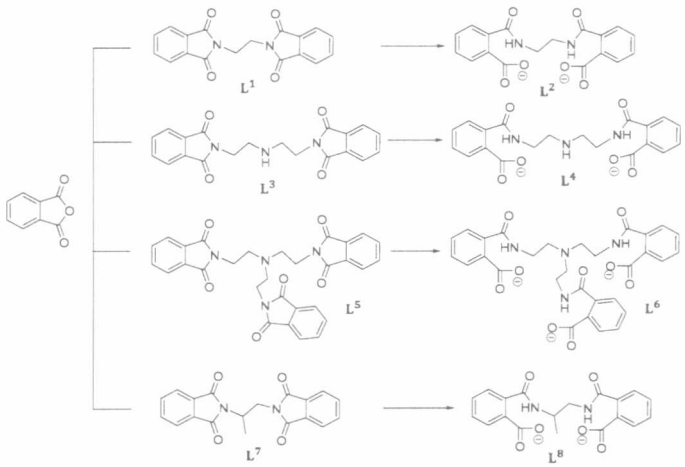

Scheme 21 Synthetic route to acyclic phthalamate derivatives ($L^{2, 4, 6, 8}$)

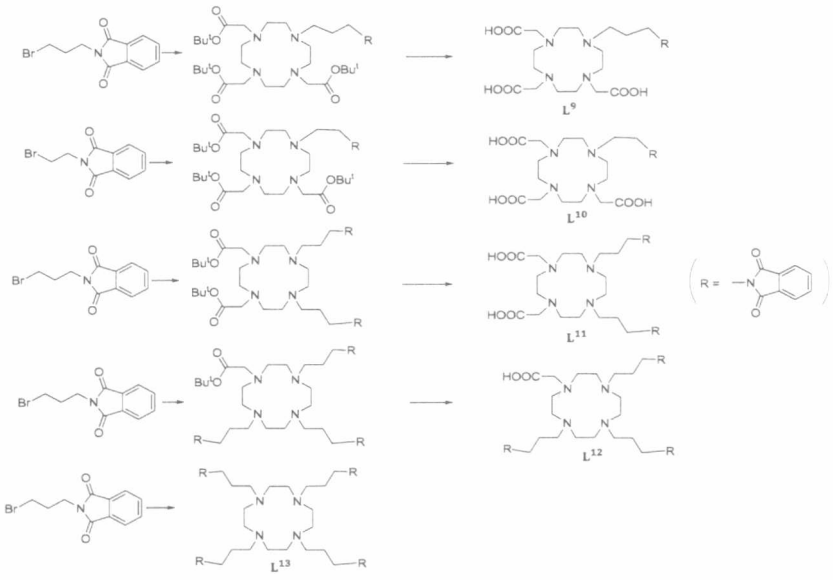

Scheme 22 Synthetic route to macrocyclic ligands (L^{9-13})

A 1:2 metal-to-ligand ratio gave the most efficient antennae effect for the acyclic phthalamate-based terbium complexes, $[Tb(L^2)_2]^-$, $[Tb(L^4)_2]^-$, $[Tb(L^6)_2]^{3-}$ and $[Tb(L^8)_2]^-$. Highly pH responsive luminescence of these four terbium complexes was observed between pH *ca.* 4.5-6.5. $[Tb(L^2)_2]^-$ showed the longest lifetime of 0.38 ms at pH *ca.* 6 while the other three terbium complexes were in the range of 0.24-0.36 ms.

The luminescence of macrocyclic terbium complex systems ($[TbL^9]^-$ - $[TbL^{12}]^-$) were enhanced significantly under basic conditions due to the replacement of bound water molecules by phthalamate functions. The luminescence of phthalamate-based macrocyclic terbium complex ($[TbL^{9H}]^-$ - $[TbL^{13H}]^-$) was maintained at a high level and then switched off at low pH due to protonation of the ligands. Scheme 23 outlines the coordinate bond between Tb^{3+} and L^9/L^{9H} at various pH. $[TbL^{9H}]^-$ exhibited the longest lifetime (2.4 ms) and highest quantum yield (46%) among all the macrocyclic terbium complexes at pH *ca.* 6 in deionised water. These values of τ and Φ are one of the top three terbium complex systems reported with a macrocyclic architecture.

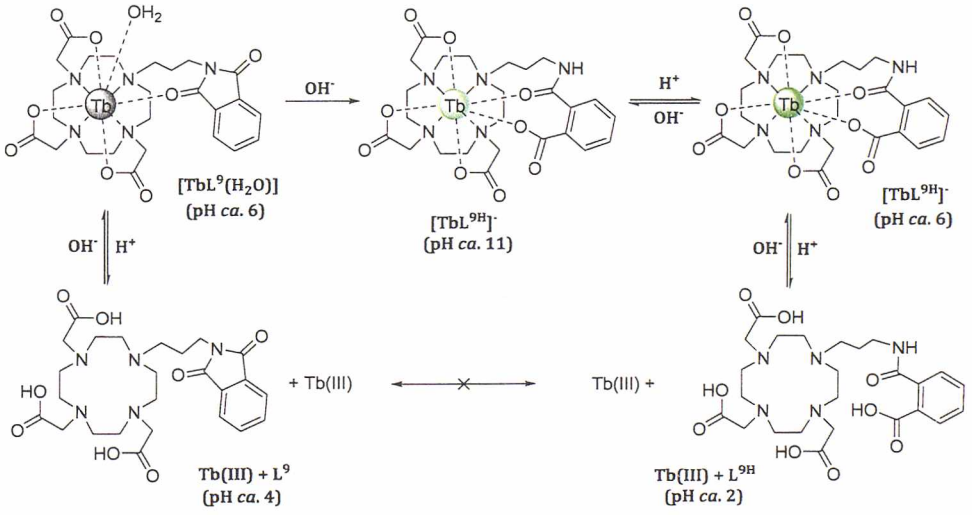

Scheme 23 Illustration of coordinate bond between Tb^{3+} and L^9/L^{9H} at various pH

The luminescence was sensitive to the presence of metal ions. $[Tb(L^2)_2]^-$ and $[TbL^{13H}]^-$ were responsive to Cu^{2+} and Fe^{3+} while their luminescence were quenched in the presence of either Cu^{2+} or Fe^{3+}. The luminescence of $[TbL^{9H}]^-$ was selectively quenched in the presence of Cu^{2+} or Co^{2+}.

6.2 Further work

Following the studies described in this work, a number of projects could be proposed to allow an investigation of the full potential applications of the lanthanide complexes of the ligands synthesized.

6.2.1 Luminescence properties of $[TbL^{9H}]^-$ in the presence of Lewis bases

The luminescence of $[TbL^{9H}]^-$ can be enhanced significantly under basic conditions. Sodium hydroxide was used so far in this work, however, Lewis bases such as ammonia, urea and tetrahydrofurans may have the same potential to activate the luminescence of $[TbL^{9H}]^-$. Further studies could be focused on the luminescence properties of $[TbL^{9H}]^-$ in the presence of different Lewis bases.

6.2.2 Luminescence properties of $[TbL^{9H}]^-$ incorporated in nanomaterials

All the luminescence studies of lanthanide complexes in this work were carried out as solutions. Recently, there has been increased interest in the potential applications of lanthanide complex in nanodevices.[320] Therefore, the high chemical stability and high quantum yield of $[TbL^{9H}]^-$ have made it potentially suitable for various biotechnological applications, such as tracking cells, drug delivery and targeting diseases.[321, 322]

A polyvinylpyrrolidone (PVP) nanofibre incorporated with a lanthanide complex, $Eu(TTA)_2phen$ (TTA: 4,4,4-trifluoro-1-(2-thenyl)1,3-butanedione, phen: 1,10-phenanthroline), has previously been synthesized successfully.[323] The luminescence results revealed that the energy transfer efficiency was enhanced while the luminescence lifetime of 7 wt%.PVP nanofibre (0.72 ms) was longer that of the powder (0.66 ms).[323] A similar nanofibre containing $[TbL^{9H}]^-$ can be electrospun with either water soluble (PVP) or non-aqueous (PCL) polymers to generate luminescent nanofibres for chemical devices.

References

1. A. Credi, B. F. Ribera and M. Venturi, *Electrochimica Acta*, 2004, **49**, 3865-3872.
2. G. P. Kittlesen, H. S. White and M. S. Wrighton, *Journal of the American Chemical Society*, 1984, **106**, 7389-7396.
3. D. C. Magri, G. D. Coen, R. L. Boyd and A. P. de Silva, *Analytica Chimica Acta*, 2006, **568**, 156-160.
4. C. J. Pedersen, *Angewandte Chemie-International Edition in English*, 1988, **27**, 1021-1027.
5. D. J. Cram, *Angewandte Chemie-International Edition in English*, 1988, **27**, 1009-1020.
6. J. M. Lehn, *Angewandte Chemie-International Edition in English*, 1988, **27**, 89-112.
7. K. A. Hutchison, J. P. Parakka, B. S. Kesler and R. R. Schumaker, in *Micro- and Nano-Photonic Materials and Devices*, ed. J. W. S. A. Perry, 1 edn., 2000, vol. 3937, pp. 64-72.
8. R. B. Dabke, G. D. Singh, A. Dhanabalan, R. Lal and A. Q. Contractor, *Analytical Chemistry*, 1997, **69**, 724-727.
9. J.-M. Lehn, *Supramolecular Chemistry: Concepts and Perspectives*, Wiley VCH, 1995, pp. 5-10.
10. V. Balzani, M. Venturi and A. Credi, *Molecular Devices and Machines: A Journey into the Nanoworld*, Wiley VCH, 2003, pp. 3-25.
11. J. Szmuszkovicz and E. Modest, *Journal of the American Chemical Society*, 1950, **72**, 571-577.
12. R. L. Zhang, Y. S. Wu, Z. L. Wang, W. Xue, H. B. Fu and J. N. Yao, *Journal of Physical Chemistry C*, 2009, **113**, 2594-2602.
13. S. Shinkai, *Pure and Applied Chemistry*, 1987, **59**, 425-430.
14. R. M. Metzger, *Journal of Materials Chemistry*, 1999, **9**, 2027-2036.
15. K. Szacilowski and W. Macyk, *Solid-State Electronics*, 2006, **50**, 1649-1655.
16. X. Fu, W. Sun, C. Fang, R. Guo and C. Yan, *Progress in Chemistry*, 2009, **21**, 957-963.
17. D. C. Magri, T. P. Vance and A. P. de Silva, *Inorganica Chimica Acta*, 2007, **360**, 751-764.
18. J. K. Tusa and H. R. He, *Journal of Materials Chemistry*, 2005, **15**, 2640-2647.
19. A. P. Desilva, H. Q. N. Gunaratne and G. E. M. Maguire, *Journal of the Chemical Society-Chemical Communications*, 1994, 1213-1214.
20. B. Bag and P. K. Bharadwaj, *Journal of Luminescence*, 2004, **110**, 85-94.
21. A. Credi, V. Balzani, S. J. Langford and J. F. Stoddart, *Journal of the American Chemical Society*, 1997, **119**, 2679-2681.
22. V. Balzani, A. Credi and M. Venturi, *Molecular Devices and Machines: Concepts and Perspectives for the Nanoworld*, 2 edn., Wiley VCH, 2008, pp. 1-11.
23. A. P. de Silva and N. D. McClenaghan, *Journal of the American Chemical Society*, 2000, **122**, 3965-3966.
24. A. P. Desilva, H. Q. N. Gunaratne and C. P. McCoy, *Nature*, 1993, **364**, 42-44.
25. R. Baron, O. Lioubashevski, E. Katz, T. Niazov and I. Willner, *Organic & Biomolecular Chemistry*, 2006, **4**, 989-991.

26. T. Gunnlaugsson, D. A. Mac Donail and D. Parker, *Chemical Communications*, 2000, 93-94.
27. T. Gunnlaugsson, D. A. Mac Donaill and D. Parker, *Journal of the American Chemical Society*, 2001, **123**, 12866-12876.
28. A. P. deSilva, H. Q. N. Gunaratne, T. Gunnlaugsson, A. J. M. Huxley, C. P. McCoy, J. T. Rademacher and T. E. Rice, *Chemical Reviews*, 1997, **97**, 1515-1566.
29. H. S. Barcena, B. Liu, M. V. Mirkin and J. W. Canary, *Inorganic Chemistry*, 2005, **44**, 7652-7660.
30. P. Yan, M. W. Holman, P. Robustelli, A. Chowdhury, F. I. Ishak and D. M. Adams, *Journal of Physical Chemistry B*, 2005, **109**, 130-137.
31. X. F. Guo, D. Q. Zhang, G. X. Zhang and D. B. Zhu, *Journal of Physical Chemistry B*, 2004, **108**, 11942-11945.
32. L. Lei, Y. Meng Xiao, L. Fu You, Y. Tao and H. Chun Hui, *Colloids and Surfaces A: Physicochemical and Engineering Aspects*, 2007, 49-53.
33. A. P. de Silva, D. B. Fox, T. S. Moody and S. M. Weir, *Trends in Biotechnology*, 2001, **19**, 29-34.
34. O. Cherniavskaya, A. Adzic, C. Knutson, B. J. Gross, L. Zang, R. Liu and D. M. Adams, *Langmuir*, 2002, **18**, 7029-7034.
35. T. Ueno, Y. Urano, K. Setsukinai, H. Takakusa, H. Kojima, K. Kikuchi, K. Ohkubo, S. Fukuzumi and T. Nagano, *Journal of the American Chemical Society*, 2004, **126**, 14079-14085.
36. B. J. Clark, T. Frost and M. A. Russell, *UV Spectroscopy: Techniques, instrumentation and data handling*, Springer, 1993, pp. 23-26.
37. J. F. Callan, A. P. de Silva and D. C. Magri, *Tetrahedron*, 2005, **61**, 8551-8588.
38. T. Miura, Y. Urano, K. Tanaka, T. Nagano, K. Ohkubo and S. Fukuzumi, *Journal of the American Chemical Society*, 2003, **125**, 8666-8671.
39. B. L. Feringa, W. F. Jager, B. Delange and E. W. Meijer, *Journal of the American Chemical Society*, 1991, **113**, 5468-5470.
40. J. P. Leonard and T. Gunnlaugsson, *Journal of Fluorescence*, 2005, **15**, 585-595.
41. S. Lis, M. Elbanowski, B. Makowska and Z. Hnatejko, *Journal of Photochemistry and Photobiology a-Chemistry*, 2002, **150**, 233-247.
42. U. Karhunen, L. Jaakkola, Q. Wang, U. Lamminmaki and T. Soukka, *Analytical Chemistry*, 2010, **82**, 751-754.
43. J. C. G. Bunzli, S. Comby, A. S. Chauvin and C. D. B. Vandevyver, *Journal of Rare Earths*, 2007, **25**, 257-274.
44. W. B. Jensen, *Journal of Chemical Education*, 1982, **59**, 634-636.
45. X. Y. Cao and M. Dolg, *Journal of Molecular Structure-Theochem*, 2002, **581**, 139-147.
46. S. G. Wang, D. K. Pan and W. H. E. Schwarz, *Journal of Chemical Physics*, 1995, **102**, 9296-9308.
47. M. Seitz, A. G. Oliver and K. N. Raymond, *Journal of the American Chemical Society*, 2007, **129**, 11153-11160.
48. R. G. Pearson, *Journal of the american chemical society*, 1963, **85**, 3533-3539.
49. R. G. Pearson, *Journal of Chemical Education*, 1968, **45**, 643-648.
50. R. G. Pearson, *Journal of Chemical Education*, 1968, **45**, 581-586.

51. K. Tanaka, Y. Kato and Y. Onuki, *Acta Crystallographica Section B-Structural Science*, 1997, **53**, 143-152.
52. F. S. Richardson, *Chemical Reviews*, 1982, **82**, 541-552.
53. A. Habenschuss and F. H. Spedding, *Journal of Chemical Physics*, 1979, **70**, 2797-2806.
54. J. Marcalo and A. P. Dematos, *Polyhedron*, 1989, **8**, 2431-2437.
55. S. A. Cotton, *Comptes Rendus Chimie*, 2005, **8**, 129-145.
56. J. C. G. Bunzli, *Accounts of Chemical Research*, 2006, **39**, 53-61.
57. E. G. Moore, A. P. S. Samuel and K. N. Raymond, *Accounts of Chemical Research*, 2009, **42**, 542-552.
58. D. Parker, *Chemical Society Reviews*, 2004, **33**, 156-165.
59. W. T. Carnall, P. R. Fields and K. Rajnak, *Journal of Chemical Physics*, 1968, **49**, 4412-4423.
60. S. S. Braga, R. A. S. Ferreira, I. S. Goncalves, M. Pillinger, J. Rocha, J. J. C. Teixeira-Dias and L. D. Carlos, *Journal of Physical Chemistry B*, 2002, **106**, 11430-11437.
61. A. Loudet, R. Bandichhor, L. X. Wu and K. Burgess, *Tetrahedron*, 2008, **64**, 3642-3654.
62. G. E. Khalil, E. K. Thompson, M. Gouterman, J. B. Callis, L. R. Dalton, N. J. Turro and S. Jockusch, *Chemical Physics Letters*, 2007, **435**, 45-49.
63. S. Cotton, *Lanthanide and Actinide Chemistry*, 2nd edn., Wiley-Blackwell, 2006.
64. K. Binnemans, *Chemical Reviews*, 2009, **109**, 4283-4374.
65. C.-H. Huang, *Rare Earth Coordination Chemistry: Fundamentals and Applications*, 1 edn., Wiley-Blackwell, 2010, pp. 9.
66. C. H. Huang, *Rare Earth Coordination Chemistry: Fundamentals and Applications*,
1 edn., Wiley-Blackwell, 2010, pp. 11.
67. D. Parker, R. S. Dickins, H. Puschmann, C. Crossland and J. A. K. Howard, *Chemical Reviews*, 2002, **102**, 1977-2010.
68. G. S. Manku, *Theoretical Principles of Inorganic Chemistry*, New edn., McGraw-Hill Education, 1982, pp. 31-33.
69. T. Gunnlaugsson and J. P. Leonard, *Chemical Communications*, 2005, 3114-3131.
70. A. Dossing, *European Journal of Inorganic Chemistry*, 2005, 1425-1434.
71. W. D. Horrocks and D. R. Sudnick, *Journal of the American Chemical Society*, 1979, **101**, 334-340.
72. A. Beeby, I. M. Clarkson, R. S. Dickins, S. Faulkner, D. Parker, L. Royle, A. S. de Sousa, J. A. G. Williams and M. Woods, *Journal of the Chemical Society-Perkin Transactions 2*, 1999, 493-503.
73. S. M. Hanagodimath, B. Siddlingeshwar, J. Thipperudrappa and S. K. B. Hadimani, *Journal of Luminescence*, 2009, **129**, 335-339.
74. A. T. R. Williams, S. A. Winfield and J. N. Miller, *Analyst*, 1983, **108**, 1067-1071.
75. K. K. ROHATGI, *Fundamentals of Photochemistry*, 1 edn., John Wiley & Sons, 1978, pp. 21-33.
76. S. Lis, *Journal of Alloys and Compounds*, 2002, **341**, 45-50.

77. J. L. Kropp and M. W. Windsor, *Journal of Chemical Physics*, 1965, **42**, 1599-1608.
78. J. C. G. Bunzli and C. Piguet, *Chemical Society Reviews*, 2005, **34**, 1048-1077.
79. R. S. Dickins, D. Parker, A. S. deSousa and J. A. G. Williams, *Chemical Communications*, 1996, 697-698.
80. A. P. Samuel, *Optimizing new classes of luminescent lanthanide complexes*, ProQuest LLC, 2011.
81. E. B. van der Tol, H. J. van Ramesdonk, J. W. Verhoeven, F. J. Steemers, E. G. Kerver, W. Verboom and D. N. Reinhoudt, *A European Journal.*, 1998, **4**, 2315-2323.
82. R. E. Whan and G. A. Crosby, *Journal of Molecular Spectroscopy*, 1962, **8**, 315-327.
83. J. L. Kropp and M. W. Windsor, *Journal of Chemical Physics*, 1965, **42**, 1599-1608.
84. S. Petoud, G. Muller, E. G. Moore, J. Xu, J. Sokolnicki, J. P. Riehl, U. N. Le, S. M. Cohen and K. N. Raymond, *Journal of the American Chemical Society*, 2007, **129**, 77-83.
85. E. A. Gastilovich, V. G. Klimenko, N. V. Korol'kova, R. N. Nurmukhametov and S. A. Serov, *Optics and Spectroscopy*, 2008, **105**, 38-45.
86. E. A. Gastilovich, N. V. Korol'kova, V. G. Klimenko and R. N. Nurmukhametov, *Optics and Spectroscopy*, 2008, **104**, 491-494.
87. M. Burton, *Comparative Effects of Radiation*, John Wiley & Sons Inc, 1960.
88. D. L. Dexter, *The journal of chemical physics*, 1953, **21**, 836-850.
89. J. R. Albani, *Principles and Applications of Fluorescence Spectroscopy*, Wiley-Blackwell, 2007, pp. 8-13.
90. S. H. Lin, W. Z. Xiao and W. Dietz, *Physical Review E*, 1993, **47**, 3698-3706.
91. A. L. Thompson, K. M. Gaab, J. J. Xu, C. J. Bardeen and T. J. Martinez, *Journal of Physical Chemistry A*, 2004, **108**, 671-682.
92. S. Faure, C. Stern, R. Guilard and P. D. Harvey, *Journal of the American Chemical Society*, 2004, **126**, 1253-1261.
93. A. P. Bassett, S. W. Magennis, P. B. Glover, D. J. Lewis, N. Spencer, S. Parsons, R. M. Williams, L. De Cola and Z. Pikramenou, *Journal of the American Chemical Society*, 2004, **126**, 9413-9424.
94. F. J. Steemers, W. Verboom, D. N. Reinhoudt, E. B. Vandertol and J. W. Verhoeven, *Journal of the American Chemical Society*, 1995, **117**, 9408-9414.
95. A. P. deSilva, H. Q. N. Gunaratne and C. P. McCoy, *Chemical Communications*, 1996, 2399-2400.
96. A. P. deSilva, H. Q. N. Gunaratne and T. E. Rice, *Angewandte Chemie-International Edition in English*, 1996, **35**, 2116-2118.
97. P. Atkinson, K. S. Findlay, F. Kielar, R. Pal, D. Parker, R. A. Poole, H. Puschmann, S. L. Richardson, P. A. Stenson, A. L. Thompson and J. H. Yu, *Organic & Biomolecular Chemistry*, 2006, **4**, 1707-1722.
98. R. Pal and D. Parker, *Chemical Communications*, 2007, 474-476.
99. R. A. Poole, F. Kielar, S. L. Richardson, P. A. Stenson and D. Parker, *Chemical Communications*, 2006, 4084-4086.
100. M. P. Lowe, D. Parker, O. Reany, S. Aime, M. Botta, G. Castellano, E. Gianolio and R. Pagliarin, *Journal of the American Chemical Society*, 2001, **123**, 7601-7609.

101. K. L. Wong, G. L. Law, Y. Y. Yang and W. T. Wong, *Advanced Materials*, 2006, **18**, 1051-1054.
102. S. Pehkonen, *Analyst*, 1995, **120**, 2655-2663.
103. M. Fujiwara, S. Tsukahara and H. Watarai, *Physical Chemistry Chemical Physics*, 1999, **1**, 2949-2951.
104. O. Kotova, S. Comby and T. Gunnlaugsson, *Chemical Communications*, **47**, 6810-6812.
105. U. C. Yoon and P. S. Mariano, *Accounts of Chemical Research*, 2001, **34**, 523-533.
106. M. Machida, H. Takechi, Y. Shishido and Y. Kanaoka, *Synthesis-Stuttgart*, 1982, 1078-1080.
107. A. G. Griesbeck and H. Gorner, *Journal of Photochemistry and Photobiology a-Chemistry*, 1999, **129**, 111-119.
108. A. G. Griesbeck, A. Henz, J. Hirt, V. Ptatschek, T. Engel, D. Löffler and F. W. Schneider, *Tetrahedron*, 1994, **50**, 701-714.
109. H. Gorner, M. Oelgemoller and A. G. Griesbeck, *Journal of Physical Chemistry A*, 2002, **106**, 1458-1464.
110. D. M. Y. Barrett, I. A. Kahwa, B. Raduchel, A. J. P. White and D. J. Williams, *Journal of the Chemical Society-Perkin Transactions 2*, 1998, 1851-1856.
111. M. de Sousa, B. de Castro, S. Abad, M. A. Miranda and U. Pischel, *Chemical Communications*, 2006, 2051-2053.
112. A. Trachsel, A. Govoni, J. Y. de Saint Lamner, E. Frerot and A. Herrmann, *Chemistry & Biodiversity*, 2008, **5**, 2621-2639.
113. E. Brunet, O. Juanes and J. C. Rodriguez-Ubis, *Current Chemical Biology*, 2007, **1**, 11-39.
114. E. G. Moore, J. Xu, C. J. Jocher, T. M. Corneillie and K. N. Raymond, *Inorganic Chemistry*, **49**, 9928-9939.
115. E. G. Moore, J. Xu, C. J. Jocher, E. J. Werner and K. N. Raymond, *Journal of the American Chemical Society*, 2006, **128**, 10648-10649.
116. E. G. Moore, J. Xu, J. Jocher, I. Castro-Rodriguez and K. N. Raymond, *Inorganic Chemistry*, 2008, **47**, 3105-3118.
117. R. Rivest, *Canadian Journal of Chemistry*, 1962, **40**, 2234-2242.
118. S. C. Jain and R. Rivest, *Journal of Inorganic and Nuclear Chemistry*, 1967, **29**, 2287-2294.
119. M. Han, H.-Y. Zhang, L.-X. Yang, Q. Jiang and Y. Liu, *Organic Letters*, 2008, **10**, 5557-5560.
120. D. M. Y. Barrett, I. A. Kahwa, J. T. Mague and G. L. McPherson, *Journal of Organic Chemistry*, 1995, **60**, 5946-5953.
121. F. Wild, *Characterization of Organic Compounds*, 2 edn., Cambridge University Press, 1958, pp. 107-142.
122. K. Eller, E. Henkes, R. Rossbacher and H. Höke, *Ullmann's Encyclopedia of Industrial Chemistry*, Wiley-VCH Verlag, 2000.
123. M. M. Sprung, *J. Am. Chem. Soc.*, 1939, **61**, 3381-3385.
124. A. Sakakura, T. Ohkubo, R. Yamashita, M. Akakura and K. Ishihara, *Organic Letters*, 2011, **13**, 892-895.
125. S. Ege, *Organic Chemistry*, 4 edn., Houghton Mifflin (Academic), 1998.
126. N. Perisic-Janjic, L. Arman and M. Lazarevic, *Bulletin of the Chemists and Technologists of Macedonia*, 1999, **18**, 15-20.

127. Y.-L. Sim, W. H. W. Ahmad, M. Y. Cheong, A. Ariffin and M. N. Khan, *Progress in Reaction Kinetics and Mechanism*, 2009, **34**, 347-359.
128. M. N. Khan and A. A. Khan, *Journal of the Chemical Society-Perkin Transactions 2*, 1979, 796-798.
129. M. N. Khan and A. A. Khan, *Journal of the Chemical Society, Perkin Transactions 2*, 1979, 796-798.
130. P. Crooy and A. Bruylants, *Bulletin des Sociétés Chimiques Belges*, 1964, **73**, 44-56.
131. M. N. Khan, *Journal of Organic Chemistry*, 1996, **61**, 8063-8068.
132. M. S. Gibson and R. W. Bradshaw, *Angewandte Chemie-International Edition*, 1968, **7**, 919-930.
133. L. Kürti and B. Czakó, *Strategic Applications of Named Reactions in Organic Synthesis*, 1 edn., Academic Press, 2005, pp. 182.
134. D. R. Klein, *Organic Chemistry*, 1 edn., John Wiley & Sons, 2011, pp. 1089.
135. B. R. Kowalski and C. A. Reilly, *Journal of Physical Chemistry*, 1971, **75**, 1402-1411.
136. Z.-P. Liang and J. Li, *Acta Crystallographica Section E-Structure Reports Online*, 2006, **62**, 5282-5283.
137. M. Zanger, *Organic Magnetic Resonance*, 1972, **4**, 1-25.
138. J. Vamecq, P. Bac, C. Herrenknecht, P. Maurois, P. Delcourt and J. P. Stables, *Journal of Medicinal Chemistry*, 2000, **43**, 1311-1319.
139. H. Toiserkani, H. Sheibani and K. Saidi, *European Polymer Journal*, **46**, 185-194.
140. J. Lambert and E. Mazzola, *Nuclear Magnetic Resoance Spectroscopy-An introduction to principles, applications, and experimental methods*, 1 edn., Pearson Education, Inc, 2004, pp. 62.
141. P. G. Henry, M. Marjanska, J. D. Walls, J. Valette, R. Gruetter and K. Ugurbil, *Magnetic Resonance in Medicine*, 2006, **55**, 250-257.
142. P. J. Stevenson, *Organic & Biomolecular Chemistry*, **9**, 2078-2084.
143. T. R. Hoye, P. R. Hanson and J. R. Vyvyan, *Journal of Organic Chemistry*, 1994, **59**, 4096-4103.
144. S. Bali, A. K. Singh, P. Sharma, R. A. Toscano, J. E. Drake, M. B. Hursthouse and M. E. Light, *Journal of Organometallic Chemistry*, 2004, **689**, 2346-2353.
145. A. K. Singh, J. Sooriyakumar, M. Kadarkaraisamy, J. E. Drake, M. B. Hursthouse, M. E. Light and R. J. Butcher, *Polyhedron*, 2002, **21**, 667-674.
146. D. L. Pavia, G. M. Lampman and G. S. Kriz, *Introduction to Spectroscopy*, 4 edn., Thomson Brooks/Cole, 2008, pp. 28-30.
147. M. Balci, *Basic 1H- and 13C-NMR Spectroscopy*, 1 edn., Elsevier Science Ltd, 2005, pp. 148.
148. T. D. W. Claridge and I. Perez-Victoria, *Organic & Biomolecular Chemistry*, 2003, **1**, 3632-3634.
149. D. F. Hunt, J. Shabanowitz, F. K. Botz and D. A. Brent, *Analytical Chemistry*, 1977, **49**, 1160-1163.
150. E. Sokol, R. J. Noll, R. G. Cooks, L. W. Beegle, H. I. Kim and I. Kanik, *International Journal of Mass spectrometer*, **306**, 187-195.
151. C. E. Rostad, *Fuel*, **89**, 997-1005.
152. A. R. Bandy, D. C. Thornton and A. R. Driedger, *Journal of Geophysical Research-Atmospheres*, 1993, **98**, 23423-23433.

153. I. Manisali, D. D. Y. Chen and B. B. Schneider, *Trac-Trends in Analytical Chemistry*, 2006, **25**, 243-256.
154. V. K. Mavrodiev, M. F. Abdullin, D. V. Gamirova, E. M. Vyrypaev, I. I. Furlei and F. Z. Galin, *International Journal of Mass spectrometer*, 2009, **279**, 37-40.
155. J. Kotz, P. Treichel and J. Townsend, *Chemistry & Chemical Reactivity*, 8 edn., Brooks/Cole, 2011, pp. 348.
156. R. J. C. Brown and R. F. C. Brown, *Journal of Chemical Education*, 2000, **77**, 724-731.
157. R. T. Myers, *Journal of Chemical Education*, 1979, **56**, 711-712.
158. R. L. DeKock, *Journal of Chemical Education*, 1987, **64**, 937-942.
159. B. C. Smith, *Fundamentals of Fourier Transform Infrared Spectroscopy*, 2 edn., CRC Press, 2011, pp. 90-96.
160. B. H. Stuart, *Infrared Spectroscopy: Fundamentals and Applications*, 1 edn., Wiley-Blackwell, 2004, pp. 242.
161. V. Krishnakumar, V. Balachandran and T. Chithambarathanu, *Spectrochimica Acta Part a-Molecular and Biomolecular Spectroscopy*, 2005, **62**, 918-925.
162. R. A. Nyquist and S. L. Fiedler, *Vibrational Spectroscopy*, 1995, **8**, 365-386.
163. I. M. Atkinson, A. R. Carroll, R. J. A. Janssen, L. F. Lindoy, O. A. Matthews and G. V. Meehan, *Journal of the Chemical Society-Perkin Transactions 1*, 1997, 295-301.
164. D. Dolphin, S. J. Rettig, H. Tang, T. Wijesekera and L. Y. Xie, *Journal of the American Chemical Society*, 1993, **115**, 9301-9302.
165. L. Y. Xie and D. Dolphin, *Journal of the Chemical Society-Chemical Communications*, 1994, 1475-1476.
166. J. L. Sessler, T. Murai and G. Hemmi, *Inorganic Chemistry*, 1989, **28**, 3390-3393.
167. M. Iyoda, J. Yamakawa and M. J. Rahman, *Angewandte Chemie-International Edition*, **50**, 10522-10553.
168. C. Ma, A. Lo, A. Abdolmaleki and M. J. MacLachlan, *Organic Letters*, 2004, **6**, 3841-3844.
169. J. A. Elvidge and J. H. Golden, *Journal of the Chemical Society*, 1957, 700-709.
170. D. Parker, *Coord. Chem. Rev.*, 2000, **205**, 109-130.
171. T. Gunnlaugsson, C. P. McCoy and F. Stomeo, *Tetrahedron Letters*, 2004, **45**, 8403-8407.
172. S. Faulkner and S. J. A. Pope, *Journal of the American Chemical Society*, 2003, **125**, 10526-10527.
173. T. J. Atkins, J. E. Richman and W. F. Oettle, *Organic Syntheses*, 1988, **50-9**, 652-662.
174. H. K. Hall, *Journal of American Chemical Society*, 1957, **79**, 5441-5444.
175. R. Linnell, *Journal of Organic Chemistry*, 1960, **25**, 290-290.
176. H.-J. A. Klaus Weissermel, Charlet R. Lindley, Stephen Hawkins, *Industrial Organic Chemistry*, Wiley-VCH, 2003, pp. 482.
177. G. R. Weisman and D. P. Reed, *Journal of Organic Chemistry*, 1996, **61**, 5186-5187.
178. T. Gunnlaugsson, R. J. H. Davies, P. E. Kruger, P. Jensen, T. McCabe, S. Mulready, J. E. O'Brien, C. S. Stevenson and A. M. Fanning, *Tetrahedron Letters*, 2005, **46**, 3761-3766.

179. Schultze, L. Bulls, Patent, WO/1996/028433, 1996.
180. C. Li and W. T. Wong, *Tetrahedron*, 2004, **60**, 5595-5601.
181. E. Hahn-Deinstrop, *Applied Thin Layer Chromatography: Best Practice and Avoidance of Mistakes*, 2 edn., Wiley VCH, 2006, pp. 69-90.
182. P. E. Wall, J. C. Berridge, P. J. Schoenmaker and C. F. Simpson, *Thin Layer Chromatography: A Modern Practical Approach*, 1 edn., Royal Society of Chemistry, 2005, pp. 7-12.
183. E. Heftman, *Chromatography: Applications Part B: Fundamentals and Applications of Chromatographic and Electrophoretic Methods*, 1 edn., Elsevier Science Ltd, 1985, pp. 142-160.
184. N. J. Wardle, A. H. Herlihy, P. W. So, J. D. Bell and S. W. A. Bligh, *Bioorganic & Medicinal Chemistry*, 2007, **15**, 4714-4721.
185. S. Buoen, J. Dale and J. Krane, *Acta Chemica Scandinavica Series B-Organic Chemistry and Biochemistry*, 1984, **38**, 773-778.
186. J. McMurry, *Fundamentals of Organic Chemistry*, 7 edn., Brooks/Cole, 2010, pp. 445.
187. W. H. Brown, C. S. Foote, B. L. Iverson and E. V. Anslyn, *Organic Chemistry* 6 edn., Brooks/Cole, 2011, pp. 495-523.
188. H. Hart, L. E. Craine, D. J. Hart and C. M. Hadad, *Organic Chemistry: A Short Course*, 13 edn., CENGAGE Learning Custom Publishing, 2011, pp. 183-189.
189. A. K. Singh, *Advanced Organic Chemistry: Reactions and Mechanisms*, 1 edn., Pearson, 2004, pp. 77-81.
190. D. R. Klein, *Organic Chemistry*, 1 edn., John Wiley & Sons, 2011, pp. 210-215.
191. J. R. Hanson, *Protecting Groups in Organic Synthesis*, 1 edn., Wiley-Blackwell 1999, pp. 130.
192. R. W. Jackson, *Tetrahedron Letters*, 2001, **42**, 5163-5165.
193. M. Meyer, V. Dahaoui-Gindrey, C. Lecomte and L. Guilard, *Coordination Chemistry Review*, 1998, **178**, 1313-1405.
194. K. Williamson and K. M. Masters, *Macroscale and Microscale Organic Experiments*, 6 edn., Brooks/Cole, 2012, pp. 318-325.
195. S. Lavoie and P. H. McBreen, *Journal of Physical Chemistry B*, 2005, **109**, 11986-11990.
196. N. S. Myshakina, Z. Ahmed and S. A. Asher, *Journal of Physical Chemistry B*, 2008, **112**, 11873-11877.
197. F. Q. Liu and L. S. Liebeskind, *Journal of Organic Chemistry*, 1998, **63**, 2835-2844.
198. M. J. Miller, M. H. Lyttle and A. Streitwieser, *Journal of Organic Chemistry*, 1981, **46**, 1977-1984.
199. W. C. Still, M. Kahn and A. Mitra, *Journal of Organic Chemistry*, 1978, **43**, 2923-2925.
200. M. Suchy and R. H. E. Hudson, *European Journal of Organic Chemistry*, 2008, 4847-4865.
201. F. Wojciechowski, M. Suchy, A. X. Li, H. A. Azab, R. Bartha and R. H. E. Hudson, *Bioconjugate Chemistry*, 2007, **18**, 1625-1636.
202. T. Chen, X. Wang, Y. He, C. Zhang, Z. Wu, K. Liao, J. Wang and Z. Guo, *Inorganic Chemistry*, 2009, **48**, 5801-5809.
203. E. E. Burnell and C. A. d. Lange, *NMR of Ordered Liquids*, 1 edn., Springer, 2003, pp. 9-21.

204. R. J. Anderson, D. J. Bendell, P. W. Groundwater and M. Berry, *Organic Spectroscopic Analysis*, 1 edn., Royal Society of Chemistry, 2004, pp. 83-88.
205. J. Humphreys, R. A. Duckett and I. M. Ward, *Polymer*, 1984, **25**, 1227-1234.
206. M. H. Norman, D. J. Minick and G. C. Rigdon, *Journal of Medicinal Chemistry*, 1996, **39**, 149-157.
207. J. H. Wengrovius, V. M. Powell and J. L. Webb, *Journal of Organic Chemistry*, 1994, **59**, 2813-2817.
208. B. Jebasingh and V. Alexander, *Inorganic Chemistry*, 2005, **44**, 9434-9443.
209. W. H. Brown, C. S. Foote, B. L. Iverson and E. V. Anslyn, *Organic Chemistry* 6 edn., Brooks/Cole, 2011, pp. 508-509.
210. M. B. Maquieira, A. B. Penenory and R. A. Rossi, *Journal of Organic Chemistry*, 2002, **67**, 1012-1015.
211. C. Steinbeck, *Natural Product Reports*, 2004, **21**, 512-518.
212. G. A. Webb, *Modern Magnetic Resonance*, 2 edn., Springer, 2006, pp. 31-62.
213. M. Oelgemoller, A. Haeuseler, M. Schmittel, A. G. Griesbeck, J. Lex and Y. Inoue, *Journal of the Chemical Society-Perkin Transactions 2*, 2002, 676-686.
214. T. S. Snowden, A. P. Bisson and E. V. Anslyn, *Bioorganic & Medicinal Chemistry*, 2001, **9**, 2467-2478.
215. F. Rizzo, A. Papagni, F. Meinardi, R. Tubino, M. Ottonelli, G. F. Musso and G. Dellepiane, *Synthetic Metals*, 2004, **147**, 143-147.
216. S. R. Chaudhari and N. Suryaprakash, *Journal of Molecular Structure*, 2012, **1016**, 163-168.
217. P. Larkin, *Infrared and Raman Spectroscopy; Principles and Spectral Interpretation*, 1 edn., An Elsevier Title, 2011, pp. 213-216.
218. S. J. Ratnakar, N. A. Samy and V. Alexander, *Polyhedron*, 2012, **38**, 1-6.
219. I. G. Binev, B. A. Stamboliyska, Y. I. Binev, E. A. Velcheva and J. A. Tsenov, *Journal of Molecular Structure*, 1999, **513**, 231-243.
220. S. Torrico-Vallejos, M. F. Erben, O. E. Piro, E. E. Castellano and C. O. Della Vedova, *Journal of Molecular Structure*, 2010, **975**, 227-233.
221. T. Matsuo, *Bulletin of the Chemical Society of Japan*, 1964, **37**, 1844-1848.
222. Y. Hase, *Journal of molecular structure* 1978, **48**, 33-42.
223. I. G. Binev, B. A. Stamboliyska and E. A. Velcheva, *Spectrochimica Acta Part a-Molecular and Biomolecular Spectroscopy*, 1996, **52**, 1135-1143.
224. S. Giordani, M. A. Cejas and F. M. Raymo, *Tetrahedron*, 2004, **60**, 10973-10981.
225. C. P. McCoy, F. Stomeo, S. E. Plush and T. Gunnlaugsson, *Chemistry of Materials*, 2006, **18**, 4336-4343.
226. M. D. Reily, L. C. Robosky, M. L. Manning, A. Butler, J. D. Baker and R. T. Winters, *Journal of the American Chemical Society*, 2006, **128**, 12360-12361.
227. R. A. Fairman, W. A. Gallimore, K. V. N. Spence and I. A. Kahwa, *Inorganic Chemistry*, 1994, **33**, 823-828.
228. T. Gunnlaugsson, H. D. P. Ali, M. Glynn, P. E. Kruger, G. M. Hussey, F. M. Pfeffer, C. M. G. dos Santos and J. Tierney, *Journal of Fluorescence*, 2005, **15**, 287-299.
229. A. Bianchi, L. Calabi, L. Ferrini, P. Losi, F. Uggeri and B. Valtancoli, *Inorganica Chimica Acta*, 1996, **249**, 13-15.
230. E. Szilagyi, E. Toth, Z. Kovacs, J. Platzek, B. Raduchel and E. Brucher, *Inorganica Chimica Acta*, 2000, **298**, 226-234.

231. A. Sassaroli and S. Fantini, *Physics in Medicine and Biology*, 2004, **49**, 255-257.
232. L. E. Sommerville, D. D. Thomas and G. L. Nelsestuen, *Journal of Biological Chemistry*, 1985, **260**, 444-452.
233. O. H. Griffith, W. A. Houle, K. F. Kongslie and W. W. Sukow, *Ultramicroscopy*, 1983, **12**, 299-308.
234. H. Abitan, H. Bohr and P. Buchhave, *Applied Optics*, 2008, **47**, 5354-5357.
235. W. F. Forbes, W. A. Mueller, A. S. Ralph and J. F. Templeton, *Canadian Journal of Chemistry*, 1957, **35**, 1049-1057.
236. V. Belluau, P. Noeureuil, E. Ratzke, A. Skvortsov, S. Gallagher, C. A. Motti and M. Oelgemoeller, *Tetrahedron Letters*, **51**, 4738-4741.
237. J. Gawronski, F. Kazmierczak, K. Gawronska, P. Skowronek, J. Waluk and J. Marczyk, *Tetrahedron*, 1996, **52**, 13201-13214.
238. F. L. Thorp-Greenwood, M. P. Coogan, A. J. Hallett, R. H. Laye and S. J. A. Pope, *Journal of Organometallic Chemistry*, 2009, **694**, 1400-1406.
239. L. Muruganandam, K.Balasubramanian, M. Ramesh and A. Sebastiyan, *Journal of Chemical, Biological and Physical Sciences*, 2012, **2**, 1184-1191.
240. R. Martin and G. A. Clarke, *Journal of Physical Chemistry*, 1978, **82**, 81-86.
241. M. V. Lucky, S. Sivakumar, M. L. P. Reddy, A. K. Paul and S. Natarajan, *Crystal Growth & Design*, **11**, 857-864.
242. G. Stojkovic and E. Popovski, *Journal of the Serbian Chemical Society*, 2006, **71**, 1061-1071.
243. V. R. More, U. S. Mote, S. R. Patil and G. B. Kolekar, *Spectrochimica Acta Part a-Molecular and Biomolecular Spectroscopy*, 2009, **74**, 771-775.
244. R. G. Pearson, *Coord. Chem. Rev.*, 1990, **100**, 403-425.
245. B. Zhao, P. Cheng, Y. Dai, C. Cheng, D. Liao-Zheng, S. P. Yan, Z. H. Jiang and G. L. Wang, *Angewandte Chemie-International Edition*, 2003, **42**, 934-936.
246. D. R. van Staveren, G. A. van Albada, J. G. Haasnoot, H. Kooijman, A. M. M. Lanfredi, P. J. Nieuwenhuizen, A. L. Spek, F. Ugozzoli, T. Weyhermuller and J. Reedijk, *Inorganica Chimica Acta*, 2001, **315**, 163-171.
247. E. J. Parks, R. A. Faltynek, F. E. Brinckman and J. Y. Peng, *Journal of the Less-Common Metals*, 1986, **126**, 300-300.
248. L. S. Starkey, *Introduction to Strategies for Organic Synthesis*, 1 edn., Wiley-Blackwell, 2012, pp. 73-81.
249. T. Z. E. Jones, D. Balsa, M. Unzeta and R. R. Ramsay, *Journal of Neural Transmission*, 2007, **114**, 707-712.
250. S. Aime, M. Botta, D. Parker and J. A. G. Williams, *Journal of the Chemical Society-Dalton Transactions*, 1996, 17-23.
251. C. R. Smith and K. Yates, *Canadian Journal of Chemistry*, 1972, **50**, 771-776.
252. P. Jansa, V. Machacek, P. Nachtigall, V. Wsol and M. Svobodova, *Molecules*, 2007, **12**, 1064-1079.
253. F. A. Bettelheim, W. H. Brown and M. K. Campbell, *Introduction to General, Organic and Biochemistry*, 9 edn., Thomson Brooks/Cole, 2008, pp. 441-457.
254. A. P. de Silva, H. Q. N. Gunaratne and T. E. Rice, *Angewandte Chemie-International Edition*, 1996, **35**, 2116-2118.
255. S. E. Plush, N. A. Clear, J. P. Leonard, A.-M. Fanning and T. Gunnlaugsson, *Dalton Transactions*, **39**, 3644-3652.

256. M. Wall, B. Linkletter, D. Williams, A. M. Lebuis, R. C. Hynes and J. Chin, *Journal of the American Chemical Society*, 1999, **121**, 4710-4711.
257. C. F. V. Mason, Chamberl.Pi and R. G. Wilkins, *Inorganic Chemistry*, 1971, **10**, 2345-2348.
258. F. Gideon and N. Carl, *Proceedings of the National Academy of Sciences of the United States of America*, 1958, **44**, 671-688.
259. P. Chakraborty and C. L. Chakrabarti, *Analytica Chimica Acta*, 2006, **571**, 260-269.
260. M. Mecozzi, M. Amici, E. Pietrantonio and G. Romanelli, *Ultrasonics Sonochemistry*, 2002, **9**, 11-18.
261. J. Zhang, F. Han, X. Wei, L. Shui, H. Gong and P. Zhang, *Industrial & Engineering Chemistry Research*, **49**, 2025-2030.
262. H. E. Ungnade and R. W. Lamb, *Journal of the American Chemical Society*, 1952, **74**, 1789-3794.
263. D. B. Kuang, S. Ito, B. Wenger, C. Klein, J. E. Moser, R. Humphry-Baker, S. M. Zakeeruddin and M. Gratzel, *Journal of the American Chemical Society*, 2006, **128**, 4146-4154.
264. A. O. Adeloye and P. A. Ajibade, *Molecules*, **16**, 4615-4631.
265. C. M. MacDermaid and G. A. Kaminski, *Journal of Physical Chemistry B*, 2007, **111**, 9036-9044.
266. H. Reuveni, N. Livnah, T. Geiger, S. Kleid, O. Ohne, I. Cohen, M. Benhar, G. Gellerman and A. Levitzki, *Biochemistry*, 2002, **41**, 10304-10314.
267. P. K. Maiti, T. Cagin, S. T. Lin and W. A. Goddard, *Macromolecules*, 2005, **38**, 979-991.
268. A. Pasha, G. Tircso, E. T. Benyo, E. Bruecher and A. D. Sherry, *European Journal of Inorganic Chemistry*, 2007, 4340-4349.
269. P. R. Selvin, *Annual Review of Biophysics and Biomolecular Structure*, 2002, **31**, 275-302.
270. B. Song, V. Sivagnanam, C. D. B. Vandevyver, I. Hemmila, H.-A. Lehr, M. A. M. Gijs and J.-C. G. Bunzli, *Analyst*, 2009, **134**, 1991-1993.
271. T. Yatabe, H. Nakai, K. Nozaki, T. Yamamura and K. Isobe, *Organometallics*, **29**, 2390-2393.
272. A. P. S. Samuel, J. L. Lunkley, G. Muller and K. N. Raymond, *European Journal of Inorganic Chemistry*, 3343-3347.
273. J. Xu, T. M. Corneillie, E. G. Moore, G.-L. Law, N. G. Butlin and K. N. Raymond, *Journal of the American Chemical Society*, **133**, 19900-19910.
274. A. P. S. Samuel, J. Xu and K. N. Raymond, *Inorganic Chemistry*, 2009, **48**, 687-698.
275. L. Armelao, S. Quici, F. Barigelletti, G. Accorsi, G. Bottaro, M. Cavazzini and E. Tondello, *Coordination Chemistry Review*, **254**, 487-505.
276. N. N. Katia, A. Lecointre, M. Regueiro-Figueroa, C. Platas-Iglesias and L. J. Charbonniere, *Inorganic Chemistry*, **50**, 1689-1697.
277. J. Andres and A.-S. Chauvin, *Inorganic Chemistry*, **50**, 10082-10090.
278. N. Chatterton, Y. Bretonniere, J. Pecaut and M. Mazzanti, *Angewandte Chemie-International Edition*, 2005, **44**, 7595-7598.
279. E. Brunet, O. Juanes, R. Sedano and J. C. Rodriguez-Ubis, *Photochemical & Photobiological Sciences*, 2002, **1**, 613-618.

280. M. P. Placidi, J. Engelmann, L. S. Natrajan, N. K. Logothetis and G. Angelovski, *Chemical Communications*, **47**, 11534-11536.
281. M. Murru, D. Parker, G. Williams and A. Beeby, *Journal of the Chemical Society-Chemical Communications*, 1993, 1116-1118.
282. R. A. Poole, G. Bobba, M. J. Cann, J. C. Frias, D. Parker and R. D. Peacock, *Organic & Biomolecular Chemistry*, 2005, **3**, 1013-1024.
283. I. Nasso, S. Bedel, C. Galaup, C. Picard and P. Jal, *European Journal of Inorganic Chemistry*, 2008, 2064-2074.
284. M. Latva, H. Takalo, V. M. Mukkala, C. Matachescu, J. C. RodriguezUbis and J. Kankare, *Journal of Luminescence*, 1997, **75**, 149-169.
285. G. F. de Sa, O. L. Malta, C. D. Donega, A. M. Simas, R. L. Longo, P. A. Santa-Cruz and E. F. da Silva, *Coord. Chem. Rev.*, 2000, **196**, 165-195.
286. C. C. C. Bejan, G. B. Rocha, R. Q. Albuquerque, F. W. J. Demnitz, G. F. de Sa and S. Alves, *Journal of Luminescence*, 2005, **113**, 79-88.
287. Y. Hasegawa, Y. Wada and S. Yanagida, *Journal of Photochemistry and Photobiology C-Photochemistry Reviews*, 2004, **5**, 183-202.
288. R. O. Freire, R. Q. Albuquerque, S. A. Junior, G. B. Rocha and M. E. de Mesquita, *Chemical Physics Letters*, 2005, **405**, 123-126.
289. O. L. Malta and F. Silva, *Spectrochimica Acta Part a-Molecular and Biomolecular Spectroscopy*, 1998, **54**, 1593-1599.
290. O. L. Malta, H. F. Brito, J. F. S. Menezes, F. Silva, S. Alves, F. S. Farias and A. V. M. deAndrade, *Journal of Luminescence*, 1997, **75**, 255-268.
291. Z. Liang, Z. Liu, L. Jiang and Y. Gao, *Tetrahedron Letters*, 2007, **48**, 1629-1632.
292. L. Fabbrizzi and A. Poggi, *Chemical Society Reviews*, 1995, **24**, 197-202.
293. B. K. McMahon and T. Gunnlaugsson, *Tetrahedron Letters*, **51**, 5406-5410.
294. T. Gunnlaugsson, B. Bichell and C. Nolan, *Tetrahedron*, 2004, **60**, 5799-5806.
295. A. P. de Silva, S. Uchiyama, T. P. Vance and B. Wannalerse, *Coordination Chemistry Review*, 2007, **251**, 1623-1632.
296. I. Oehme and O. S. Wolfbeis, *Mikrochimica Acta*, 1997, **126**, 177-192.
297. H. Wang, H. Wu, L. Xue, Y. Shi and X. Li, *Organic & Biomolecular Chemistry*, **9**, 5436-5444.
298. E. L. Que and C. J. Chang, *Journal of the American Chemical Society*, 2006, **128**, 15942-15943.
299. E. L. Que, E. Gianolio, S. L. Baker, A. P. Wong, S. Aime and C. J. Chang, *Journal of the American Chemical Society*, 2009, **131**, 8527-8536.
300. S. Goswami, D. Sen, N. K. Das and G. Hazra, *Tetrahedron Letters*, **51**, 5563-5566.
301. M. H. Keefe, K. D. Benkstein and J. T. Hupp, *Coordination Chemistry Review*, 2000, **205**, 201-228.
302. L. Fabbrizzi, A. Perotti and A. Poggi, *Inorganic Chemistry*, 1983, **22**, 1411-1412.
303. V. Bakhmutov, *Practical Nuclear Magnetic Resonance Relaxation for Chemists*, 1 edn., Wiley-Blackwell, 2004, pp. 20-29.
304. I. Bertini, C. Luchinat, L. J. Ming, M. Piccioli, M. Sola and J. S. Valentine, *Inorganic Chemistry*, 1992, **31**, 4433-4435.
305. A. M. Nonat, A. J. Harte, K. Senechal-David, J. P. Leonard and T. Gunnlaugsson, *Dalton Transactions*, 2009, 4703-4711.

306. S. C. Dodani, Q. He and C. J. Chang, *Journal of the American Chemical Society*, 2009, **131**, 18020-18021.
307. M. H. Kuok, *Solid State Communications*, 1981, **40**, 595-597.
308. S. M. Khan, E. R. Birnbaum and D. W. Darnall, *Biochemistry*, 1978, **17**, 4669-4674.
309. W. D. Horrocks, B. Holmquist and B. L. Vallee, *Proceedings of the National Academy of Sciences of the United States of America*, 1975, **72**, 4764-4768.
310. J. H. Yu and D. Parker, *European Journal of Organic Chemistry*, 2005, 4249-4252.
311. S. C. J. Meskers and H. Dekkers, *Journal of Physical Chemistry A*, 2001, **105**, 4589-4599.
312. M. J. Tapia, H. D. Burrows, M. Azenha, M. D. Miguel, A. Pais and J. M. G. Sarraguca, *Journal of Physical Chemistry B*, 2002, **106**, 6966-6972.
313. S. Lis, T. Kimura and Z. Yoshida, *Journal of Alloys and Compounds*, 2001, **323**, 125-127.
314. S. Lis, T. Kimura, Z. Yoshida and S. But, *Journal of Alloys and Compounds*, 2004, **380**, 173-176.
315. W. S. Xia, R. H. Schmehl and C. J. Li, *Tetrahedron*, 2000, **56**, 7045-7049.
316. J. Kuijt, F. Ariese, U. A. T. Brinkman and C. Gooijer, *Analytica Chimica Acta*, 2003, **488**, 135-171.
317. J.-C. G. Buenzli, S. Comby, A.-S. Chauvin and C. D. B. Vandevyver, *Journal of Rare Earths*, 2007, **25**, 257-274.
318. G. R. Choppin and D. R. Peterman, *Coordination Chemistry Review*, 1998, **174**, 283-299.
319. K. Martinelle and L. Haggstrom, *Biotechnology Techniques*, 1997, **11**, 549-551.
320. F. Gu, Z. Wang, J. Sun, D. Han and G. Guo, in *Journal of Scientific Conference Proceedings, Vol 1, Nos 2 and 3*, eds. H. Wang, J. R. H. Hie and J. Zhang, Editon edn., 2009, vol. 1, pp. 127-131.
321. F. Meiser, C. Cortez and F. Caruso, *Angewandte Chemie-International Edition*, 2004, **43**, 5954-5957.
322. P. Schuetz and F. Caruso, *Chemistry of Materials*, 2002, **14**, 4509-4516.
323. L. Wei and W. Ce, *Indian Journal of Chemistry Section a-Inorganic Bio-Inorganic Physical Theoretical & Analytical Chemistry*, 2007, **46**, 1951-1954.

Appendix: Publication, Presentations and Posters Relating to this Thesis

Publication:

G. Chen, J.L. Sarris, N.J. Wardle, S.W. Annie Bligh and N.P. Chatterton, *Chem. Commun.*, 2012, **48**, 9026-9028.

Oral presentations:

A chemically unlocked binary molecular switch.

'South East Researcher Inorganic and Materials Chemistry Meeting', University of Surrey, July 2012.

A novel terbium complex in molecular switch

'A symposium for PhD students of School of Human Sciences', London Metropolitan University, July 2012.

Posters:

A chemically unlocked binary molecular switch.

'4th European Association for Chemical and Molecular Sciences', Prague, August 2012

Phthalamate derivatives as highly luminescent lanthanide chelates.

'A Symposium for Postgraduate Inorganic Chemists', University College London, July 2011.